Technische Universität München
Fakultät für Bauingenieur- und Vermessungswesen
Institut für Baustoffe und Konstruktion
Fachgebiet Leichtmetallbau und Ermüdung

An Approach to Quality Assurance of Structural Adhesive Joints

Marianna Michaloudaki

Vollständiger Abdruck der von der Fakultät für Bauingenieur- und Vermessungswesen der Technischen Universität München zur Erlangung des akademischen Grades eines Doktor-Ingenieurs
genehmigten Dissertation.

Vorsitzender: Univ.-Prof. Dr.-Ing. Gert Albrecht

Prüfer der Dissertation:

1. Univ.-Prof. Dr.-Ing. Dr.-Ing. habil. Dimitris Kosteas
2. Prof. Dr.-Ing. Robert D. Adams,
   Univ. of Bristol / UK
3. Prof. ir. Frans Soetens,
   Univ. of Technology Eindhoven / NL

Die Dissertation wurde am 02.03.2005
bei der Technischen Universität München eingereicht und
durch die Fakultät für Bauingenieur- und Vermessungswesen
am 15.04.2005 angenommen.

στους γονείς μου,
Κωνσταντίνο και Ασπασία

Preface

The thesis provides an approach to the quality assurance of adhesively bonded joints for structural applications and focuses on the methods to quality control through destructive and non destructive testing. The proposed systematic approach is based on knowledge of the adhesive bonding technology and reliability of testing methods. As such, it is of interest for researchers who work in the field of adhesives, quality assurance experts, writers of standards, who want to apply quality management of adhesive joints in practice.

Many people contributed to this thesis. I would like to thank my supervisors, Professor Dimitris Kosteas (Technische Universität München, Faculty of Civil Engineering), Professor Robert Adams (University of Bristol, Faculty of Mechanical Engineering) and Professor Frans Soetens (Eindhoven University of Technology, Faculty of Building and Architecture) for their stimulating and fruitful comments. Furthermore, I would like to acknowledge the Paul Scherrer Institut (Dr. Eberhard Lehmann and the NEUTRA Team) and AGFA NDT Co. (Dr. Werner Roye and Mr. Uwe Wielpütz) who supported the project related to this PhD study by allowing performing the experimental non destructive testing without financial expenses and for their comments and sharpening ideas.

Then I would like to thank the members of industry Dr. Peter Born (Henkel Industrial Adhesives), Dr. Cornelis Wirth and Dr. Martin Eis (BMW AG), Dr. Heiko Wetter and Dr. Martin Bangel (AUDI AG) and Dipl.-Eng. Reinhold Gitter (ALCAN Co.), who provided this project with materials and/or laboratory facilities and they inspired me to look after practical applications of quality assurance in adhesively bonded joints. Furthermore, I am grateful to my colleagues at the Technische Universität München. In many ways they contributed to the completion of the thesis.

Munich, December 2004 Marianna Michaloudaki

Summary

With the development of advanced materials and structures, new nondestructive test techniques are being developed to evaluate material and structural integrity. Since adhesive bonding in engineering structures promises significant advantages - uniform stress distribution, enhanced fatigue properties, light weight, combination of dissimilar materials - over traditional techniques like welding and mechanical fastening, increased interest is registered in transport, construction, mechanical engineering, leisure structures.

The area of bondline integrity has been a significant "Achilles heel" in the outright acceptance of adhesive bonding in structural engineering. Design and manufacturing processes have been refined to ensure joint quality. However, bonding failures due to improper surface preparation and various manufacturing errors can not be completely avoided, thus calling for the development of reliable quality control and evaluation. Industrial fields have set increasing demands on non-destructive testing (NDT) automation and reliability both pivotal for practical implementation. To ensure the integrity of products and their fitness for purpose, an approach is described concerning the inspection effectiveness of NDT. To evaluate the reliability of non-destructive evaluation (NDE) various parameters are used on adhesive bonded systems.

It is the purpose of this thesis to present the reliability level of neutron radiography and ultrasonic method in detecting manufacturing defects, mostly dealing with debonds and cohesive weakness, as this is one of the main parameters to be considered in design of structural engineering. This is presented through systematic approach based on current knowledge about the behaviour of structural adhesive joints and quality assurance methods established through investigations on small specimens and full scale components. The material and testing parameters were estimated looking after industrial applicability and primarily the automotive field.

The NDT procedure is described and proposals to NDE are given both with neutron radiography and ultrasonic methods. The purpose of NDE was to define and classify anomalies or discontinuities in terms of size, shape, type and location. Furthermore, the possibilities and limitations of the NDT methods are presented through a comparative study. Various pulse echo and the through-transmission techniques based on ultrasonic have been performed in single lap joints in cooperation with industrial manufacturers of respective testing devices and manufacturers of adhesives. The problem how to inspect the bonded assemblies was addressed, measurement discrepancies are identified and the most suitable ultrasonic technique is selected. Artificial imperfections are introduced as reference values. The most suitable ultrasonic technique based on the amplitude measurement of the reflector is compared to the neutron radiography measurements. C-scans are compared to transmission images and the defect area is estimated with image analysis software. Neutron radiography is used for verification and reference purposes rather, as ultrasonic techniques possess distinctive advantages for applications in practice. Generally, both methods detect the same types of defects, but C-scans show significantly poorer resolution especially at smallest defects and an inability to distinguish signals at joint edges.

The high effectiveness of neutrons allows experimental investigations with neutron radiography and tomography on real components from automotive industry. Therefore the verification of the adhesively bonded area is succeeded and the applicability of the method is demonstrated through complicated structural parts. Image processing illustrates the reliability on detecting manufacturing defects. Moreover the reproducibility of the results on the testing performed on small specimens is proved to be valuable pinpointing the recognition and the evaluation of defects in the real components.

The structural response of defect free and defect adhesive joints under short term loading is presented and joint strength values were compared to NDT measurements aiming at a correlation between defect type/size and actual service behaviour. Furthermore an analysis of the

bonded joints is presented and the effect of defects and bondline thickness on ultimate stress is discussed. Attention is given towards imperfections, their consideration in theoretical stress analyses of Volkersen and Goland-Reissner and the estimation of a correction factor due to manufacturing defects. A proposal for design and quality control evaluation is given through an attempt to define quality classes and acceptance/rejection criteria.

The detectability of the imperfections depends on the adhesive-adherend system, on the inserted imperfection and on the non-destructive method used. The two NDE methods of neutron radiography and ultrasonic can detect various types of flaws occurring in adhesive joints and may give a measure of the performance of the structure. In general neutron radiography is rather reliable tool – the distribution of organic materials or imperfections can be detected – but has limitations in its applicability as it needs powerful neutron sources. The evaluation of critical structural parts or components in the development stage maybe justified. On the other hand ultrasonic testing, enhanced by ongoing further developments in instrument technology, can also lead to reproducible test results within narrow tolerances. According to the observation of the C-scans the imperfections appear larger than on the transmission images due to the geometry of the beam. Furthermore for a large number of small size contaminations ultrasonic gives a somewhat confusing image showing no exact shape of the contaminations. These investigations aim as a contribution to new international codes, either in verifying and supporting the initial assumptions of design values or providing a basis for decisions and classification in respect to execution and quality assurance of adhesive joints.

Zusammenfassung

Im Zuge der Entwicklung von neuen Materialien und Konstruktionen werden zerstörungsfreie Prüfverfahren zur Evaluierung dieser bzw. der Konstruktionsintegrität eingesetzt. Das Interesse an der Klebtechnik im Maschinenbau, Transport- und Bauwesen ist gegeben, da bedeutende Vorteile gegenüber konventionellen Verfahren, wie dem Schweißen und mechanischen Fügen aufgezeigt werden können. Beispielhaft werden erwähnt die gleichmäßige Spannungsverteilung, die verbesserten Ermüdungseigenschaften, leichtere Bauteile und das problemlose Fügen unterschiedlicher Werkstoffe.

Die Klebschichtintegrität stellt jedoch eine bedeutende "Achilles-Ferse" bei der breiten Anwendung des Klebens im konstruktiven Ingenieurbau dar. Die Gestaltung und Herstellung von Klebverbindungen wurden ständig optimiert und die Verbindungsqualität gesteigert. Trotzdem können Fehlstellen in Klebungen, z. B. aufgrund ungeeigneter Vorbehandlungsverfahren oder Fertigungsfehlern, nicht immer ausgeschlossen werden. Dieser Zustand erfordert zuverlässige Qualitäts- und Fertigungskontrollen. Von Seiten der Industrie werden deshalb verstärkt automatisierte und zuverlässige - wichtige Voraussetzungen für den Einsatz in der Praxis - zerstörungsfreie Prüfverfahren (ZfP) gefordert. In der vorliegenden Arbeit wird ein Ansatz zur Aussagequalität von ZfP und deren Einsatzfähigkeit beschrieben. Zur Beurteilung der Zuverlässigkeit der zerstörungsfreien Evaluierung werden verschiedene Parameter von Klebverbindungen berücksichtigt.

Ziel dieser Dissertation ist das Zuverlässigkeitsniveau der Neutronenradiographie und Ultraschallmethode zur Erkennung von fertigungsrelevanten Fehlstellen (insbesondere wegen mangelnder Kohäsion und Unregelmäßigkeiten) festzustellen. Deren Bestimmung und quantitative Erfassung sind signifikante Voraussetzungen bei der Berechnung und Einsatz der Verbindungen im konstruktiven Ingenieurbau. Dabei wird systematisch vorgegangen ausgehend von dem aktuellen Stand des Wissens über das Verhalten von strukturellen Klebverbindungen und die Etablierung von Qualitätssicherungsmethoden, durch Untersuchungen an kleinen Proben und realen Bauteilen. Die Material- und Prüfparameter wurden hinsichtlich ihrer industriellen Anwendbarkeit bevorzugt aus dem Bereich der Automobilindustrie gewählt.

Nach einer Beschreibung der betrachteten zerstörungsfreien Prüfverfahren, Neutronenradiographie und Ultraschalltechniken, werden Methoden der Evaluierung vorgestellt. Der Zweck ist Fehlstellen in Bezug auf Art, Größe, Form, und Lage in der tragenden Klebschicht zu bestimmen und zu klassifizieren. Darüber hinaus werden die Möglichkeiten und Einschränkungen der Prüfmethoden durch eine Vergleichsstudie dargestellt. Variierte Impuls-Echo-Techniken und die Durchschallungstechnik, im Fall der Ultraschalluntersuchung, wurden an einfach überlappte Verbindungen nach Angaben der Hersteller entsprechender Prüfgeräte und Klebstoffe durchgeführt. Die Problematik, welche Inspektionstechnik für die betrachteten Klebverbindungen angewendet werden soll wurde besprochen. Messungsdiskrepanzen wurden aufgezeichnet und das bestgeeignete Ultraschallverfahren festgestellt. Künstliche Imperfektionen wurden als Referenzwerte eingeführt. Die zuverlässigste Ultraschalltechnik, basierend auf der Amplitudenmessung des Reflektors, wurde mit Messungen aus der Neutronenradiographie verglichen. C-Scans wurden mit Transmissionsbildern verglichen und die Fehlstellen mit einem Bildbearbeitungsprogramm ausgewertet. Die Neutronenradiographie wird vorzugsweise als Referenzmethode für die Verifizierung der Ergebnisse verwendet. Die Ultraschallmethode weist signifikante, auch wirtschaftliche, Vorteile für Anwendungen in der Praxis auf. Im Allgemeinen können mit beiden Methoden die gleichen Arten von Fehlstellen entdeck werden. C-Scans beim Ultraschall haben eine niedrigere Auflösung und zeigen Schwierigkeiten bei der zuverlässigen Bestimmung der Fehlstellen, besonders bei kleinen Fehlstellen und Signalen an den Kanten.

Die hohe Wirksamkeit von Neutronen erlaubt Untersuchungen mit der Neutronen-Radiographie bzw. -Tomographie an realen Bauteilen oder Fahrzeugteilen. Besonders gut können geklebte

Überlappungen verifiziert werden. Die Anwendbarkeit der Methode wird auch an komplizierten Bauteilen demonstriert. Die Bildbearbeitung erlaubt die zuverlässige Wiedergabe fertigungsrelevanter Fehlstellen. Versuchsergebnisse an Kleinproben sind wertvoll und auf reale Bauteile reproduzierbar, und dienen zu deren Unterscheidung und Bewertung.

Das strukturelle Verhalten von fehlerfreien bzw. fehlerhaften Klebverbindungen unter quasi-statischer Belastung wird vorgestellt und die aus zerstörenden Prüfungen gewonnenen Werte der Tragfähigkeit werden den ZfP-Messungen gegenüber gestellt. Sie erlauben eine Korrelation zwischen Fehlerart bzw. -größe und Betriebsverhalten abzuleiten. Der Einfluss vorhandener Imperfektionen und der Klebschichtdicke auf die Tragfähigkeit werden diskutiert. Fehlstellen werden bei der theoretischen Spannungsverteilung nach den Vorschlägen von Volkersen und Goland-Reissner betrachtet und ein Korrekturfaktor zur Berücksichtigung fertigungsrelevanter Fehlstellen abgeschätzt. Es wird auch ein Vorschlag über Bewertungsgruppen und entsprechender Fehlstellen-Toleranzwerte zur Qualitätsklassifizierung der Klebverbindungen gemacht.

Die Feststellbarkeit von Fehlstellen hängt vom Klebstoff-Fügeteil-System, der eingebrachten Imperfektion und der verwendeten zerstörungsfreien Methode ab. Beide ZfP-Methoden, Neutronenradiographie und Ultraschall, können verschiedene Arten von Imperfektionen feststellen und Informationen über das spätere Konstruktionsverhalten liefern. I.a. ist die Neutronenradiographie ein zuverlässiges Werkzeug, vor allem zur Abbildung von organischen Werkstoffen, jedoch gibt es Einschränkungen bei der Anwendbarkeit, weil leistungsstarke Neutronenquellen benötigt werden. Bei der Untersuchung von kritischen Konstruktionsteilen in der Entwicklungsphase kann die Methode aber mit Erfolg eingesetzt werden. Andererseits vermag die Ultraschallmethode, vor allem wenn die Instrumententechnik weiter entwickelt wird, gut reproduzierbare Messergebnisse innerhalb enger Toleranzen zu liefern. Aufgrund der geometrischen Gestaltung des Prüfkopfes erscheinen die Fehlstellen auf den C-Scans größer als auf den entsprechenden Transmissionsbildern der Neutronenradiographie. Darüber hinaus kann das Ultraschallbild bei einer Ansammlung von mehreren kleinen Fehlstellen ein verwirrendes Bild liefern, ohne eine genaue Form der Fehlstellen erkennen zu lassen.

Die Forschungsergebnisse können auch als Beitrag zur Integration der Klebtechnik in neue internationale Normen, insbesondere zur Ergänzung von Berechnungsvorschlägen und Erweiterung der Datenbasis bei Metallklebverbindungen, sowie zur Qualitätsklassifizierung der Klebverbindungen verstanden werden.

List of Symbols

A	cross section area	mm^2
D	collimator diameter	mm
E	Young`s modulus	N/mm^2
E_n	neutron energy	meV
F	load	N
G	shear modulus	N/mm^2
I	transmitted neutron beam	
I_0	incident neutron beam	
L	collimator length	mm
M	bending moment	N*m
N	number density	cm^{-3}
N_A	Avogadro number	mol^{-1}
aw	atomic weight	$g*mol^{-1}$
d	bondline thickness	mm
h	Planck constant	-
k	bending moment factor	-
m	neutron mass	kg
υ	velocity	m/s
s	Standard deviation	
t	time	s
w	overlap width	mm
$\bar{x}$	mean value	
γ	elastic shear strain	mm
λ	wave length	Å
ν	Poisson's ratio	
ϱ	material density	$g*cm^{-3}$
τ	shear stress	N/mm^2

Contents

1 Introduction 1
2 Structural Adhesive Bonding Technology 3
2.1 Applications in engineering 3
2.2 Structural behaviour of adhesive bonded joints 4
2.2.1 Failure modes 4
2.2.2 Cohesion 5
2.2.3 Adhesion 6
2.2.4 Structural adhesives and surface pretreatment 7
2.2.5 Mechanical behaviour of adhesive joints 8
2.3 Production Process 9
2.3.1 Structural Design 9
2.3.2 Selection of Adhesive 10
2.3.3 Application of the adhesive 11
2.3.4 Quality control and assurance in adhesive joints 11
3 Testing and Quality Assurance 13
3.1 Measures of Quality Assurance 13
3.2 Destructive methods 13
3.3 Nondestructive methods 14
3.3.1 Quality assurance prior to bonding (pre-process) 14
3.3.2 Quality assurance during bonding (in-process) 15
3.3.3 Quality assurance after bonding (post-process) 15
3.4 Description of defects 18
3.4.1 Manufacturing defects 18
3.4.2 In-service defects 19
4 Specimens for the experimental investigations 21
4.1 Materials of the adhesive bonded systems 21
4.2 Manufacturing of specimens 22
4.3 Classification of defects during manufacturing 22
4.4 Selection of testing parameters 24
5 Neutron Radiography Measurements 27
5.1 Brief history and current developments 27
5.2 Application range 28
5.3 Application requirements 28
5.4 Components of the thermal radiography facility NEUTRA 29
5.5 Detector systems 30
5.6 Experimental set-up 30
5.6.1 Neutron digital imaging 31
5.6.2 Measurement data 32
5.7 Evaluation methodology 34
5.7.1 Digital image processing 34
5.7.2 Qualitative evaluation of ideal joints 34
5.7.3 Qualitative evaluation of defect joints 39
5.7.4 Quantitative estimations of the bondline thickness 42
5.7.5 Bitmap analysis 44
5.7.6 Quantitative estimations of the defect area 44
5.8 Concluding remarks on imperfections 50
5.8.1 Oil contamination 50
5.8.2 Teflon layers 51
5.8.3 90% relative humidity 51
6 Ultrasonic Measurements 53

6.1 Application range 53
6.2 Developments in Ultrasonic Evaluation 53
6.3 Ultrasonic physics 55
6.4 Flaw display methods 56
6.5 Pulse-echo technique 57
6.5.1 Amplitude measurement of the reflector `s echo 58
6.5.2 Amplitude measurement of the backwall echo 58
6.5.3 Amplitude measurement of the intermediate echo 58
6.6 Through-transmission technique 58
6.7 Assessment of the conventional techniques 59
6.8 Experimental set up of selected pulse echo technique 61
6.9 Evaluation methodology 61
6.9.1 Qualitative observations on the C-scans 61
6.9.2 Quantitative estimations of the defect area 64
6.10 Concluding Remarks on the two NDT methods 69
7 NDT in Full Scale Components 70
7.1 Inspections with neutron radiography 70
7.1.1 Automobile doors 70
7.1.2 Back-seat-bank 73
7.2 Inspection with neutron tomography 75
7.2.1 Bonded steel profile 75
7.2.2 Double hat profile 76
7.2.3 Hood 78
7.3 Potential of neutrons in structural application 80
8 Destructive Testing 81
8.1 A fundamental stress analysis for bonded metal structures 81
8.2 The role of destructive tests for adhesive joint strength 81
8.3 Correlation of defect area and ultimate strength 82
8.4 Chemistry and Properties of the adhesives 89
8.4.1 Teflon layers 90
8.4.2 90% pre-bond relative humidity exposure 92
8.4.3 Oil contamination on the metal sheets 94
8.5 Correlation of defects to the shear performance 95
8.6 Concluding remarks 96
9 Proposal of design and quality control evaluation 97
9.1 Considerations with the net overlap area 97
9.1.1 Results based on Volkersen and the reduced overlap length 98
9.1.2 Results based on Goland-Reissner and the reduced overlap length .99
9.1.3 Comparison of the theories 99
9.2 Considerations with the gross overlap area 102
9.3 Safety and reliability concept of design and execution 103
9.4 Quality Management 104
9.4.1 Quality Zoning Diagram and Criticality grades 104
9.4.2 Quality requirements 105
10 Conclusions and future research proposals 109

1 Introduction

Since the development of high strength structural adhesives, adhesive technology has earned interest in major fields of industrial applications. This joining method offers several advantages over more conventional methods; new materials can be combined avoiding negative effects on strength. Selection of the adhesive, surface pretreatment, manufacturing process, design concepts and quality control remain still important factors for the joint integrity.

For structural applications of adhesive bonded joints, present practice is confronted with the absence of reliable and online testing methods. A current traditional approach to evaluate the integrity of an adhesive joint for a particular application is through destructive testing of a representative sample. Several arguments are responsible and given below.

The introduction of non destructive testing comprises high fixed and maintenance costs. It also involves laboratory tests in order to produce calibration measures. The inspection procedure is expensive and requires skilled personnel. It is in fact difficult to bond test pieces without any defects or with defined defects. Various techniques have been introduced to detect irregularities in adhesively bonded joints but most of them can not ensure a high quality bond when it comes to adhesion weakness and provide a direct quantitative correlation to strength.

The limited implementation of structural adhesive bonding in new codes remains an obstacle to further innovative applications. Mutually the durability problem of adhesive joints in all industrial sectors has not yet activated standard drafting bodies to develop significantly reliable design rules for wide range of bonded systems and allow only design by testing. Thus, further efforts cannot easily concentrate on the development of new testing methods and respective standards to execution and quality control.

Another reason for the limited use of non destructive testing has a historical background. From the fifties until now developments in techniques and procedures have been accomplished in the aerospace industry only through extensive test programmes with high requirements. Any other way to proceed would have caused higher costs. Thus, this strategy has hindered innovative solution through accelerated methods. In automotive industry adhesive bonding has been introduced in the eighties. Compared to aerospace applications, design, execution and quality control processes had to be simpler and cheaper. This initiated the development of new adhesive bonded systems offering enhanced structural behaviour. The high costs of destructive testing can be afforded easily, due to the large production scale. In both automotive and aerospace industries a driving force is missing to develop automated reliable techniques for testing.

In other industrial sectors like shipbuilding, railway, mechanical and civil engineering new methods of testing quality have to be developed within inexpensive und not time consuming test programmes. The only alternative is to interdisciplinary transfer experience and data from the automotive and aerospace industry and their reliable integration to broadening industrial sectors.

Nevertheless the introduction of new materials and innovative design solutions in bonding technology demand validation through non extensive testing programmes. Mainly due to irregularities in the joints an engineering judgment and evaluation can determine if adequate strength exists or the parts need to be repaired or scrapped. When large and costly assemblies have been bonded, the importance of reliable non destructive inspections is fully appreciated.

The objective of the study presented in this thesis is a systematic approach to quality control and assurance for structural adhesive joints. To illustrate the potential of this approach the study focuses on the experimental investigations with Non Destructive Testing (NDT) and comprises the testing principle methodology. Neutron radiography and ultrasonic method are used for the inspection of bonded joints, both with some drawbacks and limitations. No single procedure can find all flaws, thus the availability and limitations are important. The approach may be used for all structural adhesive joints under various geometrical, manufacturing and loading parameters. The

defects considered are manufacturing defects and the testing methods are intended to the quality assurance of final product, i.e. structural adhesively bonded joint. This thesis provides also details on the interpretation of NDT measurements and a methodology is proposed for the qualitative and quantitative evaluation of defects and reference measures for future investigations are given.

The presented approach is based on the behaviour of structural adhesive joints and quality assurance methods established through experimental investigations on small specimens under various parameters and full scale components. To introduce both subjects various fields covered by structural adhesive bonding technology are discussed in chapter 2 and a state of the art on methods to quality assurance are presented in chapter 3. The materials selection and specimen configurations are very important issues for the performance evaluation of Non Destructive Inspection (NDI), - i.e. inspection met by established specification or procedure -. Therefore, in chapter 4 such parameters for the experimental investigations are introduced and the significance of suitable artificial imperfections is discussed. In Chapters 5 and 6 the NDT procedure is described and proposals to Non Destructive Evaluation (NDE) are given both with neutron radiography and ultrasonic methods. The purpose of NDE was to define and classify anomalies or discontinuities in terms of size, shape type and location. The possibilities and limitations of the NDT procedure are presented through a comparative study. The high effectiveness of neutrons allows experimental investigations with neutron radiography and tomography on real components from the field of the automotive industry. In chapter 7 image processing illustrates the reliability on detecting manufacturing defects. The structural response of defect free and defective adhesive joints under short term loading is presented in chapter 8. Finally, attention is given towards imperfections, their consideration in a theoretical stress analysis and the estimation of a correction factor. Furthermore quality classes and acceptance/rejection criteria are proposed in chapter 9, followed by suggestions for future research activities given in chapter 10.

2 Structural Adhesive Bonding Technology

The use of adhesives in industry generally continues to develop at a rapid pace and this is particularly the case for structural adhesives. As might be expected, developments in the properties of structural adhesives and the necessity to reduce costs in joining structural parts have led and supported the spread of these materials from the high technology aerospace industries into further fields of general engineering applications. This tendency reflects on a larger group of engineers with the need of a better understanding of the adhesive bonding technology and its multidisciplinary, i.e. chemical, physical and engineering aspects. In this chapter those aspects are highlighted.

2.1 Applications in engineering

The principle of the adhesion has been of vital importance both in nature and in the evolution of the mankind. In nature there is for instance the barnacle that affixes onto hulls of ships with the help of a protein adhesive hardened in the water, the sundew producing adhesive drops helping to catch food or the termites, that manufacture with their sticky saliva, a material out of earth, wood and chewed plants for the up to 7 m high termite towers [Gruber 2000].

One of the first well known examples of the bonding technology use is the Greek legend of Daedalus who constructed for his son Icarus a pair of wings made of birds' feathers bonded with wax. The flight became a disaster, as Icarus ignored his father's warning not to fly close to the sun. The use of adhesives based on tree resins and animals' substances goes back to the Stone Age and was applied by the Egyptians, the Romans and the Chinese to manufacture tools, weapons and wood furniture [Schindel 1988].

During industrialisation in the 19th century the performances of these plants and animals adhesives were modified synthetically and the first steps were made to develop new types of adhesives used initially in the paper and wrapping field and later on in the wood and leather workmanship for the manufacturing of furniture and shoes.

The actual era of structural bonding began with the development of reaction adhesives such as phenolic resins since 1920, polyurethanes, acrylates and epoxies since 1940 and has been applied successfully within many industrial sectors, [HBK 2001]. The aerospace industry has the longest tradition; almost every modern aeroplane contains adhesive bonded joints [Albericci 1983]. The automotive industry makes frequently use of its advantages. By bonding the front and back windows the stiffness of the car frame can be improved significantly [Lawley 1987]. Other industry branches like shipbuilding, microelectronics, mechanical and civil engineering have recognised the advantages of adhesive bonded joints for structural use [Kosteas 1969], [Brockmann 1971], [Steinhardt 1972], [Lees 1987], [Mays 1992], [Sauer 2003], [Lohse 2003].

An adhesive may be defined as a material, which when applied to surfaces of materials can join them together and resist separation. Adhesive is the general term and includes cement, glue, paste etc. The term adhesion is used when referring to the attraction between the substances. The materials being joined are commonly referred to as the substrates or the adherends, and the latter term is particularly used when the materials are part of a joint. There is no universally accepted definition of a *structural adhesive* but according to [Kinloch 1990] it is considered to be based upon monomer composition which polymerise to give high-modulus, high-strength adhesives between relatively rigid adherends, so that a load bearing joint is constructed. As a means of joining materials the use of adhesive offers many advantages when compared to other, more conventional methods such as mechanical fastening, welding or soldering. The advantages include:

- ability to bond dissimilar adherends;

- ability to join thin sheet material efficiently;
- design flexibility offering the possibility to produce complex joint configurations;
- the fact that the properties of the adherends as material are not affected;
- ability to increase the dynamic damping
- improved stress distribution in the joint imparting increased fatigue resistance;
- ability to avoid galvanic corrosion between dissimilar adherends;
- good sealing properties of the adhesive layer against gases, moisture or chemicals;
- good insulating properties of the adhesive layer against electricity, heat or sound;
- ability for automatic production sequence.

There are also disadvantages that should be taken into account:

- complicated manufacturing process with skills in surface preparation, preparation of the adhesives, control of processing temperature, pressure and humidity conditions, and use of equipment;
- curing time during which the bonded adherends have to be fixed;
- significant influence of environmental actions on durability;
- the fact that the properties of adhesive are affected by temperature;
- the fact that the properties of the adhesives are time dependent;
- possible toxicity and its effects on the environment and labour conditions;
- difficulty to apply non destructive testing to the on-line control;
- difficulty to dismantle the joint for repair or re-use of the materials.

The performance capability of bonded structures depends on basic requirements like sufficient adhesion on the adherend and cohesion strength to be accomplished during the production process. The production process includes:

- structural design of the joint;
- selection of an adhesive bonding system;
- surface pretreatment and application of the adhesive;
- use of a quality control and assurance system.

For a successful production process of a bonded construction it is necessary to understand the background of its structural behaviour, durability, and the wide variety of multidisciplinary aspects related to the above mentioned four issues.

2.2 Structural behaviour of adhesive bonded joints

2.2.1 Failure modes

In choosing an adhesive bonded joint, a variety of alternative solutions can be applied. In structural terms a distinction can be made between adhesive bonded joints globally loaded in shear, tension or peel, as indicated in Fig. 2.1. A design solution loaded in shear is preferred, while solutions loaded in tension or peel should be avoided as much as possible. This is because

for tension and peel the stress state in the vicinity of the bondline is dominated by high tensile stresses perpendicular to the bondline, which are difficult to sustain. The magnitude of these stresses is much lower for a joint primarily loaded in shear.

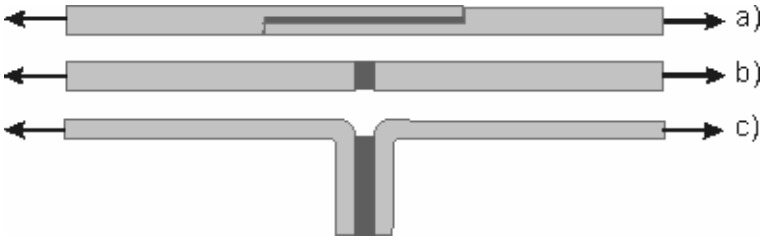

Fig. 2.1: Adhesive bonded joints globally loaded in a) shear b) tension and c) peel

Adhesive joints are composite systems whose strength depends on both the geometrical design and loading type as well as on the individual strengths of the components to be joined, the adhesive and the interlayer, Fig. 2.2. Interface between adhesive and substrate is the contact area with each other. As in every composite system consisting of different members, the overall strength is limited by the weakest member.

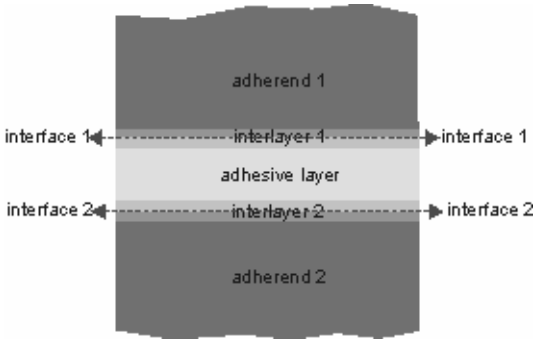

Fig. 2.2: Structure of an adhesive joint

For the performance of the adhesive bonded joint, apart from the manufacturing effects, various mechanical and environmental actions have to be taken into account. These are most of the times responsible for the failure of the joint. Actual failure occurs in one of the following locations, see Fig. 2.3:

- Adhesion failure at the interface between the bondline and the adherend. It is possible that failure is caused by an interlayer between the adherend and the adhesive occurs, for example a coating.
- Cohesion failure in the bondline. It might be expected that the failure initiates at a location with the highest stress state.
- Both cohesive and adhesive failure. This is also known by the term mixed failure.
- In one of the adherends.

Fig. 2.3: Failure of an adhesive bonded joint

2.2.2 Cohesion

Cohesion is the strength of the adhesive itself. This is a result of physical and/or chemical attractive forces between the atoms or molecules of adhesives. Since adhesives are mostly

synthetic and organic, their cohesive behaviour can be explained from the polymer technology knowledge.

Polymers are macromolecules synthesized by a reaction of simple molecules, known as monomers. The polymer technology distinguishes four different molecular structures of polymers responsible for the physical, chemical, mechanical properties of the adhesives. These are: linear, branched, crosslinked, and network structures [Habenicht 1998]. Linear polymers are based on flexible chains of macromolecules, weakly connected by physical bonds. Branched polymers are macromolecules connected with side chains, also connected by physical bonds. Cross linked polymers are connections of side chains with stronger chemical bonds. Finally the network polymer structure is based on complicated and strong chemical bonds forming a net of molecules. Adhesives belong to all four molecular structure types and especially structural adhesives belong to cross linked and network polymers.

A classification based on the properties accompanying the molecular structure proposed three types of polymers: elastomer, duromer and thermoplastic [Habenicht 1998]. An elastomer is based on a polymer with a low degree of crosslinking, is capable to stretch to a high extension and recovers without permanent deformations. A duromer is based on a polymer with a high degree of crosslinking forming a complete network polymer. This results in high strength and more rigid behaviour than of an elastomer, but both types are amorphous above a certain temperature. Therefore a distinction between adhesives based on elastomer or duromer type cannot be made easily. A thermoplastic is based on linear or branched polymers. In melting point the molecular chains become very flexible and reform continuously a new structure resulting to either an amorphous or a semi-crystalline condition.

The properties of any commercial adhesive are greatly influenced not only by the chemical type of adhesive but also by the additives typically introduced by the formulator. They often play a crucial role in influencing such factors as the rate of hardening and viscosity characteristics of the adhesive and the mechanical performance of the adhesive joint. The most important additives responsible for the structural behaviour of the adhesives are the filler, plasticizer and stabilizer. A filler interacts with the monomers and improves properties like strength, toughness, thermal insulation or conductivity. A plasticizer influences the flexibility, ductility, and toughness by increasing the distances between the polymer chains. Finally a stabilizer avoids the deterioration of the polymer due to environmental actions as ultraviolet radiation and oxidation.

2.2.3 Adhesion

Adhesive failure is located within the interface between the adhesive layer and the adherend. Design engineers try to avoid this failure type, but due to manufacturing defects or ageing of the joint, adhesive failure might become dominant.

Adhesion is defined as the interaction force acting between adhesive and substrate interface. The attainment of such interfacial contact is a necessary first stage in the formation of strong and stable adhesive joints. The next stage is the generation of intrinsic adhesion forces across the interface. They must be sufficient strong and stable both after manufacturing and subsequent service life. The various types of forces operating between the adhesive or primer and the substrate interface are commonly referred to as the *mechanisms of adhesion* and they are discussed by [Habenicht 1998] and [Kinloch 1983]. One of these mechanisms is principally based on the adsorption theory proposing bonds responsible for the interaction between atoms or molecules of the adhesive and the adherend. A distinction is made between physical and chemical bonds. Weaker physical bonds based on van der Waals, dipole, induction, or dispersion forces and hydrogen bonds are formed by an electrostatic attraction between chemical neutral molecules. The stronger chemical bonds, based on ionic, covalent and metallic bonds require reactive chemical groups that tightly bond on the adherend surface and in the adhesive. Other theories try

to give a more advanced description of the adhesion phenomena. For example the mechanical interlocking theory proposes the mechanical keying of the adhesive into the irregularities of the substrate surface. An additional theory mentioned also in the literature is the diffusion theory proposing a mutual diffusion of polymer molecules across the interface. Finally the electronic theory states an electron transfer due to different electronic band structures between the adhesive and adherend resulting in the formation of double layer of electrical charge at the interface.

Taking under consideration to avoid adhesive failure in design, less is known about the actual physical, chemical and mechanical behaviour of the interlayer. The interlayer knowledge is important for both fundamental and practical aspects. Indeed its properties determine the final over all properties of composite systems and depend on both substrate and adhesive natures. These findings are confirmed in observations by [Roche 2001]. Also, mechanisms of interphase formation indicate residual stresses as a result of structural rearrangement within the interaction of molecules in adhesive and adherend.

2.2.4 Structural adhesives and surface pretreatment

Adhesives used for structural applications are normally two-part, room temperature-cured or one-part, heat-cured. Heat-curing can generally be used for the two-part adhesives too to reduce cure time. The most widely used types are the epoxies, acrylics, polyurethanes and various aspects of these materials have to be considered in relation with the application intended. They do not only have favourable strength properties but also toughness and enhanced environmental resistance although they might need intensive surface treatment.

Epoxies are available in many formulations and can be used to bond a wide variety of materials [Garnish 1986]. The maximum load capacity of a joint in tension-shear strength of 40 MPa can be reached especially with the heat-cured epoxies at 180 °C but they are rather brittle. Through addition of rubbers, typically 5-15%, enhanced peel and impact strength and significant toughness even in thicker bondlines are obtained. The two-component epoxies cure at room temperature by additional hardener and show satisfying temperature resistance between -10 and 100 °C.

Polyurethanes are available as one- and two-component types in a wide variety of formulations. Curing of one-component system is accomplished by reaction with moisture. To reach improved mechanical properties and avoid porosity the cure process is executed under pressure with special fixturing. The two-component system cures by additional hardener; the strength is higher, the toughness and durability are excellent, even with a simple surface preparation, for example in liquid gas tankers where the temperature reaches -150 °C. Typical industrial applications for polyurethanes are mostly sandwich elements of vehicles, facades, containers, ships etc.

Acrylics are also available in various formulations although the modified acrylics are commercially very successful because of the particular benefits they offer [Martin 1986]. Strong bonds with improved adhesion and toughness can be formed rapidly under conditions well suited to industrial assembly operations. The two-component system is mostly used without mixing required; the two components are applied each on separate adherends, which are then joined together. A moderate surface treatment is necessary to provide improved durability. Overview of available formulations, the advantages and limitations of these adhesives is discussed in many handbooks, see for example [Habenicht 2001], [Gruber 2000], [DeFrayne 1983], [HBK 2001].

In common engineering practice, oxides forming on most of metal surfaces are not coherent. However the behaviour of the interlayer, between the bondline and the adherend can be positively affected by applying various treatments optimising the surface properties. The purpose of surface preparation is to remove gross contaminations, to etch away the existing oxide and to replace it with a thinner, harder and completely coherent oxide layer, called primer. The most common preparation techniques before the application of primer and/or adhesive for metal

substrates are mechanical or chemical cleaning. Chemical cleaning is widely used but often criticised for ecological and economical reasons. In order to obtain improved performance of adhesive metal bonds sophisticated and sometimes toxic pretreatments are used. Their replacement by mechanical pretreatment is of great technical interest as it is ecologically less critical. The influence of surface pretreatments on the performance of a joint and in particular on stress-strain relationships and durability is discussed by [Bockenheimer 2002], [Botter 2001] and [Price 1991]. A coating of primer immediately after cleaning serves to protect the surface until the bonding operation is carried out, it increases the wettability. Further the primer may be a coupling agent forming chemical bonds with the adherend and the adhesive or it may serve to block the pores of a porous surface and keep the adhesive within the bondline. Finally the adsorption of a primer to the substrate may be not only physical resulting to a conversion by modifying the texture of the surface. More detailed information regarding available surface preparations and their effect on joint performance are given in [Scheberger 1983], [Adams 1984], [Kinloch 1990], [Clearfield 1991], [Habenicht 2001].

2.2.5 Mechanical behaviour of adhesive joints

Among the most important properties of polymers is the glass transition temperature (T_g). This is the temperature beyond which the adhesive changes its behaviour; from an amorphous solid to a rubbery solid with completely different properties and at higher temperatures it becomes a viscous liquid. For various adhesives the glass transition temperature can be in the temperature range of practical applications, which means that the adhesive properties change significantly.

To analyse the stresses in adhesive joints requires knowledge of the basic engineering properties of the adhesive. Typically the main properties required are the tensile, or Young' s modulus, the shear modulus, the yield stresses, the fracture stresses and strains in uniaxial tension and in pure shear.

The stress-strain behaviour of adhesives is fairly complex [Gay 2000]. For low stresses the polymer's bonds are stretched and energy is stored in a quite reversible manner. This means that the stress strain behaviour shows a linear relation, which can be described by the modulus of elasticity. An additional phenomenon is the lateral strain, which can be described by the Poisson ratio. For higher stresses the stress strain behaviour is no longer linear. A part of the energy is dissipated in a viscous manner and the stress strain behaviour is not reversible. In literature this onset of yielding is described by various theories. A group of theories considers a pressure dependent yield criterion, which takes into account that for polymers the compressive yield stress is usually higher than the tensile one [Gali 1981]. For high strains the polymer's bonds fail and fracture occurs.

Under long term loads polymers normally show a kind of visco-elastic behaviour. It is a mixture of the mechanical behaviour of viscous liquids for which the stress is proportional to the strain rate and the mechanical behaviour of an elastic solid. The response depends upon the rate or time period of loading and temperature. Various theories are developed to describe the visco-elastic behaviour under different conditions, see for example [Hiel 1984].

The use of fracture mechanics to study the failure of joints is a complementary approach to that of mapping the nature and magnitude of the stresses. Both approaches have their advantages and disadvantages. Fracture mechanics has proved to be particularly useful for such aspects as characterising the toughness of adhesives, identifying mechanisms of failure and estimating the service life of "damaged" structures – the "damage" being in the form of cracks, air filled voids, debonds, etc. and having arisen from example from environmental attack, fatigue loading, subcritical impact loading. On the other hand, a detailed knowledge of the stress distribution in a bonded structure has proved to be of particular value in initial design studies and for interpreting the effects of geometric parameters.

Essentially, continuum fracture mechanics studies the strength of the structure which contains a crack [Barsom 1999]. Due to the applied load, stress and strain concentrations occur near the vicinity of the crack tip. For polymers this concentration is mostly described by a single parameter known as the strain energy release rate and provides a measure of energy required to extend a crack over unit area. Further the stress field around a sharp crack in a linear-elastic material can be defined by the stress intensity factor and fracture occurs when it exceeds some critical value. Through fracture mechanics an interrelation was established between measured fracture energy for the rupture of adhesion forces and the energy dissipated visco-elastically and plastically at the crack tip. Identifying such relationships has shown [Kinloch 1983], [Gillham 1986] and [Barton 1976] many of the observations concerning the effects of test rate, temperature and joint geometry upon the measured fracture energy or fracture toughness have been explained.

2.3 Production Process

2.3.1 Structural Design

The prediction of the structural behaviour is an essential aspect within the design process of adhesively bonded joints. The structural behaviour is influenced by the layered composition of the joint, its geometry, fabrication defects and degradation effects. For proper design knowledge about joint configurations and available methods to evaluate the mechanical performance is necessary.

There are several important aspects to be considered when designing adhesive joints. The modulus and the strength of the polymeric materials used as adhesives are far lower than those of metals. Thus, when employed to join such materials their main application is in bonding relatively thin sheets or panels. Also, the strain capability and toughness of adhesives are invariably higher when measured in compression or shear as opposed to tension cleavage or peel and this fact influences greatly the practical design of adhesive joints, Fig. 2.4. Therefore from the aspect of joint design the designer should not only attempt to keep the stress concentrations to a minimum but also attempt to distribute the imposed loads within the adhesive layer as a combination of compressive and shear stresses. Recommendations for preferable joint configurations in relation to the applied load are summarised by [Adams 1984], [Adams 1997], [Habenicht 1998] and [Kinloch 1990].

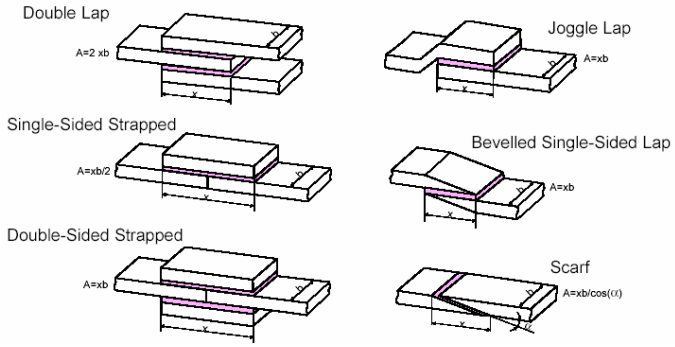

Fig. 2.4: overlap joint configurations used in practice

Theoretical methods through finite elements for measuring the basic properties of the adhesives and for analysing the stresses in the joints are reasonably well established and it is possible to make detailed calculations including physical and geometrical non-linear behaviour. Theoretical analyses are mostly used for optimisation purposes, while tests are mostly used to validate a final design. This approach does enable many aspects of the mechanical behaviour of adhesive joints to be readily understood and even predicted. In some aspects of joint design and the associated

topic of interpreting the effects of joint geometry the approach through continuum fracture mechanics can be according to [Kinloch 1983] the most valuable tool.

2.3.2 Selection of Adhesive

When designing bonded structures, one of the primary decisions to be made is the selection of the right adhesive. As there are no standard adhesives recognised for structural use, the designer needs to work with adhesives manufacturers on the selection of the specific adhesive and the appropriate surface preparation to be used. Selection of appropriate adhesives is based in practice on the required properties and the environmental conditions. However fabrication details may also dictate the adhesive type. For example some structures are too large for a heat cure to be practical, whereas for others it may not be reasonable to keep fixturing in place until a sufficient cure has been attained at room temperature. In his discussion of the various types of adhesives and their characteristics, [Minford 1993] indicates that better overall performance and environmental resistance can generally be attained with heat cure adhesives. The following section provides a guide for the potential adhesive user on how to make that choice and what to avoid by way of pitfalls during the selection process [Habenicht 2001], [Millard 1985], [Pechiney 1992].

The first factor to be evaluated is the basic type of the adhesive system to be used considering the cure temperature and the capability of the assembly to be bonded of withstanding that temperature during cure cycle. The second factor is the form of the structural adhesive i.e. films of precise thickness, liquid systems moderating to high-strength bonds and often ambient temperature curing, foam adhesives having the ability to expand and fill a gap during cure at elevated temperatures, bulk or hot-melts systems useful to be coated on skins or honeycomb core. The third factor to be considered is the cost. Adhesives vary widely in cost and although technical excellence is the ultimate concern when bonding structures, cost should not be left out of the selection process. Depending on the application, a less expensive adhesive can often perform as a high-cost material.

In primary structures there are additional factors to be considered like:

- temperature range; the estimated service temperatures must be evaluated over the entire life of the structure. This may require extensive long-term aging tests of the proposed adhesive systems before a final selection is made. These types of tests are expensive to conduct and very time consuming. However their importance to the total life of the structure cannot be overemphasised.

- environmental resistance; the environment the adhesive system is exposed apart from the already discussed temperature is very important when it comes to contaminants. Contaminants – fluids, lubricants, fuels, water in form of atmospheric moisture or normal liquid - likely to come in contact with the bonded assembly must be assessed and if found to be present at some time in the life of the structure, their effects on the adhesive must be evaluated.

- mechanical properties; the particular stresses the adhesive has to withstand in structural components is normally evaluated through mechanical tests carried out in static mode before and after specific test temperatures and/or hostile environments. In addition to these static tests, it is advisable to determine the resistance of bonded joints to fatigue loading.

- durability; a range of additional durability tests must be added to the static and fatigue tests by subjecting the adhesive to hostile environments and/or temperature while under continuous stress. The specimens are configured to evaluate the adhesive usually in shear

or cleavage in hot, wet and/or corrosive environments and a number of variation in test specimen design are available to be chosen from the engineer.

- scale-up transfer; to this point is paid the least attention when a large-scale laboratory evaluation with apparent success finds major practical problems by placing the system in production. Test assemblies simulating the complexities of typical production components should be designed with the most difficult features simulated, which would fully tax the ability of the selected adhesive to produce an acceptable bonded assembly.

2.3.3 Application of the adhesive

The manufacturing process also can have an essential effect on the strength of bonded joints. Performance is sensitive to variations in production and might have a significant influence on preventing major problems. For a proper design the engineer must have knowledge about available and implemented quality assurance systems to control the manufacturing process. The manufacturing process can be seen as a sequence of activities. The surface treatment of the adherends prior to joining is the first step in order to have an optimal adhesion force between adherent surface and adhesive layer. For this purpose, impurities i.e., dust, dirt, oil, grease, fat, water are usually removed. The next step is related to the actual bonding of the components. Aspects related to this step are the mixing of adhesive, the pot life representing the effective time for an adhesive after preparation that can be used to perform the actual bonding, the use of equipment, and the influence of temperature and humidity. Since adhesives have to be used quickly after preparation the method of manual mixing and application is obviously unsuitable and unreliable for line production. However, dispensing machines are available for this type of application, where bonding by robots is an advantage of automation in bonding technology. The curing of the adhesive follows. Although curing of the adhesive at room temperature is convenient, high-temperature curing is advantageous. In many cases the joint is fixed and pressure is applied especially for extensive bonded areas. Sometimes the curing process has to be activated by a higher processing temperature, humidity or ultraviolet radiation. After curing the joint is strong enough to be loaded. Detailed information and remarks about the manufacturing operation are given in [Habenicht 2001].

2.3.4 Quality control and assurance in adhesive joints

The development of the bonding production process and quality assurance system is not only related to the knowledge about adhesive bonding systems but also to the design and manufacturing. A quality assurance system might be very useful to ensure that all requirements are met during and after manufacturing. Aspects related to this, are the use of documentation, checklists and guidance through international standard i.e. ISO 9000 or ISO 9004. The education and training of personnel, the determination of safe handling precautions and control by destructive and nondestructive test are additional required steps for the quality assurance until the final product. Within the concept of the quality assurance belong the control of product arrival for the adhesives, control of requirements for their storage, control of the adherent surface treatment, control of dispensing and mixing equipment and finally control of the cure parameters.

The aspects of the quality control on the bonding process steps and the completed bonded product will be reviewed in the next chapter.

3 Testing and Quality Assurance

Widespread use of adhesively bonded structures has led to an urgent need for developing a reliable testing technology. The composite nature of these joints combined with the applications of new joint configurations has made the science and engineering of testing quite challenging and complex. In fact one of the major limitations in the use of adhesives as structural elements is associated with the difficulty encountered in making an accurate determination of bond quality or potential in-service performance. An important aspect of using adhesives is therefore the need to develop apart from destructive methods, nondestructive evaluation techniques that make use of simple measurements for predicting the potential level of structural bonding performance. In this chapter philosophies of testing are discussed and the criteria of quality assurance concept are considered.

3.1 Measures of Quality Assurance

The predominant strategy to quality assurance is based on destructive testing of the bonded joint with subsequent statistical evaluation. This procedure is combined with high costs and does not allow 100% controlling of the components or a repair of defects occurring during manufacturing. Testing itself or process mistakes during manufacturing (e.g. false applicator nozzle positioning) inevitably lead to product waste. Thus quality improvement is ensured by the joining method, the adjusted construction of the apparatus, recording and regulating relevant influence parameters during the task as well as nondestructive inspection of the joint directly after applying the adhesive or after curing. The concept of quality assurance in industrial process is described on Fig. 3.1.

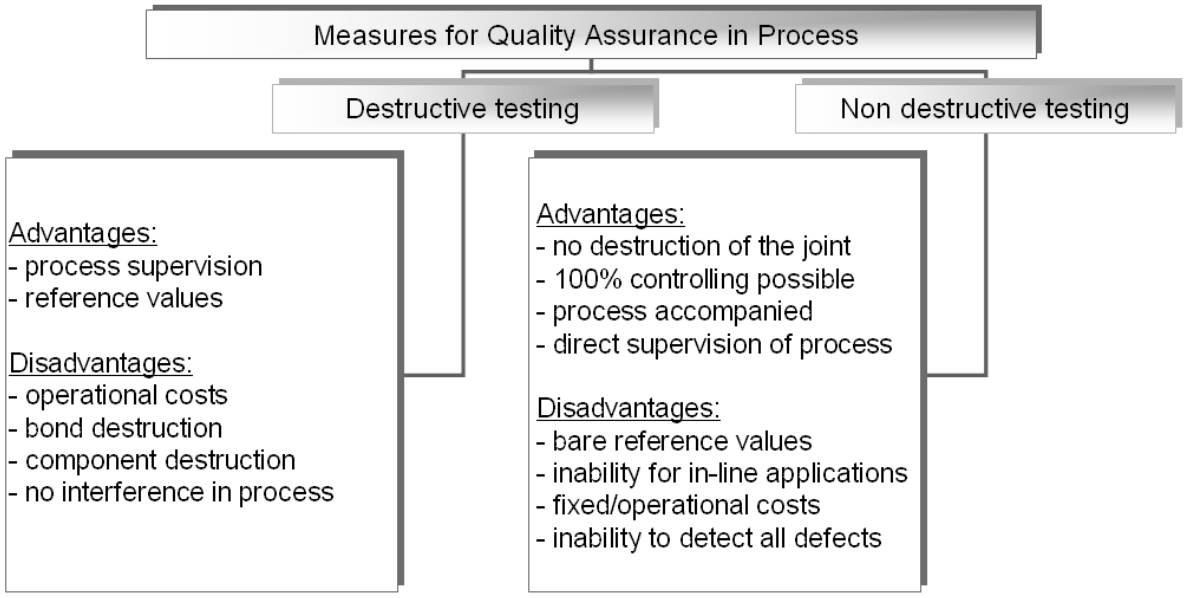

Fig. 3.1: Quality assurance concept in industrial process.

3.2 Destructive methods

An approach to evaluate the integrity of an adhesive joint for a particular application is to test destructively a representative sample of the joint. To reduce the cost of this approach, it is essential for the designer to call on reliable experience with joint design and manufacturing data before constructing a prototype. With complicated and expensive structures it is difficult to justify more than a very limited series of prototype tests before the beginning of the production. The limitation characterising of the destructive tests is that each one represents only a small

aspect of the total adhesively bonded assembly and loading. Commonly used test specimens are given by Habenicht [Habenicht 1998]. Probably the most common test used in adhesive evaluations is the lap shear test. The test specimen is inexpensive, easy to manufacture and the only test apparatus required is a machine with self-aligning grips. Sometimes tabs are bonded at the specimen ends to improve alignment. Even so, the lap shear construction being asymmetric causes a bending moment giving rise to large transverse peel stresses in the adhesive layer. The adhesive shear stress is non-uniform but concentrated at the edges of the bond, approximately being 60% higher than the average shear stress [Brockmann 1971]. Ultimately, if the concentrated forces exceed the yield strength of the adherend, it is clearly deformed and the force applied is no longer parallel to the bond plane. The bond then fails in a peel or cleavage mode beginning from the edge, where the load is most concentrated.

Another property measured by manufactures and users is the peel strength commonly by the T-peel test. Ideally, when the specimen is subjected to loading all the stresses are concentrated in a single line at the end of the bond where the failure is generated. According to work conducted by Adams and his group [Da Silva 2001], the joint strength increases with the rigidity of the joint. The stiffness of the adhesive and the adherends has significant effects on the results; the stiffer the adherend the higher the local stresses particularly in a direction across the adhesive thickness (cleavage). More special test specimens and procedures are available in [Hinopoulos 2001] and [Wirth 2004].

Adhesively bonded structures are often subjected to time-varying loads and it is therefore necessary to consider behaviour under impact, creep, and fatigue. By the impact strength measurement the energy absorbed of an adhesive bond between two blocks is determined through a test machine hammer, usually a swinging pendulum. The time-temperature behaviour of the joint is essential when it comes to creep of adhesives and there is a variety of tests assessing this [Adams 2004], [Kinloch 2004]. The fatigue properties of adhesives in shear by tension loading can provide even more useful and reliable data for estimating the durability of the joints. This procedure can be time consuming since weeks or months maybe required in testing specimens in desired conditions.

The real problem with the above mentioned tests is that they do not represent real performance situations. For example lap shear tests are mostly used to compare adhesives with each other, tension tests are important for sandwich panels, torsion or compression tests are used for honeycomb panels and peel tests for polyamide-copper composite layers. Ageing tests of bonded assemblies under continuous or intermittent loads are more representative to real performance but not so far satisfactorily developed. Thus there are no specifications or even recommendations used as guidelines for testing. Further durability and fatigue are usually time consuming and expensive to run thus used mainly for joint designs in the research and development phase. Especially fields like aerospace, marine and automotive industry have been performing tests under long term and cyclic loading and hostile environmental conditions able to estimate in various cases the behaviour of structural components. Nevertheless the application of new materials and modern designing methods proposed by Soetens and his group, demand rapid characterisation of the structural behaviour and degradation of the joint thus performing mostly short term loading tests on standardised specimens under environmental actions [Soetens 1990], [Straalen 1998], [Straalen 2001], [Straalen 2002].

3.3 Nondestructive methods

3.3.1 Quality assurance prior to bonding (pre-process)

Testing prior to bonding concerns the surface pretreatment of the substrate before applying the adhesive. The presence of excessive amounts of water vapour, hydrocarbons and other

contaminants result in poor adhesive strength, therefore surface pretreatment is a crucial issue in making a healthy bond.

A simple test involves the wettability of the surface; this is a subjected measurement of the contact angle. Clean surfaces are readily wetted and a drop of water spreads over a large area. The spread of a liquid drop of constant volume is measured quantitative through a transparent gauge placed over the drop. The Fokker contamination tester [Bijlmmer 1978] uses an oscillating probe to measure the electron emission energy of the surface. This varies greatly with the contamination degree and can even be used to detect residues from alkaline cleaning operations.

A common irregularity appearing in pre-process bonding in automotive fabrication is the oil contamination on the metal sheets. The oil degree on the surface can be almost automatically determined by a nondestructive system based on the reflection of IR beam [Eis 2003]. Specimen series with different substrates, oil products and quantities showed possible oil quantification with this method. The limitations are that the chosen transmitter and receiver provided reproducible results only for oil quantities lower than 1 g/m^2.

None of these methods are totally satisfactory and the best means of ensuring that a "good" surface exists prior to bonding is carefully to control the processes leading to its preparation, having previously established "good practice". Maintaining good control over the manufacturing process will increase the probability of achieving a defect free joint and it is particularly important in the case of the adhesive strength for which no satisfactory nondestructive testing method currently exists.

3.3.2 Quality assurance during bonding (in-process)

The use of automation in adhesive dispensing processes has taken a long time to implement due to the rigorous quality control requirements for bonded components. Comprehensive quality control systems monitor the adhesive beads laid down by a robot-held dispenser and the relative position between the bead and the object on which is being applied. This is based on a simple vision system based mostly on software and developed by Davidor and Davies [Davidor 1988]. The major success of the software is that it encodes the images at video frame rate (25 per sec) without employing specialised hardware but only by efficient use of visual information and image processing. Another automated system used in automotive industry regulates the adhesive quantity proportional to the velocity of the applicator nozzle [Eis 2003]. In this system the inspection of the viscosity grade and a maximum allowable material pressing is integrated. However no information is given about the positioning and the cross section of the fillet. A further in-process parameter for the quality is the temperature of the adhesive responsible for the lack of adhesion in case of low temperatures. The controlling is accomplished through thermoelements.

3.3.3 Quality assurance after bonding (post-process)

The majority of NDT techniques associated with adhesive bonds take place after the joint has been manufactured. The suitability of devices and procedure requirements for the industrial implementation of nondestructive testing for the inspection of adhesively bonded joints are highlighted through a calibration study carried out by Zäh et al, [Zäh 2003a].

Based on literature references and industrial "know how" there is a great number of different methods to nondestructive inspection. According to Endlich a systematic classification approach of the respective methods is based on the measurement principals [Endlich 1995]. The methods belong to four groups; these are acoustic, electric, radiography and thermal methods. Later on the "National Material's Advisory Board (NMAB) Ad Hoc Committee on Nondestructive Evaluation" [ASNDT 2002] introduced a classification system of six groups; these are visual, radiography, mechanical vibration, thermal, magnetic, electrochemical. However testing methods

from the last two groups are not suitable for the inspection of adhesive joints. Commonly used methods for adhesive joints are shown in Fig. 3.2. Moreover five main parameters are considered for the NDT classification; the energy source, the signal nature, the detectors, the display and image processing the interpretation basis of the measurements. Thereby it is possible to separate all NDT methods in the above groups.

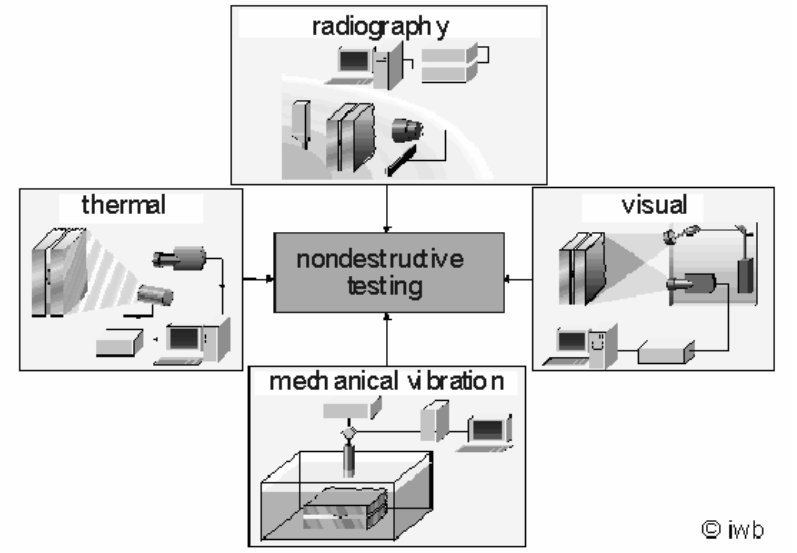

Fig. 3.2: NDT methods for adhesive joints, iwb

The evaluation of the different NDT methods carried out [Zäh 2003a], is based mainly on the experience of industrial manufacturers and users and provides through comparison of the methods` assessments a comprehensive guidance for non destructive inspection (NDI) in adhesive joints. The main evaluation criteria were accessibility of the desired inspection locations, the fixed and operating costs and finally reliability and accuracy of the measurements. Furthermore an additional or substitute medium e.g. water, or large apparatus devices are exclusion criteria for the methods. The performance expense for a measurement, the personnel safety, the automation and the specimen preparation are further implementation criteria. To the evaluation criteria belong the application experience and operation of the devices by qualified personnel, the suitability of the method especially for adhesive joints, the process compatibility in respect to the properties of the adhesive joint and the testable material combinations.

The industrial image processing often required within the NDI of bonds and their predominant inspection range is the adhesive applicator nozzle positioning. The visual NDT methods were compared and the evaluation based on the above criteria is rather economical. The use of the speckle-interferometry allows the testing of the component under mechanical loading and subsequently determines the physical properties of the bond. The 3D-speckle-interferometry compared with the shearography is rather sensitive to external interference but more reliable in comparison to holography. The potential of the shearography for the flaw detection is rather positive but there is a need in signal processing development.

A few techniques for the inspection of adhesive joints based on penetrating radiation are still in the development stage. Through radiography a multi-layered component can be registered and depicted on detectors. Thus the determination of physical properties is possible. The apparatus requires high costs for the application of such techniques; however variable characteristics can be registered at the same time by nondestructive inspection.

The principle of radar impulses is similar to those of ultrasound testing. These have the advantage, that no physical linking is required onto the sample. The limitations are the low resolution, the relatively high acquisition costs, the measurement and evaluation can be

accomplished with a high time factor. Furthermore, the reflection of the microwave radiation on metallic materials is a limitation for the implementation of the technique.

The technical relevance for the implementation of the magnetic-electric techniques for adhesive joints is of secondary importance because the bondline works as an insulator. Thus capacitive or inductive investigations are only conditionally approved. Therefore the application of these techniques is limited. For the nondestructive inspection based on chemical methods is mainly used the intrusion technique. The technical relevance is also in this case of secondary importance since no statement about the quality of the adhesive joint can be made.

For the techniques based on mechanical vibration there is already experience gained and their implementation is also driven from the low apparatus costs. Especially, inhomogeneous structures, delaminations and boundary surface conditions in the component including depth determination can be registered with ultrasound. Defect detection is enhanced through water immersion technique. Limitations are met when it comes to adhesion problems and possibly solved by non-linear ultrasound being however still in a development stage. For the ultrasound method a defined link between the probe and the sample is required through a contact medium for the transmission of the sound. This is frequently the exclusion criterion for the implementation of the technique in the manufacturing process. Exceptions to this are the air coupled ultrasound and the laser ultrasound method however being both in the development stage. The method of acoustic emission is only quasi-nondestructive since the components are subjected mechanically under loading limits, therefore damage can be caused. Furthermore, these techniques can not be widely used since available background noises can possibly influence the result of measurement. Through a vibrometer a movement fragmentation up to a few nanometers is attainable and the measurement of vibrations within megahertz field is possible.

With thermography defects can be detected concerning their position and kind through actual and anticipated performance comparison. Possibly the parts must become black before the inspection, so as to increase the absorption. Low measurement data achieved are used as reference values for the irregularities. Through necessary cooling fluids for the camera and their short application time high expenses are caused. A more favourable heating behaviour and enhanced defect detection is achieved by the sine-like modulation of the thermal waves with the Lockin- thermography.

The NDT methods were evaluated regarding to their potential for industrial implementation. The conclusions can be summarized as follows: No technique based on nondestructive inspection can provide a 100%-controlling in industrial applications. Promising techniques, i.e. the air coupled ultrasound or the lockin-thermography, are still in the development and optimisation stage. Therefore they are only used in small specimens for laboratory purposes. Due to variable parameters it must be determined which method matches to each application. The direct questioning of the sensor and system manufacturers and the users in many interviews gave helpful approaches to the classification and evaluation of the NDT methods. A high future potential is currently shown by industrial sectors in techniques with penetrating radiation. Limitations are found through the high apparatus expenses and the qualified personnel. The implementation of thermography is currently supported through the development of cheaper cameras with no cooling system. Furthermore, promising approaches are to be found in the field of the ultrasound methods through the development of non-linear ultrasound for the exploitation in adhesion problems of adhesive joints.

To ensure the integrity of products and their fitness for purpose, an approach is described by Michaloudaki and Discherl [Zäh 2003b] concerning the inspection effectiveness and implementation potential of four NDT methods - thermography, immerse ultrasonic technique, shearography and neutron radiography - in automotive applications. Neutron radiography was used for verification and reference purposes rather, as ultrasonic method possess distinctive advantages for applications in practice. Generally, both methods detected the same types of

defects, but incident scans showed significantly poorer resolution especially at smallest defects and an inability to distinguish signals at joint edges. Shearography und thermography showed on the contrary a higher implementation potential in automotive applications.

3.4 Description of defects

There are a wide variety of flaws or discontinuities occurring in adhesively bonded structures. A list of possible generic flaw types and their producing mechanisms is given through a distinction in manufacturing and in-service defects. The experimental investigations of this thesis are focussed on the manufacturing defects. Their description and producing mechanisms are based mainly on the experience of industrial partners and on personal evaluation on NDT and fracture surface. Several defects were also reported by the work of Hagemaier in Douglas Aircraft Co. [Hagemaier 1985]. A manufacturing defects catalogue and their cause occurring mostly in automotive applications and considered in this thesis is given in chapter 4. A distinction between manufacturing and in-service defects is given below.

3.4.1 Manufacturing defects

- Voids: a void is any area that should contain adhesive but it does not. There is a variety of shapes and sizes and appears usually at random locations within the bond line. They are generally surrounded by porosity if caused by a thick bondline and may be surrounded by solid adhesive if caused by entrapped gas from volatiles.
- Unbonds or disbonds: areas where the adhesive attaches to only one adherend are called "unbonds". These may be caused by inadequate surface preparation, contamination, or improperly applied pressure. Because both adherends are not bonded, the condition is similar to a void and has no strength. They are generally detectable by ultrasonic or sonic methods.
- Porosity: it might be either dispersed or localized. The frequency and or severity of porosity is random from one assembly to the next. Porosity is defined as a group of small voids clustered together or in lines. Linear porosity usually occurs near the outer edge of a bounded assembly and in many cases forms a porous frame around a bonded laminate. Porosity is usually caused by trapped volatiles and is also associated with thick bondlines which did not have sufficient pressure applied during the curing cycle. The reduced bond strength in these porous areas is directly related to its density frequency and/or severity.
- Pores or frothy fillets: this condition results from high heat up rates during curing. The volatiles are driven out of the adhesive too rapidly, causing bubbling and a porous bondline distinguished by the frothy fillets. This defect is visually detectable and should also be seen in the test specimens processed within the production parts.
- Lack of filets: Visual inspection of a bonded laminate may reveal area where the adhesive did not form a filet on both sides generally indicates a complete void. Thus high stresses near the edges of a bonded joint may cause a cracked adhesive layer due to shear or peel forces. Ultrasonic or radiographic techniques may be used to determine the depth of the void edge.
- Fractured or gouged fillets: These defects are visually detected and their consequences are the same by lack of fillets. Cracked fillets are usually caused by dropping or flexing the bond assembly. Gouges are usually made with tools such as drills or by impact with a sharp object.

- Adhesive flash: Unless precautions are taken, adhesive flows out of the joint and forms fillets plus additional adhesive flow on metal surfaces. This needs usually additional repairing. Moreover it is considered unacceptable when it interferes with ultrasonic inspection at the edges of the bonded joint where stresses are higher.
- Burned adhesive: It appears during drilling operations or when bonded assemblies are cut with a band saw. The burned adhesive is essentially overcured, causing it to become brittle and to separate from the adherend. Also the cohesive strength of the burned adhesive is drastically reduced. This defect type is detectable by ultrasonic C-scan recording methods.

3.4.2 In-service defects

- Impact Damage: Bonded assemblies made from thin materials are susceptible to damage by impact. Impact imposes strain on the adhesive causing it to crack or separate from the adherends. Thus loss in strength can possibly result. A crushed assembly can resonate during service and slowly degrade the adhesive by fatigue until it debonds from the adherends. Impact damage leaves usually a mark on the surface of the part pinpointing possible subsurface damage which can be evaluated by NDT.
- Corrosion: a stable oxide surface preparation is an essential part of the bond foundation. Improper surface preparation can result in an unstable oxide layer which may allow ingress of moisture, delamination and/or service corrosion.
- Poor fabrication: occur from weak bonds (adhesion failures) caused by poor surface preparation, unstable oxide failure and corrosion of special coatings or the base metal.

4 Specimens for the experimental investigations

Overlap joints are the simplest types of adhesive bonded joints for structural applications. These overlap joints are used mostly from the designers, because of their performances. They are globally loaded in shear, which is preferable over joints loaded in tension or peel and they can be produced with high level of quality and low costs. Especially the single lap joint is preferable also for fundamental nondestructive measurements. Results based on these are the criterion for performing further measurements in complicated components. In this chapter the adhesive bonded systems used in the experimental investigations are presented. Attention is given in parameter variations on material and dimensions of the single lap joint as well as artificial imperfections inserted.

4.1 Materials of the adhesive bonded systems

The adherends used were the high strength steel CP800, hot dip galvanised, in 2 mm sheet thickness and the aluminium alloy 6082 T6 (AlMgSi1) in 3 mm sheet thickness. The yield strength for the steel material was $R_{p0,2}$=800 Mpa and for the aluminium alloy $R_{p0,2}$=270 Mpa. Although the thickness used is the upper limit in automotive applications it was deliberately selected to test also the applicability of the NDT methods.

The structural adhesives, Betamate 1496 of Dow Automotive Co. and Terokal 5070 of Henkel-Teroson Co. were used for the manufacturing of the specimens. Both belong to high modulus epoxies and are widely used in automotive shell structure.

Similar to the stress-strain behaviour (σ-ε-diagram) of metals the shear stress-strain behaviour (τ-γ-Diagram) of adhesive joints determines the properties of the adhesive. Typically the main properties required are the tensile or Young's modulus *E*, the shear modulus *G*, the yield stress and the fracture stress and strains in uniaxial tension and pure shear. Two different approaches have been adopted by the adhesives manufacturers to measure these properties, either by bulk specimens of the adhesive or with appropriate joint geometries.

Fig. 4.1 shows schematically the stress strain curves for the aluminium alloy AlCuMg2 and an epoxy adhesive. The high modulus epoxies compared to steel or aluminium are approximately 2 to 4 order of magnitude deformable. Thus adhesives exhibit deformation behaviour very different to that of the metallic parts being joined. Although for e.g. aluminium still behaves elastically up to tensile stresses of about 200 N/mm^2 due to its modulus of elasticity, the linear correlation between stress and strain is valid for only a very narrow region for the adhesive layer. Characteristic for most polymers is the fact that the major part of the stress-strain curve is non-linear and exhibit very different stress-strain behaviour among them.

The shear modulus of the adhesive in the elastic region is defined as:

$$G = \frac{\tau}{\gamma} \qquad \text{Eq. (4-1)}$$

where: G is shear modulus below proportional limit, τ is shear stress at proportional limit and γ is elastic shear strain. Another property of the adhesive often required is Poisson `s ratio ν and this is usually deduced from the knowledge of Young's and shear moduli via the relationship:

$$E = 2G(1+\nu) \qquad \text{Eq. (4-2)}$$

Typical values of Poisson's ratio for the high modulus adhesives in load bearing structures are ν = 0,3…0,45. The Young's and shear moduli for Betamate 1496 (ν =0,40) are E = 1600 MPa and G = 570 MPa and for Terokal 5070 (ν =0,45) are E = 1340 MPa and G = 460 MPa.

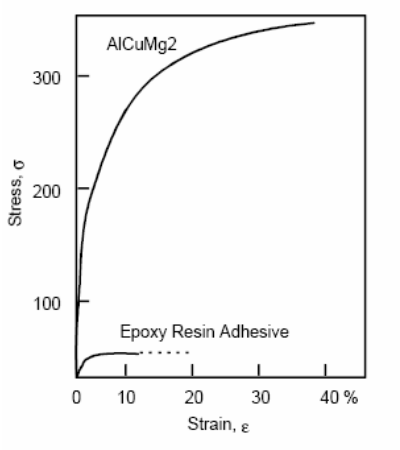

Fig. 4.1: Tensile stress-strain curve for the AlCuMg2 and an epoxy adhesive

4.2 Manufacturing of specimens

The single lap joint specimen Fig. 4.2, is used in the experimental study, both being simple and representative of the stress state in the real structure. The aluminium adherends measured 150×48×2 mm and the steel adherends, measured 110×48×3 mm. These dimensions are not as specified by various standards but larger, following recommendations of industrial partners. The main reason behind this is to increase the bonded area and successfully insert the artificial imperfections. The overlap area of aluminium specimens was 48×20 mm^2 and of steel specimens was 48×30 mm^2. The bondlines were 0,2/0,5/1,0 mm thick. The adhesives used were the single component heat cured (180° C, 40 min) epoxides "Betamate 1496"and "Terokal 5070". The aluminium surfaces were treated with a 3% solution "Alodine 2040" for 90 sec in 45 °C. In each case the two adherends were bonded manually applying the adhesive with a pistol. The correct positioning of the adherends until the adhesive had been cured, was guaranteed with a guiding bar. For a homogeneous adhesive thickness, glass balls with a specific diameter were inserted upon the overlap area and pressure of 0,03 N/mm^2 was applied. Applying pressure also reduced any air or volatiles which would otherwise be trapped between the details and affect the NDE of the artificial imperfections.

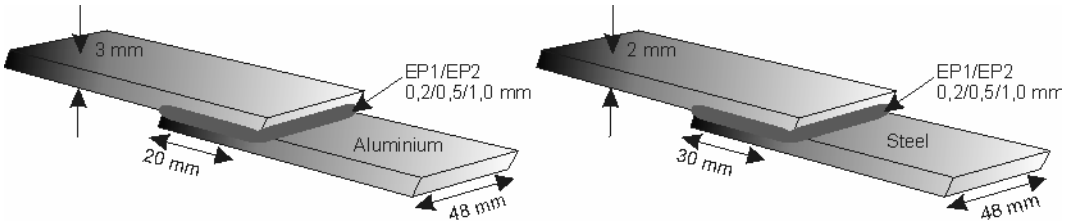

Fig. 4.2: Single lap joint specimen and overlap dimensions for aluminium and steel adherends

4.3 Classification of defects during manufacturing

There is a wide variety of defects occurring in adhesive bonded structures. A list of possible generic flaw types and their producing mechanisms is given by [Clark 1978]. According to Jiao & Rose, [Jiao 1999] defects in adhesively bonded joints can be classified either as a debond, cohesive weakness and adhesive weakness.

A debond is simply characterised and identified as a separation between the two adherends. As a result two traction free surfaces are created. The gross form of debond is illustrated in Fig. 4.3a, however, other traction-free microscopic forms of separation include voids, porosity and micro-cracking in the adhesive. During in service operations, debonds are generally associated with

moisture penetration at bonded construction edges and bolt holes, poor surface preparation, impact and /or local overheating. Debonds are usually identified using common NDE methods, such as ultrasonic inspection and acoustic emission.

Cohesive weakness Fig. 4.3b caused mostly by chemical defects such as undercured or overcured adhesive, heterogeneous adhesive mixtures and water, oil or solvent contaminants can also be detected by traditional ultrasonic techniques.

In complete contrast to debond, weakly bonded joints show no sign of separation between adherend and adhesive, Fig. 4.3c. A weakly bonded joint is still effectively bonding the two adherends together. Currently available NDE methods cannot reliably identify weak bonds during production; the only quality assurance measure is through witness coupon destructive testing.

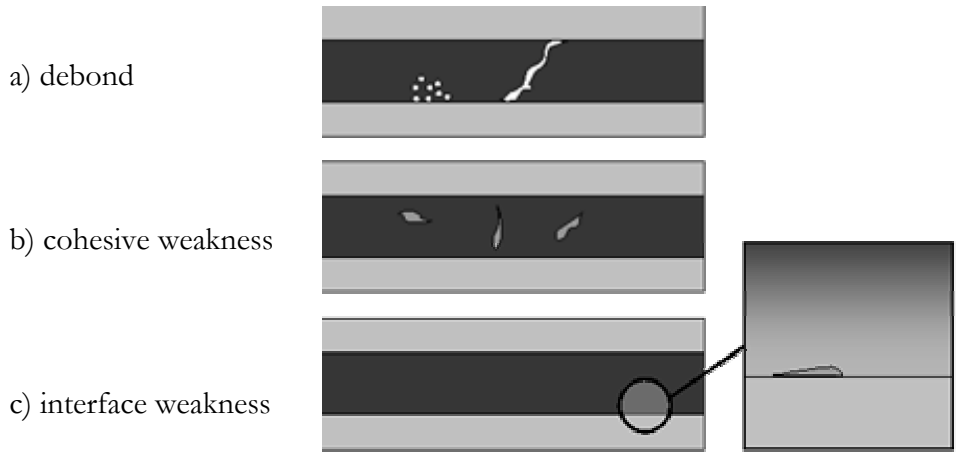

Fig. 4.3: Classification of defects in adhesively bonded joints

Common defect symptoms met in automotive fabrication, their cause and the experimental simulation through artificial imperfections are mentioned in Table 4.1. Defects considered in this investigation cover primarily either debonds or poor cohesive properties and some of them are met also in other engineering applications. The location and the form of the imperfections within the bonded area are illustrated in Fig. 4.4. Teflon layer is responsible to some extent for poor adhesion in the joint because its thickness is the same as the bondline thickness. The effectiveness of NDT on interface weakness should be investigated further with more appropriate imperfections, i.e. experimental simulation of "kissing bond" by teflon spray.

Table 4.1: Simulated artificial imperfections inserted in the joints

Defect symptom	Cause	Simulation
impurities in the bondline pass	impurities in the applicator nozzle	inserts of PTFE layer
lack of adhesion between adhesive and metal sheet	improper surface pretreatment „kissing bonds"	application of PTFE-lacquer
lack of cohesion in the adhesive	oil remaining on the sheet (>3g/m2)	oil application on the metal sheets (3/5/7 g/m2)
uneven adhesive thickness	too high/low folding pressure	folding with higher/lower pressure
air pores in the adhesive	high heat up rate / relative movement of the joined elements	adhesive stirring before application

porosity / moisture degradation of the adhesive	localisation of pores because of humidity	climate storage 21 days, 20 °C, 90% moisture
deposition of the adhesive	surface condition of panels / application speed / adhesive extrudability / nozzle diameter	moving the application nozzle positioning
residual stresses in the adhesive	relative movement of the components	provoke movement of the components

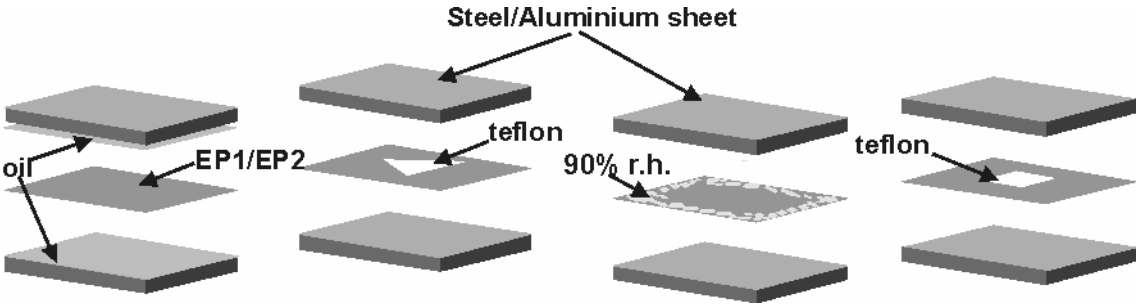

Fig. 4.4: Location and form of the artificial imperfections within the bonded area.

4.4 Selection of testing parameters

The testing program with the parameters variation and the specimen series is described explicitly in the Table 4.2 to Table 4.6. Series 1 represents the ideal -defect free- specimens and is used as basis for the bonded systems with imperfections in series 2 to 5. Each subseries within a series includes a sample size of 5 specimens. The total amount of steel specimens is 210 and aluminium is 120.

Table 4.2: Parameter variation of ideal specimens

Series 1 ideal specimens	adherend material	adhesive	bondline thickness ta [mm]
1.1	steel	EP1	0.5
1.2			0.2
1.3			1.0
1.4	steel	EP2	0.5
1.5			0.2
1.6			1.0
1.7	aluminium	EP1	0.5
1.8			0.2
1.9			1.0
1.10	aluminium	EP2	0.5
1.11			0.2
1.12			1.0
Total number of specimens: 60			

Table 4.3: Parameter variation of steel-EP1 specimens with defects

Series 2 steel/EP1/defects	adherend material	adhesive	bondline thickness t_a [mm]	defect
2.1	steel	EP1	0.5	oil 3g/m²
2.2				oil 5g/m²
2.3				oil 7g/m²
2.4				teflon 100mm²
2.5				teflon 50mm²
2.6				r.h. 90%
2.7	steel	EP1	0.2	oil 3g/m²
2.8				oil 5g/m²
2.9				oil 7g/m²
2.10				teflon 100mm²
2.11				teflon 50mm²
2.12				r.h. 90%
2.13	steel	EP1	1.0	oil 3g/m²
2.14				oil 5g/m²
2.15				oil 7g/m²
2.16				teflon 100mm²
2.17				teflon 50mm²
2.18				r.h. 90%
Total number of specimens: 90				

Table 4.4: Parameter variation of steel-EP2 specimens with defects

Series 3 steel/EP2/defects	adherend material	adhesive	bondline thickness t_a [mm]	defect
3.1	steel	EP2	0.5	oil 3g/m²
3.2				oil 5g/m²
3.3				oil 7g/m²
3.4				teflon 100mm²
3.5				teflon 50mm²
3.6				r.h. 90%
3.7	steel	EP2	0.2	oil 3g/m²
3.8				oil 5g/m²
3.9				oil 7g/m²
3.10				teflon 100mm²
3.11				teflon 50mm²
3.12				r.h. 90%
3.13	steel	EP2	1.0	oil 3g/m²
3.14				oil 5g/m²
3.15				oil 7g/m²
3.16				teflon 100mm²
3.17				teflon 50mm²
3.18				r.h. 90%
Total number of specimens: 90				

Table 4.5: Parameter variation of aluminium-EP1 specimens with defects

Series 4 aluminium/EP1/defects	adherend material	adhesive	bondline thickness t_a [mm]	defect
4.4 4.5 4.6	aluminium	EP1	0.5	teflon 64mm² teflon 32mm² r.h. 90%
4.10 4.11 4.12	aluminium	EP1	0.2	teflon 64mm² teflon 32mm² r.h. 90%
4.16 4.17 4.18	aluminium	EP1	1.0	teflon 64mm² teflon 32mm² r.h. 90%
Total number of specimens: 45				

Table 4.6: Parameter variation of aluminium-EP2 specimens with defects

Series 5 aluminium/EP2/defects	adherend material	adhesive	bondline thickness t_a [mm]	defect
5.4 5.5 5.6	aluminium	EP2	0.5	teflon 64mm² teflon 32mm² r.h. 90%
5.10 5.11 5.12	aluminium	EP2	0.2	teflon 64mm² teflon 32mm² r.h. 90%
5.16 5.17 5.18	aluminium	EP2	1.0	teflon 64mm² teflon 32mm² r.h. 90%
Total number of specimens: 45				

5 Neutron Radiography Measurements

Nondestructive testing with neutrons can yield important information not obtainable by other traditional NDT methods. For example, thermal neutrons are particularly attenuated by low atomic number materials such as hydrogen, lithium and boron. Also, neutrons are transmitted with relative ease through most metals including iron lead, bismuth and uranium. This reversal from X-ray attenuation properties for neutrons has helped make neutron radiography particularly useful for the nondestructive evaluation of materials such as explosives, fluids, rubber, plastic and adhesives, even when they are combined in metal assemblies.

5.1 Brief history and current developments

Industrial neutron and X-radiography are similar in the principle of their techniques and are complementary in the nature of the information supplied. Therefore it is of interest to view the history of neutron radiography development in comparison with that of X-radiography.

It was in 1895 that X-rays were discovered by Röntgen in Germany. Although the principle of X-radiography was realised and proven, it was not until reliable X-ray sources became available 20 years later that industrial X-radiography began to be widely applied. Three factors contributed to wide industrial use: availability of economic methods, familiarity and confidence among industrial manufacturers and the specification of the method in codes.

By comparison, neutron radiography is a young field. The high penetrating nature of neutron radiation was discovered, on a sense, before the neutron itself. Bothe and Becker in Germany, the Joliot Curies in Paris, and Chadwick at Cambridge were all intrigued by the peculiarly penetrating nature of the radiation emitted when alpha rays from polonium impinged on beryllium, and it was this that led to discovery of the neutron 1932. However it was not until 1955, that the available neutron intensities were sufficient for practical industrial applications.

Since 1965 the activity has increased appreciably and separated in three main phases, [Barton 1976]. The first phase was the spreading of neutron radiography ideas to a large number of research centres interested in nuclear technology and explored some of the potential applications. The second phase, about 1968 was the beginning of "service", where the industries could have any item wished with neutrons inspected. In the last phase three new factors have been introduced. First, standards have been established through the American Society for Testing and Materials (ASTM) as neutron radiography takes place alongside with other testing techniques, such as X-radiography and ultrasonics. Second, centres with considerable needs have begun to purchase and optimise their own neutron radiography facilities for their own work. Third, a trend can be seen, where for certain problems development work has been undertaken to tailor techniques especially for particular industrial needs. An example of this is the development of highly transportable neutron radiography equipment for inspection of aircraft.

To summarise this section, neutron radiography is following a development pattern similar to that of X-radiography, but with a 40 year time lag. For both techniques, source availability, industrial knowledge and the adoption in standards and specifications are of major value.

In trying to give a perspective on possible future trends for neutron radiography, two possibly negative influences must be mentioned against three positive ones. The foreseeable main negative influences are of course: (1) the possibility of a deep and sustained reduction in world industrial activity, and (2) the possibility of reduced government financial support for research and development in nuclear techniques. Foreseeable positive influences are: (1) increasing industrial familiarity with neutron radiography, (2) increasing need for quality control as manufactured equipment becomes more complex, and (3) improvements in neutron radiography techniques.

5.2 Application range

There is a broad range of possible applications for neutron radiography which have been performed or proven feasible by preliminary investigations at the NEUTRA station at Paul Scherrer Institute, [Lehmann 2001a]. The following list gives the engineering application fields together with some objects and the goals of their investigations at NEUTRA stations in our days in addition to other neutron source stations worldwide since the early 70s [Berger 1976]:

- automotive industry for the inspection of motors, castings, composite materials and the detection of lubricants` distribution, adhesives and material defects
- nuclear industry for the inspection of fuel pins, the detection of cladding leaks in irradiated fuel elements, fuel burn-up measurements and defect localization
- material science for defect detection, homogeneity analysis of composite materials, alloys and solderings
- civil engineering in structure analysis, moisture content, effectiveness of impregnating agents of soil samples, concrete, wood, tiles
- electronics, electrical engineering for the detection of defects and electrochemical processes analysis of switches, isolators and batteries
- aerospace industry for corrosion detection and adhesive bonding defects in metal honeycombs, phenolic fiberglas-to-metal structures pyrodevices, space vehicle heat pipes, cooling channels

5.3 Application requirements

The extent to which neutrons can be utilized for practical radiography depends on several parameters mentioned by [Cutforth 1976]. These application requirements are in general contradictory. There are conflicts between neutron intensity and cost and between neutron intensity and portability. Although it is difficult to be specific about requirements without first evaluating the application, the following performance characteristics apply to almost any practical application.

- Neutron energy: Thermal neutrons are the energy region 2meV-100meV, exhibiting the most useful attenuation characteristics. Moreover thermal neutron images have been easier to detect and record.
- Beam Collimation: The collimator L/D ratio (L = length collimator guiding neutrons, D = entrance diameter) mentioned by should be 10 to give a useful resolution or more than 50 for most practical applications. This ratio nowadays reaches the 550 at the NEUTRA station.
- Neutron Intensity: A radiographic source should produce a thermal neutron flux of 10^6 neutrons/cm^2/s or more for beam extraction for practical applications. With a given source assembly, beam intensity (speed) can be increased only by sacrificing collimation (resolution) and vice versa. The thermal neutron flux density at standard measuring position at NEUTRA is $3{,}4*10^6$ neutrons/cm^2/s at 1 mA proton current.
- Background radiation: A high γ background radiation can greatly reduce the radiographic contrast of low atomic number materials in the inspected sample. The γ background of primary beam reaches at NEUTRA station 1,5 mSv/h.

- Physical size and portability of source: These requirements must be determined for each application. Generally it is difficult and costly to incorporate portability into a very intense neutron source assembly.
- Cost: Neutron sources are more costly to produce, maintain and operate than X-ray sources. Therefore, each application must be evaluated if neutron inspections are economically justified.

5.4 Components of the thermal radiography facility NEUTRA

Fig. 5.1 shows the principal components of the radiography facility [Lehmann 2001b] used for the experimental investigations of this thesis. Neutrons are generated in the target of the Spallation Neutron Source (SINQ) by high energy proton radiation. Their velocity is reduced to thermal energies in the heavy water filled moderator tank. Another major component is the beam collimator i.e. an evacuated straight pipe guiding the neutrons to the sample position. In order to form a suitable parallel field for radiography purposes, a converging and then diverging collimating pipe is guided through a small aperture. The main parameters of the collimator are the total length L and the diameter of the entrance opening D. These define the angular divergence of the beam and the neutron intensity at the object inspected. The divergent collimator, 11m long, can provide a large uniform beam coverage, but some image distortion occurs at the edges because the neutron paths are radial than parallel. The beam distortion is usually too small to cause problems except in a few special cases. Hence, the divergent beam is the type of collimator used and recommended for most practical applications.

The object observation where the measurements are performed is located at the end of the collimator. The station surrounded by concrete shield contains the object-positioning device, the detector-positioning device and a beam catcher where the beam ends. The positioning devices consist of modular sets of frames that can be adapted to a great diversity of objects and to different detectors. It can be moved remotely with the sample from outside the shielding. A special rotating desk is used for tomography experiments.

A so called "Local Access Control" system is protecting the users against the hazard of direct exposure of the human body by an uncontrolled opening of shutter systems.

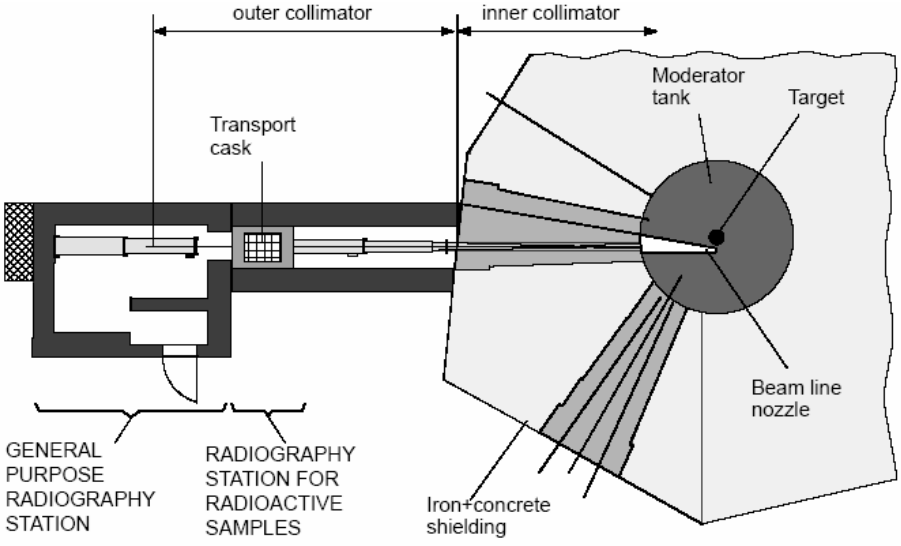

Fig. 5.1: View on the thermal radiography facility NEUTRA, source PSI

5.5 Detector systems

Four detector systems are available at NEUTRA station; a track-etch film/converter device, a silver halide film / Gd- converter device, an imaging plate detector and an electronic detector based on the combination of a scintillator screen with a nitrogen-cooled CCD camera and used for the investigations of this thesis

Although neutron scattering experiments are based on single event counting, the radiography detector integrates respective parameters of time, energy and space. It converts all transmitted neutrons to an adequate image of the tested object. Traditionally used films are insensitive to the neutron irradiation and a conversion process has to be applied for neutron detection. Beside the film method applied for many years, new concepts were realised on the basis of cameras which detect the light output of scintillator screens [Lehmann 1999]. Because the light intensity during neutron exposition is very low, these cameras have to be as sensitive as possible to ensure reasonable frames rates or exposure time respectively. Only the strongest neutron sources are able to allow conditions for real-time imaging with neutrons. A typical arrangement with a CCD-camera is shown in Fig. 5.2. To protect the camera against radiation, a suited shielding around it is recommended. Another detector is the imaging plates; the information about the applied radiation can be carried to the imaging plate scanner where it is extracted in digital form. Because imaging plates are sensitive for beta- and gamma radiation too, they should be used at radiography facilities with low background in the beam. The higher sensitivity, good resolution, large dynamic range (5 orders of magnitude) and the high linearity, are good reasons to replace film methods completely with cameras.

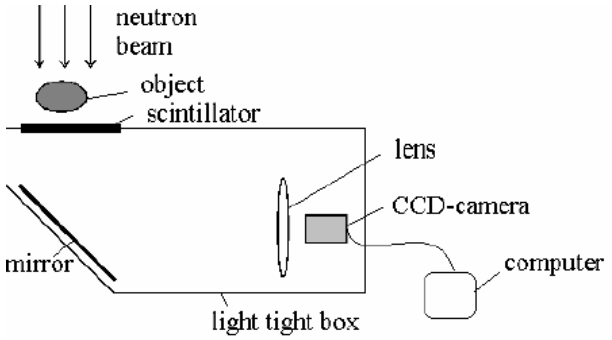

Fig. 5.2: Principle set-up of a camera based neutron radiography detector system

5.6 Experimental set-up

Neutron radiography is similar to x-ray radiography in that both depend on ability to achieve object contrast on the resultant image. However there are significant differences in the effectiveness of the two methods, especially when certain contaminations of elements are examined. The mass attenuation coefficients of the different elements for x-rays assume a near-linear increase with atomic number, whereas the coefficients for neutrons do not show such proportionality. Attenuation of x-rays is determined mainly by the density of the material being examined. Thicker and/or denser materials appear more opaque. The attenuation of neutrons is a function of both scattering and capture possibilities for each element. Adhesives inspected by neutron radiography can be delineated from other elements in many cases where x-ray radiography is inadequate. However neutron radiography inspection does not appear to be cost effective for routine inspection of adhesive bonded structures. It is extremely useful for evaluating the quality of built-in defect reference values or for failure analysis.

The basic experimental set-up is given by the following schematic illustration in Fig. 5.3, where the neutron generating source is the target of the spallation source SINQ [Lehmann 2001c], surrounded with heavy water for moderation of thermal neutron energies. The collimator is a

beam forming assembly, which determines the geometric properties of the beam and may also contain filters to modify the energy spectrum or to reduce the content in gamma rays of the beam. The image resolution achievable with the beam depends mostly on the collimator geometry and is expressed by the L/D ratio, where L is the collimator length and D is the diameter of the inlet aperture of the collimator on the side facing the source. The beam is transmitted through the joint and recorded by a plane position sensitive detector, as a two dimensional image.

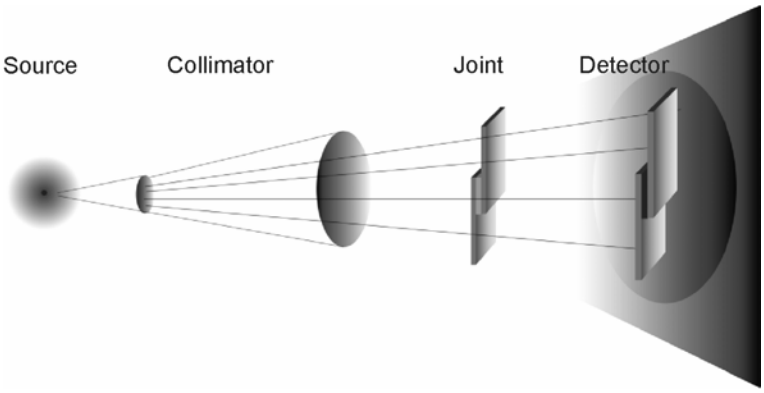

Fig. 5.3: Schematic illustration of a radiographic projection.

5.6.1 Neutron digital imaging

A majority of neutron detectors, especially those which are new or still under development, deliver the obtained image in digital form, Fig. 5.4. In this way, the result of a neutron radiography experiment has to be considered more as a data set instead of a nice clear picture. There are many advantages in digital information, mainly:

- the application of all powerful techniques for image post-processing; in this way, the application range can be shifted and extended regarding sensitivity, contrast and resolution;
- faults during the exposure process can be removed by adapted methods like filtering and transformations;
- a quantification of the amount of material in the sample or of processes in the sample becomes possible with high precision;
- methods of tomography with neutrons based on many projections of the rotated sample can now be implemented as powerful and competing tool;
- the image transfer is much easier without any loss of information or quality;
- by image subtraction methods it becomes possible to measure and to visualise very small amounts of substances even if the background level is much higher.

The digital techniques for neutron imaging can take profit from the recent developments in computer technique regarding speed and memory. However, all high quality neutron images represent data sets of tens to hundreds of MBytes which have to be handled and saved. In this way, digital imaging represents a front-running and demanding method also in the future with an important potential.

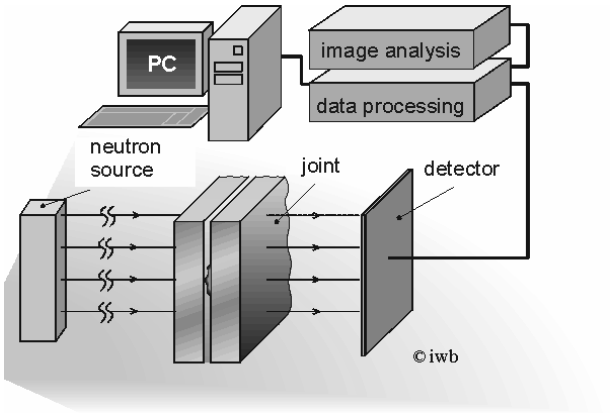

Fig. 5.4: Neutron radiography testing and data processing; source: iwb.

5.6.2 Measurement data

Neutron transmission radiography is based on the application of the attenuation law of radiation passing through matter. Because different materials have different attenuation behaviour the neutron beam passing through an adhesive bond can be interpreted as signal carrying information about the composition and the structure of the joint. The macroscopic inspection of an adhesively bonded joint with neutrons is limited in two respects [Lehmann 2001d]:

- ability to penetrate the joint

- ability to distinguish different materials or zones in the joint.

The transmitted beam signal I through a single lap joint with total thickness d and a macroscopic cross-section A can be described by the basic law of radiation attenuation in matter, see Fig. 5.5:

$$I = I_0 \cdot e^{-A \cdot d} \qquad \text{Eq. (5-1)}$$

where I_0 represents the incident neutron flux signal. The ratio between the emerging neutron flux and incident flux is called transmission T. Depending on the attenuation properties of the different materials investigated, quantitative data of the material penetrated can be obtained from Eq. (5-1) and subsequently the macroscopic cross-section A_{Al} for the adherend can be estimated. The incident intensity I_0 and the transmitted intensity for the adherend and the adhesives were obtained from the neutron radiography measurements, Table 5.1.

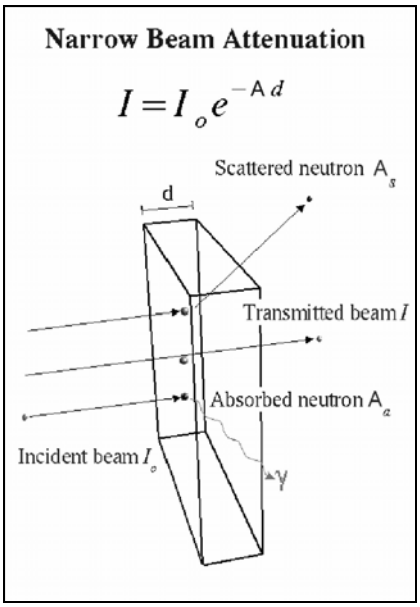

Fig. 5.5: Neutron matter interaction

Table 5.1: Overview of measured data for the adhesives Betamate 1496 and Terokal 5070

		Adhesive "Betamate 1496"				Adhesive "Terokal 5070"			
adherend	bondline thickness [mm]	specimen	incident intensity I_0	transmitted intensity I_{St} / I_{Al}	transmitted intensity $I_{adhesive}$	specimen	incident intensity I_0	transmitted intensity I_{St}/I_{Al}	transmitted intensity $I_{adhesive}$
steel	0,2	1.2.1	43784	36192	27162	1.5.1	43942	12201	8026
		1.2.2		36179	28587	1.5.2		12214	8161
		1.2.3		35958	28009	1.5.3		12139	7904
		1.2.4		36199	28076	1.5.4		12205	8150
		1.2.5		36135	27727	1.5.5		12151	7852
steel	0,5	1.1.1	33107	26239	18755	1.4.1	43850	36186	27043
		1.1.2		27475	19879	1.4.2		36168	27392
		1.1.3		27685	20172	1.4.3		36009	28016
		1.1.4		27148	19856	1.4.4		36200	26454
		1.1.5		27098	19593	1.4.5		36183	25879
steel	1,0	1.3.1	40140	33158	21126	1.6.1	14590	36336	28746
		1.3.2		33179	21046	1.6.2		36309	28529
		1.3.3		33165	21269	1.6.3		36324	27216
		1.3.4		33218	20980	1.6.4		36337	28939
		1.3.5		33198	20801	1.6.5		36290	28597
aluminium	0,2	1.8.1	43690	42528	39201	1.11.1	44063	42874	38934
		1.8.2		42615	37247	1.11.2		42956	38576
		1.8.3		42555	38170	1.11.3		42896	39870
		1.8.4		42598	39132	1.11.4		42939	39594
		1.8.5		42628	38385	1.11.5		42895	37195
aluminium	0,5	1.7.1	43902	42716	35742	1.10.1	43830	42644	34817
		1.7.2		42757	34889	1.10.2		42730	35690
		1.7.3		42748	35503	1.10.3		42682	35251
		1.7.4		42792	34453	1.10.4		42679	34381
		1.7.5		42739	34396	1.10.5		42684	35008
aluminium	1,0	1.9.1	43607	42432	30807	1.12.1	44195	43034	38749
		1.9.2		42513	31012	1.12.2		43048	39519
		1.9.3		42467	30896	1.12.3		43051	39698
		1.9.4		42547	31440	1.12.4		43098	39868
		1.9.5		42471	30871	1.12.5		43052	39371

The macroscopic cross-section $A_{adhesive}$ can be calculated by processing the same formula for the theoretical values of bondline thickness. Thus with known aluminium adherend thickness we can determine the thickness of the adhesive or the variation in bondline thickness as follows:

$$I = I_0 \cdot e^{-A_{Al} \cdot d_{Al} - A_{adhesive} \cdot d_{adhesive}} \qquad \text{Eq. (5-2)}$$

The mean value of the macroscopic cross-sections for the adherend A_{Al} and the two adhesives $A_{adhesive}$ are given in Table 5.2. It is worth noting here that the value $A_{adhesive}$ decreases, the thicker the bondline appears due to respective attenuation of neutrons in the adhesive.

Table 5.2: Mean value of the estimated macroscopic cross section for the adherend and the two adhesives

		Adherend	Adhesive "Betamate 1496"	Adhesive "Terokal 5070"
adherend	bondline thickness [mm]	mean value of macroscopic cross section overlap area A_{St} or A_{Al}	mean value of macroscopic cross section adhesive area $A_{adhesive}$	mean value of macroscopic cross section adhesive area $A_{adhesive}$
steel	0,2	0,955	3,310	2,160
	0,5		2,471	2,013
	1,0		2,651	2,379

aluminium	0,2	0,087	3,864	3,684
	0,5		3,473	3,415
	1,0		2,890	3,083

5.7 Evaluation methodology

5.7.1 Digital image processing

A neutron radiograph is an image of a visual representation of an object. Experienced personnel has the enhanced ability to qualitatively extract information from images. This ability is based also on any mechanical means of image analysis, if quantitative information has to be achieved from the image. Obtaining quantitative data from the images is the principal added value of image analysis systems. In order to process an image with a computer, the image must be converted into numeric form. This process is known as image digitisation. The digitisation process divides an image into a horizontal grid, or array, of very small regions called "picture elements", or "pixels". In these investigations the digital image of a neutron radiograph is characterised by a 16 bit depth greyscale with 65.535 levels of grey. At the NEUTRA station of Paul Scherrer Institute this level of analysis of the images enables visual inspection, optical density, profiles and dimensional measurements.

5.7.2 Qualitative evaluation of ideal joints

Fig. 5.6 and Fig. 5.7 show typical transmission images of six lap joints with steel or aluminium in each case. Steel specimens 1.1.1, 1.2.5, 1.3.4 and aluminium specimens 1.7.4, 1.8.1, 1.9.5 were bonded with "Betamate 1496". Steel specimens 1.4.5, 1.5.4, 1.6.4 and aluminium specimens 1.10.3, 1.11.5, 1.12.1 were bonded with "Terokal 5070". All bonds are considered to be ideal bonds without defined imperfections inserted (s. also Annex A).

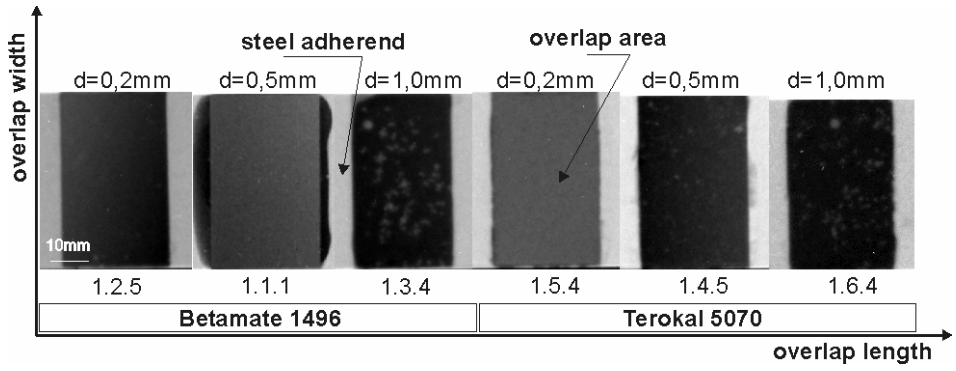

Fig. 5.6: Transmission images of aluminium ideal bonds with 0,2, 0,5 and 1,0 bondline thickness.

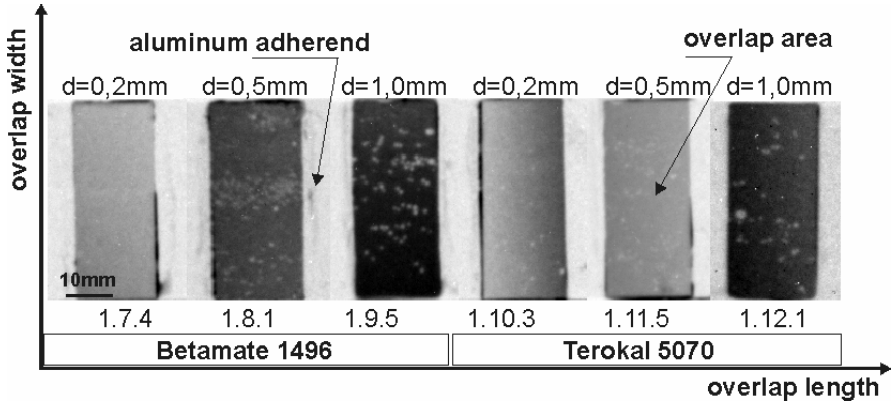

Fig. 5.7: Transmission images of aluminium ideal bonds with 0,2, 0,5 and 1,0 bondline thickness.

Observing the bond areas, a contrast difference between the specimens due to adhesive thickness is noticed. The 1,0 mm thickness in both adhesives shows the richest contrast relative to 0,5 and 0,2 mm thickness. Furthermore the glass balls inserted during manufacturing limiting the bondline thickness are easy to recognize especially in the specimens with adhesive thickness 1,0 and 0,5 mm.

Preliminary investigations of Michaloudaki and Kosteas showed that steel and aluminium adherends look fairly transparent in contrast to both adhesives in the joint due to hydrogen detection even between metal parts [Kosteas 2002a]. The hydrogen atoms in the adhesive absorb neutrons rendering it opaque. In fact aluminium looks even more transparent in comparison with steel due to higher interaction probability of steel (and even higher of adhesives) with neutrons, Fig. 5.8. Hereby the relation, defining the macroscopic neutron interaction cross section Σ as a function to the microscopic neutron interaction cross section σ known from database given in Eq. (5-3):

$$A = N * \sigma \quad [cm^{-1}] \qquad \text{Eq. (5-3)}$$

and

$$N = \frac{\rho}{aw} * N_A \quad [cm^{-3}] \qquad \text{Eq. (5-4)}$$

where:

N: number density $[cm^{-3}]$

ϱ: material density $[g*cm^{-3}]$

aw: atomic weight $[g*mol^{-1}]$

N_A: Avogadro number $6{,}022*10^{23}$ $[mol^{-1}]$

The experimental A values for steel and aluminium given in Table 5.2 approximate significantly - and thus verified- the following evaluated A values for iron and aluminium with applied from database σ values.

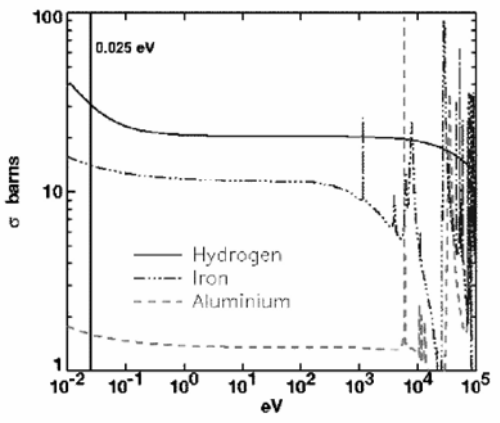

Thermal Neutron Cross Sections at 0.025eV

Material	ρ	σ	Å
Water	1	103	3.45
Iron	7.9	14	1.18
Aluminium	2.7	1.7	0.1

Fig. 5.8: Neutron cross sections for several elements or chemical combinations, Paul Scherrer Institute

The data of each digital image can be used for calculations of quantitative information regarding the content of the joint. Due to data linearity within the wide dynamic range of the digital system

- slow scan CCD-camera - a high accuracy can be obtained. On the following diagrams, Fig. 5.9 and Fig. 5.10 the bondline thickness *d* along the overlap width w = 48 mm of the above specimen series - with a sample size of 5 specimens for each adhesive and each bondline thickness - is given. The digital measurements relating to the neutron distribution along the overlap width according to Eq. (5-2) provide information about the variation in bondline thickness. The line profiles in the diagrams approximate the 0,2, 0,5 and 1,0 mm defined bondline thickness. Some of these curves show a clear deviation though, which means thicker or thinner bondline at the respective overlap area. This fact can be confirmed also from the transmission images of Fig. 5.7, where the contrast on specimens 1.7.1, 1.10.1 and 1.11.1 varies along the overlap width or/and length.

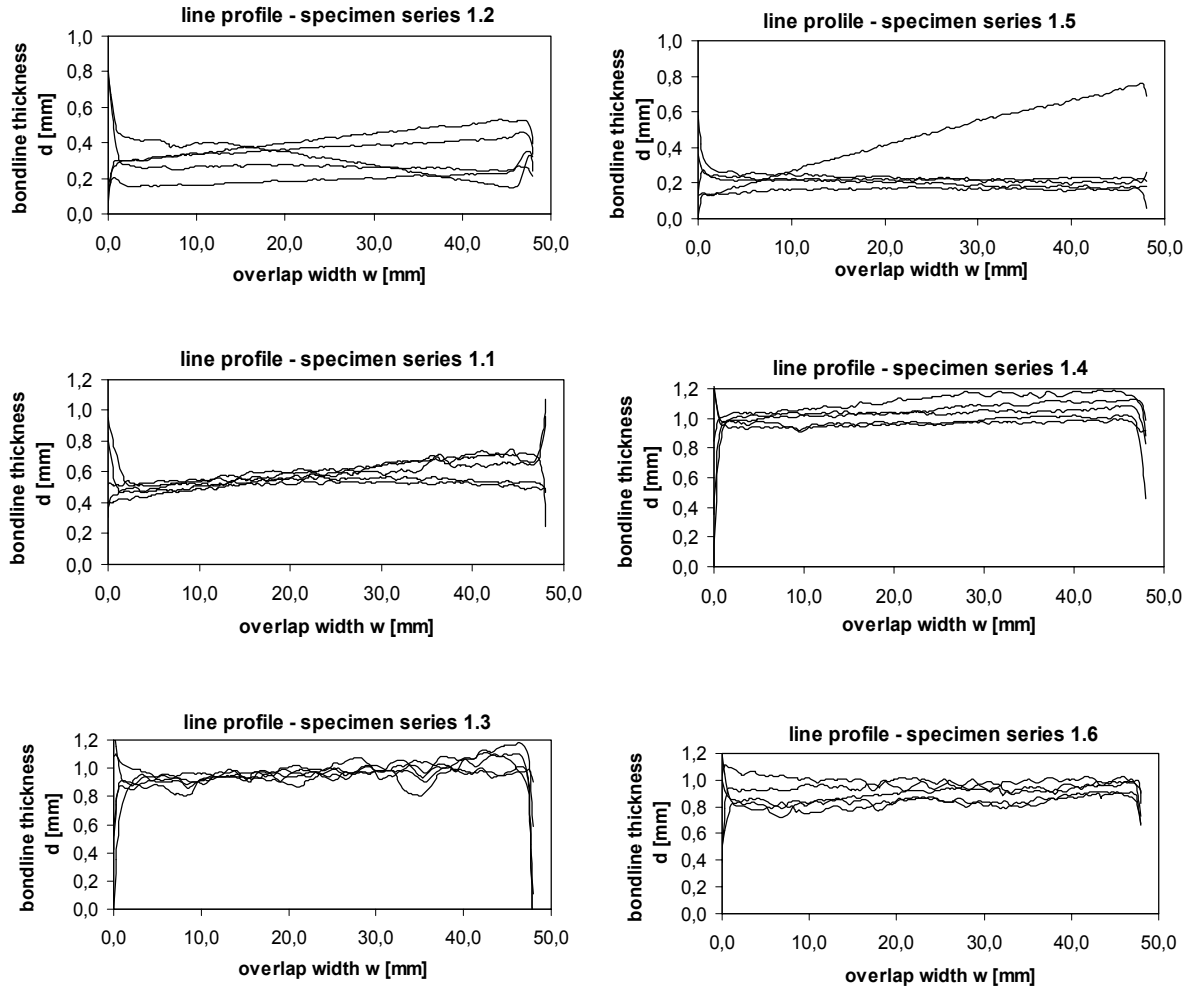

Fig. 5.9: Line profiles of the bondline thickness for the adhesives "Betamate 1946" and "Terokal 5070" within an overlap area 30x48 mm² and with steel adherends.

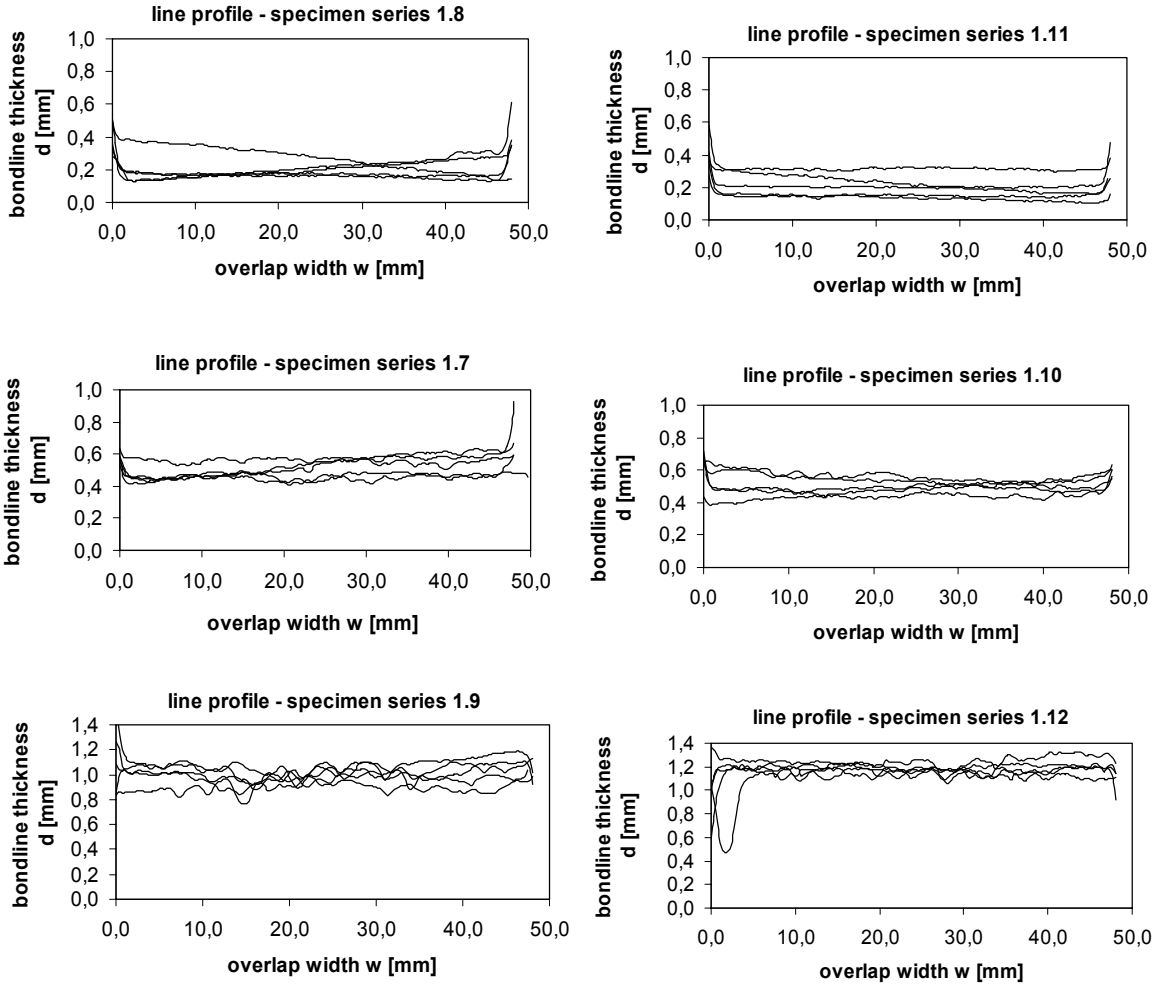

Fig. 5.10: Line Profiles of the bondline thickness for the adhesives "Betamate 1946" and "Terokal 5070" within an overlap area 20x48 mm² and with aluminium adherends.

The variation of the bondline thickness over the bonded area (for steel 1440 mm^2 and aluminium 960 mm^2) is shown on the Fig. 5.11 for the steel specimens 1.5.4, 1.4.5, 1.6.4 and Fig. 5.12 for the aluminium specimens 1.7.4, 1.8.1, 1.9.5. The resolution of the detection system reaches 1024 x 1024 pixels with 1 pixel being approximately 0,27 mm. This means that 175 pixels in overlap width multiplied with approximately 73 pixels in the overlap length offers approximately 12780 points, i.e. measurements of the bondline thickness [Michaloudaki 2003].

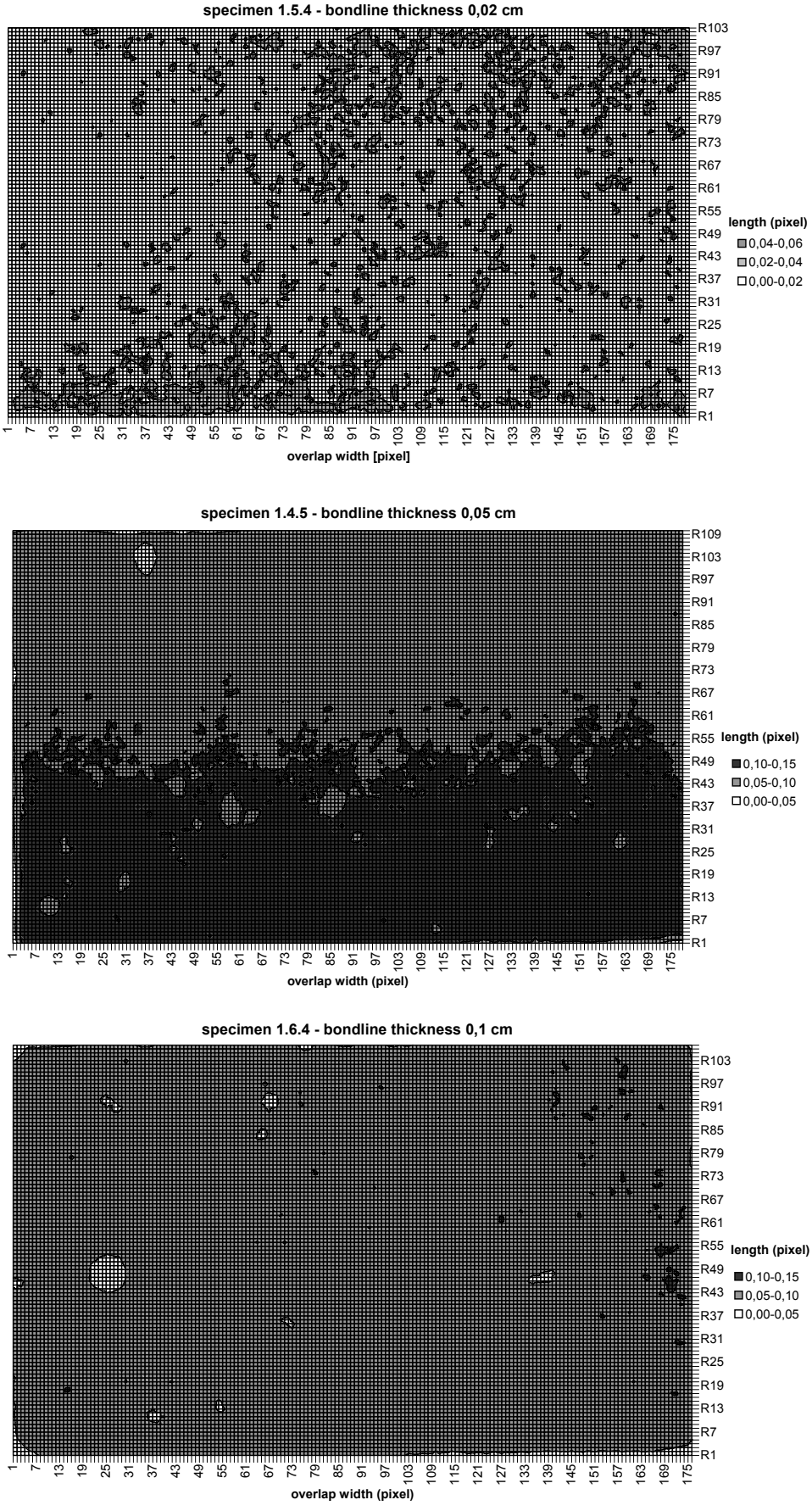

Fig. 5.11: Measurements of the bondline thickness variation [cm] within an overlap area for the adhesive "Terokal 5070" with steel adherends.

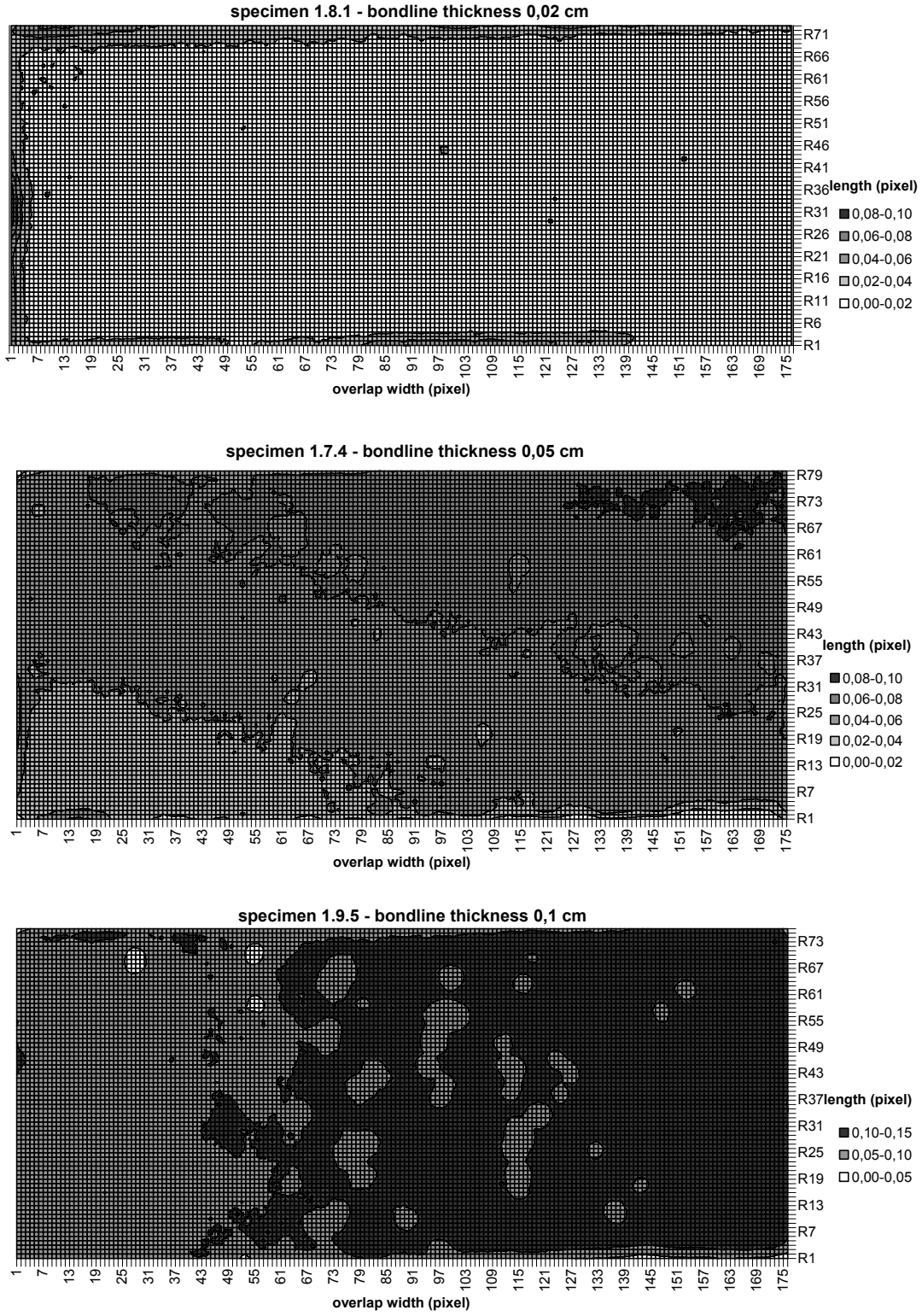

Fig. 5.12: Measurements of the bondline thickness variation [cm] within an overlap area for the adhesive "Betamate 1496" with aluminium adherends.

5.7.3 Qualitative evaluation of defect joints

Fig. 5.13 and Fig. 5.14 show transmission images of the overlap area (1440 mm^2) of the steel joints bonded with the adhesives "Betamate 1496" and "Terokal 5070" after evaluation. Fig. 5.15

and Fig. 5.16 show also transmission images of the overlap area (960 mm^2) of the aluminium joints bonded with the above mentioned adhesives after evaluation with image analysis software. This evaluation is described in detail in 5.8.4 and transmission images of the specimen series are presented in Annex A. The detectability of the imperfections with neutron radiography was in general very good because of the presence of hydrogen in the adhesive, and the high resolution of the transmission images. The artificial imperfections were evaluated by means of image analysis software and the results are given in Table 5.3 to Table 5.6. Each mean value is representative of a sample size of 5.

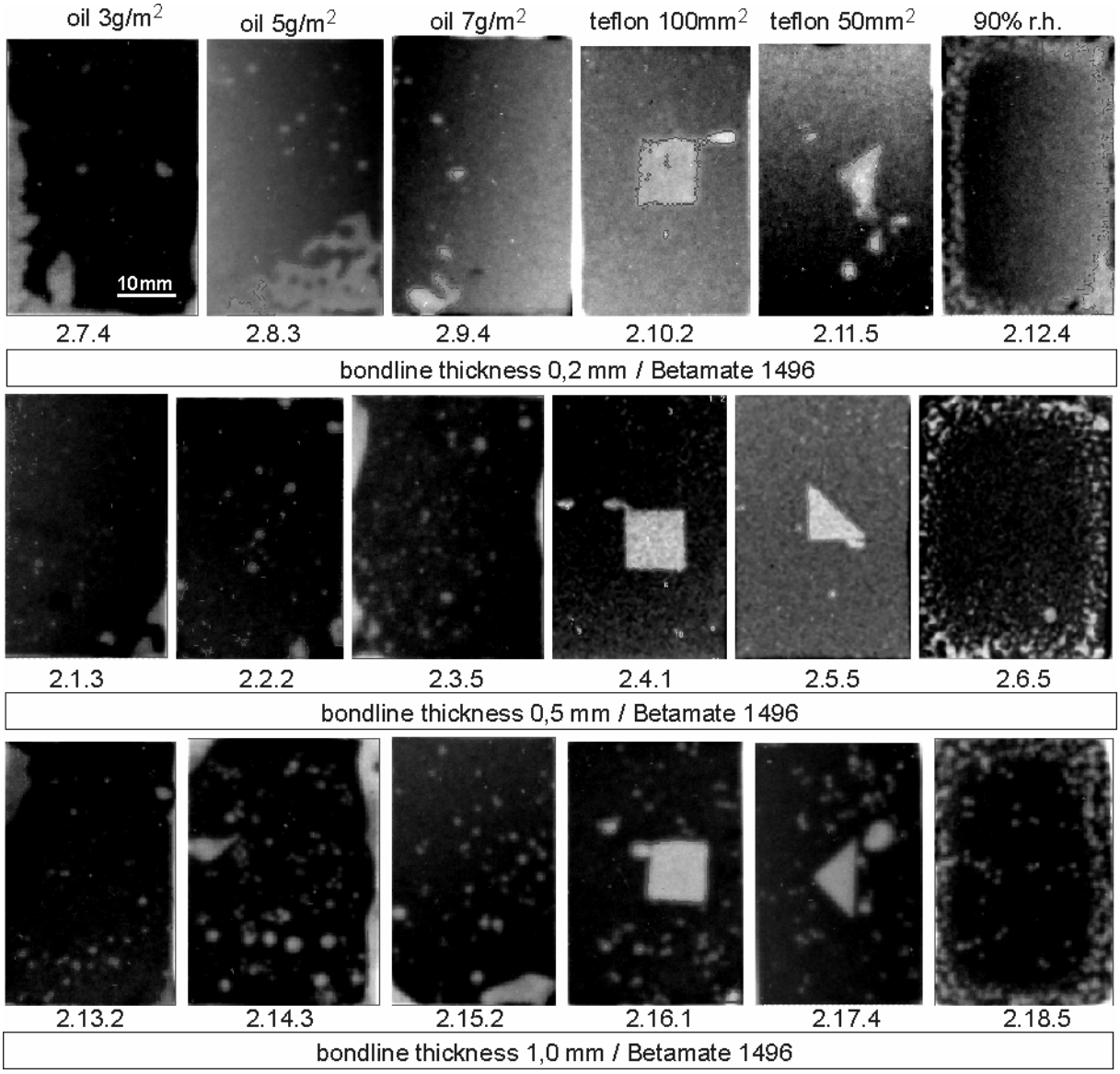

Fig. 5.13: Transmission images of steel lap joints bonded with "Betamate 1496" with imperfections.

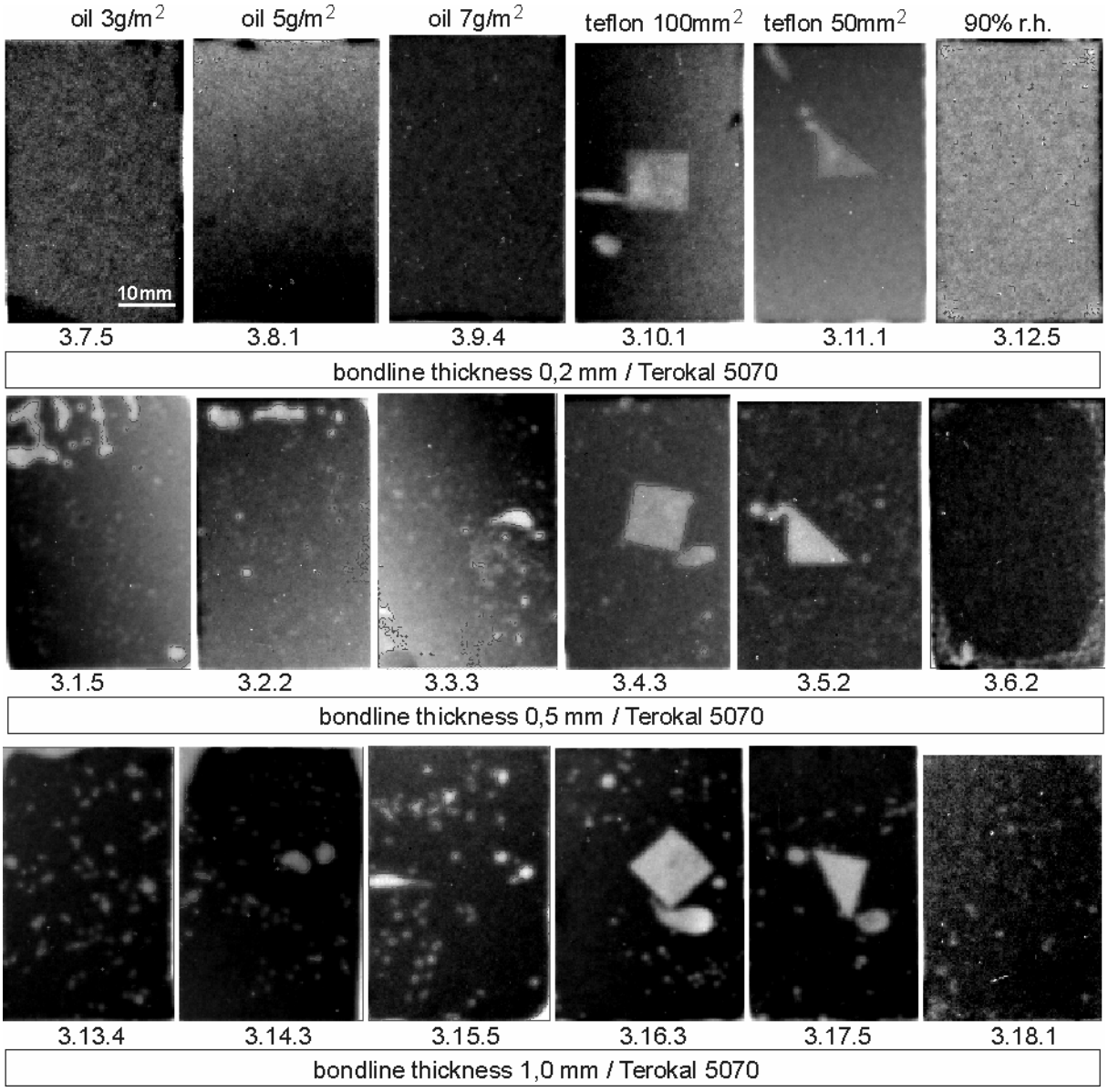

Fig. 5.14: Transmission pictures of steel lap joints bonded with "Terokal 5070" with imperfections.

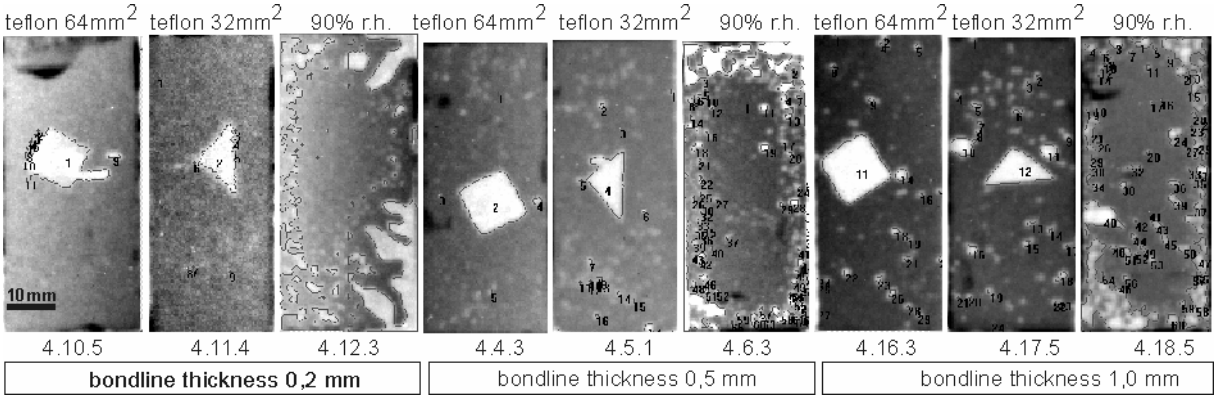

Fig. 5.15: Transmission images of aluminium lap joints bonded with "Betamate 1496" with imperfections.

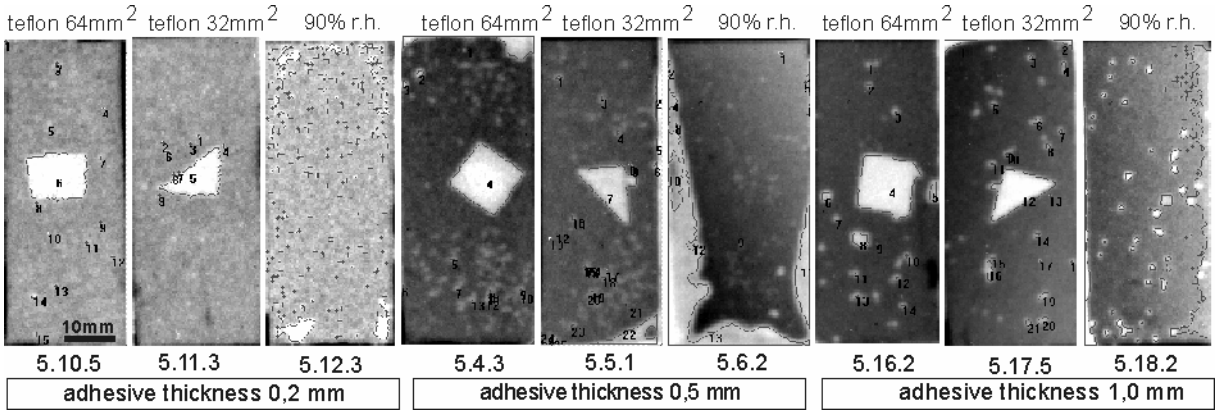

Fig. 5.16: Transmission pictures of aluminium lap joints bonded with "Terokal 5070" with imperfections.

On the transmission images of the overlap areas we observe that very small imperfections - pores or glass balls for the determination of bondline thickness - are also detectable in addition to the artificial imperfections. The detectability of internal flaws or structural defects is influenced by the possibility to separate different grey levels in the images obtained. Theoretically, a 16 bit format allows distinguishing between ca. 65000 levels. Imperfect areas are indicated through a contrast difference - adhesive tends to black, imperfections tend to white - size and form being detectable with high accuracy. This fact is associated to the geometry of the beam. The latter being almost parallel assures that no significant distortions will arise.

5.7.4 Quantitative estimations of the bondline thickness

A further task apart from the qualitative observations on the images is to perform measurements upon them by means of the image analysis software *Image Pro* and extract quantitative information concerning the irregularities in the bonds for e.g. variation in bondline thickness. A useful tool on the Measure menu is the Line Profile command obtaining a plot of the intensity values of a single line within image. By the selection of the Line Profile command, the Line Profile window is opened and two defining-lines are placed within the image. The defining-lines specify the line of pixels to be plotted. The lines (Line option) can be drawn to any length. The two discontinuous defining-lines were positioned over the area of pixels to be measured, i.e. on the upper and lower specimen side, Fig. 5.17. Thus the average intensity values over the overlap area ware plotted with a single curve.

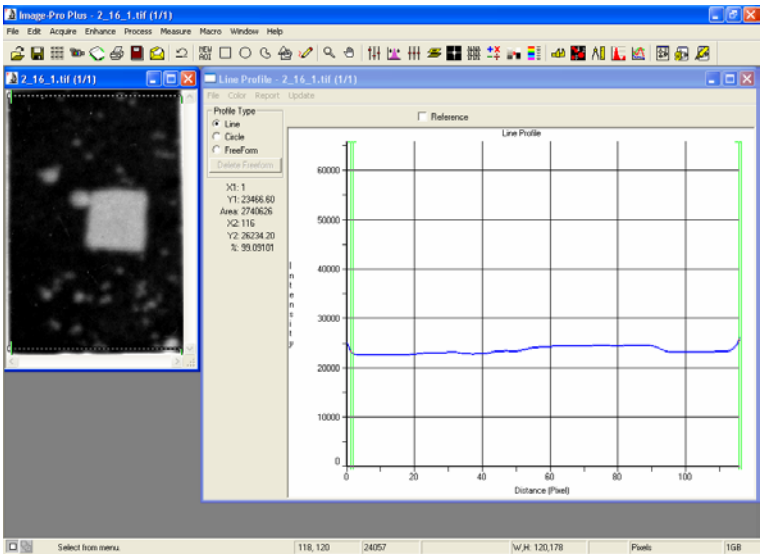

Fig. 5.17: Plot of intensity values as line profile in relation to pixels across the overlap width.

The graph in the Line Profile window displays the type of plot selected in the Line Profile Report Menu i.e., Normal, Thick Horizontal, or Thick Vertical. The used *Thick Horizontal* lines plotted intensity values (Y-axis) along the overlap width of the specimen, given in pixels (X-axis). The Table option in the Report Menu was selected to display the line profile data in tabular form, as shown below in Fig. 5.18. The data behind the digital image were used for calculations of quantitative information regarding the bond.

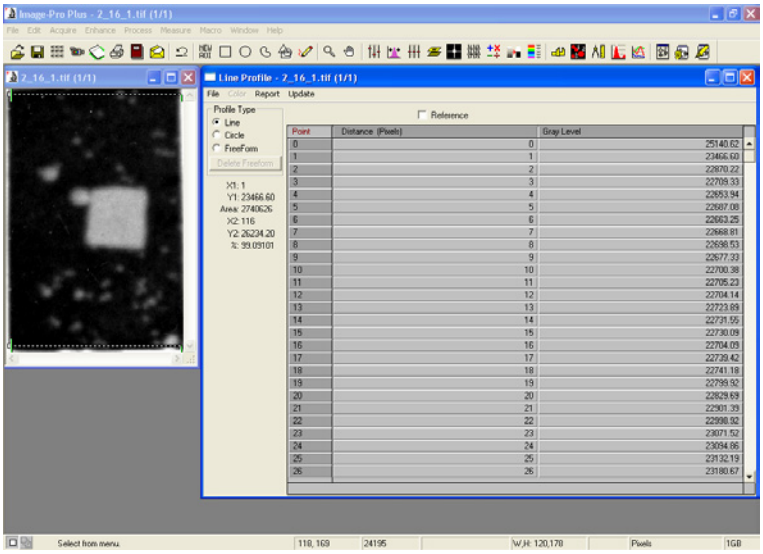

Fig. 5.18: Tabular form of the intensity values of the image bitmap for every pixel across the overlap width.

The DDE *(Dynamic Data Exchange)* to Excel command was selected to transfer the above measured data to Microsoft's Excel spreadsheet. The data export is followed by calibration of pixels in millimetres of specimen, Fig. 5.19. Respective calculations through the attenuation law reflect the depicted intensity values on the image as adhesive thickness on the graph. Thus a plot of the average thickness over the total overlap area as a line profile is gained for further evaluation.

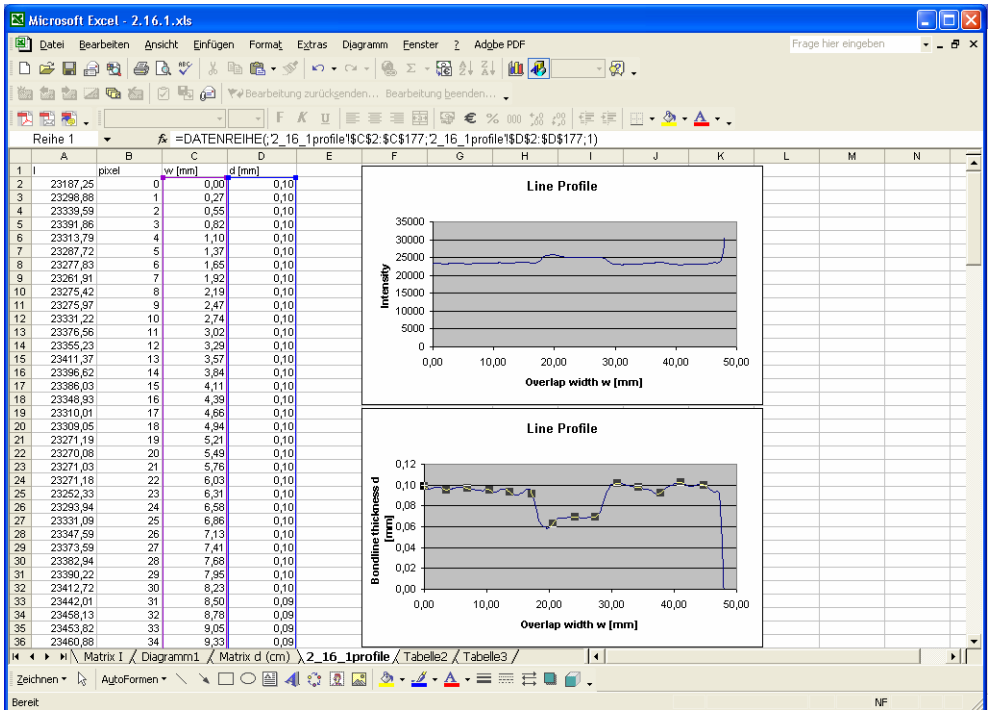

Fig. 5.19: Plot of bondline thickness across the overlap width.

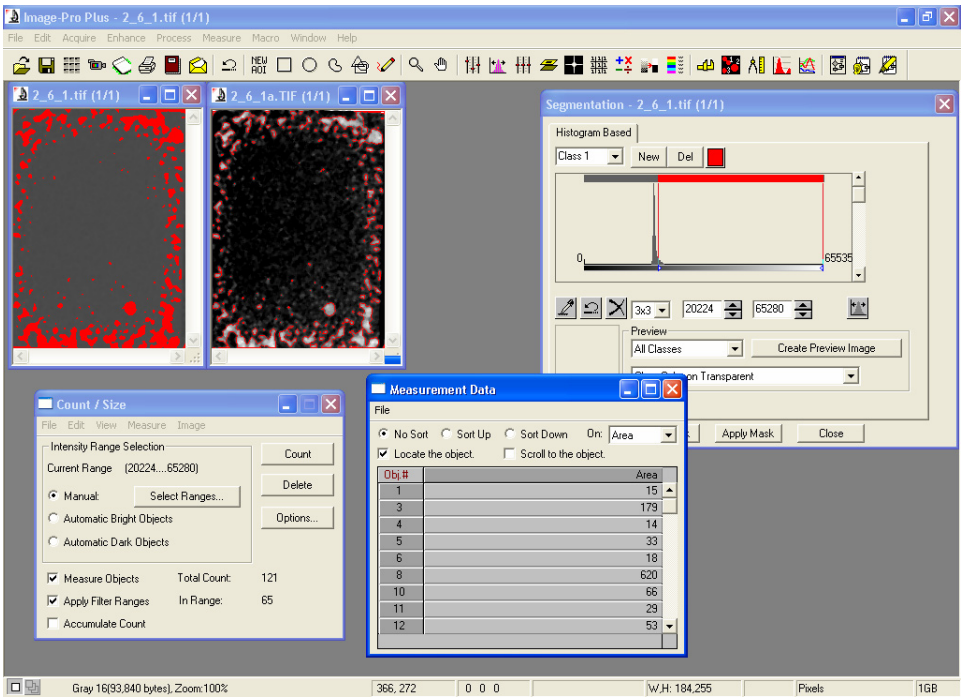

Fig. 5.21: Estimation of the defect area through image analysis software.

The basic steps involved in a counting task are to:

set the range of intensities (monochrome images) or the colours (colour images) that identify the object you want to count using the tools in the Intensity Range Selection group box.

select the kinds of measurement you want to record in the Count/Size: Measure menu's Select Measurements dialog box.

count and measure the objects using the Count button.

When the Count/Size command is selected, the Count/Size window is displayed. Then, using the Count/Size menu commands, the measurements can be viewed, saved, and edited. Moreover using the menu commands the data can be classified, sorted and graphed.

It is worth here noting that the smallest defect evaluated had only 0,08 mm^2 area equal to 1 pixel. One pixel is after all the smallest unit able to be estimated with image processing. In terms of maximum defect volume for a defect 0,08 mm^2 big across the overlap area could be 0,016/0,040/0,080 mm^3 respectively for 0,2/0,5/1,0 mm bondline thickness.

Based on the methodology described for the evaluation of defects through neutrons image processing and analysis software the defect area estimated for the specimens with introduced imperfections are given in Table 5.3 to Table 5.6. The total amount of defect steel specimens is 222 and aluminium is 90. The mean value and standard deviation were determined for every parameters combination with a sample size of 5 specimens.

Table 5.3: Evaluated defect area within an overlap bonded area of 1440mm2 for adhesive Betamate 1496 and steel adherends

	Bondline thickness 0,2 mm				Bondline thickness 0,5 mm				Bondline thickness 1,0 mm			
inserted defect	specimen	defect area [mm²]	mean value of defect area [mm²]	standard dev. [mm²]	specimen	defect area [mm²]	mean value of defect area [mm²]	standard dev. [mm²]	specimen	defect area [mm²]	mean value of defect area [mm²]	standard dev. [mm²]
oil 3 g/m²	2.7.1	140,11	92,46	82,13	2.1.1	28,71	51,27	43,74	2.13.1	75,14	72,06	33,78
	2.7.2	24,92			2.1.2	12,59			2.13.2	109,61		
	2.7.3	22,64			2.1.3	87,94			2.13.3	97,64		
	2.7.4	212,32			2.1.4	18,82			2.13.4	26,73		
	2.7.5	62,29			2.1.5	108,82			2.13.5	51,19		
oil 5 g/m²	2.8.1	3,21	49,28	88,15	2.2.1	65,70	69,95	10,65	2.14.1	130,22	129,71	55,19
	2.8.2	9,93			2.2.2	76,62			2.14.2	85,42		
	2.8.3	206,73			2.2.3	81,90			2.14.3	216,73		
	2.8.4	9,38			2.2.4	71,28			2.14.4	78,80		
	2.8.5	17,17			2.2.5	54,25			2.14.5	137,40		
oil 7 g/m²	2.9.1	11,79	41,49	39,26	2.3.1	19,92	89,65	40,78	2.15.1	73,44	75,03	22,83
	2.9.2	14,92			2.3.2	109,04			2.15.2	111,02		
	2.9.3	24,11			2.3.3	102,89			2.15.3	63,29		
	2.9.4	50,35			2.3.4	91,62			2.15.4	77,72		
	2.9.5	106,27			2.3.5	124,79			2.15.5	49,69		
teflon foil 100 mm²	2.10.1	107,37	119,79	8,91	2.4.1	133,86	122,89	8,11	2.16.1	120,86	143,82	33,01
	2.10.2	132,28			2.4.2	123,71			2.16.2	115,52		
	2.10.3	119,26			2.4.3	126,79			2.16.3	129,27		
	2.10.4	121,90			2.4.4	113,63			2.16.4	194,80		
	2.10.5	118,16			2.4.5	116,46			2.16.5	158,67		
teflon foil 50 mm²	2.11.1	55,98	59,62	5,51	2.5.1	65,31	67,34	15,22	2.17.1	63,07	88,03	19,47
	2.11.2	61,89			2.5.2	65,74			2.17.2	89,66		
	2.11.3	54,34			2.5.3	90,14			2.17.3	75,16		
	2.11.4	57,81			2.5.4	47,35			2.17.4	100,22		
	2.11.5	68,09			2.5.5	68,15			2.17.5	112,05		
90% r.h.	2.12.1	120,52	136,64	43,53	2.6.1	202,95	192,29	28,02	2.18.1	170,73	207,82	27,99
	2.12.2	159,32			2.6.2	171,47			2.18.2	244,45		
	2.12.3	179,88			2.6.3	212,02			2.18.3	193,33		
	2.12.4	156,25			2.6.4	154,66			2.18.4	208,42		
	2.12.5	238,81			2.6.5	220,37			2.18.5	222,16		

Table 5.4: Evaluated defect area within an overlap bonded area of 1440mm² with Terokal 5070 steel adherends

	Bondline thickness 0,2 mm				Bondline thickness 0,5 mm				Bondline thickness 1,0 mm			
inserted defect	specimen	defect area [mm²]	mean value of defect area [mm²]	standard dev. [mm²]	specimen	defect area [mm²]	mean value of defect area [mm²]	standard dev. [mm²]	specimen	defect area [mm²]	mean value of defect area [mm²]	standard dev. [mm²]
oil 3 g/m²	3.7.1	20,23	20,79	8,14	3.1.1	62,37	83,57	43,74	3.13.1	76,23	83,65	23,52
	3.7.2	33,87			3.1.2	91,03			3.13.2	100,27		
	3.7.3	17,80			3.1.3	93,69			3.13.3	61,09		
	3.7.4	20,44			3.1.4	73,40			3.13.4	115,67		
	3.7.5	11,60			3.1.5	97,38			3.13.5	65,00		
oil 5 g/m²	3.8.1	21,41	45,12	16,86	3.2.1	31,94	65,54	28,64	3.14.1	70,84	97,01	23,90
	3.8.2	36,46			3.2.2	72,99			3.14.2	98,39		
	3.8.3	51,88			3.2.3	46,93			3.14.3	135,13		
	3.8.4	65,85			3.2.4	107,26			3.14.4	95,64		
	3.8.5	50,01			3.2.5	68,58			3.14.5	85,03		
oil 7 g/m²	3.9.1	35,92	34,56	3,47	3.3.1	105,14	102,82	25,54	3.15.1	101,79	102,77	8,99
	3.9.2	37,60			3.3.2	114,94			3.15.2	115,17		
	3.9.3	33,32			3.3.3	68,47			3.15.3	94,67		
	3.9.4	36,88			3.3.4	136,00			3.15.4	94,11		
	3.9.5	29,08			3.3.5	89,56			3.15.5	108,09		
teflon foil 100 mm²	3.10.1	131,63	115,61	13,01	3.4.1	109,85	128,79	18,31	3.16.1	129,95	139,09	15,82
	3.10.2	105,60			3.4.2	139,86			3.16.2	121,33		
	3.10.3	127,90			3.4.3	117,98			3.16.3	162,69		
	3.10.4	107,31			3.4.4	121,27			3.16.4	145,22		
	3.10.5	105,59			3.4.5	155,00			3.16.5	136,25		
teflon foil 50 mm²	3.5.1	69,79	65,02	12,23	2.5.1	83,75	66,53	17,68	3.17.1	121,04	88,22	26,60
	3.5.2	75,68			2.5.2	60,28			3.17.2	61,95		
	3.5.3	75,79			2.5.3	50,49			3.17.3	71,17		
	3.5.4	50,75			2.5.4	87,00			3.17.4	112,40		
	3.5.5	53,08			2.5.5	51,11			3.17.5	74,53		
90% r.h.	3.6.1	95,14	46,68	32,14	2.6.1	123,30	192,29	19,77	3.18.1	108,96	64,81	26,04
	3.6.2	12,93			2.6.2	139,30			3.18.2	47,68		
	3.6.3	50,56			2.6.3	131,91			3.18.3	52,58		
	3.6.4	52,46			2.6.4	119,48			3.18.4	47,14		
	3.6.5	22,29			2.6.5	169,21			3.18.5	67,70		

Table 5.5: Evaluated defect area within an overlap bonded area of 940mm² for adhesive Betamate 1496 and aluminium adherends

	Bondline thickness 0,2 mm				Bondline thickness 0,5 mm				Bondline thickness 1,0 mm			
inserted defect	specimen	defect area [mm²]	mean value of defect area [mm²]	standard dev. [mm²]	specimen	defect area [mm²]	mean value of defect area [mm²]	standard dev. [mm²]	specimen	defect area [mm²]	mean value of defect area [mm²]	standard dev. [mm²]
teflon foil 64 mm²	4.10.1	150,32	94,72	31,42	4.4.1	71,33	81,12	9,97	4.16.1	93,60	96,63	8,61
	4.10.2	77,30			4.4.2	93,93			4.16.2	88,48		
	4.10.3	88,81			4.4.3	72,68			4.16.3	89,74		
	4.10.4	78,59			4.4.4	78,75			4.16.4	103,39		
	4.10.5	78,60			4.4.5	88,93			4.16.5	107,94		
teflon foil 32 mm²	4.11.1	37,83	36,27	2,61	4.5.1	52,48	50,89	7,36	4.17.1	66,81	60,86	10,36
	4.11.2	39,51			4.5.2	49,92			4.17.2	50,96		
	4.11.3	33,07			4.5.3	59,44			4.17.3	67,14		
	4.11.4	36,66			4.5.4	39,30			4.17.4	48,42		
	4.11.5	34,28			4.5.5	53,30			4.17.5	70,96		
90% r.h.	4.12.1	223,24	277,89	53,24	4.6.1	204,33	195,63	25,64	4.18.1	228,40	248,57	19,02
	4.12.2	221,90			4.6.2	215,65			4.18.2	228,89		
	4.12.3	336,52			4.6.3	175,65			4.18.3	270,40		
	4.12.4	318,49			4.6.4	220,53			4.18.4	260,26		
	4.12.5	289,32			4.6.5	161,97			4.18.5	254,90		

Table 5.6: Evaluated defect area within an overlap bonded area of 940mm² for adhesive Terokal 5070 and aluminium adherends

	Bondline thickness 0,2 mm				Bondline thickness 0,5 mm				Bondline thickness 1,0 mm			
inserted defect	specimen	defect area [mm²]	mean value of defect area [mm²]	standard dev. [mm²]	specimen	defect area [mm²]	mean value of defect area [mm²]	standard dev. [mm²]	specimen	defect area [mm²]	mean value of defect area [mm²]	standard dev. [mm²]
teflon foil 64 mm²	5.10.1	85,27	73,27	8,54	5.4.1	79,00	86,97	12,57	5.16.1	76,28	89,83	9,15
	5.10.2	65,00			5.4.2	94,50			5.16.2	91,15		
	5.10.3	79,02			5.4.3	101,40			5.16.3	90,62		
	5.10.4	69,37			5.4.4	69,83			5.16.4	89,11		
	5.10.5	67,69			5.4.5	90,13			5.16.5	102,01		
teflon foil 32 mm²	5.11.1	40,80	41,04	3,62	5.5.1	77,19	50,68	16,91	5.17.1	37,51	84,23	39,06
	5.11.2	45,71			5.5.2	54,48			5.17.2	110,12		
	5.11.3	35,72			5.5.3	42,61			5.17.3	70,12		
	5.11.4	40,55			5.5.4	47,12			5.17.4	136,63		
	5.11.5	42,43			5.5.5	31,99			5.17.5	66,79		
90% r.h.	5.12.1	112,54	97,22	34,56	5.6.1	42,79	131,40	70,69	5.18.1	169,24	122,61	71,13
	5.12.2	151,29			5.6.2	189,67			5.18.2	184,55		
	5.12.3	74,99			5.6.3	75,71			5.18.3	67,51		
	5.12.4	71,19			5.6.4	205,56			5.18.4	165,72		
	5.12.5	76,07			5.6.5	143,28			5.18.5	26,01		

The neutron distribution across the overlap width in pixels is shown on the upper diagram of Fig. 5.19 and the respective adhesive thickness on the lower diagram. The thickness is approximately 1,0 mm with insignificant variation. The reduction of thickness between 20 and 30 mm overlap width is due to teflon layer inserted in the adhesive and the fact of lower neutron absorption.

5.7.5 Bitmap analysis

The Bitmap Analysis command on the Measure menu has been used to view the pixel values of the active window in numeric format, Fig. 5.20. The intensity values have been exported to Microsoft's Excel spreadsheet and through calibration and use of radiation attenuation law in matter the bondline thickness for the overlap area was estimated as described in 5.7.2. It is worth here noting that the table of Bitmap analysis includes approximately 20.000 values over 1440 mm^2 of an steel overlap and that means that one measurement value corresponds to only 0,3 mm on the x,y coordinates. For an aluminium overlap of 960 mm^2 a bitmap analysis includes approximately 13.000 intensity values.

The Surface Plot (or 3-D Plot) tool creates a three-dimensional representation of the intensity of an image being able to evaluate the image and the defects from several aspects by rotating the image in the axis.

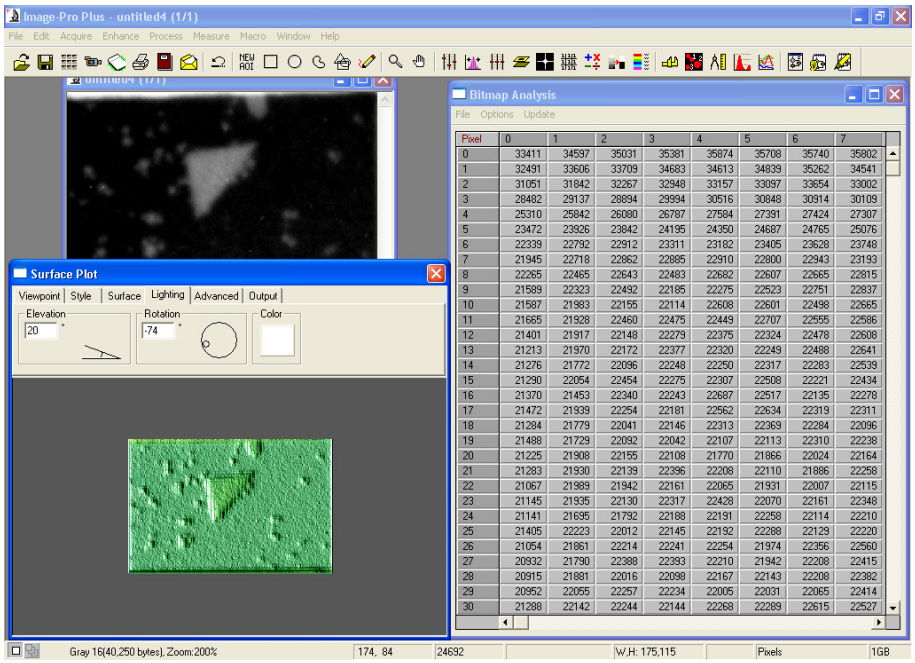

Fig. 5.20: Surface plot between the metals and respective intensity measurements for every x/y-coordinates-pair.

5.7.6 Quantitative estimations of the defect area

Through further tools in the Measure Menu, it is possible to count the number of cells in a sample and measure multiple objects i.e. defect area within a single image, Fig. 5.21. Once the objects have been counted and measured, you can use the Count/Size window's Measure menu options to automatically sort and classify the objects by any of the measured characteristics.

5.8 Concluding remarks on imperfections

The results given in Table 5.3 to Table 5.6, show that the mean value of the total defect area is more or less independent of the adhesive applied. The mean value of the defect area and the scatter band 2s for every sample series are demonstrated separately for every bondline thickness in the diagrams of Fig. 5.22. The effect of the artificial imperfections on the strength of the joints is further studied in chapter 8.

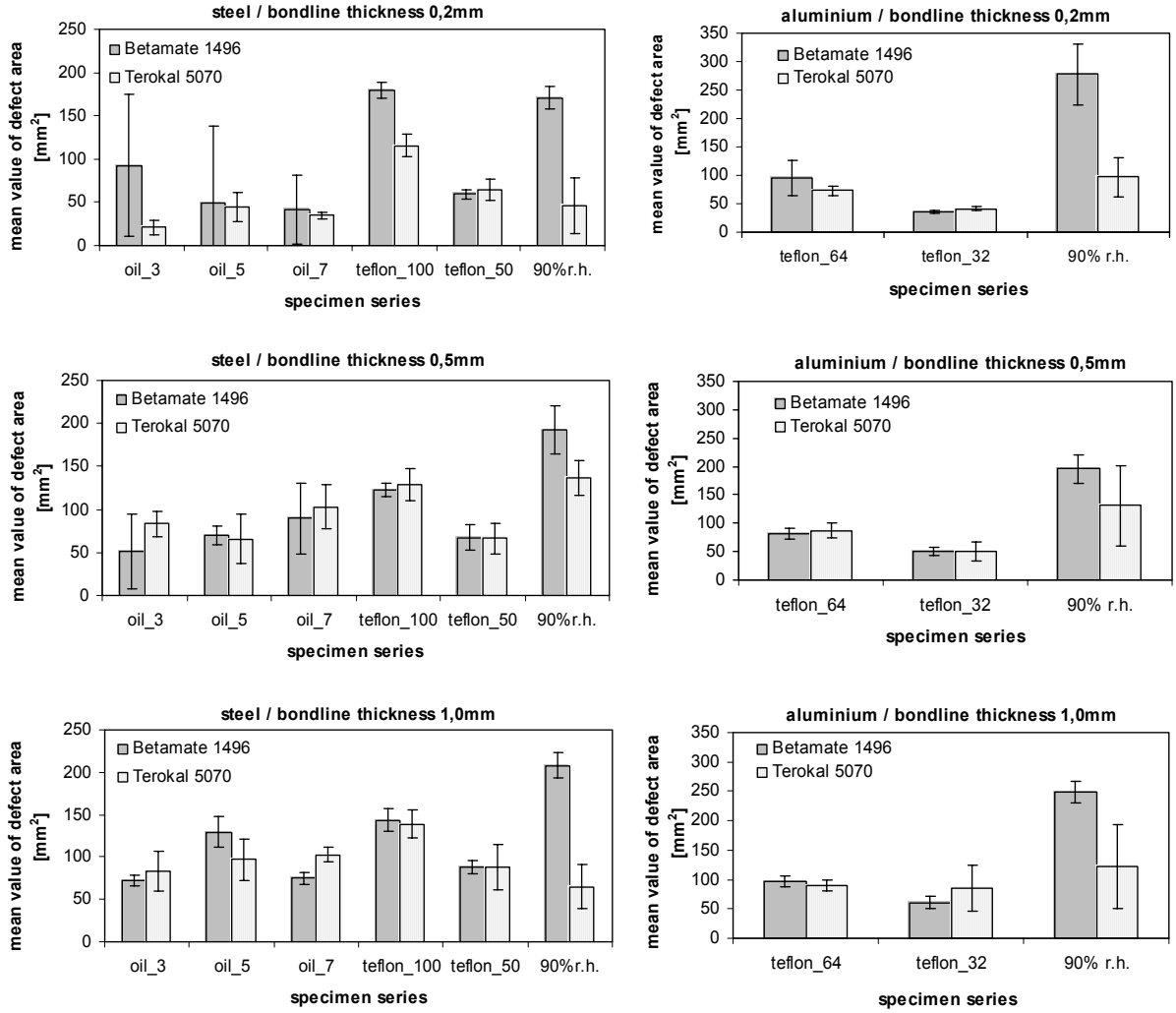

Fig. 5.22: Mean value and the scatter band 2s of evaluated imperfections in steel or aluminium single lap joints bonded with "Betamate 1496" and "Terokal 5070" in 0,2, 0,5 and 1,0 mm bondline thickness.

5.8.1 Oil contamination

Based on Fig. 5.13 and Fig. 5.14 (and Figures of Annex A) the evaluated defect area was always smaller than the initially intended defect area because, an amount of oil during manufacturing was spread out over and outside the overlap area. To make matters worse the structural adhesives used under consideration have the ability to absorb oil contamination to some extent during curing, thus rendering them even more difficult to detect defects. Another possible explanation for this reduced detectability is that oil is being squeezed into pores of the adhesive. The transmission images seem to estimate this situation rather reliably after all.

5.8.2 Teflon layers

The inserted teflon foil, had in each case the same thickness as the bondline, i.e. 0,2/0,5/1,0 mm. In all specimens with teflon inserts as imperfection, Fig. A1 to Fig. A12 of Annex A, the evaluated total defect area appears – because of the inserted glass balls or random pores during manufacturing – somewhat larger than the actual artificial imperfection. This is due to the observations on the transmission images that inserted glass balls or random pores occurring during manufacturing of specimens are indeed detected by neutron radiography, and, consequently, evaluated by image analysis software along with the teflon imperfections as belonging to the defect area. The fine depiction of the imperfections, random or defined, is gained due to the high resolution images, and the approximation to the parallel beam geometry.

5.8.3 90% relative humidity

Similar conclusions are reached for specimens with 90% relative humidity. The transmission images show the water contamination at the edges of the overlap area with great refinement. According to [Fassbender 1980], investigations applying ultrasonic methods showed that C-scans do not record the full extent of the bonded area, i.e. defects at the edges of overlap; this was also observed by the authors [Michaloudaki 2004a], when performing experimental investigations through ultrasonic inspection on the specimens of Fig. 5.13 to Fig. 5.16. Results on this issue are presented in Chapter 6. The effect of humidity in transmission images was observed in three characteristic types; in form of large voids, gross porosity, i.e. oblong pores close to each other, or finally, as slight porosity. The neutron attenuation in water is similar to the adhesive, showing also similar contrast on the transmission images. Moisture uptake was absorbed in the adhesive's chemical structure leaving voids or porosity at its former position. The water absorption confirms the dendritic porosity, gross or slight identified by visual inspection of the fracture surface of the specimens, Fig. 8.5 und Fig. 8.6.

The mean value of individual results (humid area in mm^2), Table 5.3 to Table 5.6, specimens with 0,2 and 1,0 mm, differ for the two different adhesives by more than 50%. The structural adhesive "Terokal 5070" absorbs water contamination possibly to some small extent during curing - without producing voids or porosity -, thus rendering it even more difficult to detect defects due to humidity. Another possible explanation for this reduced detectability is that humidity cannot penetrate at all into the chemical structure of this adhesive, but remains as a dispersed irregularity within its mass. Neutron attenuation in water and hydrogen bearing adhesive is similar, thus preventing estimation through various contrast levels. The effect of moisture contamination was investigated by Kosteas & Michaloudaki in steel bonded joints including also destructive tests, ultimately aiming at a correlation with actual strength values [Kosteas 2003] and [Michaloudaki 2004b]. These observations will be further evaluated in chapter 8, in an attempt to explain the different behaviour and quantify ultimate strength of the joints for the two adhesives.

6 Ultrasonic Measurements

The most popular ultrasonic testing application has been associated with thickness measurement of a test object and defect location within a material or a joint. Recent work has extended the basic ultrasonic test philosophy in the field of adhesive bonding inspection. Due to different physical and mechanical properties, adhesives do not permit the full implementation of the ultrasonic method. This chapter reviews the physical principles associated with ultrasonic testing and the particular items that must receive special attention when inspecting adhesively bonded parts in a structure, as well as describe the respective evaluation of test specimens.

6.1 Application range

Nothing is "perfect" and for reasons of safety and costs, materials have to be inspected whether they really fulfil the desired properties. Details on numerous application possibilities of ultrasonic and the appropriate techniques are given by [Müller 1973], [Lehfeldt 1973] and [Krautkrämer 1977]. A few significant application areas in engineering discussed are:

- transportation means for inspection of rolling stocks, aircrafts, rails,
- metal producing industries for testing cast, forged and rolled products,
- in ship building for testing joints
- in the machine manufacturing and electronics industries for testing semi-finished products, for welded, soldered, and bonded joints
- in the chemical industry for testing products and compounds, for monitoring parts of installations subject to corrosion
- in science and research for determining solid body and molecular properties

The significant advantages and development of the method show even today that ultrasonic still remains the most widespread used among other non-destructive methods.

6.2 Developments in Ultrasonic Evaluation

In work reported by Rose and Mayer [Rose 1973] attempts were made to correlate single ultrasonic testing measurements with the potential performance of the adhesive joint structure. Results were obtained for a few specific defect situations in structures. A general approach for the overall identification of irregularities and/or potential structure performance though, was not tackled in detail. Chang et al. [Chang 1975] reported extensive studies where correlation was attempted of various testing parameters with adhesive bond strength of a multilayered structural system. Also here reasonable results were reported only for a few specific situations. Trying to advance the state of the art in non destructive testing approach, Meyer and Rose [Meyer 1977] reported a physical model analysis where ultrasonic attenuation influences were considered in an adhesively bonded system. A variety of undercure and overcure cases were studied in detail. Changes in the ultrasonic signal are based on reflection-signals of overcured or undercured adhesively bonded layers within the structure. Success was obtained by analysing the frequency profile curve and evaluating the changes due to the presence of defects. This work provided guidelines for transducer selection and resolution requirements referring to the difficult adhesive bond inspection problem.

Interesting work was reported by Chernobelskays et al. [Chernobelskays 1979], where a high resolution ultrasonic probe was used to carefully resolve the echoes from each side of a bonded layer. Chaskelis and Clark [Chaskelis 1980] attempted to explain some of the degradation

problems by means of ultrasonic evaluation. Also, wave propagation modes beyond the commonly used compression- and shear-wave through an adhesive system are evaluated. Alers and Elsley [Alers 1970] reported their quantitative ultrasonic signal evaluation techniques used in establishing a test method for studying the adhesive bond strength as a function of wave propagation parameters. Budenkov et al. [Budenkov 1977] examined the possibility of testing the strength of the joints by means of ultrasonic interference waves. Rose [Rose 1976] pointed out the simplicity of void or delamination detection in adhesively bonded structure. Difficulties in the detection arise by improper surface preparation and the subtle edge effects. Woodmansee [Woodmansee 1978] described a trough transmission technique for detecting porosity in bondlines.

Rokhlin et al. [Rokhlin 1981] described an ultrasonic interference wave technique useful for predicting the strength of bonded joints. Djordjevic and Venables [Djordjevic 1981] outlined their experiences in ultrasonic A-scan, C-scan and resonance measurements for evaluating the quality of adhesively bonded components. Williams and Zwicke [Williams 1982] described their approaches in pattern recognition reliable for evaluating the integrity of bonded structures for a variety of defect cases.

The popular Fokker bond tester and its resonance concept was discussed by Schlieckelmann [Schlieckemann 1982] who indicated some of his experiences and values of the procedure. Knollman and Hartog [Knollman 1982] described a shear modulus gradient technique based on ultrasonic Rayleigh waves that propagate through the bonded joint. A detailed state-of- the-art was reported by Curtis [Curtis 1982] discussing the factors that control the joint strength. A variety of resonant- and pulse echo-techniques were reviewed along with the discussion of plate and interfacial waves and their potential for evaluating the integrity of bonded components. Rose et al.[Rose 1983] reported a feasibility study based on pulse echo techniques and some physical modelling aspects used in pattern recognition technique. Fundamental results were obtained for solving the lack of surface preparation problem in a metal-to-metal adhesively bonded component using a transfer function feature and spatially averaged peak to peak amplitude feature. Exploitation of the normal beam technique is well demonstrated by Rose et al. A specific selection of test parameters and specimens and utilisation of high frequencies in the ca. 30 MHz region indicated a promise in solving specific problems. Rokhlin et al. [Rokhlin 1986] have considered shear vibrations on the interface to measure adhesion properties. Such assertations have led to the extension of the mostly used longitudinal waves in normal incidence compared to other kinds of waves such as plate surface, and interface ones with transverse components of displacements. The huge difficulties in the generation and reception of such waves in a field inspection have led recently to the application of low frequency oblique incidence technique. Claus and Kline [Claus 1979] and later Rose and Pilarski [Rose 1986] studied the utility of waves to interrogate the interface between the adhesive and the substrate. Many of the procedures outlined in the literature have been adopted in an attempt to solve the general defect identification problem in an adhesively bonded structure. These procedures have been also utilised in tackling problems associated with quality control, process control, and in-series inspection. Some of the methodologies associated with these new developments are outlined in a paper by [Rose 1985]) that reviewed a feature-based ultrasonic test technique and the physical modelling associated with data collection and analysis of identifying defects.

The lack of satisfactory testing in the adhesive-adherend interlayer is particularly important, as it is the layer that governs the susceptibility of the joint to the environmental attack. This problem has been the subject of intensive research of a theoretical nature for over 20 years and a review of early work in the field is given by Thompson and Thompson [Thompson 1999] and later by Achenbach [Achenbach 1991], [Tang 1999]. Several models about the ultrasonic analysis of non-linear response of adhesive bonds have been suggested and theoretically investigated. It may, however, be possible to monitor the onset of environmental attack and this has been the subject of extensive recent work by [Cawley 2002]). Recent experimental investigations by Roye and

Michaloudaki based on ultrasonic measurements with pulse echo, through transmission, spectroscopy and impact resonance techniques regarding their implementation potential and their reliability, lead to reproducible test results within narrow tolerances only enhanced by ongoing further developments in instrument technology [Roye 2003].

6.3 Ultrasonic physics

Ultrasonic waves can be generated inside a material by placing an ultrasonic transducer on a test object as illustrated in Fig. 6.1. Commonly employed ultrasonic transducers are made of piezoelectric crystals. The piezoelectric device converts electrical energy applied to the crystal into mechanical energy that produces a wave or pulse that travels through the material. A couplant – water, mineral oil, or glycerine - is required between the ultrasonic transducer and a test material that allows efficient transfer of energy from the transducer to the test object. One of the most important parameters associated with ultrasonic wave propagation is the wave velocity v of the material. It takes a finite time for a wave or pulse to travel from one position to another inside the joint. The faster the wave speed, the shorter the time between two points. The pulse travels to a reflecting surface, which could be the back surface of the bonded joint or possibly an inclusion in it. When the echo returns to the crystal by way of a reversed piezoelectric effect, the sound energy is now converted into electrical energy. A suitable display can be obtained on an oscilloscope. By employing the wave velocity property v of a material in question, the arrival time t, mentioned on an oscilloscope, can be related to the thickness d or distance to a particular reflector through the formula:

$$t = \frac{2d}{v} \qquad \text{Eq. (6-1)}$$

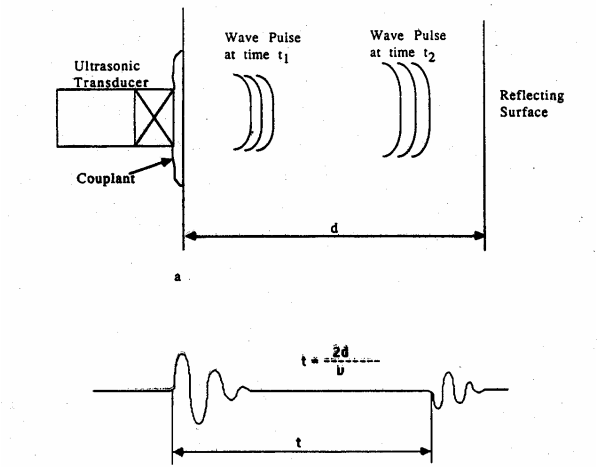

Fig. 6.1: Basic ultrasonic test principle. (a) pulse echo setup, (b) oscilloscope display

According to Rose (1991), the majority of ultrasonic investigations carried out makes use of arrival time analysis and subsequently a wave velocity value for thickness measurement and for defect location. However it is difficult to use precisely the wave velocity in a complex system like metal – adhesive joints because of its inhomogeneous and anisotropic characteristics.

A distinction between pulse-echo and through-transmission modes about the ray paths of a single pulse is made by Adams (1987). When ultrasonic is used in the pulse-echo mode, the returning signals are composed of a series of reflections, some of which have traversed the bondline and others of which have not. A high resolution (high frequency) probe is necessary to separate the various components, shown schematically in Fig. 6.2. For instance, pulse B has passed twice through the top adherend while pulse C has also passed twice through the adhesive. An indication of the quality of the adhesive can be obtained by amplitude changes between these two

pulses. If there is a void or some other form of defect, pulse C will be usually reduced in height and shifted in time. Pulse A is by far the strongest and subsequent reflections between the surface of the top adherend and the front of the transducer can cause interference with B and C.

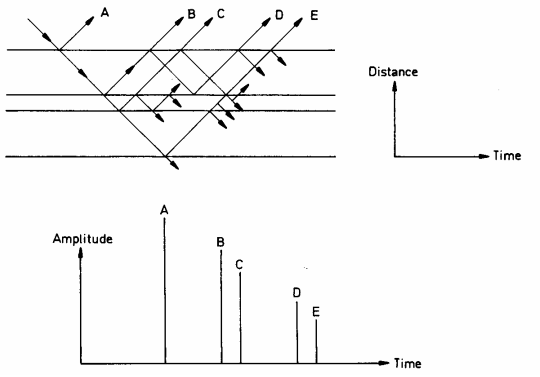

Fig. 6.2: Pulse echo ultrasonic in a bonded joint. (a) ray paths of a single pulse, (b) amplitude time relationship

When using the through-transmission mode, the first pulse received, A in Fig. 6.3 has travelled only once through the adhesive and this is quickly followed by a series of smaller pulses B, C, D etc. which have additionally passed, 2, 4, 6 times through the adhesive. If a void is present, little or no energy is transmitted, giving a clear indication of its presence.

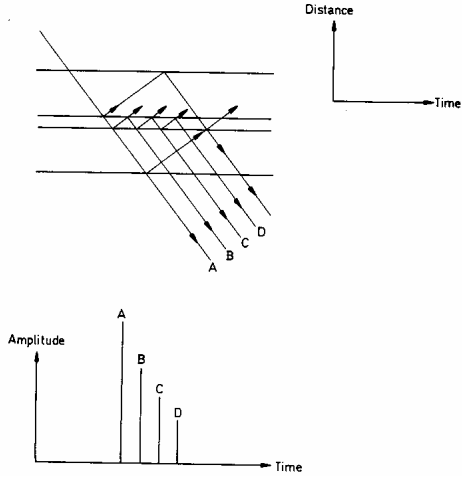

Fig. 6.3: Through-transmission ultrasonic in a bonded joint. (a) ray paths of a single pulse, (b) amplitude time relationship

Pulse echo and through-transmission techniques were performed initially only in a small sample size appointing the optimum technique in relation to applicability and reliability. The techniques are described in the next paragraphs and the results compared with each other. The amplitude measurement of the reflector echo was consequently selected for performing testing in the complete specimen series and the reasons for this selection are given in 6.8.

6.4 Flaw display methods

The most commonly used methods for displaying ultrasonic information are designated as A-, B- and C-scans, Fig. 6.4. The A-scan displays the voltage amplitude as a function of time and it can be read on an oscilloscope. The relative amplitudes of the reflected echoes are indicative of the existence of a defect and the time for an echo to appear serves to locate the depth. Naturally, each measurement gives only the situation in one position and several points have to be tested to obtain information from the whole specimen.

In the B-scan the vertical axis of an oscilloscope screen displays the time required for a pulse to leave the front surface and be reflected back to the transducer from the bonds and the back surface. The horizontal axis shows the distance the transducer moves along the front surface. The B-scan visualises any void in the adhesive layer easily by showing almost no signal from the interfaces below the defect. Thus, the B-scan also permits determination of the depth of the void.

Ultrasound imaging is a special method and it uses the principle of the C-scan [Nieminen 1991]. In the C-scan mode of operation, the transducer scans the surface in a regular raster fashion and the defects are shown as bright patches. A C-scan shows clearly the defect areas, but it does not give any information in the through-thickness direction of the flaw. However, mechanical scanning is slow and the resolution is severely limited by the beam diameter. If focused ultrasound is used, the field width is smaller and the resolution better.

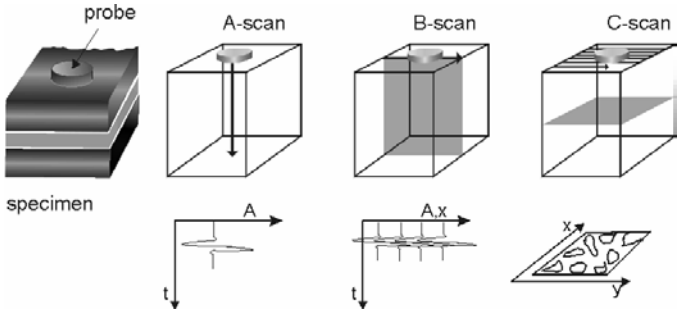

Fig. 6.4: Flaw display methods in ultrasonic method; above: testing schema and below: measurement result

Using the above mentioned flaw display methods with through-transmission and pulse-echo techniques it is possible to analyse simple lap joints and detect flaws as thin as 10 nm and as small as approximately 150 μm in diameter [Camahort 1979]. However, several transducers are required for samples of different sizes and the resolution depends on the frequency of the ultrasound, the diameter of the transducer and the point density of the measurements.

6.5 Pulse-echo technique

The pulse – echo technique utilizes short ultrasound pulses and observes individual echoes from each interface in the sample. Since there is only one transducer, which works both as transmitter and receiver, the technical problems associated with the access of both sides of the sample can be avoided. The specimens and the transducer / receiver were placed inside a water filled tank. The amplitude and position of the echoes are used to detect the defect. A void or a debonding region can be observed and its position relative to the interfaces in the specimen determined easily, since the echoes from the lower interfaces are drastically decreased or totally missing. Although the interpretation of the echo pattern is usually quite straightforward with simple lap joints, the evaluation of more complex structures and shapes requires qualified personnel. The purpose of ultrasonic equipment used in the pulse-echo method is to make the difference between "sound input" and "sound output" technically measurable. With the technique used for our investigations, the amplitude measured and evaluated was reflector echo, either a backwall echo, or an intermediate echo Fig. 6.5.

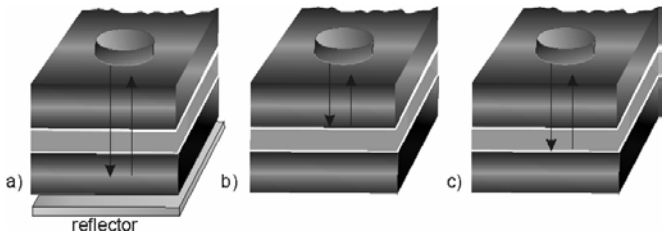

Fig. 6.5: Measurement of the a) reflector echo, b) backwall echo and c) intermediate echo

6.5.1 Amplitude measurement of the reflector `s echo

The configuration for the pulse-echo technique is shown in Fig. 6.5a) and belongs to the conventional ultrasonic techniques. An ultrasonic pulser/receiver (Model USD 15X) was used to excite the ultrasonic transducer and to receive the ultrasonic signals. An ultrasonic transducer with a central frequency of 5 MHz was used. The distance between the pulser and the specimen was 50 mm in the water tank. An aluminium sheet (reflector) was placed under the specimens. The use of a reflector in our investigations demanded that both sides of the sample should be easy to access. The ultrasonic pulse propagated into all layers of the bond and the signal was reflected on the surface of the aluminium sheet. The reliability of measurement comprising the whole joint can be significantly enhanced by the reflector.

6.5.2 Amplitude measurement of the backwall echo

Another option of the pulse-echo technique is the amplitude measurement of the backwall echo. A pulser/receiver (Model USD 15X) with a central frequency of 10 MHz was used to excite the ultrasonic pulse and to receive the ultrasonic signals. The distance between the pulser and the specimen in the water tank was 30mm. The pulse travels through the upper adherend and is reflected by a discontinuity or the surface of the upper interlayer, Fig. 6.5b). In this way we get information about the upper interlayer but no assessment about the bondline itself.

6.5.3 Amplitude measurement of the intermediate echo

In case that there is also another reflector within the sound beam, then between the initial echo and the backwall echo appears another one, caused by partial reflection of the sound wave on the discontinuity. An ultrasonic transducer with a central frequency of 10 MHz was used. The advantage in this case is that a declaration is provided for the whole joint, Fig. 6.5c), but this is not reliable enough, as the intermediate echo is within the initial pulse and therefore covered by it.

6.6 Through-transmission technique

In the through-transmission technique we follow the magnitude of the transmitted energy. In contrast to the pulse echo technique, separate transducers are used for transmitting and receiving the pulses and they are located on opposite sides of the sample, Fig. 6.6. When the pulse reaches an imperfection, the signal at the receiver disappears or decreases significantly. Thus, this technique can be used to locate and roughly determine the size of the flaws. A pulser and a receiver (Model USD 15X) were used to excite the ultrasonic transducer and to receive the ultrasonic signals respectively. An ultrasonic transducer with a central frequency of 5 MHz was used. Through-transmission technique requires a liquid coupling agent on both sides of the specimen. Transducers were placed in water and the testing was carried out by immersing the bonded specimen into water, Fig. 6.7. The main disadvantage of this technique is the lack of information, as to where the flaws are positioned in pulse direction. Complex structures cannot be analysed, and even with specimens of constant thickness it is difficult to keep the relative positioning of the transducers constant.

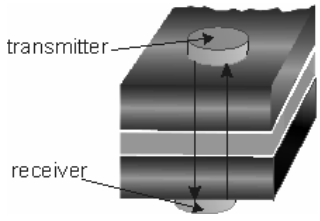

Fig. 6.6: Through-Transmission technique

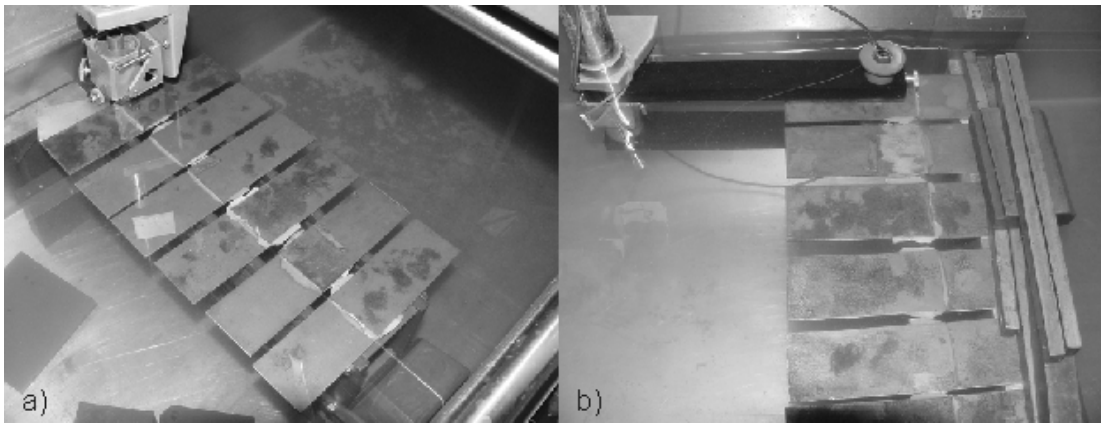

Fig. 6.7: Experimental set up of a) pulse echo technique with one probe as transmitter and receiver and b) through transmission technique with two probes as transmitter and receiver

6.7 Assessment of the conventional techniques

Fig. 6.8 and Fig. 6.9 show typical 5 and 10 MHz C-scans from six lap joints. In both figures the left joint is an ideal bond with no "artificial" imperfections. In automotive fabrication such a joint does not exist, since approximately 3g/mm^2 of oil always remain on the sheets. Joints 2 and 6 are contaminated with two different types of oil, app. 3g/mm^2 in each joint. Joints 3 and 5 contain a teflon layer 100 or 50 mm^2 respectively. The teflon layer is 0,5 mm thick, exactly the same as the adhesive layer itself representing the absolute lack of adhesion on both adherends. Specimen 4 represents the moisture content in an adhesive bonded joint, a common case appearing both during the application of the adhesive and during service performance. The joint was treated for 21 days at 20 °C with 90% relative humidity before the heat curing.

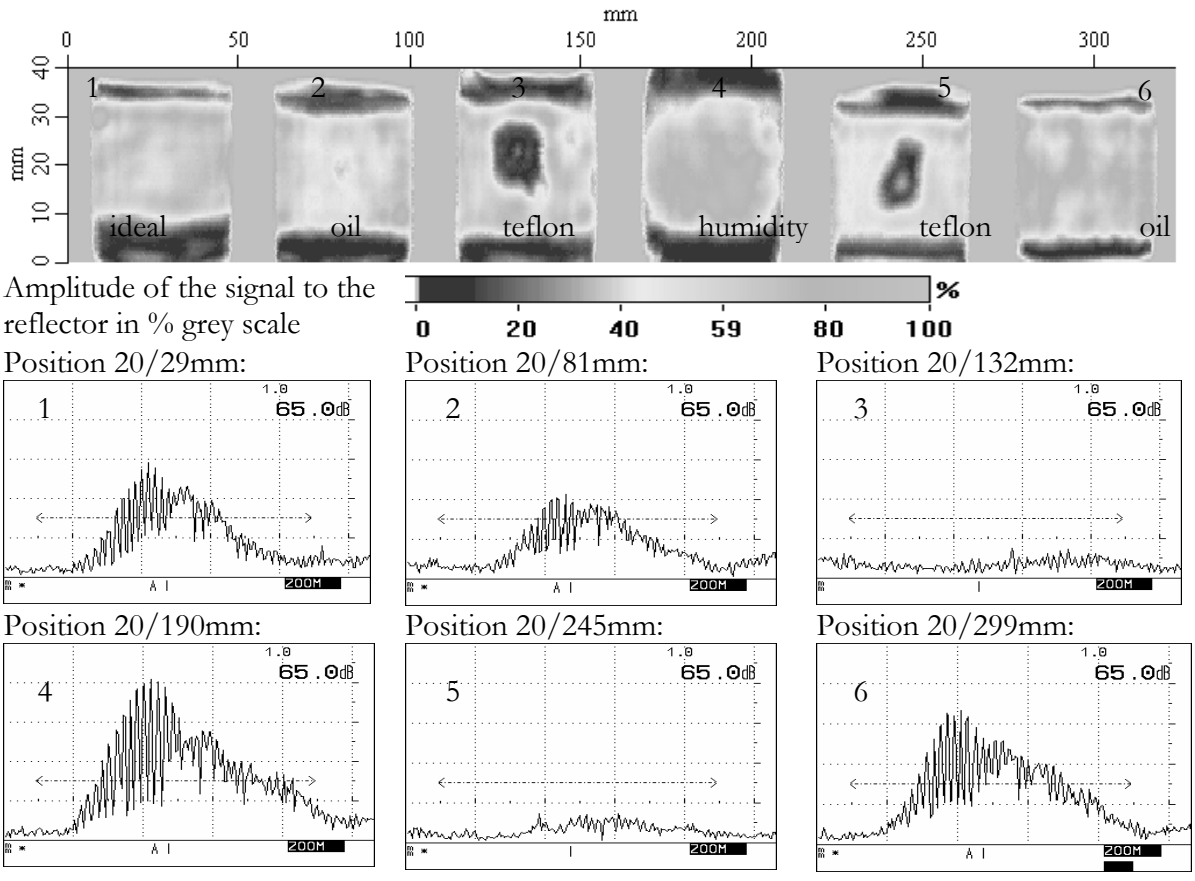

Fig. 6.8: 5 MHz C-scan of reflector echo of an ideal bond (1) and bonds with imperfections such as oil drops (2, 6), teflon layers (3, 5), moisture (4)

Flaw detection is illustrated in Fig. 6.8 with the pulse-echo technique and the amplitude measurement of the reflector ´s echo. The ultrasonic pulse was generated in the transmitter and propagated into all layers of the bond and the signal was reflected on the surface of the aluminium reflector sheet. The amplitude, Fig. 6.8, supplies information about the propagation of the sound not only through the adhesive but also the layers of the joint. High amplitudes declare a good bonding and high propagation ability of the sound through the adhesive. However with this technique the exact position of the defects cannot be attributed to specific layers of the joint. The percentage colour scale from red to blue in Fig. 6.8 provides an indication about the adherend-adhesive interlayer and information about possible contaminations, i.e teflon is shown in black, oil contaminants in light grey. The fact that at the beginning and the end of the joint the area is in black colour does not indicate a defect but the difference in thickness between adherend and joint.

The flaw detection with the pulse-echo technique and the amplitude measurement of the backwall echo is illustrated in Fig. 6.9. The ultrasonic pulse propagated through the upper adherend and the signal was reflected on the upper interlayer. The amplitude measurements of the backwall echo are shown on the displays. In all cases the fifth backwall echo was evaluated for reliability reasons. The amplitude informs only about the propagation of the sound through the first interlayer of the joint. That means that for the adhesive and the second interlayer we gain no information. On the other side we can determine readily the position of an imperfection since the detection does not cover the whole joint but only the upper adherend-adhesive interlayer. Comparing Fig. 6.8 and Fig. 6.9 we come up with many differences in the detection techniques. The C-scans and the amplitude on the displays show that the amplitude measurement of the reflector is more reliable than the amplitude measurement of the backwall echo as the scan information correlates better to the actual inserted flaws. Joint 4 with the water contaminantion exhibits a lower reflection coefficient.

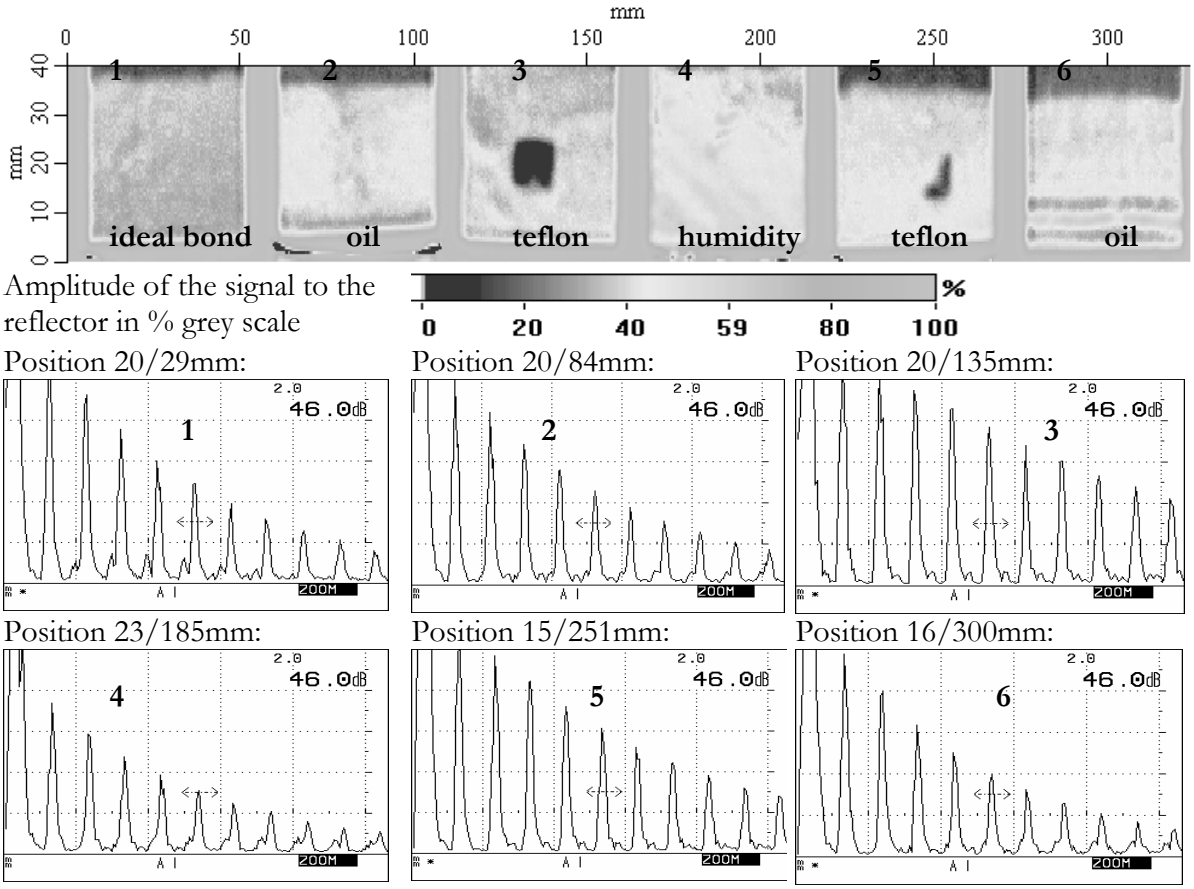

Fig. 6.9: 10 MHz C-scan of backwall echo of an ideal bond (1) and bonds with imperfections such as oil drops (2, 6), teflon layers (3, 5), moisture (4)

6.8 Experimental set up of selected pulse echo technique

Considering preliminary investigations of Kosteas & Michaloudaki the pulse echo technique with the amplitude measurement of the reflector, Fig. 6.10, was preferred for the experimental investigations of the complete testing program due to the following reasons [Kosteas 2002b]:

- It offers more accurate results i.e. reliable depiction of imperfections on the C-scans in comparison with the techniques of the amplitude measurements of the backwall echo or the intermediate echo.
- The ultrasonic pulse propagating into all layers gives an indication of the complete joint until the first or before the second interlayer.
- It appears more flexible for industrial applications in contrast with the through transmission technique, where the opening distance between transmitter and receiver remains constant during testing whereas the thickness of the component varies.

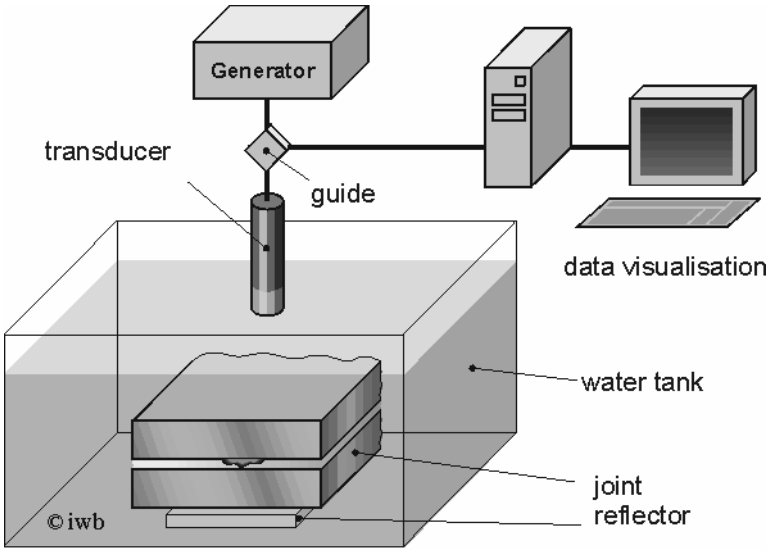

Fig. 6.10: Experimental set-up – specimens and transducer inside a water filled tank

6.9 Evaluation methodology

The evaluation methodology for the estimation of the defect area was accomplished as described in chapter 5.8.

6.9.1 Qualitative observations on the C-scans

Fig. 6.11 to Fig. 6.14 show typical 5 MHz C-scans of the overlap area for the steel or aluminium joints bonded with two epoxies "Betamate 1496" and "Terokal 5070" with 0,2/0,5/1,0 mm adhesive thickness after evaluation. The artificial imperfections were subsequently evaluated by means of image analysis software, Fig. 6.15. Each mean value is representative of a sample size of 5 specimens. Teflon layer in square and triangle form had each time equal thickness as the bondline aiming to represent simultaneously the absolute lack of adhesion and cohesion. Moisture content in an adhesively bonded joint is a common case appearing both during the manufacturing and service performance. The joints were treated for 21 days at 20 °C with 90% relative humidity prior to the heat curing, simulating a defect due to manufacturing. Additional parameters of bondline thickness 0,2/0,5/1,0 mm and aluminium/steel adherends offer a systematic and extensive approach of image evaluation of respective C-scans.

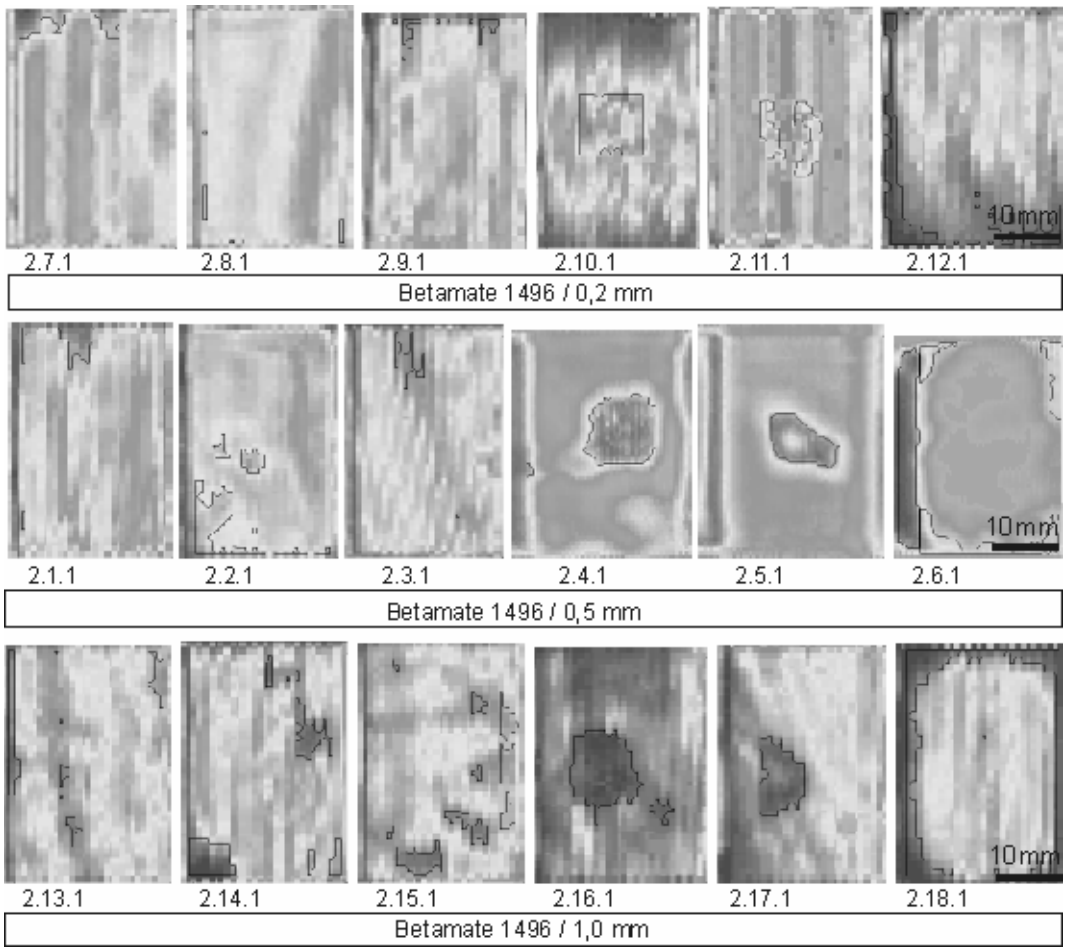

Fig. 6.11: C-scans of the overlap area (1440mm2) for the steel joints bonded with "Betamate 1496".

The detectability of the artificial imperfections is lower than with neutron radiography by distinguishing only between ca. 250 grey levels on the scans. Moreover the poor resolution of the images is responsible for the low detectability especially at smallest defects, i.e. random pores or glass balls. The grey levels from black to white, i.e. teflon foil is shown in black, provide an indication about the adherend-adhesive interlayer and information about possible contaminations, without being able to classify their nature. The fact that around the joint the area is in black colour does not indicate a defect but the difference in thickness between adherend and joint and consequently inability to distinguish signals at joint edges.

The detectability of a given size or depth of defect depends to some extent on the criterion used to decide whether a given area of structure is defective; thus the criterion choice depends on the relative importance of detecting all defects and not rejecting good areas of the structure. The simplest criterion is to reject all areas whose intensity is below a threshold value. This works very satisfactorily when the measured intensity is effectively controlled with calibration measurements. Since the intensity of the joint varies with position, variations in measured intensity are obtained over a good structure. This means that good areas can have a lower intensity than defect zones in other parts of the structure. Hence depending on the threshold value chosen, either defects are missing or good areas are identified as defects. This problem is evident in the C-scans presented here. This difficulty could be reduced by comparing each point measurement with one made at the same point of a similar structure which is known to be free of defects. However this would involve considerable data storage and would not completely overcome the problem since the introduction of defect does not necessarily reduce the intensity.

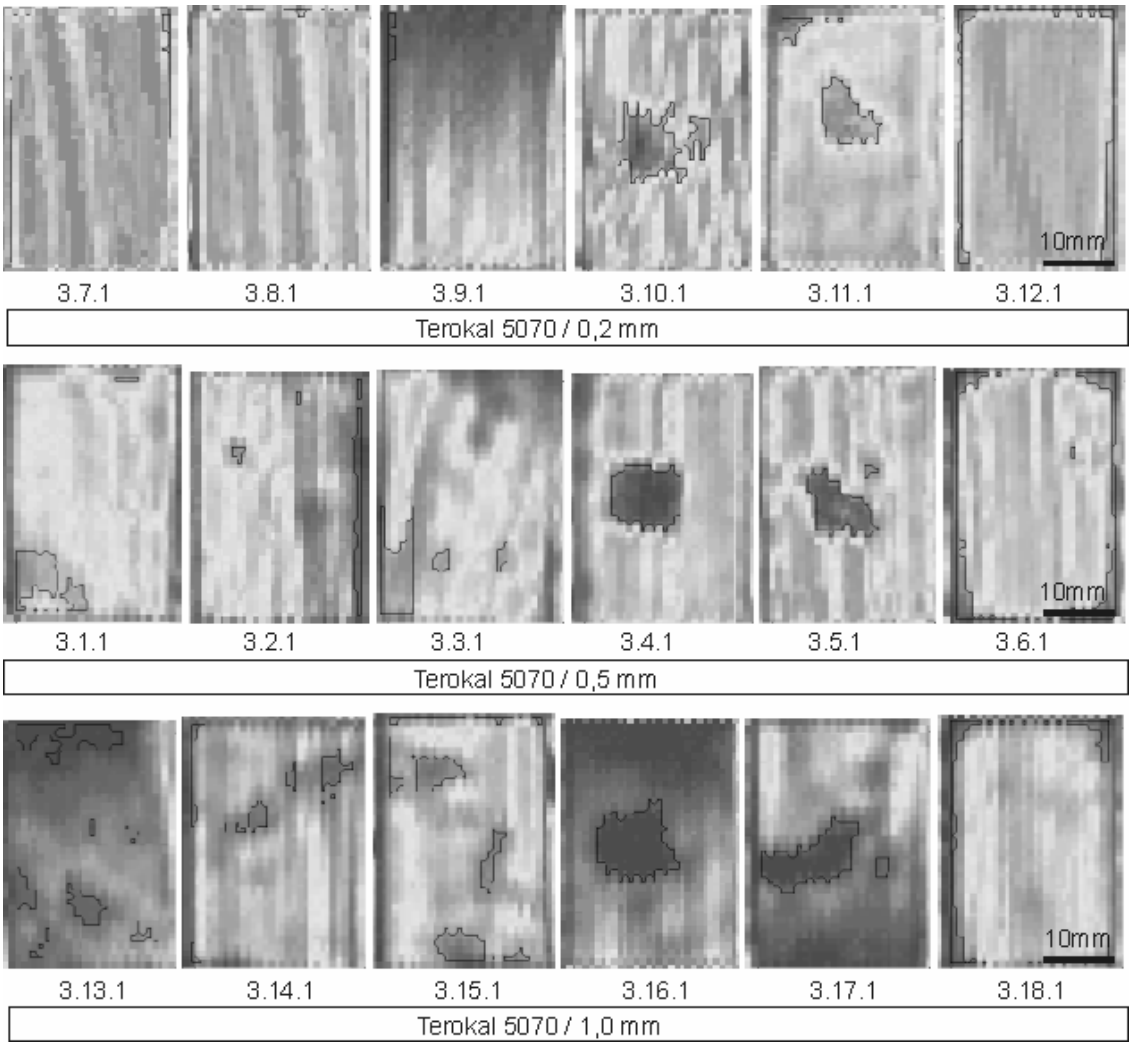

Fig. 6.12: C-scans of the overlap area (1440 mm²) for the steel joints bonded with "Teroka 5070"

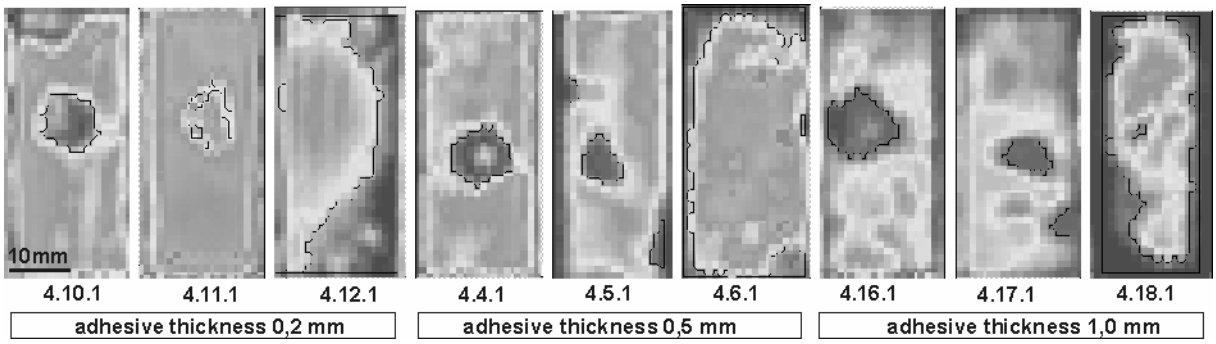

Fig. 6. 13: C-scans of the overlap area (960mm²) for the aluminium joints bonded with "Betamate 1496".

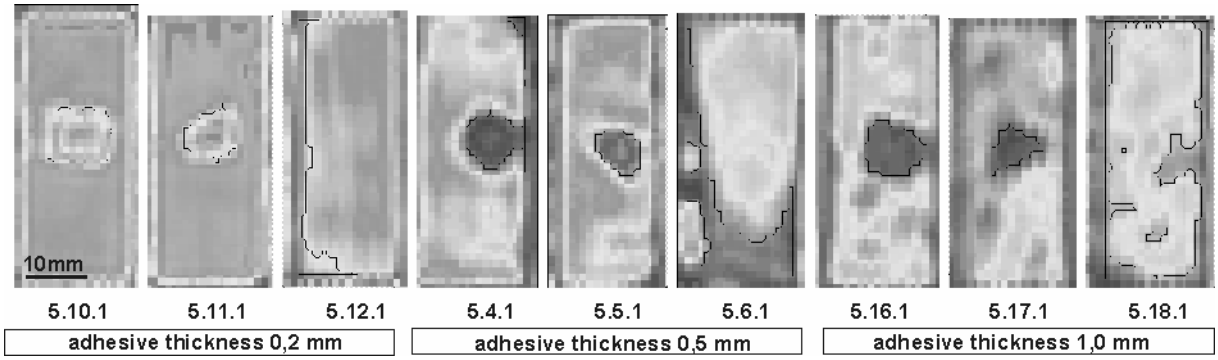

Fig. 6.14: C-scans of the overlap area (960 mm²) for the aluminium joints bonded with "Terokal 5070"

6.9.2 Quantitative estimations of the defect area

If we compare the C-scans, between the two adhesives for the same adherend material, reproducible observations are noted. Very small defects are not detectable or are indicated through the difference in colour, though neither their size nor their form can be exactly deducted. The mean values of humid area, in specimens with 0,2 and 1,0 mm bondline thickness, differ more than 50%, Table 6.1 to Table 6.4. Further detectable defects in the C-scans appear larger than they really are. This is also confirmed in the diagrams of Fig. 6.15, where the mean value of evaluated defects is always higher than expected due to hose-shaped sound beam.

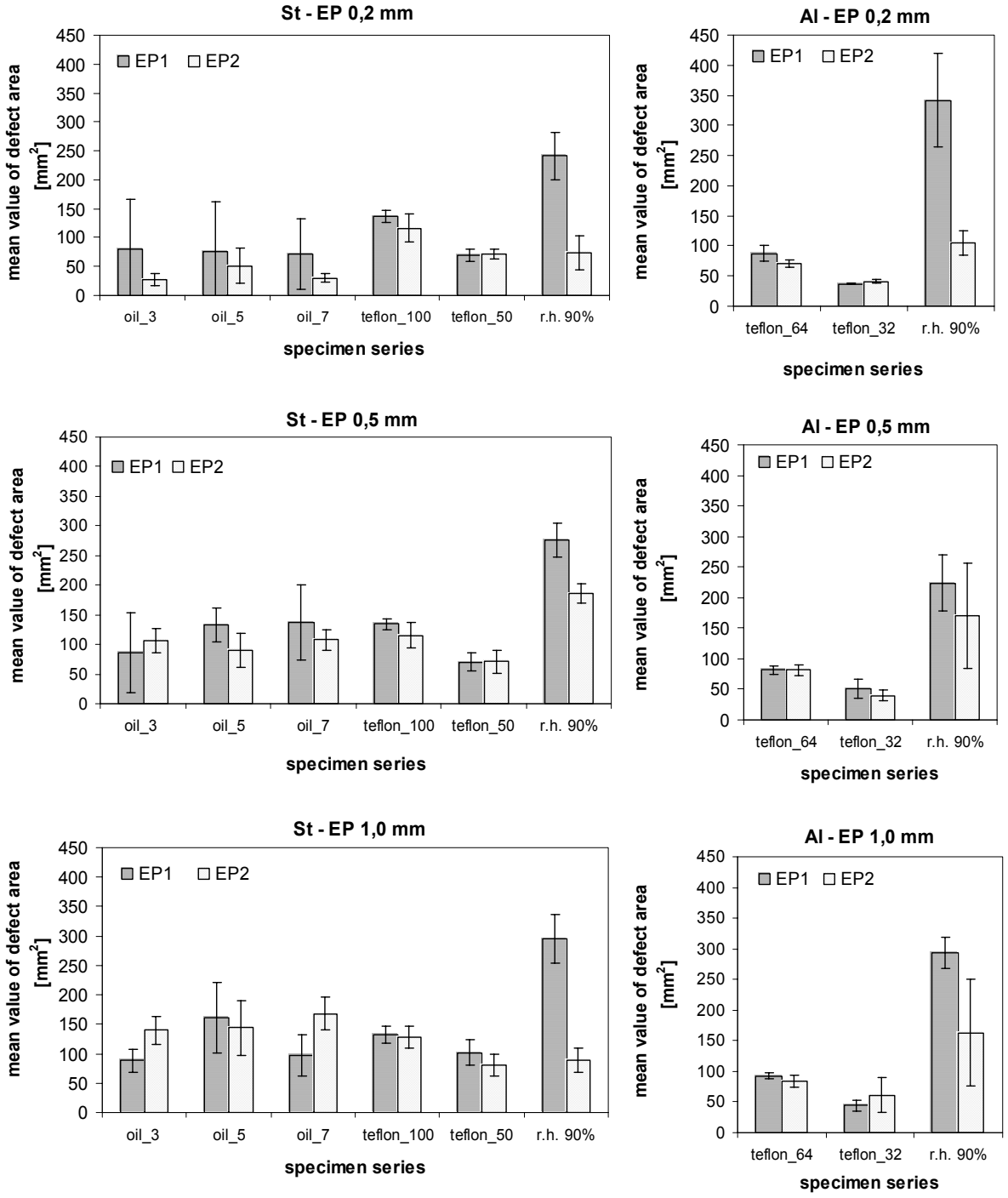

Fig. 6.15: Mean value and the scatter band 2s of evaluated imperfections in steel and aluminium single lap joints bonded with "Betamate 1496" (EP1) and "Terokal 5070" (EP2) in 0,2, 0,5 and 1,0 mm bondline thickness

Table 6.1: Evaluated defect area within an overlap bonded area of 1440 mm² for adhesive "Betamate 1496" and steel adherends

	Bondline thickness 0,2 mm				Bondline thickness 0,5 mm				Bondline thickness 1,0 mm			
inserted defect	specimen	defect area [mm²]	mean value of defect area [mm²]	standard dev. [mm²]	specimen	defect area [mm²]	mean value of defect area [mm²]	standard dev. [mm²]	specimen	defect area [mm²]	mean value of defect area [mm²]	standard dev. [mm²]
oil 3 g/m²	2.7.1	50,11	80,88	85,66	2.1.1	58,09	85,35	67,39	2.13.1	94,80	87,97	19,27
	2.7.2	33,83			2.1.2	26,81			2.13.2	116,19		
	2.7.3	19,79			2.1.3	129,91			2.13.3	88,74		
	2.7.4	229,50			2.1.4	31,28			2.13.4	69,90		
	2.7.5	71,18			2.1.5	180,66			2.13.5	70,22		
oil 5 g/m²	2.8.1	17,21	75,91	86,21	2.2.1	128,32	137,27	28,58	2.14.1	139,81	160,23	60,01
	2.8.2	81,08			2.2.2	149,38			2.14.2	112,99		
	2.8.3	223,12			2.2.3	163,11			2.14.3	253,44		
	2.8.4	19,15			2.2.4	133,10			2.14.4	110,44		
	2.8.5	38,94			2.2.5	87,46			2.14.5	184,49		
oil 7 g/m²	2.9.1	29,68	71,50	60,00	2.3.1	35,43	137,00	63,90	2.15.1	150,34	97,54	35,41
	2.9.2	34,79			2.3.2	130,55			2.15.2	117,14		
	2.9.3	24,90			2.3.3	158,32			2.15.3	79,48		
	2.9.4	108,53			2.3.4	150,66			2.15.4	75,01		
	2.9.5	159,60			2.3.5	210,03			2.15.5	65,75		
teflon foil 100 mm²	2.10.1	118,10	136,9	10,82	2.4.1	148,42	134,51	9,13	2.16.1	134,06	132,66	14,21
	2.10.2	140,76			2.4.2	128,00			2.16.2	131,83		
	2.10.3	137,25			2.4.3	130,87			2.16.3	110,44		
	2.10.4	139,81			2.4.4	138,85			2.16.4	149,70		
	2.10.5	146,51			2.4.5	126,40			2.16.5	137,25		
teflon foil 50 mm²	2.11.1	67,03	69,07	10,52	2.5.1	72,14	70,48	16,19	2.17.1	74,69	102,14	20,82
	2.11.2	64,16			2.5.2	66,39			2.17.2	120,34		
	2.11.3	60,97			2.5.3	93,84			2.17.3	93,20		
	2.11.4	65,75			2.5.4	48,52			2.17.4	125,44		
	2.11.5	87,46			2.5.5	71,50			2.17.5	97,03		
90% r.h.	2.12.1	183,54	240,99	41,19	2.6.1	316,64	276,55	28,99	2.18.1	253,12	295,00	41,27
	2.12.2	229,18			2.6.2	265,57			2.18.2	294,93		
	2.12.3	278,02			2.6.3	251,84			2.18.3	254,40		
	2.12.4	230,14			2.6.4	251,84			2.18.4	335,15		
	2.12.5	284,08			2.6.5	296,85			2.18.5	337,39		

Table 6.2: Evaluated defect area within an overlap bonded area of 1440 mm² with "Terokal 5070" steel adherends

	Bondline thickness 0,2 mm				Bondline thickness 0,5 mm				Bondline thickness 1,0 mm			
inserted defect	specimen	defect area [mm²]	mean value of defect area [mm²]	standard dev. [mm²]	specimen	defect area [mm²]	mean value of defect area [mm²]	standard dev. [mm²]	specimen	defect area [mm²]	mean value of defect area [mm²]	standard dev. [mm²]
oil 3 g/m²	3.7.1	35,11	26,75	10,19	3.1.1	89,69	106,74	20,34	3.13.1	151,30	139,42	24,35
	3.7.2	37,35			3.1.2	121,61			3.13.2	128,95		
	3.7.3	26,81			3.1.3	110,12			3.13.3	110,76		
	3.7.4	22,34			3.1.4	82,35			3.13.4	174,60		
	3.7.5	12,13			3.1.5	129,91			3.13.5	131,51		
oil 5 g/m²	3.8.1	10,53	51,26	30,08	3.2.1	66,07	89,98	28,60	3.14.1	92,25	144,47	46,42
	3.8.2	27,45			3.2.2	120,02			3.14.2	165,34		
	3.8.3	72,78			3.2.3	57,77			3.14.3	160,23		
	3.8.4	74,37			3.2.4	117,14			3.14.4	202,69		
	3.8.5	71,38			3.2.5	84,91			3.14.5	101,82		
oil 7 g/m²	3.9.1	26,81	30,45	8,29	3.3.1	114,91	107,57	17,00	3.15.1	189,92	167,83	27,45
	3.9.2	36,07			3.3.2	120,34			3.15.2	196,62		
	3.9.3	19,15			3.3.3	121,61			3.15.3	130,55		
	3.9.4	29,68			3.3.4	81,08			3.15.4	171,41		
	3.9.5	40,54			3.3.5	100,55			3.15.5	150,66		
teflon foil 100 mm²	3.10.1	103,74	116,51	24,29	3.4.1	103,42	114,97	21,85	3.16.1	125,76	127,87	18,86
	3.10.2	126,40			3.4.2	125,76			3.16.2	112,04		
	3.10.3	154,81			3.4.3	103,10			3.16.3	157,68		
	3.10.4	97,35			3.4.4	94,48			3.16.4	111,72		
	3.10.5	100,23			3.4.5	148,11			3.16.5	132,15		
teflon foil 50 mm²	3.5.1	75,01	71,37	8,66	3.5.1	74,37	70,73	19,15	3.17.1	94,48	80,57	18,21
	3.5.2	80,44			3.5.2	74,69			3.17.2	60,65		
	3.5.3	76,93			3.5.3	52,99			3.17.3	60,65		
	3.5.4	60,33			3.5.4	98,95			3.17.4	92,25		
	3.5.5	64,16			3.5.5	52,67			3.17.5	94,80		
90% r.h.	3.6.1	119,06	73,03	29,19	3.6.1	178,43	185,58	16,55	3.18.1	118,10	89,05	21,06
	3.6.2	49,16			3.6.2	163,11			3.18.2	79,16		
	3.6.3	81,39			3.6.3	205,56			3.18.3	64,16		
	3.6.4	67,35			3.6.4	183,54			3.18.4	82,03		
	3.6.5	48,20			3.6.5	197,26			3.18.5	101,82		

Table 6.3: Evaluated defect area within an overlap bonded area of 940 mm² for adhesive "Betamate 1496"and aluminium adherends

	Bondline thickness 0,2 mm				Bondline thickness 0,5 mm				Bondline thickness 1,0 mm			
inserted defect	specimen	defect area [mm²]	mean value of defect area [mm²]	standard dev. [mm²]	specimen	defect area [mm²]	mean value of defect area [mm²]	standard dev. [mm²]	specimen	defect area [mm²]	mean value of defect area [mm²]	standard dev. [mm²]
teflon foil 64 mm²	4.10.1	107,57	87,08	13,34	4.4.1	73,41	81,65	6,87	4.16.1	90,97	92,63	5,25
	4.10.2	75,01			4.4.2	84,59			4.16.2	98,31		
	4.10.3	87,46			4.4.3	77,24			4.16.3	86,82		
	4.10.4	90,01			4.4.4	81,71			4.16.4	97,99		
	4.10.5	75,33			4.4.5	91,29			4.16.5	89,05		
teflon foil 32 mm²	4.11.1	37,66	36,64	0,99	4.5.1	41,50	50,82	16,00	4.17.1	33,83	44,17	8,89
	4.11.2	35,43			4.5.2	62,24			4.17.2	35,11		
	4.11.3	37,66			4.5.3	73,10			4.17.3	51,71		
	4.11.4	36,07			4.5.4	36,07			4.17.4	50,11		
	4.11.5	36,39			4.5.5	41,18			4.17.5	50,11		
90% r.h.	4.12.1	259,82	341,98	78,29	4.6.1	144,91	223,75	45,80	4.18.1	267,16	293,21	25,39
	4.12.2	287,27			4.6.2	263,65			4.18.2	286,00		
	4.12.3	457,08			4.6.3	242,59			4.18.3	292,06		
	4.12.4	378,24			4.6.4	230,14			4.18.4	335,47		
	4.12.5	327,49			4.6.5	237,48			4.18.5	285,36		

Table 6.4: Evaluated defect area within an overlap bonded area of 940 mm² for adhesive "Terokal 5070" and aluminium adherends

	Bondline thickness 0,2 mm				Bondline thickness 0,5 mm				Bondline thickness 1,0 mm			
inserted defect	specimen	defect area [mm²]	mean value of defect area [mm²]	standard dev. [mm²]	specimen	defect area [mm²]	mean value of defect area [mm²]	standard dev. [mm²]	specimen	defect area [mm²]	mean value of defect area [mm²]	standard dev. [mm²]
teflon foil 64 mm²	5.10.1	67,03	71,24	6,44	5.4.1	75,01	81,20	19,92	5.16.1	70,54	83,56	9,77
	5.10.2	65,75			5.4.2	94,48			5.16.2	77,56		
	5.10.3	81,39			5.4.3	84,91			5.16.3	90,01		
	5.10.4	73,73			5.4.4	70,22			5.16.4	84,59		
	5.10.5	68,31			5.4.5	81,39			5.16.5	95,12		
teflon foil 32 mm²	5.11.1	38,30	40,73	3,09	5.5.1	35,43	39,96	9,34	5.17.1	42,13	61,48	27,67
	5.11.2	45,33			5.5.2	52,99			5.17.2	92,89		
	5.11.3	38,30			5.5.3	35,75			5.17.3	37,03		
	5.11.4	39,26			5.5.4	42,45			5.17.4	90,33		
	5.11.5	42,45			5.5.5	33,20			5.17.5	45,01		
90% r.h.	5.12.1	111,72	100,55	19,92	5.6.1	5.6.1	170,51	8,06	5.18.1	221,20	163,17	87,47
	5.12.2	69,58			5.6.2	5.6.2			5.18.2	240,67		
	5.12.3	122,89			5.6.3	5.6.3			5.18.3	110,44		
	5.12.4	99,59			5.6.4	5.6.4			5.18.4	208,43		
	5.12.5	98,95			5.6.5	5.6.5			5.18.5	35,11		

6.10 Concluding Remarks on the two NDT methods

Comparing the two NDT methods used the following may be noted. The detectability of the imperfections with neutron radiography was in general better than with ultrasonic because of the high detection of hydrogen bearing adhesive, and the high resolution of the transmission images. In specimens with inserted PTFE layers the evaluated total defect area appears – because of the inserted glass balls or random pores during manufacturing – larger than the actual imperfection. This fact does not seem to influence the evaluation of the tomography so much because of the high resolution pictures that are gained. Moreover C-scan evaluation with the ultrasonic method produces larger defect sizes because of the sound beam geometry.

For specimens with oil contamination, the evaluated defect area on the transmission images was sometimes smaller than the initially intended defect area because, an amount of oil during manufacturing was spread out over and outside the overlap area. Furthermore, this structural adhesive under consideration has the ability to absorb oil contamination to some extent during curing, thus rendering it even more difficult to detect defects. Another possible explanation for this reduced detectability is that oil is being squeezed into pores of the adhesive. The transmission image seems to estimate this situation rather reliably after all. The relatively high scatter band on the estimated defect area was due to the difficulty in reproducing the defect. On the other hand these observations are not confirmed in the case of the C-scans. The defect area is always significantly larger (white colour) than the defect inserted. This was an unexpected result, but the ultrasonic signal for a large number of small size contaminations gives only a general declaration about the joint without providing the exact position and shape of the contaminations. The ultrasonic measurement in this case can not be justified as the ultimate strength of the defect joints which is almost equal to the strength of the defect free joints [Michaloudaki 2004a].

The same conclusions can be reached for specimens with moisture content. The transmission image shows the water contaminants at the edges of the joint with great refinement, but the C-scan provides only general information of the existing imperfection. However the evaluated defect area with the image analysis software is about the same no matter which method is used. The consequences of the humid environment upon strength are discussed in chapter 8.

Within further investigations of Kosteas & Michaloudaki every imperfection, artificial (PTFE layer) or random, was evaluated separately, i.e. as individual artificial imperfection and not the total defect area, by image analysis software [Kosteas 2002c]. In this way the reliability of the images gained with ultrasonic and neutron radiography is estimated. For instance the evaluation through image analysis in case of the tomography of a teflon layer (100 mm^2) in the bond showed that the results differ only 15% from the actual inserted imperfection and 40% respectively in case of the C-scan. It is demonstrated further that the area of individual artificial imperfections is lower than the whole defect area, since random and perhaps non-significant imperfection readings are not included.

It is worth noting that the smallest defect evaluated on transmission images had a size of only 0,08 mm^2 and on C-scans 0,32 mm^2 equal to 1 pixel.

7 NDT in Full Scale Components

Adhesive bonding is used as a low temperature joining method in the automotive industry particularly for the manufacturing of hang on parts like doors and hoods, or also roofs and suspensions. In contrast to other joining techniques like bolting, riveting or welding, where the connection can be immediately loaded, in bonding technology there is a number of process parameters -surface pretreatment, adhesive application, curing etc.- to be followed. Thereby the joint can successfully transfer forces and its strength can only attain the design values. The mechanical behaviour of the bonded joint depends also on defects during manufacturing. This chapter presents illustrative applications of neutrons through radiography and tomography both providing information about the inner structure of industrial components.

7.1 Inspections with neutron radiography

7.1.1 Automobile doors

A steel car door was used as real structural component to validate the adhesively bonded area by means of neutron radiography, Fig. 7.1a. Different contrast of greyscale on the transmission image, Fig. 7.1b, reveals variation in metal sheet thickness -the higher contrast the thicker metal sheet-. This is clearly illustrated with the internal steel sheet where the thickness varies from 1,8 mm (left side) to 0,8 mm (right side).

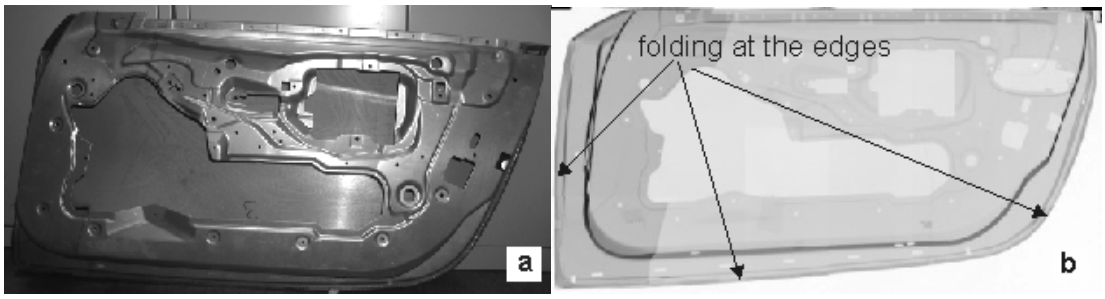

Fig. 7.1: a) Photograph of steel car door and b) transmission image of the door by means of neutron radiography

The bondline is applied at the edges of the left, lower, and right door side. Actually the joint is accomplished through folding by 180° of the external steel sheet and adhesively bonding on both sides of the internal steel sheet. A schematical illustration of the manufacturing steps and joint design is shown on Fig. 7.2. Fig. 7.3 shows the transmission images of the door and in magnification the defect bonded areas around it. Steel sheets look fairly transparent in contrast to the adhesive in the flange due to lower interaction of metals with neutrons and consequently, higher detection of hydrogen bearing compounds even between metal parts. Thus, the hydrogen atoms in polymers absorb neutrons rendering it opaque.

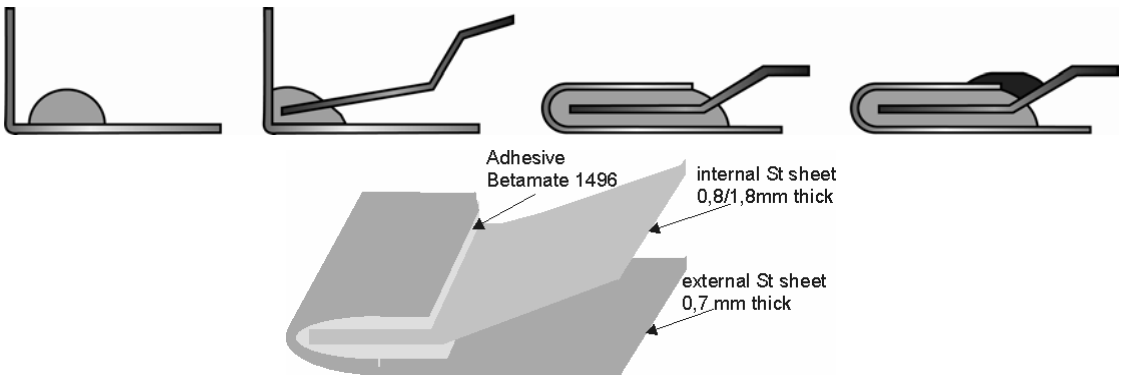

Fig. 7.2: Flange adhesively bonded on three sides around the car door

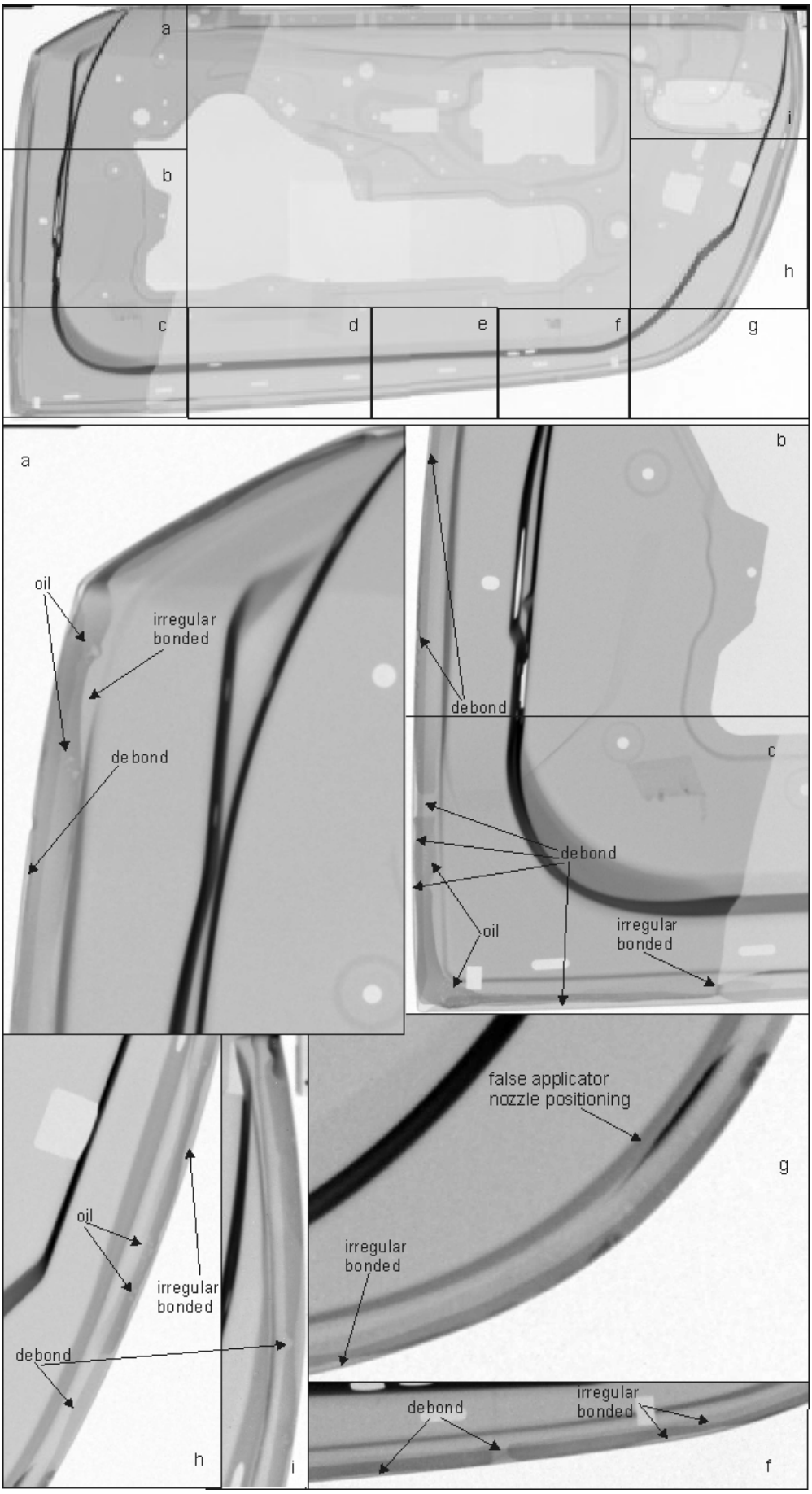

Fig. 7.3: Manufacturing defects detected by means of neutron radiography in steel car door

Commonly detected manufacturing defects were:

- oil remaining on the sheets due to rolling production
- adhesive coming out of the overlap due to false positioning of the applicator nozzle
- debonds due to unfilled gaps
- pores due to possible relative movement of the sheets before curing
- wide or narrow bonding pass due to irregular bonding
- variation in thickness indicated through contrast difference -black: thick bondline and light grey: thin bondline- in the joint.

The above defects were simulated with defined artificial imperfections covering either debonds, poor cohesive properties or adhesive weakness. Typical imperfections considered in this investigation were inserts of PTFE layer, PTFE lacquer, oil application on the metal sheets, too high/low folding pressure and interruption of the bondline.

Also, an aluminium car door was used to demonstrate possibilities for the non destructive validation of the adhesively bonded area, Fig. 7.4. The bondline was applied at the edges all around the back side of the door. Actually the joint was accomplished in a similar way like the steel door, through folding of the external aluminium sheet and adhesively bonding on both sides of the internal sheet, Fig. 7.2. Fig. 7.5 shows the transmission image of the door and defect bonded areas all around it in magnification. Aluminium sheets look fairly transparent in contrast to the adhesive in the flange and the sealing material due to hydrogen detection even between metal parts. Commonly introduced defects are similar to those described for the steel door. Another detected defect in case of the aluminium bond is the foam shape structure due to high folding pressure [Michaloudaki 2004c].

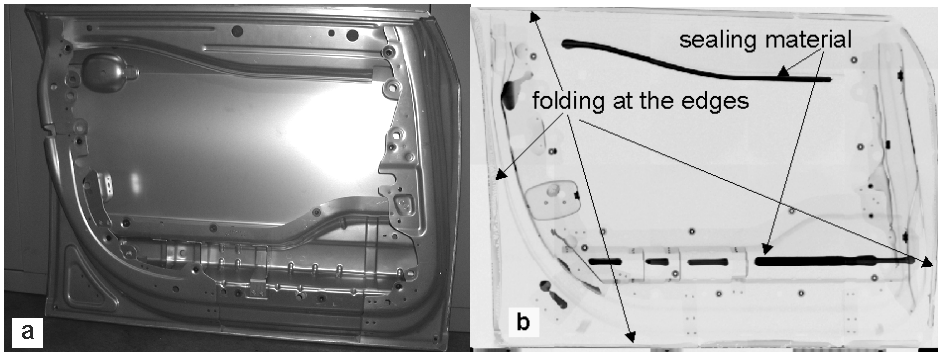

Fig. 7.4: a) Photograph of aluminium car door and b) transmission image of the door

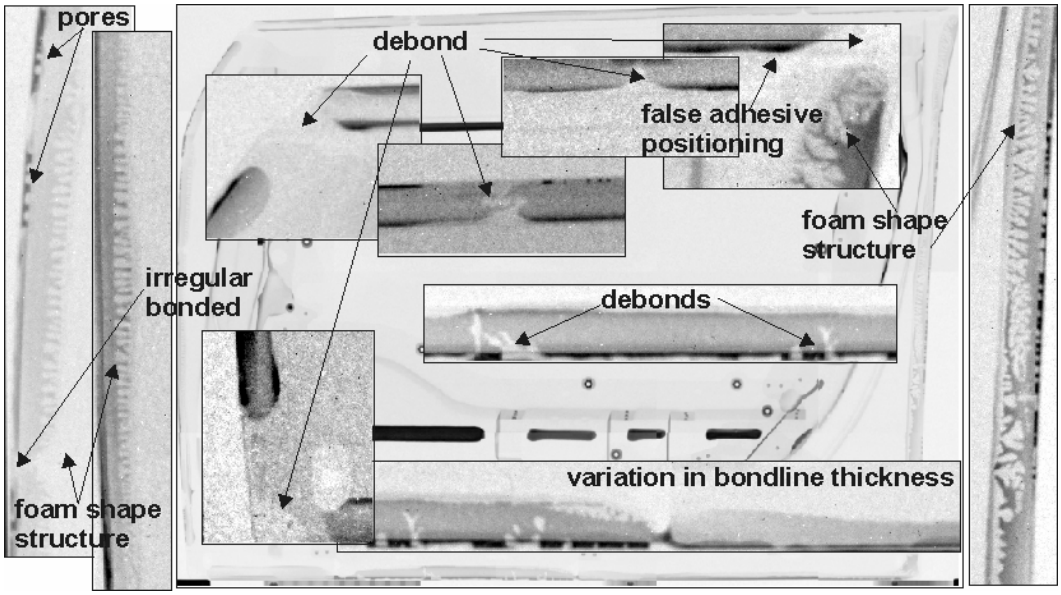

Fig. 7.5: Manufacturing defects detected by means of neutron radiography in aluminium car door

7.1.2 Back-seat-bank

A further investigation example is given with an aluminium back-seat-bank, Fig. 7.66a. This component is a layered composition of various materials connected with a number of joining methods. The main body is a sandwich element, i.e. two aluminium sheets bonded together through a third corrugated aluminium sheet. Different contrast of greyscale on the transmission image reveals a rather clear illustration of the bonded area, through a dense distribution of the adhesive. The only random defects detected, were a few debonds covering an insignificant area in comparison with the whole bonded area of the sandwich component. Further bonding was applied at several parts on the back side of the bank. The joints were accomplished by overlapping aluminium profiles on the main body of the sandwich element. The bandage attached offers high strength and stiffness due to crash resistant adhesives. The bonded parts are additionally riveted or welded to ensure an enhanced long term structural behaviour of the hybrid connections [Kosteas 2001].

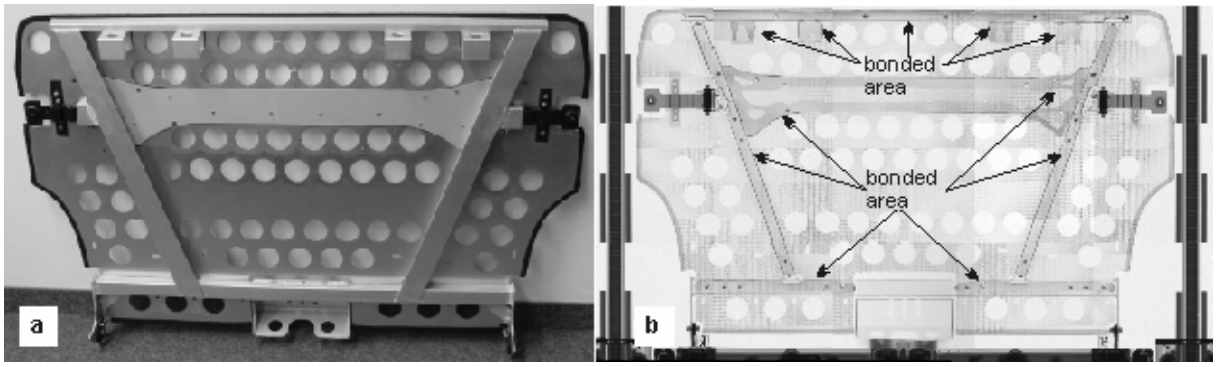

Fig. 7.6: Photograph of aluminium back-seat-bank and b) transmission image of the back-seat-bank by means of neutron radiography

Fig. 7.7 shows the location of the defects of the bonded parts attached on the sandwich element in magnification. Common random defects are debonds, especially in the area around the rivets, slight porosity probably due to relative movement of the parts before the adhesive attained its final strength. Furthermore, adhesive coming out of the overlap due to false positioning of the applicator nozzle and irregular bonding through too narrow or too wide bondlines are usual defects detected.

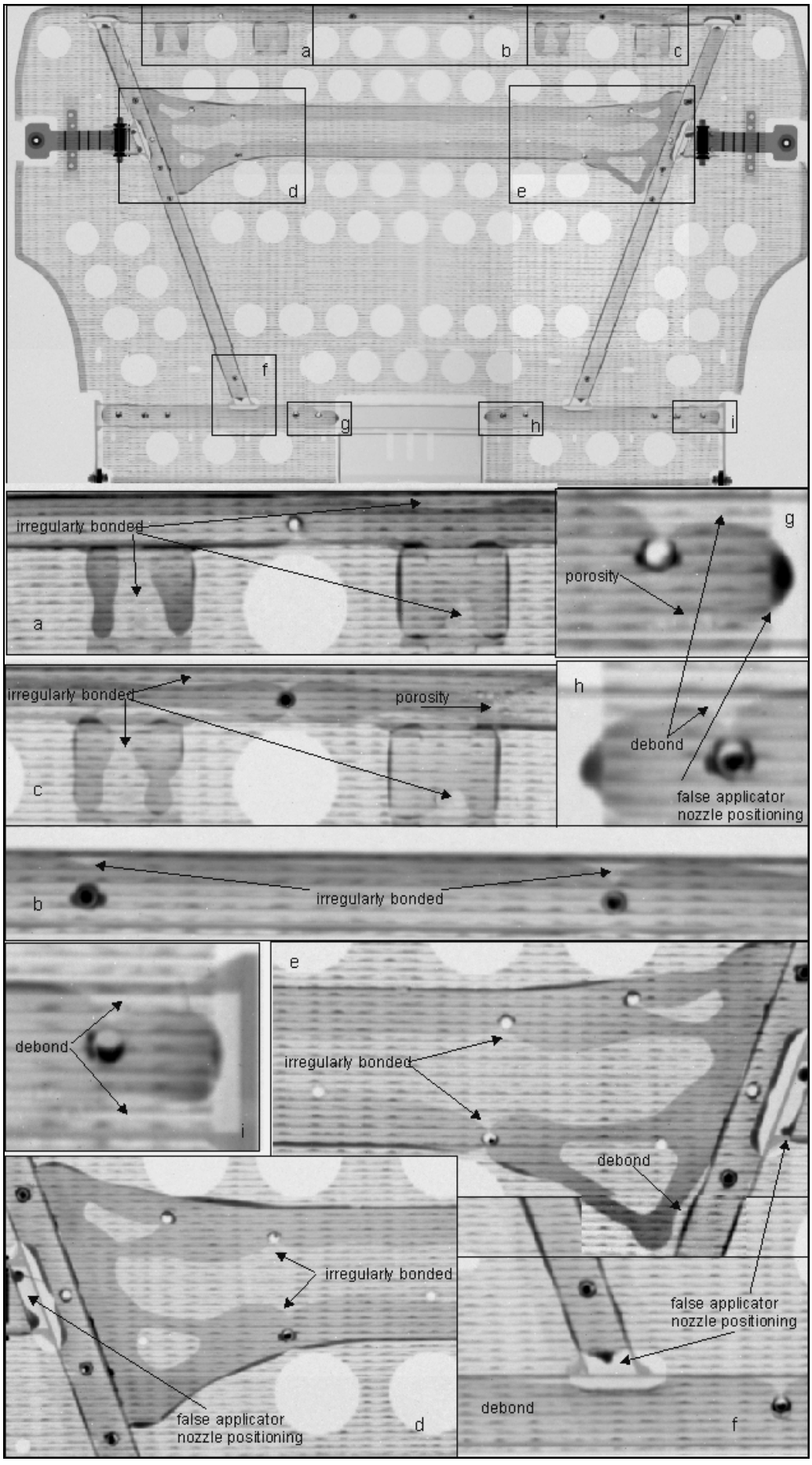

Fig. 7.7: Manufacturing defects detected by means of neutron radiography in back-seat-bank

7.2 Inspection with neutron tomography

Radiography simply involves irradiating an object and recording a projection or "shadow image", as ordinary X-ray radiographs. Tomography involves recording images of the object taken from many directions. In industrial tomography the sample is placed on a table rotating through a fixed beam to obtain projections of the sample over an angular range of 180 degrees. The obtained image data allow the reconstruction of the internal structure of the sample.

Components of the automotive shell and hang on parts were inspected with neutron tomography at the Position 3 of NEUTRA station in Paul Sherrer Institute, each of them with 300 projections within an angle of 180°. The image data were subsequently visualized with the VG-Studio software; thus a clear segmentation between steel and adhesive distribution was possible. The reason for the materials` differentiation is again the high contrast of the adhesive even in between the metal layers due to high water concentration. Neutron tomography allows even the clear visualisation of the metal sheet structure. Various views of the tested components are given representing different materials combined.

7.2.1 Bonded steel profile

The steel component of Fig. 7.8 is spot welded and adhesively bonded all around the edges. Bonding increases the fatigue resistance of the joint and providing enhanced sealing and stiffness. The photograph shows that the profile was tested in two parts i.e. upper part - detail A, lower part - detail B, as its dimensions were larger than the dimensions of the detector. The tomograph surface views of the details illustrate the metal parts, steel materials or various sheet thicknesses with different contrast of greyscale. The tomograph transparent views show the metal being relatively transparent i.e. foggy distribution with some sharp curves. Further the adhesive distribution is with red colour illustrated and manufacturing defects such as porosity and debonds are clearly recognised.

According to Dance [Dance 1976], inspections of pit corrosion within metal structures with neutrons is feasible due to detection of moisture, hydroxides, oil, or other hydrogenous substances accumulating at the hidden corrosion locations. From the data gathered in the radiographic comparison of corrosion products and lubricating grease placed in an aluminium assembly, it appeared that the presence of significant amounts of grease or oil at the exact corrosion locations would tend to suppress the differentiation between the two hydrogenous materials detected. The size of the corrosion products imaged was 0,75 mm in diameter and 0,05 mm in thickness. Details C and D show possibly pit corrosion near the weld nugget, clearly imaged by differential neutron absorption. Corrosion products, i.e. metal oxides absorb more neutrons than metals and fewer neutrons than hydrogenous substances. Thus the marked corrosion in Fig. 7.8 is in between contrasted.

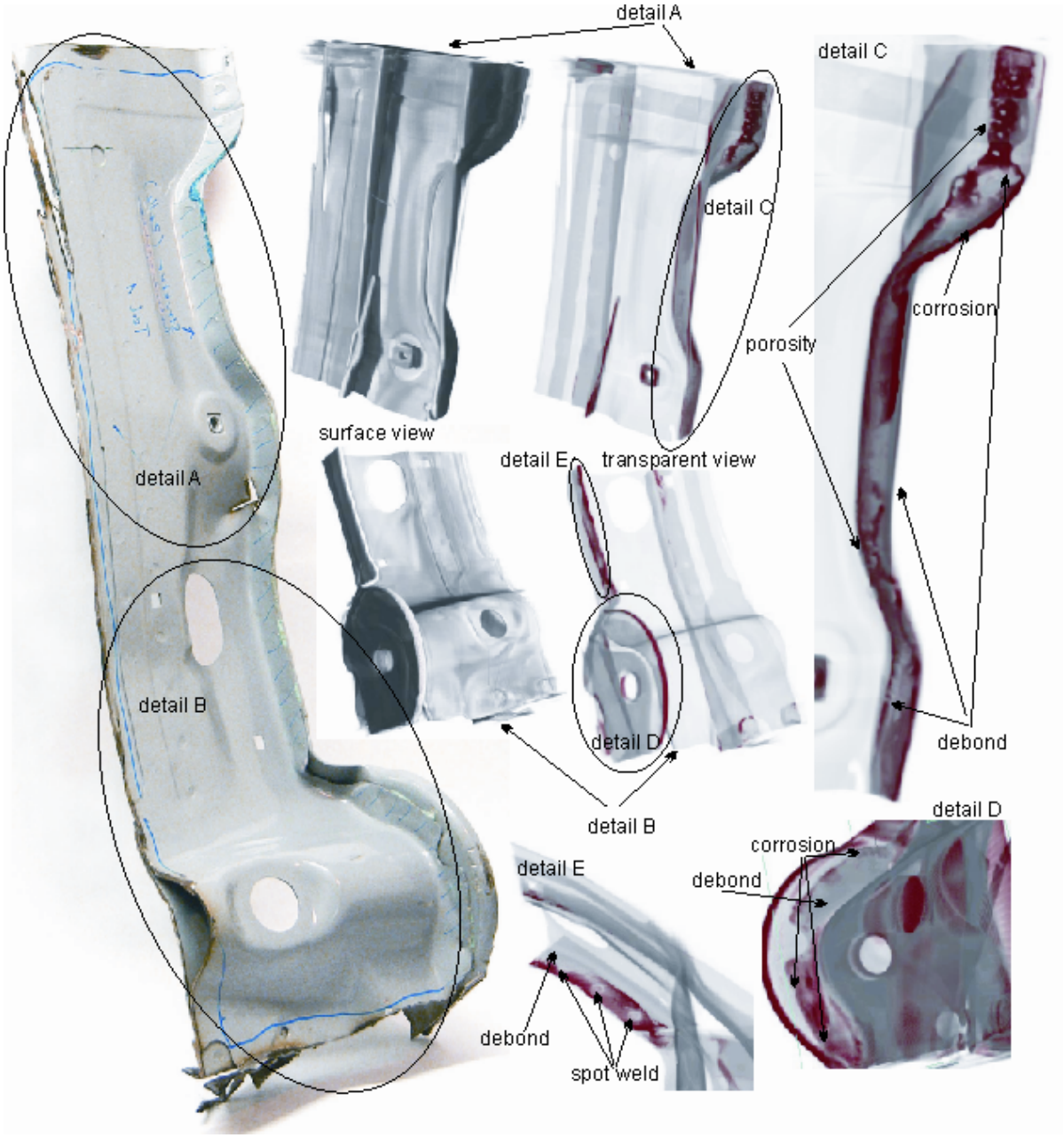

Fig. 7.8: Manufacturing defects detected by means of neutron tomography in bonded steel profile

7.2.2 Double hat profile

The steel double hat profile of Fig. 7.9 was further used for the non destructive validation of the adhesively bonded area through neutron tomography. The component is adhesively bonded and spot welded offering an enhanced structural behaviour at the joint. The photograph shows the cut profile into two pieces before testing. The surface views of the components illustrate the individual metal structures with contrasts of greyscale. Cross sections of the components in surface view give indications about the distribution of the adhesive.

Electronic image processing was used to remove the metal completely from the image, i.e. increasing brightness, transparency is assigned each time to different materials. The hat profile shows within the same image its upper part as surface view and its lower part as transparent view. Thus the image reveals more than just three-dimensional view; it provides access to hidden data, making visible the adhesive layer and defects, shown in the transparent views of Fig. 7.9. Details A to D show the weld-bond area in magnification. The spot welds are clearly recognised and the

debonds are spread to a larger area around the weld nuggets. Further defects are slight porosity in several regions or large pores distant with each other. The different contrast of the red coloured adhesive distribution reveals bondline thickness variation, i.e. too thin adhesive layer is shown in light red colour and thick adhesive in dark red.

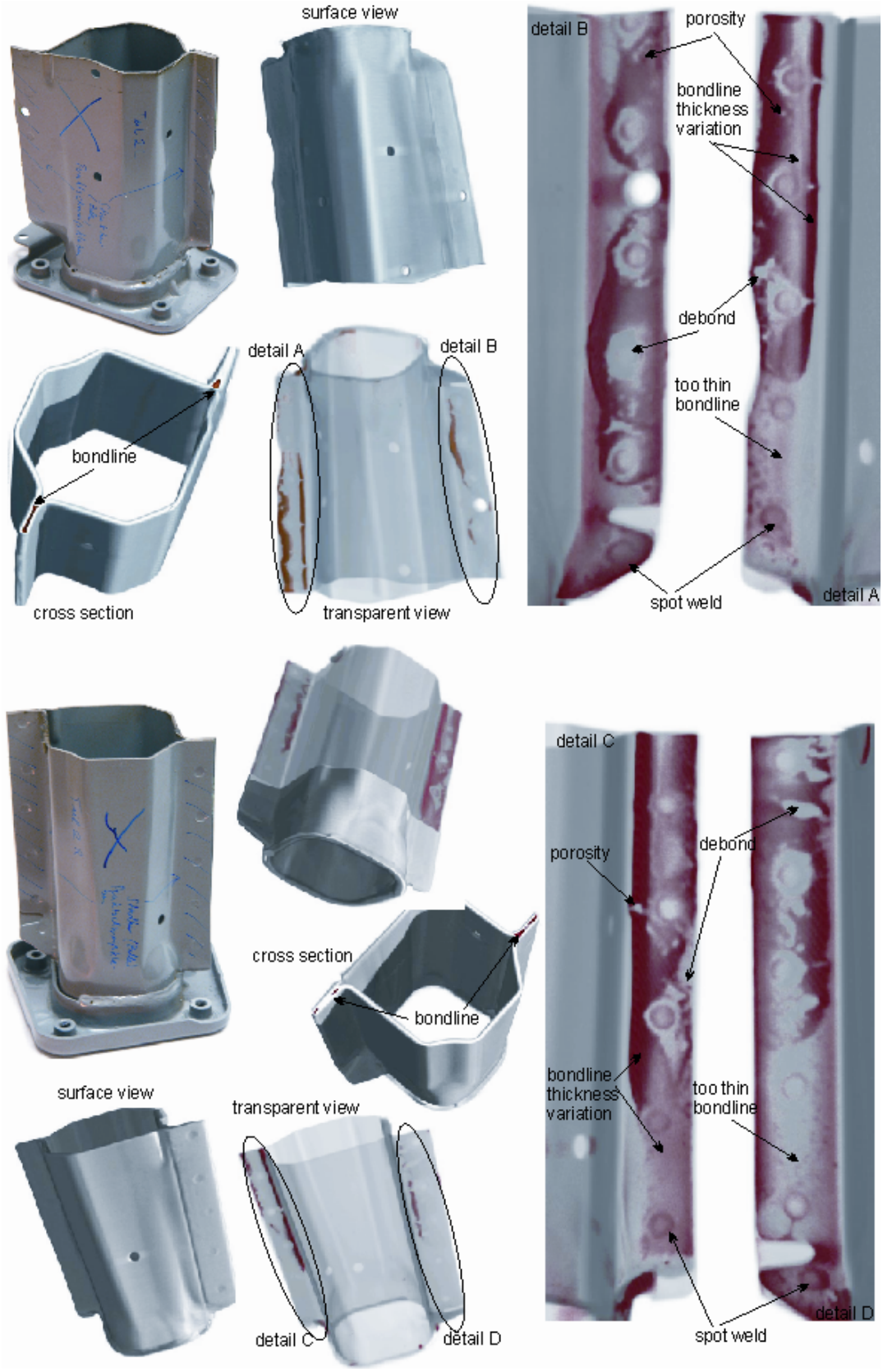

Fig. 7.9: Manufacturing defects detected by means of neutron tomography in double hat profile

Based on investigations of Sharp et al [Sharp 1996], sufficient spot welds are generally accomplished by using enough electrode force to obtain electrical contact of the bonded adherends and somewhat increased current. A fairly common weld-process problem, expulsion, is the spraying of molten aluminium out of the weld nugget. Even though this problem generally doesn't affect the static or fatigue strength of spot welds themselves, the weld parameters are adjusted to reduce its occurrence. However, expulsion was shown to lower the fatigue strengths of weld bonds by forcing out the adhesive, thus starving the bond within an area often extended to a joint edge. This conclusion is also observed for the steel spot weld-bond on the details C and D of Fig. 7.9. Naturally, the loss of bond in this critical high stressed area lowers the fatigue strength.

The effect of weld discontinuities on the fatigue performance of lap joints and low-load-transfer joints in aircraft alloys was included in a study by Scarich and Chanani, [Scarich 1982]. Weld bonding or bonding produced significantly higher fatigue strengths than spot welding for both joint types. For low-load-transfer joints, bonding had an advantage over weld bonding. Tests of bonded lap joints demonstrated that an intentional central 25% debond did not reduce the fatigue strength. The fact that load transfer is concentrated at the joint extremities is the reason that spot welds are placed in that central area without appreciably lowering the fatigue performance.

However in case of high strength steel a debond increase leads to almost linear reduction in strength and the whole adhesive yields starting from the joint-ends until the middle. Moreover the spot welds as peel stoppers are inserted near enough to a lap end to prevent peel loadings but it is often likely to crack and destroy the bond in the highest loaded area. If so, such a joint would probably have the fatigue performance of a spot welded joint. If it is considered that a spot weld is a disrupted bond area then a careful balance of end distance, and spot welds number is important to stay underneath the critical debond value leading otherwise to linear static strength reduction and subsequently to unexpected fatigue failure.

7.2.3 Hood

The last investigation was conducted on a steel car hood, Fig. 7.10. The bondline is applied at several edges of the hood parts. Actually the joint is accomplished at folding 180° the external steel sheet and adhesively bonding it on both sides of the internal steel sheet. The photograph shows the hood into two pieces before testing. The surface views of the components illustrate the individual metal structures with contrasts of greyscale. Cross sections of the components in metal view give indications about the distribution of the adhesive.

Electronic image processing allowed the surrounding metal adherends to be illustrated as transparent haze. Details B and C show defect free bond areas in magnification. The bondline is orderly, i.e. not too wide or too narrow applied. The instant contrast across the adhesive layer reveals an instant bondline thickness. Details A and D show several irregularities in the adhesive application. Debonds and bondline thickness variation are easily detected on the transparent views of the tomographs, caused mostly from the false positioning of the adhesive applicator nozzle.

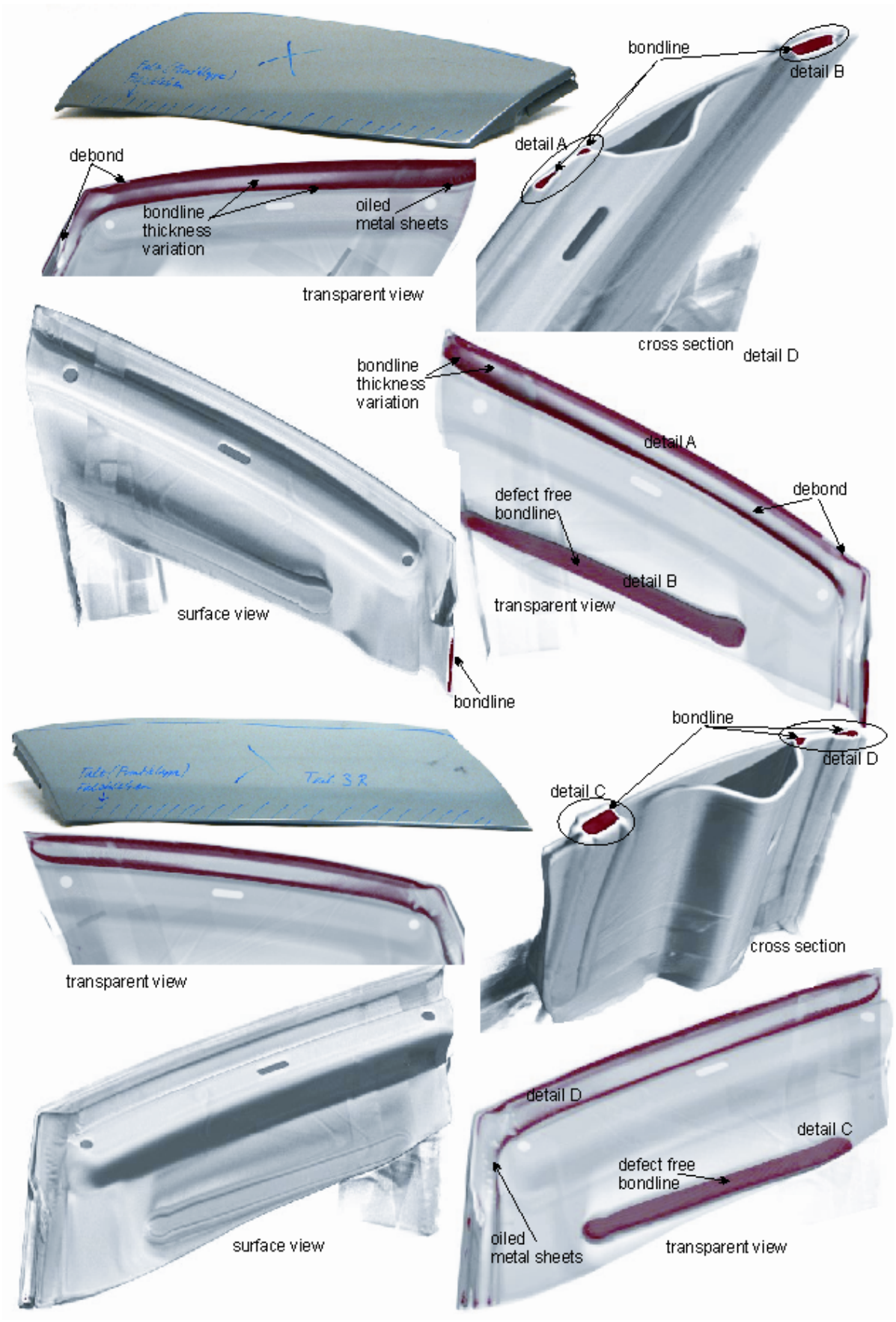

Fig. 7.10: Manufacturing defects detected by means of neutron tomography in a hood

7.3 Potential of neutrons in structural application

To verify the qualitative observations on small scale specimens and the applicability of the method in industrial products several components have been tested and evaluated. In general neutron radiography and tomography are rather reliable tools and invaluable supplements to conventional NDT techniques for real components [Michaloudaki 2004d]. Experimental investigations on structural components of the automotive industry have demonstrated that for certain inspections neutrons may have more to offer for the evaluation of structural integrity than the more frequently used methods, like ultrasonic or thermography, [Michaloudaki 2004e]. The refinement provided by neutron radiography over scan techniques for inspecting the adhesive structure and distribution within complicated metal parts is a prime advantage. In most of the cases deliberately introduced imperfections or random defects during manufacturing were qualitatively recognised. For detection of hidden corrosion, neutron radiography appears to hold a distinct advantage over other techniques in its ability to image corroded locations. It is worth here noting that the initial experimental investigations on overlap joints considering various parameters highly contributed to the detection and identification of the defects due to reproducible results gained from the small specimens.

The development and application of neutron radiography and tomography demonstrate the unique contribution of these techniques toward higher product reliability but have limitations in their industrial applicability as they need powerful neutron sources. The evaluation of critical structural parts or components in the development stage maybe justified. For large components radiography on a production basis, and particularly for in-situ inspections, improved imaging techniques for reducing exposure times required for good resolution radiographs must be pursued. Continuous improvements in the development of portable neutron sources must be sought for realising the full potential of neutron radiography in industrial "on-line" inspections. It is expected that as present limitations in these areas are lifted, neutron radiography will assume an active role in the non destructive evaluation of many types of bonded structure.

There is a potential use of the method apart from the aircraft and automotive industry as in cases of civil engineering and shipbuilding structures, where large and complicated components with bonded or hybrid joints are formed, often even realised as a series product. Not only in prototype design but also in the establishment of basic detail category classification data and reference values neutron radiography offers several benefits.

8 Destructive Testing

Quantitative evaluation of the degradation of adhesive bonds remains one of the most challenging problems to be solved in the widespread use of bonded structures. Bonding failures due to improper manufacturing have led to an urgent need for developing a reliable testing technology. Since non destructive methods have not yet reached the demanded level in automation and reliability for several industrial applications, an approach to evaluate the integrity of an adhesive joint is to destructively test a representative sample. In these investigations mechanical test results help to interpret complementary nondestructive detection of deliberately introduced defects and correlate the strength sensitivity with the nature of the defects.

8.1 A fundamental stress analysis for bonded metal structures

When a load F is applied to a single lap joint of width w and length l, the average applied shear stress, τ, is given by Eq. (8-1):

$$\tau = \frac{F}{w \cdot l} \qquad \text{Eq. (8-1)}$$

However, because of differential shear in the adherends [Volkersen 1938], there is a non-linear distribution of these stresses, with peaks at the two ends. Goland and Reissner [Goland 1944] showed that because the forces F are displaced, there will, be a bending moment M at the joint ends, given by Eq. (8-2).

$$M = \frac{k \cdot F \cdot t}{2} \qquad \text{Eq. (8-2)}$$

where t is the adherend thickness and k is the bending moment factor which is a function of the joint parameters and also of the load, F. In general, k decreases as F increases [Adams 1997]. The main effect of the bending moment applied to the joint is to create peel stresses (tensile stresses perpendicular to the adhesive layer) which peak sharply at the joint ends. Because of these effects in shear and peel, both of which peak at the joint ends, it may be considered that defects towards the middle of the overlap will have an insignificant effect on joint strength. Thus detecting defects in this area through NDT would also be of minor importance and all efforts should be concentrated in the highly stressed region at the joint-ends. Adams et al (Adams 1997) have discussed the mechanics of bonded joints and supported their considerations with finite element analysis and testing. They have shown that the theories of Volkersen and Goland & Reissner are sufficient for a preliminary understanding of joint mechanics. However, there are other important factors which need to be considered in real joints. These factors include, in particular, the non linear yield and plasticity of real materials, both adhesives and adherends.

8.2 The role of destructive tests for adhesive joint strength

The main contribution of non destructive evaluation (NDE) methods in adhesive joints is the detection of various types of flaws, observation of degradation processes with time, and with accumulating experience a product qualification procedure. The implementation of adhesive technology in new codes would encourage further innovative applications. Lack of reliable data for different adhesive bonded systems could be offset through design by testing, and it is here that NDE could offer a valuable quantification and control tool. However, NDE cannot estimate directly joint strength. Parallel destructive tests commonly contribute to the desired correlation. Industrial fields have set increasing demands on NDT automation and reliability, both pivotal for practical implementation.

In case of adhesively bonded joints, it was for a long time believed that the presence of defects in the middle of the joint could not lead to consequences on the mechanical behaviour of the joint. Work by Schonhorn`s group [Zalucha 1983] had frequently been used to validate this. They showed that, when high-strength aluminium alloy adherends (2024-T3) were used with a structural epoxy adhesive and inserting a polypropylene layer inserted into the middle of the joint, there was no reduction of lap shear strength as the bonded area was reduced to 40% of the original (unaffected) area. Closer observations showed that the results were dominated by the yield of the adherends. Once the metallic substrates yielded, the joint failed in the limited ductility adhesive. The fracture conditions appeared more severe at the joint-ends. Thus, joint failure was almost entirely dominated by the "end" effects revealed by Volkersen and Goland & Reissner.

Since Schochorn`s work was carried out, there have been considerable improvements in structural adhesives. His work was extended by Adams et al [Adams 1999] by using low and high strength steel adherends and a commercial toughened epoxy. Defined defects were introduced by inserting PTFE strips symmetrically in the middle of the joint with 150/300/400 mm^2 area in a total overlap area of 625 mm^2. For the mild steel adherends there was an effect of defect size on the strength only when more than 50% of the bonded area was removed, confirming also Schonchorn's results. In the case of high strength steel there was almost a linear reduction in the strength with increasing area of debond.

These results relate to the relative plasticity of the adhesive and the adherends. Using a very ductile adhesive e.g. acrylic or polyurethane with the mild steel, it is likely that the adherend yield strength would have ceased to dominate the results. However since the mild steel is much more ductile than a brittle adhesive, adherend yield at the joint end leads to failure. On the contrary, when a toughened adhesive is used with high strength steel the whole adhesive yields starting from the joint-ends towards the middle. Therefore the significance of these results for the NDT is obvious when the adherends are no ductile materials i.e. high strength metals, advanced composites, ceramics and glasses.

The above investigations of Schonhorn's and Adams' groups were extended by performing tension-shear tests on high strength steel and aluminium with brittle adhesives and defined imperfections not only in the middle of the overlap but also at the joint-ends. Aiming to a preliminary understanding on the effect of defects on the structural behaviour of adhesive joints analytical methods through continuous mechanics were used. These investigations are presented below.

8.3 Correlation of defect area and ultimate strength

Destructive tests were performed with the specimens used in NDT investigations, aiming to monitor mechanical behaviour and to relate deliberately introduced defects to the strength of metal-epoxy joints. Specimens were loaded in axial tension Fig. 8.1, ensuring load symmetry through additional metal sheets in the machine grips. The test was displacement controlled. The applied load and the displacement over a length of 55 mm were continuously recorded and respective load-displacement diagrams are shown in *Annex C*. The ultimate load value for every specimen, the mean value and the standard deviation for every sample series with aluminium or steel adherends are given in the Table 8.1 to Table 8.4.

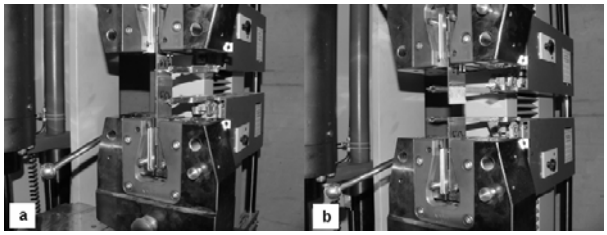

Fig. 8.1: Tension-shear test of single overlap joints before and after failure.

Table 8.1: Ultimate load values for the steel lap joints with the adhesive Betamate 1496 and overlap area 1440 mm².

	Bondline thickness 0,2 mm				Bondline thickness 0,5 mm				Bondline thickness 1,0 mm			
inserted defect	specimen	ultimate strength [N]	mean value [N]	standard dev. [N]	specimen	ultimate strength [N]	mean value [N]	standard dev. [N]	specimen	ultimate strength [N]	mean value [N]	standard dev. [N]
ideal	1.2.1	39535	38078	2647	1.1.1	38077	42880	3007	1.3.1	34518	30101	3764
	1.2.2	37929			1.1.2	42965			1.3.2	32494		
	1.2.3	41602			1.1.3	46137			1.3.3	30091		
	1.2.4	34715			1.1.4	44455			1.3.4	24622		
	1.2.5	36611			1.1.5	42767			1.3.5	28741		
oil 3 g/m²	2.7.1	34986	39217	4673	2.1.1	33144	35143	3974	2.13.1	32675	32157	1380
	2.7.2	41658			2.1.2	37765			2.13.2	31342		
	2.7.3	45626			2.1.3	36592			2.13.3	30754		
	2.7.4	34485			2.1.4	39009			2.13.4	34287		
	2.7.5	39332			2.1.5	29205			2.13.5	31728		
oil 5 g/m²	2.8.1	44200	40047	6732	2.2.1	37053	34136	1772	2.14.1	28547	28812	1665
	2.8.2	45547			2.2.2	32359			2.14.2	31262		
	2.8.3	28698			2.2.3	34095			2.14.3	29427		
	2.8.4	42230			2.2.4	33207			2.14.4	28012		
	2.8.5	39559			2.2.5	33965			2.14.5	26812		
oil 7 g/m²	2.9.1	39630	39802	8063	2.3.1	33584	31652	2158	2.15.1	27500	28723	2837
	2.9.2	45255			2.3.2	30494			2.15.2	26398		
	2.9.3	47770			2.3.3	31864			2.15.3	28899		
	2.9.4	39465			2.3.4	28608			2.15.4	33537		
	2.9.5	26891			2.3.5	33712			2.15.5	27279		
teflon foil 100 mm²	2.10.1	40715	38053	1720	2.4.1	43407	39677	4276	2.16.1	26288	25775	993
	2.10.2	36895			2.4.2	36487			2.16.2	24994		
	2.10.3	38719			2.4.3	45155			2.16.3	26651		
	2.10.4	37520			2.4.4	35898			2.16.4	26502		
	2.10.5	36416			2.4.5	37234			2.16.5	24442		
teflon foil 50 mm²	2.11.1	37800	37812	2229	2.5.1	40941	41157	1163	2.17.1	32734	31131	1686
	2.11.2	34731			2.5.2	41774			2.17.2	32564		
	2.11.3	40884			2.5.3	39440			2.17.3	28632		
	2.11.4	37134			2.5.4	41845			2.17.4	31282		
	2.11.5	38511			2.5.5	42236			2.17.5	30441		
90% r.h.	2.12.1	38100	31110	4179	2.6.1	37301	35803	1220	2.18.1	35061	33195	1554
	2.12.2	30904			2.6.2	36198			2.18.2	33780		
	2.12.3	28563			2.6.3	36424			2.18.3	33839		
	2.12.4	27337			2.6.4	34454			2.18.4	31084		
	2.12.5	30644			2.6.5	34640			2.18.5	32210		

Table 8.2: Ultimate load values for the steel lap joints with the adhesive Terokal 5070 and overlap area 1440 mm².

	Bondline thickness 0,2 mm				Bondline thickness 0,5 mm				Bondline thickness 1,0 mm			
inserted defect	specimen	ultimate strength [N]	mean value [N]	standard dev. [N]	specimen	ultimate strength [N]	mean value [N]	standard dev. [N]	specimen	ultimate strength [N]	mean value [N]	standard dev. [N]
ideal	1.5.1	39792	37714	1449	1.4.1	36258	36523	1117	1.6.1	21986	27414	3131
	1.5.2	37460			1.4.2	38455			1.6.2	30106		
	1.5.3	35815			1.4.3	35769			1.6.3	28311		
	1.5.4	37298			1.4.4	36386			1.6.4	28240		
	1.5.5	38205			1.4.5	35748			1.6.5	28427		
oil 3 g/m²	3.7.1	36856	37049	909	3.1.1	36525	35910	1629	3.13.1	27429	26706	2221
	3.7.2	36353			3.1.2	36500			3.13.2	29481		
	3.7.3	36060			3.1.3	36908			3.13.3	27503		
	3.7.4	38126			3.1.4	36607			3.13.4	25465		
	3.7.5	37851			3.1.5	33010			3.13.5	23652		
oil 5 g/m²	3.8.1	34663	38855	2508	3.2.1	35548	36568	1983	3.14.1	30657	28076	2051
	3.8.2	40911			3.2.2	33789			3.14.2	29094		
	3.8.3	40672			3.2.3	36950			3.14.3	28144		
	3.8.4	38944			3.2.4	38973			3.14.4	27338		
	3.8.5	39086			3.2.5	37982			3.14.5	25146		
oil 7 g/m²	3.9.1	41453	40481	1449	3.3.1	36070	35513	1590	3.15.1	24416	27357	2712
	3.9.2	39674			3.3.2	35385			3.15.2	30742		
	3.9.3	42415			3.3.3	33363			3.15.3	25557		
	3.9.4	38778			3.3.4	37729			3.15.4	26428		
	3.9.5	40085			3.3.5	35016			3.15.5	29641		
teflon foil 100 mm²	3.10.1	30977	33552	2442	3.4.1	33876	31794	1410	3.16.1	30021	29452	1694
	3.10.2	33895			3.4.2	32250			3.16.2	27027		
	3.10.3	32605			3.4.3	31815			3.16.3	31646		
	3.10.4	36756			3.4.4	30775			3.16.4	29729		
	3.10.5	33871			3.4.5	30256			3.16.5	28835		
teflon foil 50 mm²	3.5.1	33370	35305	2088	2.5.1	33852	34886	1226	3.17.1	30267	28936	2647
	3.5.2	35359			2.5.2	34744			3.17.2	28931		
	3.5.3	33885			2.5.3	36404			3.17.3	24373		
	3.5.4	38721			2.5.4	33582			3.17.4	30856		
	3.5.5	35192			2.5.5	35846			3.17.5	30255		
90% r.h.	3.6.1	33843	35063	998	2.6.1	35231	35497	457	3.18.1	31128	29703	1057
	3.6.2	35350			2.6.2	34996			3.18.2	28422		
	3.6.3	34735			2.6.3	36203			3.18.3	29622		
	3.6.4	36562			2.6.4	35449			3.18.4	30298		
	3.6.5	34823			2.6.5	35607			3.18.5	29044		

Table 8.3: Ultimate load values for the aluminium lap joints with the adhesive Betamate 1496 and overlap area 960 mm².

	Bondline thickness 0,2 mm				Bondline thickness 0,5 mm				Bondline thickness 1,0 mm			
inserted defect	specimen	ultimate strength [N]	mean value [N]	standard dev. [N]	specimen	ultimate strength [N]	mean value [N]	standard dev. [N]	specimen	ultimate strength [N]	mean value [N]	standard dev. [N]
ideal	1.8.1	22220	22635	1657	1.7.1	19937	21260	1646	1.9.1	15094	17526	1835
	1.8.2	19902			1.7.2	23151			1.9.2	18861		
	1.8.3	23750			1.7.3	22944			1.9.3	16541		
	1.8.4	23538			1.7.4	19864			1.9.4	19716		
	1.8.5	23767			1.7.5	20405			1.9.5	17418		
teflon foil 64 mm²	4.10.1	18792	22515	2695	4.4.1	20383	22026	1736	4.16.1	19976	17361	2140
	4.10.2	20694			4.4.2	24072			4.16.2	14510		
	4.10.3	25317			4.4.3	23728			4.16.3	18890		
	4.10.4	23525			4.4.4	20802			4.16.4	17013		
	4.10.5	24249			4.4.5	21144			4.16.5	16418		
teflon foil 32 mm²	4.11.1	22780	22710	1697	4.5.1	21711	22666	1178	4.17.1	20901	19038	1091
	4.11.2	24480			4.5.2	21203			4.17.2	18974		
	4.11.3	22114			4.5.3	24044			4.17.3	18625		
	4.11.4	20184			4.5.4	23013			4.17.4	18625		
	4.11.5	23994			4.5.5	23360			4.17.5	18066		
90% r.h.	4.12.1	26035	20990	3736	4.6.1	22288	23252	3580	4.18.1	22217	20503	1518
	4.12.2	22689			4.6.2	21275			4.18.2	19908		
	4.12.3	15877			4.6.3	19065			4.18.3	21914		
	4.12.4	20068			4.6.4	28137			4.18.4	18633		
	4.12.5	20280			4.6.5	25495			4.18.5	19845		

Table 8.4: Ultimate load values for the aluminium lap joints with the adhesive Terokal 5070 and overlap area 960 mm².

	Bondline thickness 0,2 mm				Bondline thickness 0,5 mm				Bondline thickness 1,0 mm			
inserted defect	specimen	ultimate strength [N]	mean value [N]	standard dev. [N]	specimen	ultimate strength [N]	mean value [N]	standard dev. [N]	specimen	ultimate strength [N]	mean value [N]	standard dev. [N]
ideal	1.11.1	23562	21814	2190	1.10.1	20581	20040	943	1.12.1	17620	16078	1499
	1.11.2	19508			1.10.2	21304			1.12.2	14149		
	1.11.3	24632			1.10.3	19116			1.12.3	17582		
	1.11.4	21078			1.10.4	19140			1.12.4	15574		
	1.11.5	20288			1.10.5	20060			1.12.5	15467		
teflon foil 64 mm²	5.10.1	17164	17749	1971	5.4.1	18150	17202	2012	5.16.1	15796	16535	919
	5.10.2	17672			5.4.2	15920			5.16.2	16764		
	5.10.3	15979			5.4.3	16988			5.16.3	15441		
	5.10.4	16831			5.4.4	20069			5.16.4	17078		
	5.10.5	21099			5.4.5	14883			5.16.5	17640		
teflon foil 32 mm²	5.11.1	16693	19927	2004	5.5.1	17430	13859	3983	5.17.1	16560	17601	754
	5.11.2	19242			5.5.2	16666			5.17.2	18381		
	5.11.3	21344			5.5.3	14971			5.17.3	17590		
	5.11.4	21190			5.5.4	12714			5.17.4	18257		
	5.11.5	21268			5.5.5	7510			5.17.5	17215		
90% r.h.	5.12.1	22030	23132	2016	5.6.1	19322	19176	2177	5.18.1	18532	17748	957
	5.12.2	23411			5.6.2	17105			5.18.2	16096		
	5.12.3	23502			5.6.3	21652			5.18.3	18247		
	5.12.4	20646			5.6.4	16854			5.18.4	17937		
	5.12.5	26073			5.6.5	20945			5.18.5	17929		

The mean value of the ultimate load and the scatter band 2s for every sample series with aluminium or steel adherends are given in the diagrams of the Fig. 8.2. The evaluation of 'ideal' i.e. defect-free joints shows that, for both substrates and both adhesives, the optimum bondline thickness is in the region of 0,2 to 0,5mm; a significant reduction in strength is observed when the bondline thickness is at 1,0mm. Generally Betamete 1496 (EP1) shows slightly better structural behaviour than Terokal 5070 (EP2) for both ideal and defect bonds.

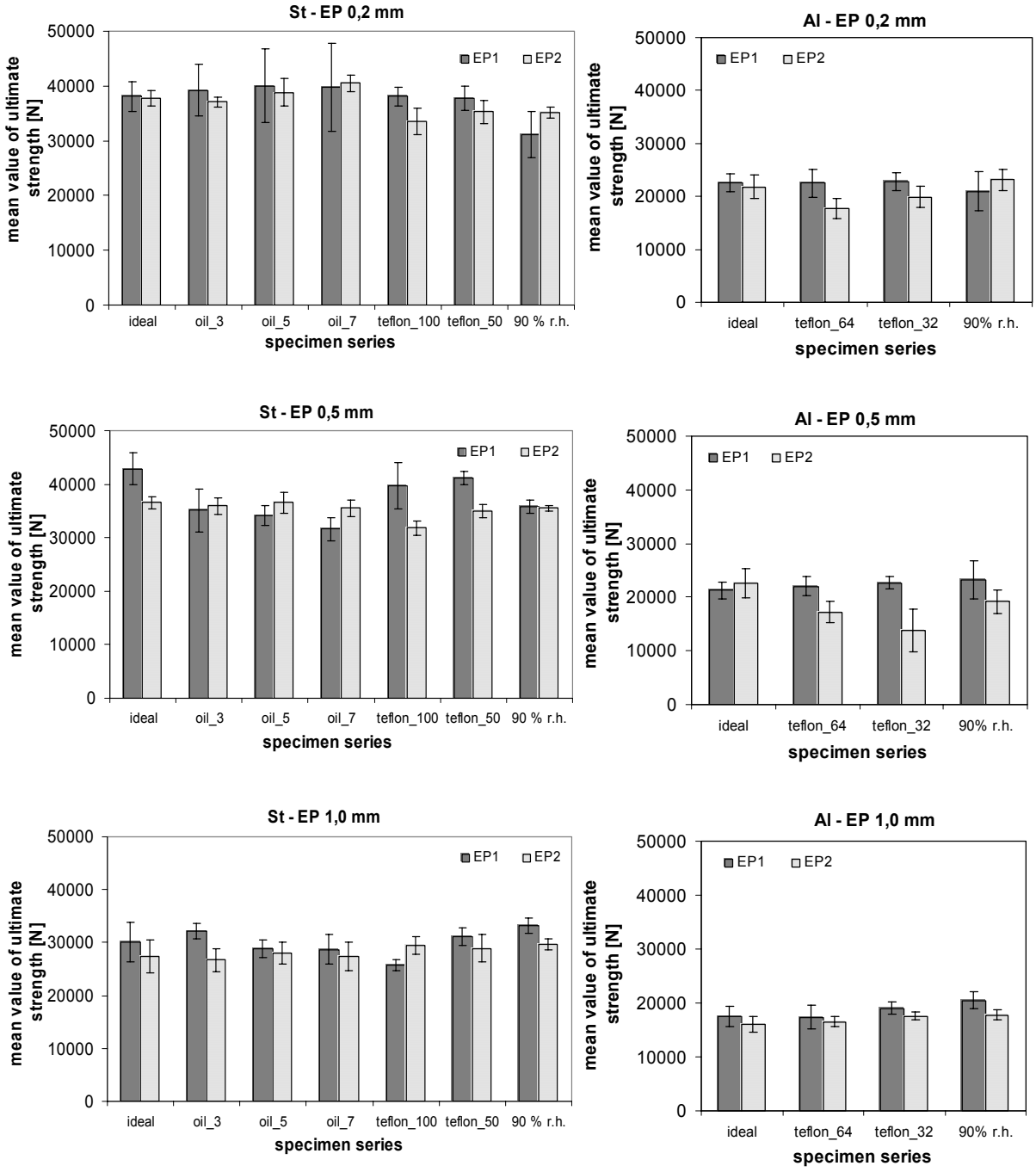

Fig. 8.2: Mean values of ultimate strength and the scatter band 2s for the adhesives Betamate 1496 (EP1) and Terokal 5070 (EP2)

There is a reduction of approximately 25% of the aluminium joint strength for the ideal specimens and both epoxies as the bondline thickness increases from 0,2 to 1,0 mm. The same tendency is also observed in case of specimens with imperfections, where the reduction of the joint strength varies between approximately 2% and 30%. It is worth here mentioning that in

spite of deliberately introduced imperfections the ultimate strength has not been significantly reduced. The same tendency on the strength reduction is not observed between 0,2 and 0,5 bondline thickness. The thickness variation in this case seems to be insignificant either for the ideal or defect bonds. Clear differences in the structural behaviour appear in bondline thickness higher than 0,5 until 1,0 mm.

There is a reduction of the steel joint strength for the ideal specimens with Betamate 1496 reaching 27% and Terokal 5070 38% as the bondline thickness increases from 0,2 to 1,0 mm. The same tendency is also observed in the case of specimens with imperfections, where the reduction of the joint strength varies between app. 20% and 50%. Thus, there is definitely, apart from the thickness variation, a significant influence of the imperfections upon ultimate strength. Between 0,2 and 0,5 mm bondline thickness, the maximum strength reduction reaches 20% although in most of the cases thickness variation appears negligible upon strength or the structural behaviour is app. 15% amplified with 0,5mm bondline. Clear differences in strength reduction appear indeed with bondline thickness higher than 0,5 until 1,0 mm.

More specifically, the inclusion of Teflon defects in bonded steel joints seems to have little detrimental effect; i.e. within a few percentage points, either way, of the control values, as shown in Table 8.5. Very much the same sort of conclusions can be drawn for the aluminium bonded joints although, in this case, the results using Terokal 5070 do appear to have greater associated scatter accompanied by a slightly more negative effect.

Table 8.5: Percentage (%) of the joint strength reduction due to imperfections in relation to ideal bonds.

$\frac{(F_{defected} - F_{ideal})}{F_{ideal}} \cdot 100\%$		Bondline thickness 0,2 mm		Bondline thickness 0,5 mm		Bondline thickness 1,0 mm	
Adherends	Imperfection	Betamate 1496	Terokal 5070	Betamate 1496	Terokal 5070	Betamate 1496	Terokal 5070
steel	oil_3	-3,0	-1,4	18,0	1,7	-6,8	2,6
	oil_5	-5,2	-6,4	20,4	-0,1	4,3	-2,4
	oil_7	-4,5	-10,8	26,2	2,8	4,6	0,2
	teflon_100	0,1	8,1	7,5	12,9	14,4	-7,4
	teflon_50	0,7	3,3	4,0	4,5	-3,4	-5,6
	90 % r.h.	18,3	4,0	16,5	2,8	-10,3	-8,3
aluminium	teflon_64	0,5	18,6	-3,6	23,6	0,9	-2,8
	teflon_32	-0,3	8,7	-6,6	38,4	-8,6	-9,5
	90 % r.h.	7,3	-6,0	-9,4	14,8	-17,0	-10,4

It is worth noticing that for specimen series both with steel and aluminium adherends exposured to 21 days pre-bond humidity 90% r.h. in room temperature and the results are not so clear cut. The performance for both adhesives on steel substrates appears to drop when the thinner bondlines are considered (0,2 and 0,5 mm) but increase where the bondline thickness is 1,0 mm. On aluminium substrates, however, there is no such clear-cut pattern but, once again, an apparent strength increase is seen for bondline thicknesses of 1,0 mm.

For the specimen series with steel adherends and oil contamination (3, 5 and 7 g/m²), the lap-shear performance is very confused with an apparent random pattern of performance increases and decreases as the oil content, the bondline thickness and the adhesive type changes. With the EP1 adhesive, however, the performance does appear to worsen, at oil coatings of over 3 g/m², as the bondline thickness increases. With the EP2 adhesive, the pattern appears to be a random one.

Two questions are, therefore, posed:

- Structural adhesives often are plasticized when water uptake takes place after curing. Can that also be the case when water uptake takes place before curing? Does plasticization usually only cause higher deformability or can it lead to higher shear strength?
- When the adhesive is applied onto oily substrates, why does the strength increase in most specimens with 0,2 mm bondline thickness (five out of six cases), whilst it decreases when 0,5 and 1,0 mm bondline thickness are encountered (nine out of twelve cases)?

To gain an insight into these observations it is important to understand the chemistry and recorded properties of each adhesive and then to examine, in detail, the results obtained to date. Further consulting by Bishopp [Bishopp 2004] and observations on the fracture surfaces contributed for the better understanding of the results. These results are explained below.

8.4 Chemistry and Properties of the adhesives

Betamate 1496 V (EP1) of Dow Automotive is a one-component epoxy paste adhesive which can be dispensed 'warm' by a conventional cartridge gun. It can be cured in 60 minutes at 155°C or 30 minutes at 170°C to give a tough crosslinked matrix which imparts good impact resistance to bonded joints.

The Material Specification Data Sheet (MSDS) shows that it contains two Bisphenol A based epoxies (30 to 60% and 1 to 25% respectively) plus 2, 3-epoxypropyl neodecanoate (1 to 10%); there are some indications that the second of the two Bisphenol A epoxies is a solid resin. The MSDS contains no indications of nitrogen-containing products but they must, surely, be present in the hardener component; the section on fire hazards simply states that 'toxic gases' are produced; but doesn't identify them. Further physical and mechanical properties of EP1 are given in the Table 8.6:

Table 8.6: Properties of the adhesive "Betamate 1496 V"

Viscosity at 23°C	~ 3000 Pa.s
Viscosity at 40°C	~ 300 Pa.s
Tensile strength	32 N/mm²
Elongation at failure	15%
Lap-shear strength at 23°C on steel substrates*	30 N/mm²
T-Peel strength at 23°C on steel substrates	>100 N/25mm
Impact strength*	28 N/mm
*: Cured for 30 minutes at 170°C	

Henkel's Terokal 5070MB-25 (EP2) is a one-component epoxy paste adhesive which can be dispensed -ideally at temperatures up to 55°C- by a conventional cartridge gun. It can be cured in 12 minutes at 160°C but can tolerate cures up to 45 minutes at 190°C to give a tough crosslinked

of the original bonded area lead to insignificant reduction of lap shear strength. That was more or less expected since earlier investigations of Schonhorn [Zalucha 1983], showed that even with 40% reduction of the original unaffected area there is no loss of strength. Furthermore Adams showed that after more than 50% bond area reduction, strength loss is noticable. These results refer to low strength steel and aluminium alloy i.e. yield strength values of $R_{p0,2}$=170-200 N/mm^2. The strength results of aluminium bonds in Table 8.5 do not allow coming up to similar conclusions because the inserted imperfection was rather small and the strength among thickness and adhesive either reduces up to 40% or increases above the strength of ideal bonds without following a specific parameter. This means that relative plasticity of the adherends and the adhesive are also responsible for the mechanical behaviour of the joint preventing a classification of the effect of small size imperfections.

In the case of high strength steel, Adams showed that imperfection 20% of the total bond area caused a noticeable strength reduction around 30%. Table 8.5 shows that for high strength steel adherends teflon layer with 5% or even less of the total bond area cause strength reduction up to almost 5%. Similar observations are noted for a teflon layer of 10% or even less of the total bond area, where strength reduction reaches 15%. This result confirms the almost linear reduction in joint strength with increasing debond area pointed out by the investigations of the Adams' group [Adams 1999].

A teflon layer inserted within a thick bondline (1,0 mm) seems to increase the strength (six out of eight cases) in comparison to defect free specimens. This means that, although a defect within a thin bondline (0,2/0,5 mm) commonly reduces the joint strength, when the bondline is thick an enhanced strength behaviour is observed no matter what adherend material is used. The triangle shaped teflon layer reaches in some cases somewhat lower strength ranges than the square teflon layer (twice as large as the triangle). This fact is associated probably with the local stress concentrations and stress redistribution in the joint, where the average shear stress due to introduced imperfections is higher. The macroscopic observation of the specimens identifies, that failure has occurred by lack of cohesion mixed and lack of adhesion as the bondline thickness increases from 0,2/0,5/1,0mm, Fig. 8.3 and Fig. 8.4.

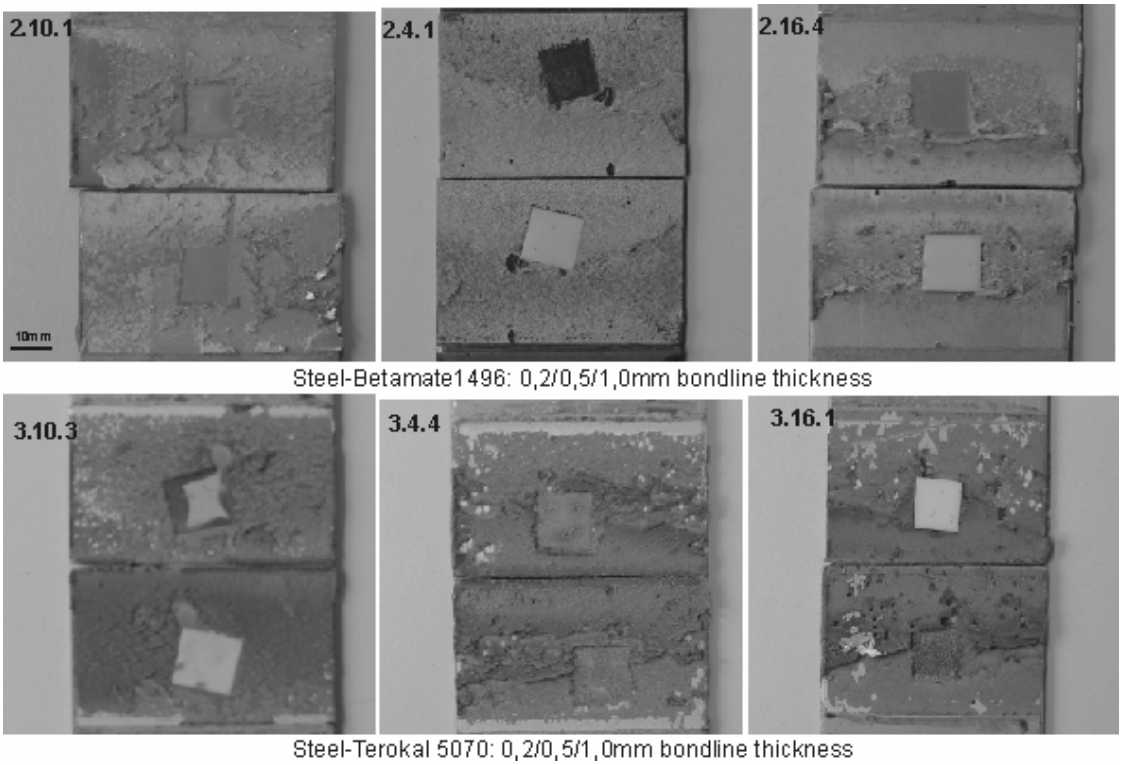

Fig. 8.3: Macroscopic observations on the fracture surface of steel lap joints bonded with the adhesives "Betamate 1496" and "Terokal 5070" and inserted PTFE layer.

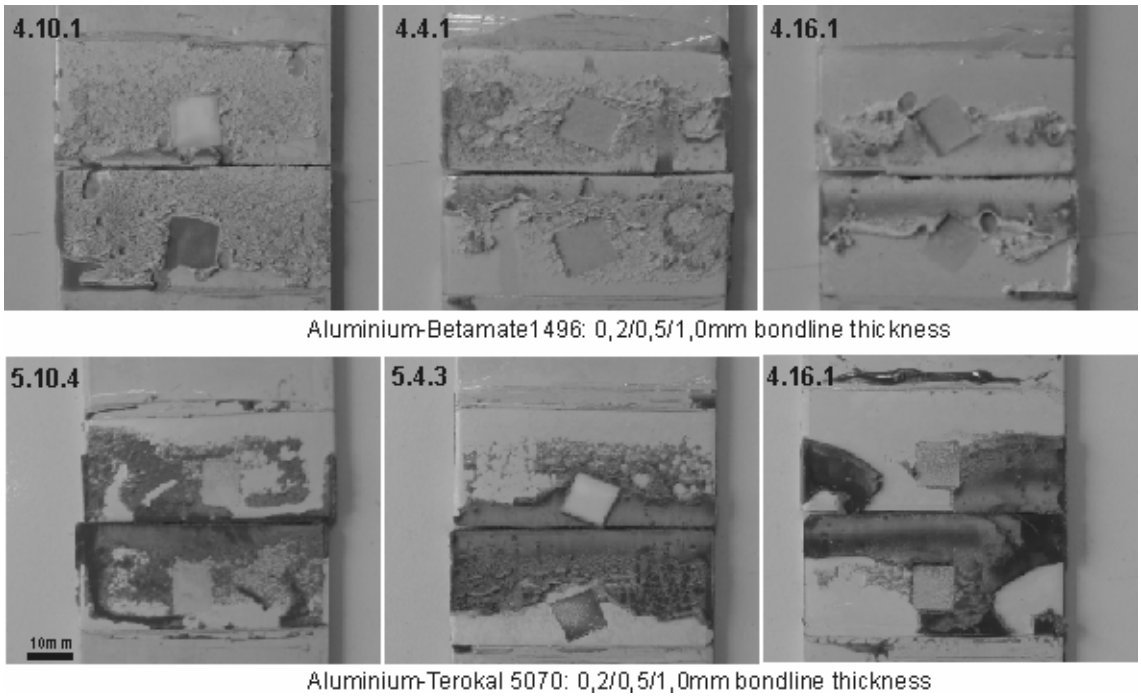

Fig. 8.4: Macroscopic observations on the fracture surface of aluminium lap joints bonded with the adhesives "Betamate 1496" and "Terokal 5070" and inserted PTFE layer.

8.4.2 90% pre-bond relative humidity exposure

The 21-day conditioning period should be sufficient to ensure that not only equilibrium is reached but also that there should be a significant level of surface moisture on the adhesives before closure of the joints.

The argument that this moisture will be released by the system as the temperature is raised to cure temperature is a valid one. However, as the gelation temperature, under dynamic cure conditions, is likely to be considerably above 100°C – independent of whether the curative is diamino diphenyl sulphone (DDS) or a substituted diamino diphenyl methanes (DDM) – no moisture should be trapped inside the joint after cure; any such residual moisture in the cured joint would lead to voiding, bubbled squeeze-out and possibly adhesive starvation within the joint: the so-called 'blown' bondlines. Most, if not all of these would obviously lead to undesirable stress concentrations and poor strengths.

The pressure applied to the joints during cure should compensate for material lost - follow-up pressure consolidating the bondline – unless the bondlines are artificially shimmed to control thickness. Further, provided that the applied pressure is not too high, volatiles should not be trapped. It is only if the volatile loss is so excessive that serious reduction in strengths should be seen.

The fact that moisture can escape before the onset of gelation, therefore, should make it extremely unlikely that 'plasticization' of the cured matrix will occur under these conditions. 'Plasticization' of the cured matrix generally allows stress relaxation in the cured joint; making the matrix appear 'tougher'; this can manifest itself with an apparent improvement in lap-shear and peel performance at ambient -but not elevated- temperatures.

However, it is very clear from neutron radiograph analyses Fig. 5.13 to Fig. 5.16 that the joints do, indeed, contain considerable quantities of water. The effect on the Betamate 1496 appears to be considerably more marked than on the joints made with Terokal 5070. This is confirmed when an estimate of the total areas occupied by defects is calculated and compared with the values for defects induced by the addition of controlled quantities of Teflon, Fig. 5.22.

The results of the neutron radiography are further confirmed when the fracture surfaces of the joints are examined. Not only is there considerable 'damage' but the failure patterns on the Terokal joints are 'less severe' than for the Betamate. This is clearly seen in Fig. 8.5 und Fig. 8.6.

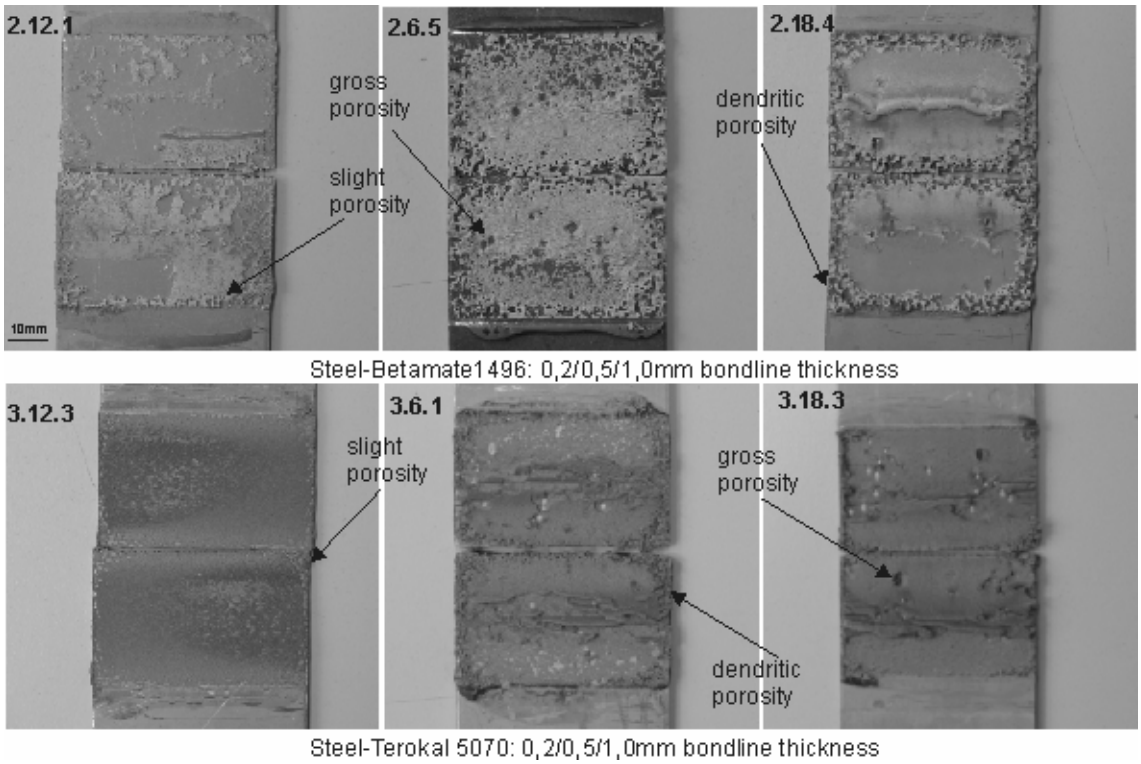

Fig. 8.5: Macroscopic observations of moisture uptake on the fracture surface of the steel lap joints bonded with the adhesives "Betamate 1496" and "Terokal 5070" and exposed to 90% r.h. pre-bond humidity.

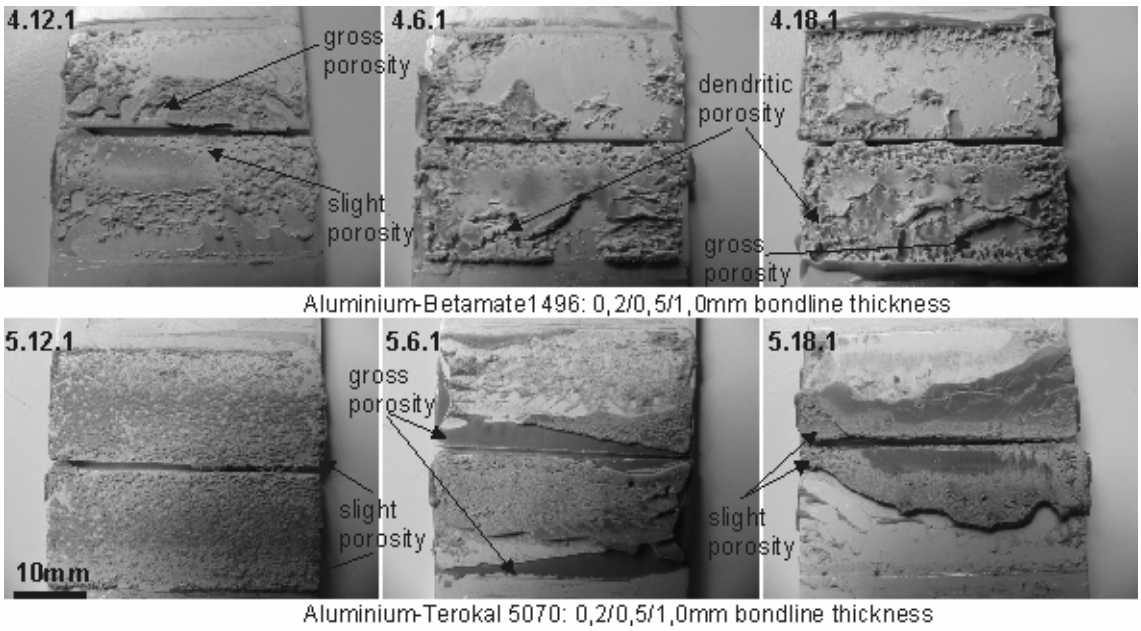

Fig. 8.6: Macroscopic observations of moisture uptake on the fracture surface of the aluminium lap joints bonded with the adhesives "Betamate 1496" and "Terokal 5070" and exposed to 90% r.h. pre-bond humidity.

The failure patterns themselves are worth of more detailed examination. The water absorption in steel and aluminium bonds confirms the dendritic porosity, gross or slight, identified by visual inspection of the fracture surface of the specimens. At the edge of each joint, a distinct series of

voids can be seen where moisture vapour has bubbled into the squeeze-out. This is particularly unfavourable in the joints with bondline thicknesses of 0,2 and 0,5 mm and also seems to be worse for the Betamate 1496 adhesive. The level of voids in the depth of the joints appears to be far worse with the Betamate 1496 adhesive; indeed, for the Terokal 5070 joints with bondline thicknesses above 0,2 mm, bubbles/voids within the joint are at a significantly low level.

Further, the Betamate 1496 joints exhibit a significant degree of adhesion failure, Fig. 8.6, whereas the Terokal 5070 joints show cohesive failure at a bondline thickness of 0,2 mm and the more typical 'half-and-half' pattern associated with structural adhesive joints: i.e. half of one joint has thick cohesive failure whilst the other half has thin/weak cohesive failure the second half of the broken joint being the mirror image of the first.

Clearly, the effect of pre-bond humidity is to cause damage and is very unlikely to give any degree of plasticization to the bonded joint as water is unlikely to remain in a dispersed state with the epoxy matrix during such a high temperature cure (180 °C).

8.4.3 Oil contamination on the metal sheets

As mentioned before, these types of adhesive are relatively compatible with any oil on the substrates to be bonded; particularly, as in these cases, when 160°C to 180°C cure cycles are employed.

However, it is likely that any resulting 'oil plasticization' of the adhesive matrix will only take place close to the interface. Thus, with thicker bondlines it is highly likely that, on cure, two distinct matrices will exist: one which is 'oil plasticized' and one which comprises just the original adhesive formulation. Fig. 8.7 shows, that the failure modus observed varies, i.e. lack of cohesion, mixed and lack of adhesion as the bondline thickness increases from 0,2/0,5/1,0mm.

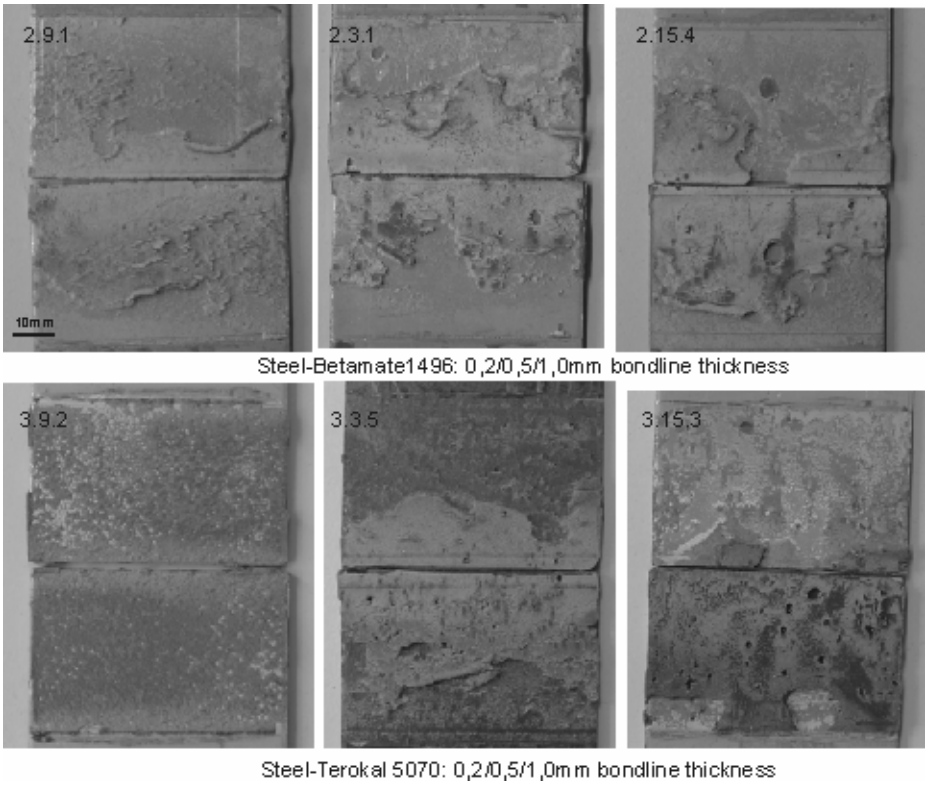

Fig. 8.7: Macroscopic observations on the fracture surface of steel lap joints bonded with the adhesives "Betamate 1496" and "Terokal 5070" and inserted PTFE layer.

Again, one would expect that the effect of plasticization on the cured adhesive – it is very unlikely that any oil inclusion will be lost during cure – would lead to stress relaxation in the

cured joint; making the matrix appear "tougher". Again, this can manifest itself with an apparent improvement in lap-shear and peel performance at ambient – but not elevated – temperatures.

The presence of two distinct matrices – i.e. as has been indicated for thicker bondlines – leads to different failure patterns and possibly, to a different shear performance.

8.5 Correlation of defects to the shear performance

From the available chemical analysis, neither formulation, on the face of it, appears to possess a chemistry which is likely to make it susceptible to, particularly, moisture attack. Indeed, the Betamate 1496 contains an epoxy resin - 2, 3-epoxypropyl neodecanoate – which should protect the cured adhesive against moisture ingress.

It is quite clear, from the micrographs, that the Betamate 1496 is significantly more susceptible to moisture than the Terokal 5070 adhesive. This could, indeed, be due to the overall chemistry of the adhesives. One possibility which springs to mind is that the Betamate 1496 contains dicyandiamide as the curative – this is particularly susceptible to moisture attack – and the Terokal 5070 contains something like an aromatic amine – DDS, for instance.

Whatever the explanation, it is very clear that both adhesives are significantly affected by pre-bond humidity exposure under the conditions used in this piece of work.

Turning to the shear performance, especially as it is accepted that the current sample size is small, it is very difficult to arrive at hard and fast conclusions concerning any possible adhesive-to-adhesive and/or bondline thickness variations.

If one examines the effect of pre-bond humidity on the steel and the aluminium adherends then, once the scatter bands are taken into account, it is very difficult to see any real trend across the bondline thicknesses used or from adhesive to adhesive. What is surprising, however, is how well both adhesives perform at bondline thicknesses of 0,2 and 0,5 mm when one considers the damage seen within the fracture surfaces.

It is feasible that, at the highest bondline thickness of 1,0 mm, the much reduced level of damage, coupled with any commensurate, overall reduction in bondline thickness following enhanced squeeze out, could just improve the apparent joint strength.

For the same reasons, it is very difficult to see any real trends in the performance on oily steel substrates; if anything the scatter bands are often much more pronounced in these cases.

The differences in shear performance between the thinnest and the thicker bondlines, indicate that, in the case of the thicker bondlines, the epoxy/oil matrix close to the interface is more ductile than the stiffer matrix in the centre of the joint; oil not having penetrated this far. The stresses in these joints, therefore, would be different, or even very different, to those in the joints with the much thinner bondline; leading to very different failure loads and/or patterns.

The presence of defects, consequently, is more likely to be indicative of poor joint manufacture than of impending failure, especially for short term loading. Former investigations on aluminium-joints with disbonded areas have shown that the presence of this large artificial imperfection caused virtually no change in joint strength [Drinkwater 2001]. The presence of defects however could be of high importance for the long term behaviour of structural components; contact corrosion when various materials combine. Fatigue and crash behaviour are also vital issues to be considered and defects could lead to earlier bonding failure. Furthermore manufacturing defects, such as displacement of the adhesive bondline out of the overlap area, require rectification, bearing consequently the production process.

8.6 Concluding remarks

Pre-bond humidity is causing considerable damage within the joint. Thus, it is unlikely that water remains dispersed with the adhesive after cure; hence no plasticization. There is too much scatter with such a small experimental sample to draw any hard and fast conclusions concerning strength trends. However, the results do give the appearance that the thicker adhesive layers could actually benefit from exposure to pre-bond humidity. This could well be as a result of a change in joint geometry – thinner than expected bondlines – rather than any plasticization.

Oil most certainly 'dissolves' in the epoxy matrices during cure; the key to performance could well be the depth of penetration into the joint; a 1.0 mm bondline is thick. 'Dissolved' oil in structural epoxy adhesives has been known to plasticize the cured matrix at room temperature in the same way as water appears to. Again, there is too much scatter with such a small experimental sample to draw any hard and fast conclusions concerning strength trends. It seems that the results with thicker adhesive bondlines show a significant down turn possibly behaving like a ductile adhesive at the interfaces and a rigid adhesive in the centre changing the failure patterns in the joint.

The major concern of these investigations is the degradation of joint mechanical properties due to improper manufacturing conditions. The structural behaviour of the joint depends on the adhesive-adherend system and on the inserted imperfection. The weak bondline problem has a significant and measurable effect on the load transfer capability of the joint. Although the strength reduction under short term loading seems to be insignificant due to the presence of defects, these can lead to unexpected consequences when it comes to production process and in-service performance.

9 Proposal of design and quality control evaluation

Overlap joints are the simplest types of adhesively bonded joints for structural applications, mainly used by designers and in standard test methods. However the stresses in the adhesive layer are not uniform in practice, and the stress concentrations arise from differential straining of the substrates and from the eccentricity of the loading path. The early work of Volkersen, who considered only the former of the factors and Goland and Reissner, who were the first to consider both factors, is given below. Attention is given towards imperfections, their consideration in the models and the estimation of a correction factor.

9.1 Considerations with the net overlap area

The main goal of this chapter is to compare the experimental average shear stress τ_0 to the calculated-predicted maximum shear stress τ_{max} of defective single lap joints based on the assumptions and analytical expressions of Volkersen (V) and Goland-Reissner (G-R). If the adherends behave as a rigid material (inextensible), the shear stress distribution would be even and equal to the applied load divided by the bonded area. However calculations are based upon the assumption that the adhesive and the substrates behave as linear elastic materials and the stress is proportional to strain. The real shear stress distribution is illustrated in Fig. 9.1 (hatched area).

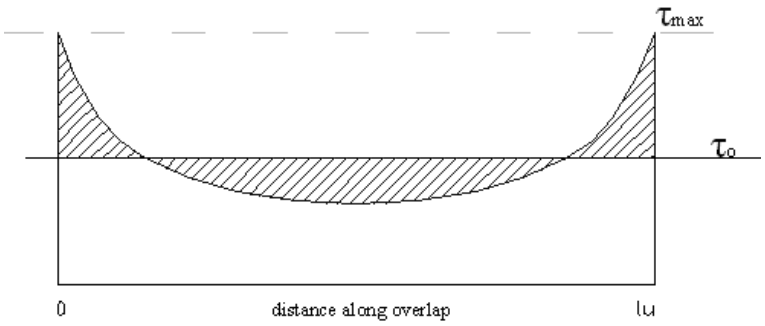

Fig. 9.1: Nominal shear stress distribution τ_0 in a single lap joint with linear elastic materials

The experimental failure load divided by the bonded area is equivalent to τ_0 i.e. the nominal stress at failure, and the theoretical maximum stress τ_{max}, is near the overlap end. The areas below τ_0 and between τ_{max} and τ_0 are of course equal. In both theories the maximum stress in the joint is expressed by Eq. (9-1):

$$\tau_{\max,th} = \mathrm{K} \cdot \tau_0 \qquad \text{Eq. (9-1)}$$

where:

$$\tau_0 = \frac{F}{w \cdot l_u} \text{ (= failure load/overlap area)} \qquad \text{Eq. (9-2)}$$

The K value depends on the theory used and the respective assumptions.

To calculate τ_{max} with V and G-R theories in case of joints with defects, the following simplification is made; the defect area, estimated through neutron image processing, is used to calculate a new overlap area (net area), Fig. 9.2. The models of V and G-R depend on the overlap length and not the area, consequently knowing the defect area for every specimen and for a constant overlap width $w = 48$ mm an overlap length lu_2 is calculated from Eq. (9-3) Thus a new overlap length lu_1 is calculated from Eq. (9-4) used also in the theories of V and G-R. This approach is rather general and approximate considering the defect and without taking into account the actual location and the shape of the defect. The actual consideration is that the

failure load is reached for a smaller overlap area and the nominal shear stress is respectively higher. Based on considerations of Adams et al the positioning of a defect at the edges of the overlap and transverse to the loading axis is the worst case of debond due to higher stress peaks concentrated at the outer area [Adams 1999].

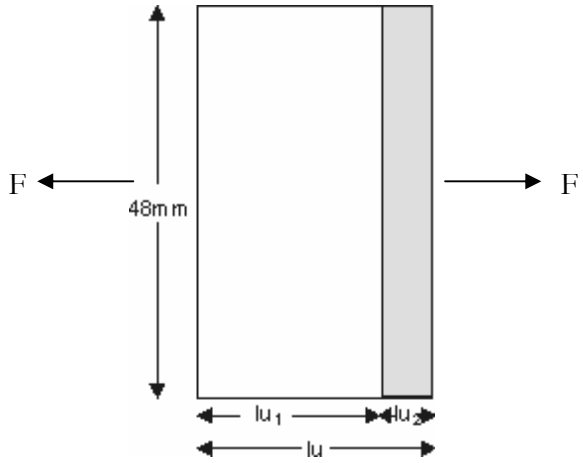

Fig. 9.2: Simplification where the net area represents the overlap area

$$l_{u_2} = \frac{A_{defect}}{w} \quad (A_{defect} \text{ given in Table 5.3 to Table 5.6 and w = 48 mm}) \qquad \text{Eq. (9-3)}$$

$$l_{u_1} = l_u - l_{u_2} \quad (l_u = 30 \text{ mm for steel and 20 mm for aluminium}) \qquad \text{Eq. (9-4)}$$

9.1.1 Results based on Volkersen and the reduced overlap length

Volkersen's stress analysis is based upon the assumption that the joint is loaded in pure tension-shear. A number of parameters characteristic for every bonded system are taken into account, i.e. shear modulus of the adhesive G_a, bondline thickness t_a, tensile modulus of the substrate E_s, thickness of substrate d_s and the reduced overlap length l_{u1} (s. Eq. (9-4)) influencing the stress distribution of the adhesive joint. The value of K_V is obtained from the following equations:

$$K_V = \left(\frac{\Delta}{W}\right)^{1/2} \cdot \left[\frac{W - 1 + \cosh(\Delta \cdot W)^{1/2}}{\sinh(\Delta \cdot W)^{1/2}}\right] \qquad \text{Eq. (9-5)}$$

where W is defined by:

$$W = \frac{E_{s1} \cdot d_1 + E_{s2} \cdot d_2}{E_{s1} \cdot d_1} \qquad \text{Eq. (9-6)}$$

where Δ is a dimensionless coefficient:

$$\Delta = \frac{G_a \cdot l_{u_1}^{\,2}}{E_{s2} \cdot d_2 \cdot t_a} \qquad \text{Eq. (9-7)}$$

For the substrates of these investigations, $E_{s1}d_1$ and $E_{s2}d_2$ are equal and W reduces to a value of 2. Eq. (9-5) becomes then:

$$K_V = \sqrt{(\Delta/2)} \cdot \coth\sqrt{(\Delta/2)} \qquad \text{Eq. (9-8)}$$

The model suggested by Volkersen does not take into account the tensile stresses generated in the adhesive as a result of the bending moment related to the eccentricity of the joint design. The results of the maximum stress with the assumption of the reduced overlap length l_{u1} are given in Annex D.

9.1.2 Results based on Goland-Reissner and the reduced overlap length

Goland and Reissner, after performing a series of experiments, came to the conclusion that the bending of the substrates at the extremities of the bonded area has a considerable effect upon the stress distribution of the joint itself. This consideration was described through the following equations, where $\varkappa$ is the bending moment factor:

$$\kappa = 1 + 2\sqrt{2}\cdot\tanh\left\{(3/2)\cdot\sqrt{(1-\nu_s^{\,2})}\cdot(l_{u_1}/2d)\cdot\sqrt{(F/E_s\cdot b\cdot d)}\right\} \qquad \text{Eq. (9-9)}$$

$$K_{G-R} = \frac{\tau_{\max}}{\tau_0} = f(\kappa) = \frac{1+3\kappa}{4}\cdot\sqrt{(2\Delta)}\cdot\coth\sqrt{(2\Delta)} + \frac{3\cdot(1-\kappa)}{4} \qquad \text{Eq. (9-10)}$$

where ν_s is the Poisson's ratio of the substrate (0,33 for aluminium and 0,30 for steel) and Δ is calculated through Eq. (9-7). The values of the maximum stress assuming a reduced overlap length l_{u1} are given in Annex D.

9.1.3 Comparison of the theories

The diagrams in Fig. 9.3 and Fig. 9.4 show the ratio τ_{max}/τ_0 in relation to the bondline thickness for the defect free and defect bonds and arise from the diagrams of Annex D. The diagrams of Annex D express the magnitude of the discrepancy among the defect types with the result that this magnitude is practically the same for all types of investigated defects but differs for different bondline thickness [Suárez 2004]. Thus, the factors K_V and K_{G-R}, (Fig. 9.3 and Fig. 9.4) estimated with the assumption of the reduced overlap length l_{u1}, give a measure between ideal and defect bonds using the mean value of defect types for each bondline thickness.

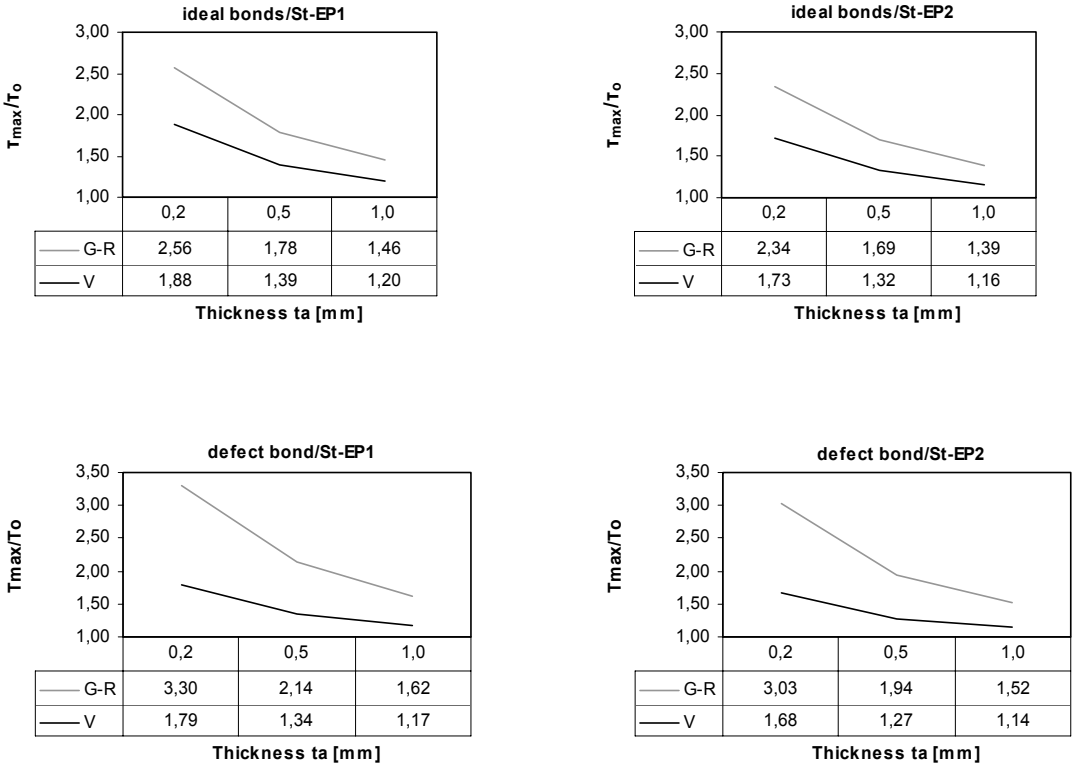

Fig. 9.3: Mean values of factors K_{G-R} and K_V for steel-epoxy defect free and defect joints (EP1=Betamate 1496 and EP2=Terokal 5070).

matrix which is said to give high peel strengths and to impart good impact-peel resistance to bonded joints.

The MSDS only shows that it contains less than 50% of a liquid Bisphenol A epoxy resin. It is clear, though, that it also contains nitrogenous components; almost certainly the hardener. There are also indications that it contains a solid filler. Further physical and mechanical properties of EP2 are mentioned on the Table 8.7:

Table 8.7: Properties of the adhesive "Terokal 5070MB-25"

Sg	1.10
Shrinkage on cure	6.8%
Viscosity at 50°C	75 Pa.s
Average size of solid particles	< 30 μm
Lap-shear strength on oily [2 – 3 g/m²] steel substrates*	
at -40°C**	>25 MPa
at 23°C	>20 MPa
at 90°C**	>15 MPa
Service temperature [short excursion]	-40° to +90°C [120°C]
*: Cured for 30 minutes at 180°C **: Following 24 hours conditioning at temperature	

Both adhesive Data Sheets state that these systems impart enhanced toughness (peel and impact and/or impact-peel performance) but give no indication as to the toughening mechanism. What is declared would generally lead to a fairly brittle end-product thus a toughener must be present; it is likely in both cases that this will be a carboxylated nitrile rubber (i.e. Hycar CTBN), a polyurethane or some such polymeric modifier.

In both cases no indication is given as to the curing system. This could be dicyandiamide -water sensitive- but, in view of both systems' ability to cure at 155° to 160°C it is likely that it is an aromatic amine such as diamino diphenyl sulphone [DDS, Dapsone®], which does have good water resistance; there is just a possibility that it could be a 'Lonza amine': substituted diamino diphenyl methanes (DDM).

It is likely that both systems contain fillers; these could impart thixotropy or give some environmental protection. In the first case the most likely material would be a fumed silica (particle size is generally smaller than 7 μm). In the second case, many formulations include finely-divided calcium carbonate to provide cataplasma resistance; this would fit with the particle size quoted for EP2.

Both adhesives are quoted as being tolerant to many -but not all- oils encountered in engineering, particularly automotive, applications. This is not really surprising as most epoxy resins exhibit some compatibility towards oil. Further, EP1 contains 2, 3-epoxypropyl neodecanoate which, not only is a specific for protection of the cured matrix against moisture attack, but should enhance the system's oil compatibility. If both systems contain something like Hycar CTBN, this will also aid in tolerance to oily substrates [Sprenger 2003].

8.4.1 Teflon layers

The diagrams of Fig. 8.2 show that high strength steel or aluminium alloys bonded with structural epoxy adhesives including PTFE layers of less than 10% (square layer) or even 5% (triangle layer)

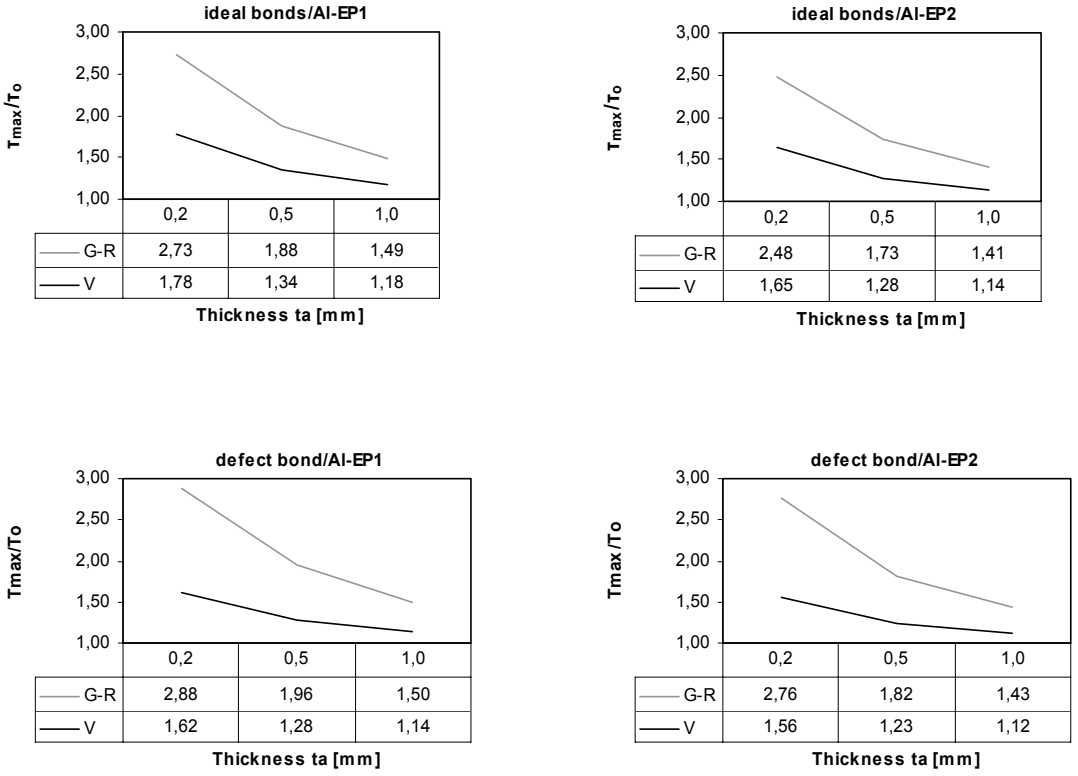

Fig. 9.4: Mean values of factors K_{G-R} and K_V for aluminium-epoxy defect free and defect joints (EP1=Betamate 1496 and EP2=Terokal 5070).

In diagrams of Annex D the ideal joints with 0,2 mm thickness reach the highest failure stress. Nevertheless, for the defect free steel-Betamate 1496 joints the mean value of stress with 0,5 mm bondline thickness, is almost 6 % higher, than bonds with 0,2 mm thickness. Specimens with defects show a better behaviour with 0,2 mm bondline as well. Only in the case of introduced defect of 90% r.h., an enhanced structural behaviour is observed with 1,0 mm bondline thickness and not 0,2 mm as expected. The theoretical stress values of V and G-R show similar tendency to the experimental values; the value of τ_{max} increases with decreasing thickness, Fig. D.1 and Fig. D.2 of Annex D.

In comparison with steel joints, aluminium joints present similar behaviour with bondline thickness variation but a lower failure load range (Fig. D.3 and Fig. D.4 of Annex D) due to the decreased rigidity of aluminium adherends.

The effect of the defect on the carrying capacity or the structural strength of the joint can be expressed more accurately through the analogy of τ_{max} (as the critical stress value in failure) than the nominal value τ_0. Table 9.1 gives a measure of maximum stress by the effect of the defect compared to the ideal bond. The maximum stress values were estimated with the G-R theory being more representative to the real loading conditions.

Table 9.1: Percentage (%) of the maximum stress of defective bonds in relationship to ideal bonds.

$\frac{(\tau_{\max_{defect}} - \tau_{\max_{ideal}})}{\tau_{\max_{ideal}}} \cdot 100\%$		Bondline thickness 0,2 mm		Bondline thickness 0,5 mm		Bondline thickness 1,0 mm	
Adherends	Imperfection	Betamate 1496	Terokal 5070	Betamate 1496	Terokal 5070	Betamate 1496	Terokal 5070
steel	oil_3	33,48	31,10	10,29	22,50	26,32	15,60
	oil_5	40,80	31,83	5,57	20,79	15,32	18,05
	oil_7	37,71	35,62	-5,23	18,74	10,77	13,98
	teflon_100	38,64	20,99	14,29	12,88	4,20	23,73
	teflon_50	40,76	26,36	26,39	19,03	28,20	21,17
	90 % r.h.	9,56	22,91	2,22	29,72	36,13	26,82
aluminium	teflon_64	16,58	-0,36	22,85	0,73	10,65	16,76
	teflon_32	22,45	9,22	25,57	-18,47	18,10	20,42
	90 % r.h.	4,74	21,90	23,52	5,63	29,79	26,01

Considering the net bond area on the stress calculations, the joint failure stress under short term static loading is sometimes higher with defects than ideal bonds (positive results in Table 9.1). Actually this fact is significantly influenced by the position of the defect. On the contrary to the almost even stress distribution along the overlap length, when a defect zone (e.g. porosity or small contaminants close to each other) is present, implies a stress concentration point - possibly stress in this point is lower than at the end of the bondline (τ_{max}) -, that could reduce the τ_{max} value at the end of the overlap to a new value τ'_{max} (area above and below the τ_0 line must be equal), Fig. 9.5.

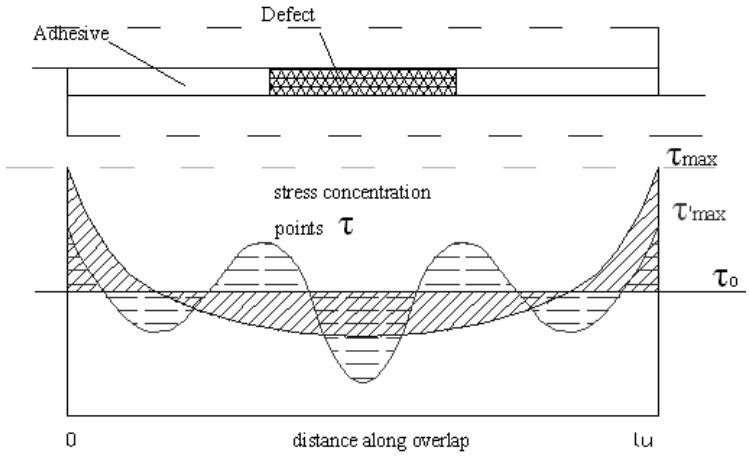

Fig. 9.5: Possible stress concentration effect with presence of defect.

9.2 Considerations with the gross overlap area

In practice, NDT is used only for limited applications. Thus, the following approach deals with the assumption that the size of the defects can not be estimated. Considering that critical manufacturing defects are a threat to the structural integrity of the joint and due to lack of reliable NDI in a production series, a coefficient multiplied by the G-R factors is determined; this approximates to a corrected G-R factor in order to estimate the τ_{max}, in the adhesive joints. This was accomplished through $f(\varkappa)_n$ values estimated for the net or reduced area (w^*l_{u1}), and the new $f(\varkappa)_g$ values, calculated with the non reduced or gross area (w^*l_w). For this approach the factors of Goland and Reissner theory were used being more representative to the real loading conditions than the earlier theory of Volkersen.

The $f(\varkappa)_n/f(\varkappa)_g$ ratio represents the constants determined for each series of specimens. Table 9.2 and Table 9.3 show the mean value for every series obtained each time out of 5 specimens.

Table 9.2: Mean value of $f(\varkappa)_n/f(\varkappa)_g$ ratio for Steel-Epoxy (Betamate 1496 or Terokal 5070)

	Steel-Betamate 1496			Steel-Terokal 5070		
Inserted defect	Bondline thickness			Bondline thickness		
	0,2 mm	0,5 mm	1,0 mm	0,2 mm	0,5 mm	1,0 mm
oil 3 g/m²	1,28	1,22	1,14	1,32	1,17	1,11
oil 5 g/m²	1,32	1,20	1,10	1,30	1,18	1,10
oil 7 g/m²	1,33	1,18	1,13	1,32	1,16	1,09
teflon foil 100 mm²	1,26	1,18	1,08	1,23	1,13	1,08
teflon foil 50 mm²	1,31	1,22	1,12	1,28	1,18	1,11
90% r.h.	1,19	1,13	1,06	1,29	1,14	1,12

Table 9.3: Mean value of $f(\varkappa)_n/f(\varkappa)_g$ ratio for Aluminium- Epoxy (Betamate 1496 or Terokal 5070)

	Aluminium- Betamate 1496			Aluminium- Terokal 5070		
Inserted defect	Bondline thickness			Bondline thickness		
	0,2 mm	0,5 mm	1,0 mm	0,2 mm	0,5 mm	1,0 mm
teflon foil 64 mm2	1,09	1,07	1,02	1,09	1,04	1,02
teflon foil 32 mm2	1,17	1,10	1,05	1,14	1,07	1,03
90% r.h.	0,89	0,97	0,93	1,08	1,01	1,01

In the above tables values greater than one are mostly observed, meaning that the $f(\varkappa)$ values are higher, when the size of the defect is estimated and its area is not included to the bonded area. To accomplish a practical use of the above tables a representative value is adopted. For every bonded system and bondline thickness the $f(\varkappa)_n/f(\varkappa)_g$ ratio was determined out of the mean value of a sample size of 5 defects for steel bonds and 3 defects for aluminium bonds, Table 9.4.

Table 9.4: Mean values of ratio $f(\varkappa)_n/f(\varkappa)_g$ (EP1=Betamate 1496 or EP2=Terokal 5070)

Bondline thickness mm	Steel-EP1 %	Steel-EP2 %	Aluminium-EP1 %	Aluminium-EP2 %
0,2	1,28	1,29	1,05	1,11
0,5	1,19	1,16	1,05	1,04
1,0	1,11	1,10	1,00	1,02

From Table 9.4 can be concluded that the general tendency is $n_{1,0}<n_{0,5}<n_{0,2}$, which indicates that the value of these coefficients is always lower for higher thickness. These values serve as a contribution to the estimations of a correcting factor $f(\varkappa)_n/f(\varkappa)_g$, in respect to manufacturing defects used in the calculation of the G-R bending moment factors. Thus, realistic values of G-R bending moment factors regarding the net area are attained and the subsequent maximum stress can be estimated. A practical approximation of the values is shown in Table 9.5. These results may be extrapolated to another type of joint with different geometric parameters, when further experimental investigations of the new parameters are performed.

Table 9.5: Final values of $f(k)_n/f(k)_g$ (EP1=Betamate 1496 or EP2=Terokal 5070)

Thickness mm	Steel-EP1 %	Steel-EP2 %	Aluminium-EP1 %	Aluminium-EP2 %
0,2	1,30	1,30	1,05	1,10
0,5	1,20	1,15	1,05	1,05
1,0	1,10	1,10	1,00	1,05

Table 9.5 expresses the magnitude of the discrepancy between critical theoretical (maximum) stress and engineering maximum stress with the result that this magnitude is practically the same for all types of investigated defects but differs for different bondline thickness. These values are higher for steel than in aluminium due to the deformation capacity i.e. lower elastic modulus of the aluminium adherends.

9.3 Safety and reliability concept of design and execution

Structural integrity is ensured through the estimation of boundary conditions between safety and failure in engineering structures. Specifications have provided guidance by defining "allowable" loads/stresses, a limit value derived from the bearing capacity of a component assuming an overall safety margin, initially based on past experience. This definition has undergone many refinements, mainly through more reliable, statistically supported estimates for loading and the bearing capacity, and the familiar attempts to identify partial safety factors, separately for the action and reaction side. It must also be considered that design is a multiple and interdisciplinary task requiring a clear allocation of responsibilities in order to realise safety and reliability as well as economy. It is a recent achievement only, during the Eurocode drafting process, international code harmonisation efforts and the linking of manufacturing, quality control and inspection criteria with component behaviour in service that a consistent system of rules has been produced [Kosteas 2004]. These aspects had to be taken into account in both codes for aluminium structures, i.e. for design [prEN 1999] and execution [prEN 1090].

A dialogue between science/university and industry/manufacturer/client/operator/authorities /society has to be carried on. On the national level there are at times too many and fragmented bodies, on the European level the ESIS (European Structural Integrity Society) is still a fledgling

organisation, and internationally there is not a single organisation. Standards organisations may undertake this task. In this sense the Eurocode EN 1990, Part 2.2, Annex B identifies reliability management of design and execution work, Fig. 9.6 and Fig. 9.7.

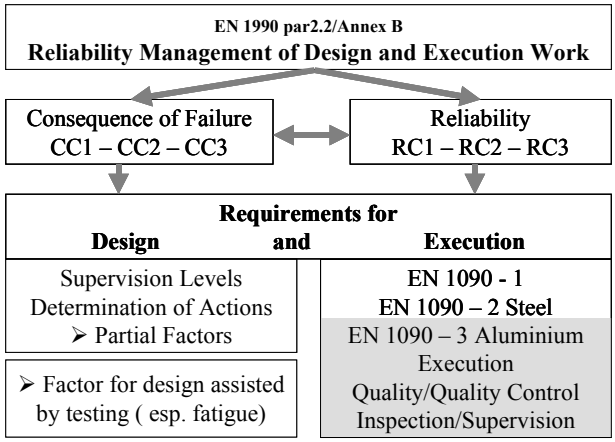

Fig. 9.6: Elements for reliability in design and execution

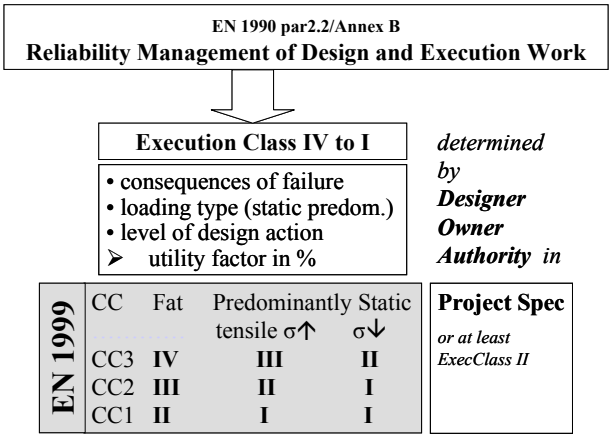

Fig. 9.7 Execution classes in the Eurocode for aluminium

The National Annex may further define rules for a) application of the reliability class, b) the connection between reliability and execution class, c) supervision/execution. Execution classes provide these links. The factors introduced to account for reliability are given below:

- the partial factors for loading and component strength,
- the factor for design assisted by testing, and
- the utilisation factor expressing the level of design action.

Especially the first two are linked inherently to sample sizes of evaluated data. The third is used for linking design values to actual behaviour in practice or at least to current execution quality standards. Further information on these factors as they appear in the Eurocode and a discussion of procedural steps for their definition and correlation to actual test data is given in [Kosteas 2004].

9.4 Quality Management

9.4.1 Quality Zoning Diagram and Criticality grades

NDT serves as a basis for process control and to establish quality control standards. The acceptance or rejection of a bonded assembly is related directly to the quality level desired by the designer. The quality level, in turn, is based on the importance of the part or component in terms of performance or safety. The frequency/severity flaw criteria and sensitivity of the test should be based on the desired quality levels. To avoid unwarranted inspection costs, it is advisable to divide the bonded joints into zones based on stress levels or criticality of the part function [Hagemaier 1985]. Bonded joints are generally designed to withstand shear loads. Stress analysis of bonded joints reveals that the outer edges of a bonded joint will be subjected to higher stress levels than the middle of the joint. Therefore, higher quality may be desired at the edges, and parts should be zoned accordingly. The zoned area should be dimensioned so that the inspector can define the two different zones prior to inspection. Fig. 9.8 shows an example of quality zoning for an overlap joint. A definition of inspection grade numbers versus allowable defect size is illustrated on the diagram. Quality grade 1 is within ¼ of the overlap length and grade 2 is the bond between any two grade 1 bonds. The boundary between the two grades is at $\tau_{max} = \tau_0$. For example for the overlap joint the quality grades were defined as follows:

Quality grade 1:

If $l_{max\ unbonded}$=25% unbond length, then $w_{max\ unbonded}$=¼*100% =25% unbond width;

If $w_{max\ unbonded}$=100% unbond width, then $l_{max\ unbonded}$=¼*25% = 6,25% unbond length;

Quality grade 2:

If $l_{max\ unbonded}$=50% unbond length, then $w_{max\ unbonded}$=¼*100% =25% unbond width;

If $w_{max\ unbonded}$=100% unbond width, then $l_{max\ unbonded}$=¼*50% = 12,5% unbond length;

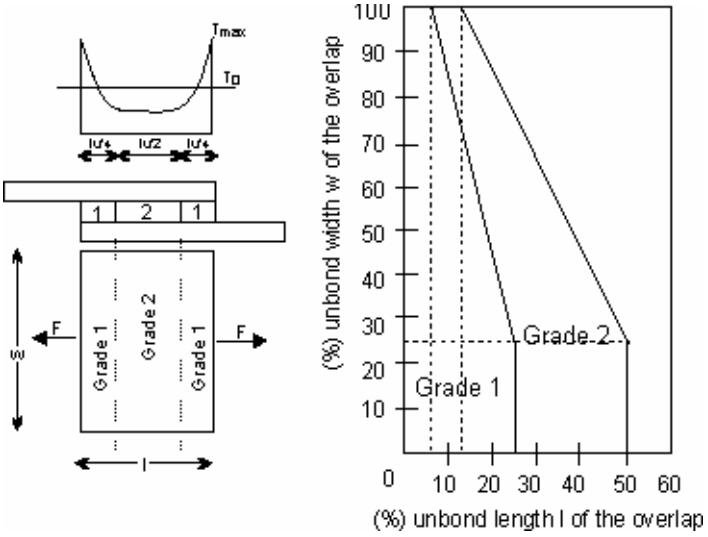

Fig. 9.8: Zoning diagram of acceptance grades for defect area.

For multiple bondline joints, it may not be possible to inspect to a high quality at the edge of all adherends because of the loss of test sensitivity at each successive bondline below the surface. If the edges of the joint are stepped or staggered, high quality inspection is possible at the edges of all bondlines. The width of the step should be large enough to accommodate the test instrument probe through ultrasonic inspection. Joint edges that are not stepped should be inspected from opposite sides.

The above definition of the acceptance grades within an overlap area is used to fulfill the quality requirements described in the 3 following steps.

9.4.2 Quality requirements

Before inspection can be performed on a bonded structure, acceptance/rejection criteria must be established. These are usually in form of frequency (number of defects per unit area) and/or severity (maximum allowable defect size). To avoid unnecessary rejections the boundary conditions between bold and conservative criteria must be adopted. The frequency and severity criteria should be based on NDT readings and subsequent strength levels. To avoid excessive, unnecessary inspection or to underestimate the quality requirements, quality classes are specified making use of experimental investigations.

Step 1: Indication of Criticality Grades.

Fig. 9.9 shows an example of quality zoning for bonded laminate skin splices. The numbers 1 and 2 on the drawing indicate the zones with different criticality grades. Quality grade 1 is within ¼ of the overlap length of the edge of any bonded member and grade 2 is the bond between any two grade 1 bonds.

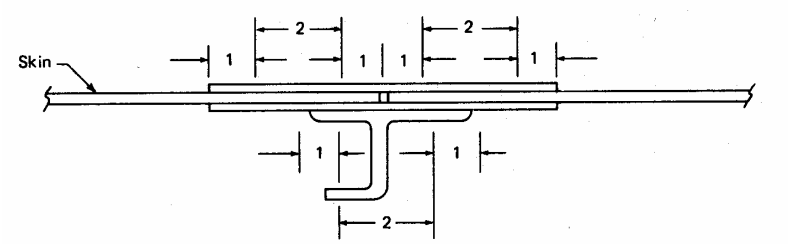

Fig. 9.9: Indication of quality zones on a complex bonded component

Step 2: Acceptance/Rejection Criteria.

Based on the geometry of the specimens used for the experimental investigations and on the zoning concept of the Fig. 9.8 the zones with the criticality grades are shown in Fig. 9.10. The actual unbonded area (defect) should be within the maximum allowable unbonded area for the two grades. The acceptance/rejection criteria for the adhesive joints are determined through the following requirements for the unbonded area:

- If $A_{actual\ unbonded} \leq A_{allowable\ unbonded}$ in Grade 1 and Grade 2 then the joint is accepted;
- If $A_{actual\ unbonded} > A_{allowable\ unbonded}$ in Grade 1 or Grade 2 then the joint is rejected;

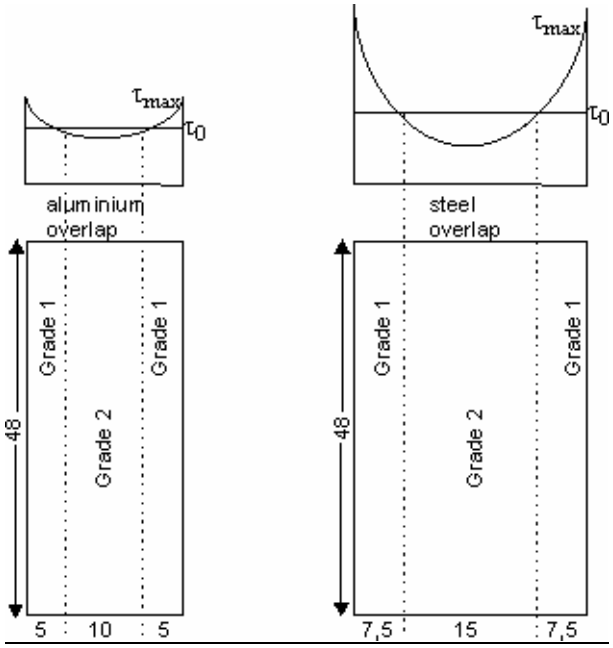

Fig. 9.10: Indication of zones for the aluminium and steel bonds

The actual unbonded area ($A_{actual\ unbonded}$) is estimated through NDT readings (Table 5.3 to Table 5.6) and the maximum allowable unbonded area ($A_{allowable\ unbonded}$) is calculated from the zoning diagram of Fig. 9.8.

If the joint is accepted then Step 3 follows.

Step 3: Specification of Quality Classes.

For every grade of the zoning diagram the actual bonded area is equal to the maximum bonded area without the defect area: $A_{actual\ bonded} = A_{maximum\ bonded} - A_{defect}$.

For mild steel adherends und subsequently aluminium according to chapter 8 there is no effect of the defect size until more than 50% of the bond area has been removed, Fig. 9.11 (diagram on the left). In case of high strength steel adherends, there is a clear and almost linear reduction in the joint strength with increasing debond area, Fig. 9.11 (diagram on the right). The maximum

allowable unbonded area can be up to 25% of the bonded area for every grade. A defect beyond that limit leads to the rejection area of the diagrams.

Referring to Fig. 9.11 and considering that $l_{max}*w_{max}$ = 100% bonded area belongs to Class A, the following quality classes for each criticality grade are specified:

- Class A: bonded area greater than 85%;
- Class B: bonded area greater than 50%;
- Class C: bonded area greater than 25%;

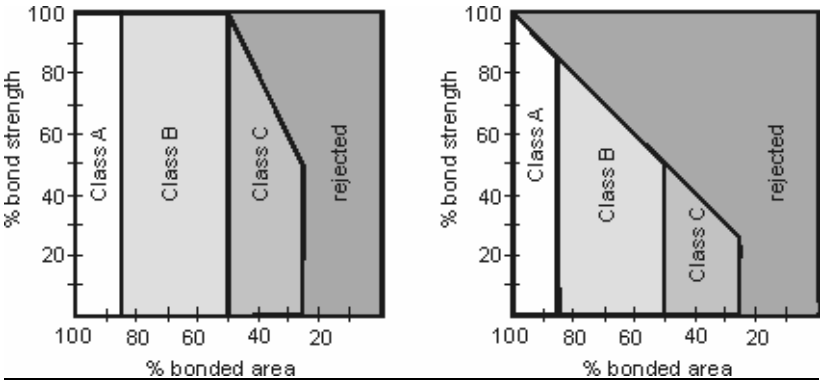

Fig. 9.11: Quality classes for bonded joints with aluminium or mild steel (left) and high strength steel (right) adherends.

The diagrams of Fig. 9.11 are based on the diagrams of the failure bond strength versus debonded area of the work of [Adams 1999]. For the better understanding of the above, two examples follow.

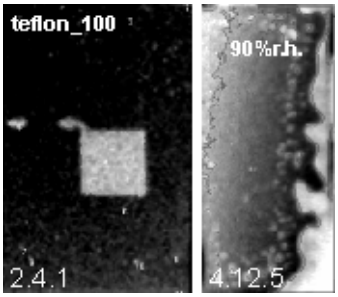

Fig. 9.12: Specimens for checking the quality requirements

Specimen 2.4.1: The pore on the left of the transmission image belongs to the zone of quality grade 1. Obviously the pore is very small and it does not negatively affect the quality of the joint. The artificial imperfection of the steel overlap area belongs to the zone of quality grade 2. Its size is approximately 130 mm^2. The unbonded length is approximately 11 mm i.e. 37% of the overlap length. The unbonded width is approximately 12 mm i.e. 25% of the overlap width (within the limits of zone for quality grade 2, Fig. 9.8) Thus the joint is accepted. The maximum bonded area (100%) in grade 2 is 720 mm^2. The actual bonded area is then 540 mm^2, i.e. 75% bonded area, leading to Class B: greater than 50% of the diagram on the right of the Fig. 9.11.

Specimen 4.12.5: the artificial imperfection of 90% r.h. is taking mostly place at the left and right sides of the overlap and belongs to grade 1. Its size is approximately 290 mm^2 (100 mm^2 on the left and 190 mm^2 on the right. The unbonded length $l_{unbonded}$= 5mm 25%, then the unbonded width is 100mm2 unbonded area/5mm unbonded length = 20 mm width equal to 42% overlap width but greater than the allowable $w_{unbonded}$=¼*100% =25% unbond width. Thus, this bond is rejected.

10 Conclusions and future research proposals

The aim of this study has been to evaluate the inspection effectiveness of NDT in assessing structural integrity of adhesive joints. To this purpose specimens with inserted and random defects were tested by neutron radiography and ultrasonics, analysed and evaluated by image analysis software. These results were then correlated to their respective shear strength values and fracture surface from destructive tests. Based on the findings of this thesis the following conclusions have been made.

The detectability of the imperfections depends on the adhesive-adherend system, on the type of imperfection, and on the NDT method used. The two methods of neutron radiography and ultrasonics can detect various types of flaws occurring in adhesive joints and may give a measure of the performance of the structure. In general, neutron radiography is a rather reliable tool – the distribution of organic materials or imperfections can be detected – but has limitations in on-site applicability as it needs powerful neutron sources and expensive equipment. The evaluation of critical structural parts or components in the development stage may be justified. The high detectability of defects is enhanced by the possibility to separate between a large number of grey levels in the transmission images obtained. This fact is associated with the geometry of the beam. The latter being almost parallel assures that no significant distortions will arise. It is worth noting that the smallest defect evaluated had only 0,08 mm^2 area equal to 1 pixel, the smallest unit able to be estimated with image processing. Neutron radiography is used as a reference method for the comparison of results with respective measurements on the same specimen series with ultrasonic techniques.

Contrary to transmission images of neutron radiography, C-scans in ultrasonics do not record the full feature extent of the overlap area. This is an important deficiency of the ultrasonic method, since humidity takes place mostly at the edges. According to observation of the C-scans, the imperfections appear larger, due to the geometry of the beam than on respective transmission images. For a large number of small size contaminations, ultrasonics gives a somewhat confusing image showing no exact shape of the contamination. The limited resolution on the C-scans is responsible for the smallest possible detected area of 0,32 mm^2 equal to 1 pixel. Nevertheless, the ultrasonic method, enhanced by ongoing developments in instrument technology, can also lead to reproducible test results within stated tolerances.

Experimental investigations on examples of structural components for the automotive industry have demonstrated that, for certain components neutrons may have more to offer for the evaluation of structural integrity than conventional methods. The refinement provided by neutron radiography or tomography for inspecting the adhesive structure and distinction between complicated metal parts is a prime advantage. Deliberately introduced imperfections or random defects during manufacturing have been qualitatively identified. It is worth noting that the initial experimental investigations considering various parameters on overlap joints with small specimens decisively contributed to the detection and identification of defects. This fact supports the concept of utilising neutron radiography as a tool to establish reference values for structural integrity management.

The major concern of the investigations is the mechanical properties reduction in joints due to improper manufacturing conditions. The structural behaviour of the joint depends on the adhesive-adherend system and on the inserted imperfection. The problem of adhesive weakness has a significant and measurable effect on the load transfer capability of the joint. Pre-bond humidity causes considerable damage within the joint. It is unlikely that water remains dispersed within the adhesive after cure; hence no plasticization of the adhesive. There is significant scatter within a small experimental sample to draw any hard and fast conclusions concerning strength trends. However, the results do give the appearance that the thicker adhesive layers could actually benefit from exposure to pre-bond humidity. Oil most certainly ‘dissolves’ in the epoxy matrices

during cure; 'Dissolved' oil in structural epoxy adhesive plasticizes the cured matrix at room temperature in the same way as water appears to. Again, there is significant scatter within a small experimental sample to draw any hard and fast conclusions concerning strength trends. It seems that the results with thicker adhesive bondlines show a significant reduction possibly behaving like a ductile adhesive at the interfaces and a rigid adhesive in the centre changing the failure patterns in the joint. The Teflon layer insert is to some extent responsible for a stress redistribution in the joint. Although the strength reduction under short term loading seems to be insignificant due to the presence of defects, these can lead to unexpected consequences when it comes to production process and in-service performance under service or fatigue loads.

Attention has been given towards imperfections though their consideration in theoretical stress analyses of Volkersen and Goland-Reissner and the estimation of a correction factor due to manufacturing defects. This factor expresses the magnitude of the discrepancy between critical theoretical (maximum) stress and engineering maximum stress with the result that this magnitude is practically the same for all types of investigated defects but differs for different bondline thicknesses. These values are higher for steel than for aluminium due to the deformation capacity of the aluminium adherends. A proposal for design and quality control evaluation is given by an attempt to define quality classes and acceptance/rejection criteria.

The presented straightforward methodology with various parameters and techniques aims towards establishment of standard limit values for actual defects in structural components by quality classes for adhesive joints, and discusses the industrial implementation options. Various aspects of reliable NDT and NDE methods to qualify the images processed and to quantify the manufacturing defects have been studied and extensively discussed. The systematic approach is a novel method to develop reliable NDE methodologies for structural adhesive bonded joints.

Future research activities within the field of structural adhesive bonded joints have to follow new developments in industry. The main contribution of NDE methods in adhesive joints is the detection of various types of flaws, the observation of degradation processes with time and, with accumulating experience, a product qualification procedure. With recent developments, applications of NDT in the aviation, automotive and electronic fields are often encountered. Adhesive joints, also in combination with other joining types in hybrid connections, offer advantageous solutions in aluminium structures – and also in in civil engineering. Their implementation in new codes would encourage further innovative applications. Lack of reliable data for different adhesive bonded systems could be offset through design by testing, and it is here that NDE could offer a valuable quantification and control tool. However, NDE cannot estimate joint strength directly. Parallel destructive tests commonly contribute to the desired correlation. Industrial fields have set increasing demands on NDT automation and reliability, both of which are pivotal for practical implementation. The thesis specifically focuses on the second parameter; the role of digital signal processing and, consequently, defect detectability and characterisation. A further important aspect is the implementation potential of NDI methods in industrial applications. Continuous improvements in the development of portable neutron sources must be sought for realising the full potential of neutron radiography in industrial "on-line" inspections. It is expected that as present limitations in these areas are lifted, neutron radiography will assume an active role in the non destructive evaluation of many types of bonded structure. Ultrasonic testing has been already widely performed in industry. Nevertheless, ultrasonic techniques enhanced by ongoing further developments in instrument technology, will prove to be a feasible alternative for online inspections in combination with reproducible test results within narrow tolerances.

Various questions about the structural mechanical actions are partly related to relevant manufacturing defects. In the present study, only short-term load condition have been considered. The presence of manufacturing defects is also significant for the long term behaviour of structural components and for contact corrosion when various materials are combined.

Fatigue and crash behaviour are also vital issues to be considered and defects could lead to earlier bonding failure. To validate the response of defects in crash resistance, creep behaviour or progressive failure processes, respective impact loads, long-term static loads, or low/high cycle fatigue loads within further experimental investigations have to be performed.

Most of the artificial imperfections considered as manufacturing defects assume failure due to lack of cohesion, while in many practical situations adhesion failure or a mixture of both failure modes is dominant. In this thesis, cohesion failure was ensured through suitable surface preparation, although oil contamination was often responsible for mixed or adhesive failure. The phenomenon of adhesion failure has been ignored for many years because, for various applications, the occurrence of this failure mode is not allowed. But there are no arguments why failure due to lack of adhesion is refused, as long as the target reliability level is guaranteed. Thus, further NDE should be focussed in the interlayer between the adhesive bondline and the adherend by studying various parameters of surface pretreatment or other possible manufacturing defects which can cause adhesive failure.

To evaluate the performance of NDI, the materials selection and specimen configurations are very important issues. Further, bonded systems with various geometrical parameters and structural adhesives on polyurethane basis would contribute to the validation of the proposed NDE. Study of inserted imperfections using further parameters regarding the position, size and magnitude is also essential. An additional methodology through theoretical considerations with finite element methods studying the effect of inserted imperfections on the structural response of adhesively bonded joints would be a valuable tool for structural integrity predictions in combination with experimental investigations.

An important aspect within the development of reliable quality control is the effect of the manufacturing process. In the present investigations, there is significant scatter in some cases, possibly due to the difficulty in reproducing artificial imperfections in the manufacturing process. Less is known about the actual influences of industrial manufacturing process on quality assurance. Researching the manufacturing process to find the defects cause might provide knowledge about procedures to be followed, sensitivity of the selected adhesive bonding system and the necessity of qualified personnel. Based on this, a qualification system can be developed for adhesive bonded joints, for example similar to those used for welded joints. The proposal for a design concept and quality evaluation methodology indicates the necessity of further tests.

Future research activities on testing techniques, evaluation methodologies, the influences of manufacturing defects, and correlation between irregularities and mechanical behaviour will support further developments of quality assurance in adhesively bonded joints. Using the presented systematic approach, the quality of bonded components under the investigated parameters can be estimated. A drawback of this approach is that the proposed process is complicated and needs optimisation suggestions for practical applications. This is because attention was given mainly in the reliability of testing performance and evaluation and not on technical developments regarding industrial implementation. For daily quality assurance, it is essential to develop easy to use testing methods. For this reason researchers also have to look after a combination of simplified testing methods and compilation of defect catalogues and quality classes. These investigations were initially aiming as a contribution to the work of the Eurocode [prEN 1999], [prEN 1090], either in verifying and supporting the initial assumptions of design values or providing a basis for decisions and classification in respect to execution and quality control standards.

References

[Achenbach 1991] Achenbach, J.D, Parikh O.K. Adhesion Sci. Technology, 1991, p. 601-618

[Adams 1984] Adams, R. D., Wake, W. C., Structural adhesive Joints in Engineering, Elsevier Applied Science Publ., United Kingdom (1984)

[Adams 1987] Adams R. D. Industrial applications of adhesive bonding edited by M. M. Sadek, Elsevier applied science publishers, UK (1987)

[Adams 1997] Adams, R.D., Comyn, J. and Wake W.C. "Structural Adhesive Joints in Engineering – 2nd Edition, pp. 359, Chapman & Hall (1997)

[Adams 1999] Adams, R.D., Guild, F.J. Karachalios, E., Mahon A.R., Journal of Adh. & Adh., "The significance to NDT of defects in adhesively bonded structures". (1999)

[Adams 2004] Adams R. D. What controls the strength of adhesive lap joints when exposed to aggressive environments. Proc. 7th European Adhesion Conference, Freiburg, Germany (2004)

[Albericci 1983] Albericci, P. Aerospace Applications, Durability of Structural Adhesives, ed. by Kinloch A. J, Elsevier Publ. New York (1983)

[Alers 1970] Alers G. A., Elsey R. K., Applications of quantitative ultrasonic signal analysis to adhesive bond strength prediction. Proc. Structural Adhesives and Bonding, pp. 119-137 (1970)

[ASNDT 2002] American Society for Nondestructive Testing: classification of ndt methods. <http://www.asnt.org/whatndt/primer4.htm> (2002).

[Barsom 1999] Barsom, J. M., Rolfe, S. T., Fracture and Fatigue Control in Structures: Applications of Fracture Mechanics. 3rd Edition. American Society for Testing and Materials Publ. (1999)

[Barton 1976] Barton, J. P. "Neutron radiography – An Overview", Practical Applications of Neutron radiography and Gaging, ASTM STP 586, American Society for Testing and Materials, ed. by Berger, H., pp. 5-19. (1976)

[Berger 1976] Berger, H. Practical Applications of Neutron radiography and Gaging, ASTM STP 586, American Society for Testing and Materials. (1976)

[Bijlmmer 1978] Bijlmmer, P. F. A. Adhesion 2, ed. K. W. Allen, Applied Science, London (1978)

[Bishopp 2004] Bishopp, J. Report: The effect of oil up-take on the mechanical performance of Dow's Betamate 1496V and Henkel's Terokal 5070MB-25. Star Adhesion Limited (2004)

[Bockenheimer 2002] Bockenheimer, C., Valeske, B., Possart, W. Network structure in epoxy aluminium bonds after mechanical treatment. Int. Journal of Adhesion & Adhesives. Vol. 22, pp.349-356 (2002)

[Botter 2001] Botter, H., van den Berg, A., Soetens, F., van Straalen, IJ. J.,Vlot, A. Influence of surface pre-treatment on the shear stress-strain relationships of structural adhesives. Proc. 6th Int. Conference on Structural Adhesives in Engineering, Bristol, UK (2001)

[Brockmann 1971] Brockmann, W. Grundlagen und Stand der Metallklebtechnik, VDI-Verlag, Düsseldorf (1971)

[Budenkov 1977] Budenkov G. A., Volegov Yu. V., Pepelyaev V. A., Redko V. I. Ultrasonics Vol. 7 pp. 194 (1977)

[Camahort 1979] Camahort, J.L., Carver, D., Pfeil, R., Mulroy, Jr.J.: Nat SAMPE Symp. Exhib., p. 377 (1979)

[Cawley 2002] Cawley, P.: NDE of Adhesive Joints.-What can be detected? Proc. The Second World Congress on Adhesion and Related Phenomena (WCARP-II), 2002, p. 127-129

[Chang 1975] Chang F. H., Couchman, J. C., Bell J. R., Gordon D. E. Correlations of NDE parameters with adhesive bond strength in multi-layered structures, Proc. ASNT 10th Symposium on NDT, San Antonio Texas, pp. 266-273 (1975)

[Chaskelis 1980] Chaskelis H. H., Clark A. V. Materials Evaluation, Vol. 38 (34) pp.20-26 (1980)

[Chernobelskays 1979] Chernobelskays T. Kovnovich S., Harnik E. J. Applied Physics, Vol. 12, pp. 815, (1979)

[Clark 1978] M. T. Clark, Definition and Non-destructive Detection of Critical Adhesive Bond-Line Flaws, U.S. Air Force Materials Lab. Techn. Rep. AFML-TR-78-108 (1978)

[Claus 1979] Claus R. O., Kline R. A. J. Applied Physics, Vol. 50, pp. 806 (1979)

[Clearfield 1991] Clearfield, H. M., Mc Namara, D. K., Davis, G., D. Adherend Surface Preparation for Structural Adhesive Bonding. Adhesive Bonding. Ed. by Lieng-Huang Lee. Plenum Publ. New York (1991)

[Curtis 1982] Curtis G. J. Ultrasonic Testing: Non conventional Testing techniques, pp.495-454 (1982)

[Cutforth 1976] Cutforth, D. C. "Neutron Sources for Radiography and Gaging", Practical Applications of Neutron radiography and Gaging, ASTM STP 586, American Society for Testing and Materials, ed. by Berger, H., pp. 20-34. (1976)

[Da Silva 2001] Da Silva, F. M. Lucas, Adams, R. D. The Strength of Adhesively Bonded T-Joints. Proc. 6th Int. Conference on Structural Adhesives in Engineering, Bristol, UK (2001)

[Dance 1976] Dance, W. E. "Neutron radiographic Nondestructive Evaluation of Aerospace Structures", Practical Applications of Neutron radiography and Gaging, ASTM STP 586, American Society for Testing and Materials, ed. by Berger, H., pp. 137-151 (1976)

[Davidor 1988] Davidor Y., Davies B. L. Int. J of Adhesion and Adhesives Vol. 8 (1). (1988)

[DeFrayne 1983] DeFrayne, G. High Performance Adhesive Bonding. 1st Edition. Adhesives for bonding metals. Society of Manufacturing Engineers. Michigan, USA (1983)

[Djordjevic 1981] Djordjevic B. B., Venables J. D. Proc. 13th Symposium on NDE, pp. 68-76. San Antonio Texas (1981)

[Drinkwater 2001] Drinkwater, B. W., Brotherhood C. J., Guild, F. J.: The Ultrasonic detectability of kissing bonds in adhesive joints. In Proc. SAE VI, Bristol, UK, (2001)

[Eis 2003] Eis, M. Qualitätsüberwachung beim Kleben. Proc. 17th Congress Swissbonding, Rapperswil, Switzerland (2003)

[Endlich 1995] Endlich, W.: Fertigungstechnik mit Kleb- und Dichtstoffen: Praxishandbuch der Kleb- und Dichtstoffverarbeitung. Braunschweig: Vieweg 1995.

[Fassbender 1980] Fassbender RH, Hagemaier DJ, Radecky RL, Int. J. Adhesion and Adhesives, 1(2): 79. (1980)

[Gali 1981] Gali, S., Dolev, G. Ishai, O. An effective stress/strain concept in the mechanical characterisation of structural adhesive bonding. Int. J. Adhesion and Adhesives. (1981)

[Garnish 1986] Garnish E. W. Epoxy Based Adhesives, Structural Adhesives – Developments in Resins and Primers, ed. by A. J. Kinloch, Elsevier Publ. N.Y. (1986)

[Gay 2000] Gay, C. Does stretching affect adhesion? Int. J. Adhesion and Adhesives. Vol.20 (2000)

[Gillham 1986] Gillham, J.K. Cure and Properties of Thermosseting Polymers. Structural Adhesives – Developments in Resins and Primers. Edited by A.J. Kinloch. Elsevier Applied Sciences Publishers, London and New York (1986)

[Goland 1944] Goland, M., Reissner, E.: Journal of Applied Mechanics, Trans. ASME, Vol. 66, p. A17 (1944)

[Gruber 2000] Gruber, W. Kleben von Aluminium - Aluminium Merkblatt V6. 4th Edition. Aluminium Zentrale e.V. Aliminium-Verlag, Düsseldorf

[Habenicht 1998] Habenicht, G. Kleben Grundlagen Technologie Anwendungen, 3rd Edition, Springer Verlag, Berlin (1998)

[Habenicht 2001] Habenicht, G. Kleben – erfolgreich und fehlerfrei, Vieweg Verlag, Germany (2001)

[Hagemaier 1978] Hagemaier D., Fassbender R. Nondestructive testing of adhesive bonded structures, SAMPE Q., Vol. 9(4), (1978)

[Hagemaier 1985] Hagemeier D. J. Nondestructive Inspection. Adhesive bonding of aluminium alloys. Ed. Thrall EW, Shannon RW. NY & Basel: Marcel Dekker Inc., (1985)

[HBK 2001] Handbuch Klebtechnik. Ed. by Adhäsion Kleben & Dichten, Industrieverband Klebstoffe e.V., Vieweg Verlag Germany (2002)

[HBKD] Handbook Kleben & Dichten

[Hiel 1984] Hiel, C., Cardon, A. H., Brinson, H. F. Viscoelastic Modelling of Epoxy-Resins for Adhesive and Composite Applications. Proc. 5th Int. Congress on Experimental Mechanics, Montreal (1984)

[Hinopoulos 2001] Hinopoulos G., Broughton WR. Evaluation of the T-peel joint using finite element analysis. Proc. 6th Int. Conference on Structural Adhesives in Engineering, Bristol, UK (2001)

[Jiao 1999] Jiao, D., Rose, J.L.: Adhesion Sci. Technol., p. 631-646 (1991)

[Kinloch 1983] Kinloch A. J. Introduction - Durability of Structural Adhesives, ed. by A. J. Kinloch, Elsevier Publ. N.Y. (1983)

[Kinloch 1990] Kinloch, A. J., Adhesion and Adhesives, Science and Technology, Chapman and Hall Publ., London, New York (1990)

[Kinloch 2004] Kinloch A. J., Korenberg C. F., Tan K. T. The durability of structural adhesive joints. Proc. 7th European Adhesion Conference, Freiburg, Germany (2004)

[Knollman 1982] Knollman G. C., Hartog J. J. J. Applied Physics Vol. 53, Part I, pp. 1516, (1982)

[Kosteas 1969] Kosteas, D: Επικόλληση μεταλλικών κατασκευών, Τεχνικά Χρονικά, Τεύχ. 5 (1969)

[Kosteas 2001] Kosteas D., Michaloudaki M. Aluminium adhesive bonding. State of the art. In Proc. 1st Hellenic Conf. in Metallic Materials, Nov. 2001,Volos, GR., pp. 94-99.

[Kosteas 2002a] Kosteas D, Michaloudaki M. In: Proc EURADH 2002/ADHESION ΄02. p. 353. Glasgow (2002)

[Kosteas 2002b] Kosteas, D. & Michaloudaki, M. The Method of Ultrasonic as a Tool for the Inspection of Technical Epoxy-Metal Bonds. Proc. 4th Nat. Conf. of HSNT & 2nd Balkan Conf. of BSND. Athens (2002)

[Kosteas 2002c] Kosteas, D. & Michaloudaki, M. NDE and Quality Control in Adhesive Joins. What can be detected? Proc. Colloquium on Aluminium in Shipbuilding, Munich (2002)

[Kosteas 2003] Kosteas D, Michaloudaki M. In: Proc. Int. Conf. Advances in Structures (ASSCCA `03) p. 453. Sydney (2003)

[Kosteas 2004] Design by Testing – A Look behind the Scenes Into prEN1999-1-3. Proc. ISAAG Conference, Munich (2004)

[Krautkrämer 1977] Krautkrämer J. u. H. Ultrasonic testing of materials, Springer Verlag, Berlin (1977)

[Lawley 1987] Lawley, E. D. Adhesives in the Automotive Industry, Industrial Applications of Adhesive Bonding, ed. by M.M. Sadek, Elsevier Publ. N.Y (1987)

[Lees 1987] Lees, W. A. & Baldwin, T. R. Adhesives for the Structural and Mechanical Engineer Industrial Applications of Adhesive Bonding, ed. by M.M. Sadek, Elsevier Publ. N.Y (1987)

[Lehfeldt 1973] Lehfeldt W. Ultraschall – kurz und bündig, Vogel Verlag, Würzburg (1973)

[Lehmann 1983] Lehmann, S. L. Primers for structural adhesives. High-Performance Adhesive Bonding. 1st Edition by G. DeFrayne. Society of Manufacturing Engineers (1983)

[Lehmann 1999] Lehmann, E et al., Application of new radiation detection techniques at PSI, especially at the spallation neutron source, NIM A 424, pp 158- 164. (1999)

[Lehmann 2001a] Lehmann, E. H., Vontobel, P., Frei, G. "Neutron radiography at the Spallation Neutron Source SINQ of the Paul Scherrer Institute", Villigen PSI (2001)

[Lehmann 2001b] Lehmann, E. H., Kühne, G. "Eigenschaften der Anlagen für Neutronenradiographie am Paul Scherrer Institut". In Proc. Anwender-Workshop zur Nutzung der Neutroneradiographie. 2001, Villigen PSI, CH (2001)

[Lehmann 2001c] Lehmann E, Vontobel P, Wiezel L. Nondestructive Testing and Evaluation. 16(2-6): 191. (2001)

[Lehmann 2001d] Lehmann E, Vontobel P. Examples for neutron imaging as a tool for industry related inspections. Annual Report PSI, Annex VI, p. 57. (2001)

[Lohse 2003] Lohse, H., Klebstoffe für Fahrzeuge und Bauwesen, 13. Fachforum Kleben, - Grundlagen, Forschungsergebnisse, Anwendungen, Würzburg (2003)

[Martin 1986] Martin F. R. Acrylic Based Adhesives, Structural Adhesives – Developments in Resins and Primers, ed. by A. J. Kinloch, Elsevier Publ. N.Y. (1986)

[Mays 1992] Mays, G. C., Hutschinson, A. R. Adhesives in Civil Engineering, Cambridge University Press, United Kingdom (1992)

[Meyer 1977] Meyer P. A., Rose J. L. J. Applied Physics Vol. 48, pp. 3705, (1977)

[Michaloudaki 2003] Michaloudaki M., Lehmann, E., Kosteas, D. Neutron Imaging as a Tool for the Non-Destructive Evaluation of Adhesive Joints in Aluminium. 17th International Adhesion and Bonding Congress Swiss Bonding, Rupperswil, CH (2003). Publ. in: Int, Journal of Adhesion & Adhesives, in press

[Michaloudaki 2004] Michaloudaki, M., Kosteas, D.: NDE and Product Qualification of Adhesive Joints in Aluminum. In Proc.: 9th INALCO, OH, USA (2004)

[Michaloudaki 2004a] Michaloudaki M., Kosteas D.: Ultrasonic Imaging of Adhesive Joints in Correlation to Strength. Proc. 7th European Adhesion Conference EURADH, Freiburg, D, pp.398-403. (2004).

[Michaloudaki 2004b] Michaloudaki M., Kosteas D.: The effect of fabrication defects on the strength of metal - epoxide joints. Proc. 7th Int. Conference on Structural Adhesives in Engineering SAEVII), 2004, Bristol, UK, pp. 180-183 und Proc. 2nd Hellenic Conf. in Metallic Materials, Nov. 2004, Athens, GR.

[Michaloudaki 2004c] Michaloudaki, M.: Vortrag „Qualitätssicherung an Klebverbindungen-Untersuchungen an realen Automobilbauteilen" an der Seminarstunde bei AUDI AG, Abteilung Fügetechnik/Klebtechnik, März 2004

[Michaloudaki 2004d] Michaloudaki M., Lehmann E., Kosteas D.: Neutron Imaging as Tool for Industry Related Inspections on Structural Adhesive Joints. In Proc. 28th Annual Meeting of the Adhesion Society, Febr. 2005, Alabama, US, in press.

[Michaloudaki 2004e] Michaloudaki M., Schlieckenrieder K.: Kleben im Automobilbau – Notwendigkeit zur zerstörungsfreien Prüfung,Vortrag an der Veranstaltung von IHK für München und Oberbayern und TUM Tech GmbH: Der FRM-II – Werkzeug für den Mittelstand, Okt. 2004, München, D

[Millard 1985] Millard, E. C., Adhesive Selection from the User's Viewpoint. Adhesive Bonding of Aluminium Alloys, ed. by E. W. Thrall & R. W. Shannon, M. Dekker Inc., New York and Basel (1985)

[Minford 1993] Minford, J. D., Handbook of Aluminium Bonding Technology and Data, Marcel Dekker, New York (1993)

[Müller 1973] Müller E. A. W. Handbuch der zerstörungsfreien Materialprüfung, Verlag Oldenburg, München (1973)

[Nieminen 1991] Nieminen, A.O.K., Koening, J.L.: Int. J. Adhesion a. Adhesives, p. 5-9 (1991)

[Pechiney 1992] Guide of Pechiney Renalu, Aluminium Bonding, ed. by Pechiney Renalu, Courbevoie (1992)

[prEN 1090] Technical rules for execution of aluminium structures.- Part 3. CEN TC 135 /WG 3, working document N 70, 2003.

[prEN 1999] Eurocode 9: Design of Aluminium structures – Part 1-1: General rules and rules for buildings Brussels, 2002.

[Price 1991] Price, A., Baldwin, T., Gregson, P. J. Effect of simple pretreatments on the durability of adhesive-bonded Al-Li-Cu-Mg- alloy. Int. Journal of Adhesion & Adhesives Vol. 11 (1) (1991)

[Roche 2001] Roche, A. A, Bouchet, J., Formation of epoxy/metal interfaces, Proc. 6th Int. Conference on Structural Adhesives in Engineering, Bristol, UK (2001)

[Rokhlin 1981] Rokhlin S. I., Hefets M., Rosen M. J. Applied Physics. Vol. 52 pp. 2847 (1981)

[Rokhlin 1986] Rokhlin S. I., Marom D. J. Acoust. Soc. Am. Vol. 80 pp. 585-590 (1986)

[Rose 1973] Rose J. L., Meyer P. A. Materials Evaluation Vol. 42 pp. 109, (1973)

[Rose 1976] Rose J. L. Aspects of the adhesive bond strength classification problem. Proc. Applied Polymer Symposium 32, Pitcatinny Arsenal, NJ (1976)

[Rose 1983] Rose J. L., Avioli M. J., Bilgram R. J. Non Destructive Testing Vol. 25, pp. 67 (1983)

[Rose 1985] Rose J. L. Materials Evaluation Vol. 40, pp. 541-546 (1985)

[Rose 1986] Rose J. L., Pilarski A., Da-Le J. J. Acoust. Soc. Am. Vol 80, Part I, pp.105 (1986)

[Roye 2003] Roye W., Michaloudaki M.: Methoden zur zerstörungsfreien Qualitätssicherung von Klebverbindungen. Proc. Fachtagung Fertigungssysteme Kleben, FSK, Okt. 2003, Bremen, pp. 138-146. and Fachzeitschrift Adhäsion - Kleben und Dichten, März 2004, pp.32-38

[Sauer 2003] Sauer, J., Kalthärtende Klebstoffe für die Luftfahrtindustrie und andere Anwendungen, 13. Fachforum Kleben, - Grundlagen, Forschungsergebnisse, Anwendungen, Würzburg (2003)

[Scarich 1982] Scarich, G. V., and Chanani, G. R. Fatigue behaviour of Weldbonded Joints, J. Aircraft, Vol. 19. Iss. 9 (1982)

[Scheberger 1983] Scheberger, G. L. Surface preparation for adhesive bonding. High-Performance Adhesive Bonding. 1st Edition by G. DeFrayne. Society of Manufacturing Engineers (1983)

[Schindel 1988] Schindel-Bindelli, E.H., Gutherz, W. Konstruktives Kleben, VCH-Verlagsgesellschaft mbH, Deutschland, (1988)

[Schlieckemann 1982] Schlieckemann R. J. Nondestructive testing of adhesive bonded joints., Fokker-VFW Technical Report, NTIS (N81-28190), pp. 38 (1982)

[Sharp 1996] M.L. Sharp, G.E. Nordmark, G.C. Menzemer: Fatigue design of aluminum components and structures, McGraw Hill Companies, , p. 220-227. New York (1996)

[Soetens 1990] Soetens F. Int. J. Adhesion and Adhesives. Vol. 10 (3), pp. 143-152 (1990)

[Sprenger 2003] Sprenger, S., Eger, C., Kinloch, A.J., Lee, J.H., Taylor, A. C., Egan, D. Symposium: Current aspects of epoxy resins, London, UK (2003)

[Steinhardt 1972] Steinhardt, O., Mang F. Geklebte Leichtmetallverbindungen, Technische Mitteilungen Heft 7 p 314-317 (1972)

[Straalen 1998] Straalen IJ. J. van, Wardenier J., Vogelesang L. B., Soetens F. Int. J. Adhesion and Adhesives. Vol. 18, pp. 41-49 (1998)

[Straalen 2001] Straalen, IJ. J. Van. PhD thesis: Development of design rules for structural adhesive bonded joints. ISBN 90-9014507-9. Technische Universiteit Delft. (2001)

[Straalen 2002] Straalen I.J. J. van, Tooren M.J. L. Van Development of Design Rules for adhesive bonded joints. Heron Publ. TNO. Vol 47. pp. 263-274 (2002)

[Suárez 2004] Suárez Acero J. A. Structural Response of Defects in Adhesively Bonded Joints. Diploma Thesis Nr. 327. Technische Universität München. (2004)

[Tang 1999] Tang, Z., Cheng, A., Achenbach, J.D.: J. Adhesion Sci. Technology, 1999, p. 837-854

[Thompson 1999] Thompson, R.B., Thompson, D.O.: J. Adhesion Sci. Technology, 1991, p. 583-599

[Thrall 1985] Thrall EW, Shannon RW. Adhesive bonding of aluminium alloys. NY & Basel: Marcel Dekker Inc., (1985)

[Volkersen 1938] Volkersen, O. Luftfahrtforschung, Vol. 15, p.41, (1938)

[Wang 1972] Wang, T.T., Ryan, F.W., Schonchorn, H. Journal of Applied Polymer Science, Vol. 16, pp 1901-1909 (1972)

[Williams 1982] Williams R. S., Zwicke P. E. Materials Evaluation Vol. 40 pp. 312 (1982)

[Wirth 2004] Wirth, C. PhD thesis: Berechnungskonzept für die Klebflanschfestigkeit in Gesamtkarosseriemodellen. Technische Universität München (2004)

[Woodmansee 1978] Woodmansee W. E. Through transmission ultrasonic attenuation measurements on adhesively bonded structures. Proc. 1st Int. Symposium, Gaitherburg, MD (1978)

[Young 1986] Young, R. J. Rigid Partculate Reinforced Thermosseting Polymers. Polymers. Structural Adhesives – Developments in Resins and Primers. Edited by A.J. Kinloch. Elsevier Applied Sciences Publishers, London and New York (1986)

[Zäh 2003a] Zäh F. M., Schlickenrieder K., Mosandl T., Adhäsion - Kleben und Dichten, .(2003)

[Zäh 2003b] Zäh F. M., Kosteas, D. Lammel, C., Schlickenrieder, K., Mosandl, T., Michaloudaki, M. Discherl, F. Adhäsion - Kleben und Dichten, Vol.8 pp.18-23 (2003)

[Zalucha 1983] Zalucha, J. D. Testing adhesives: philosophy and practice. High Performance Adhesive Bonding. 1st Edition by G. DeFrayne, Society of Manufacturing Engineers. Michigan, USA (1983)

Annex A for Chapter 5

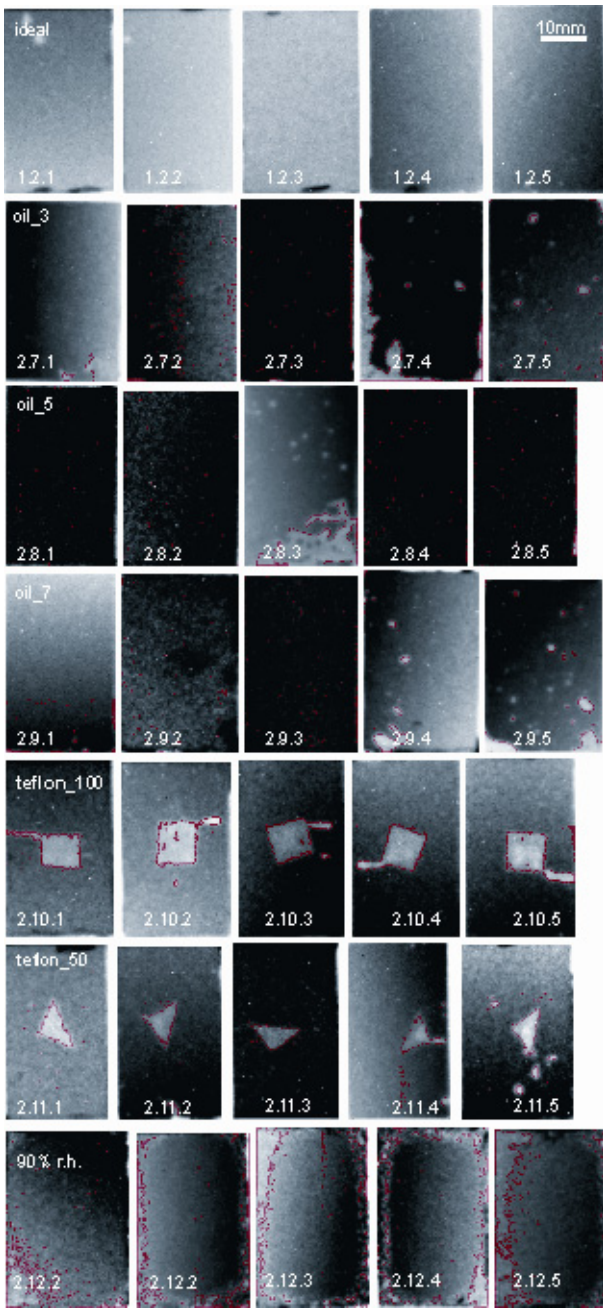

Fig. A1: Transmission images of steel-Betamate 1496 overlaps with 0,2mm bondline thickness.

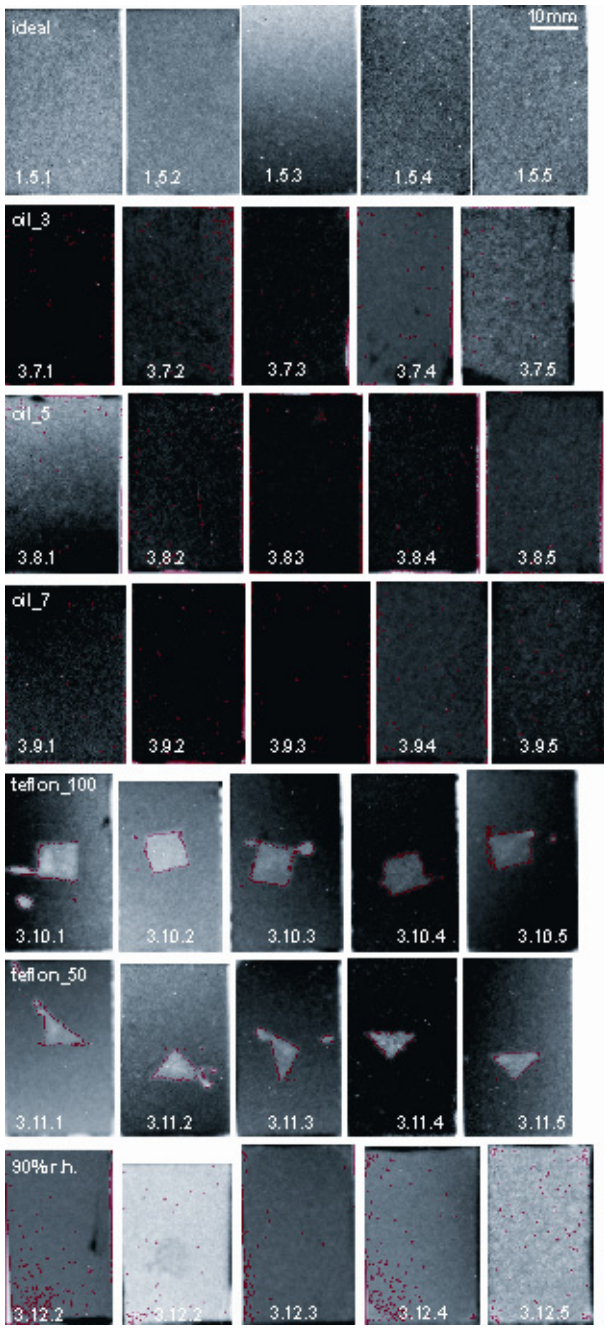

Fig. A2: Transmission images of steel-Terokal 5070 overlaps with 0,2mm bondline thickness.

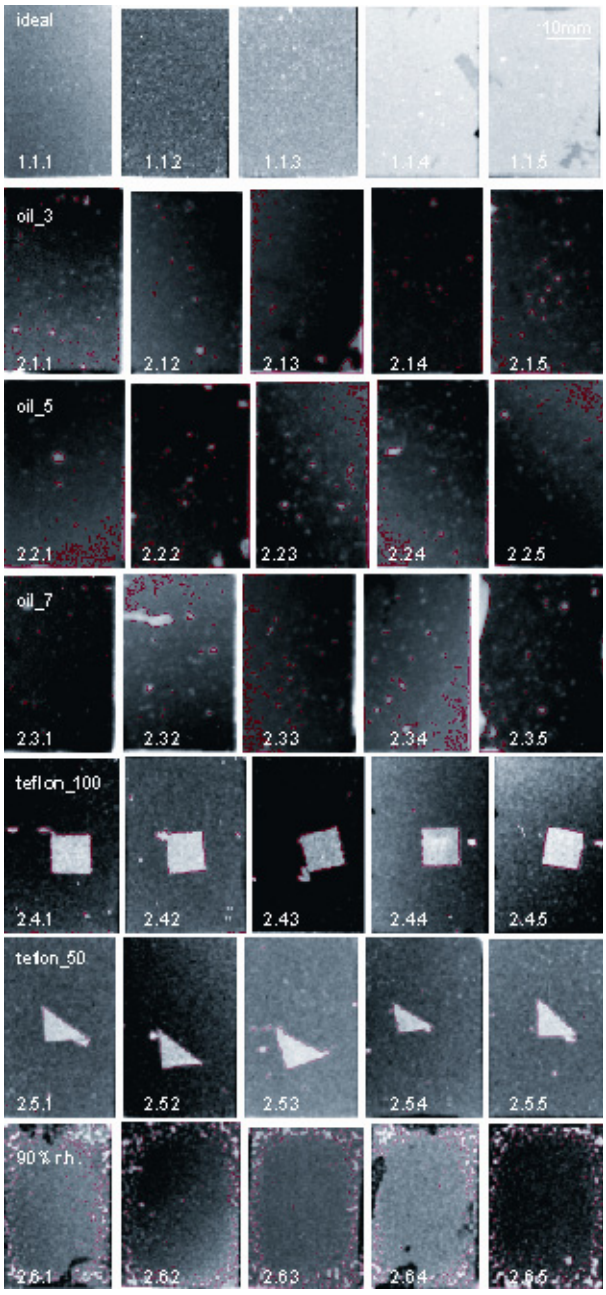

Fig. A3: Transmission images of steel-Betamate 1496 overlaps with 0,5mm bondline thickness.

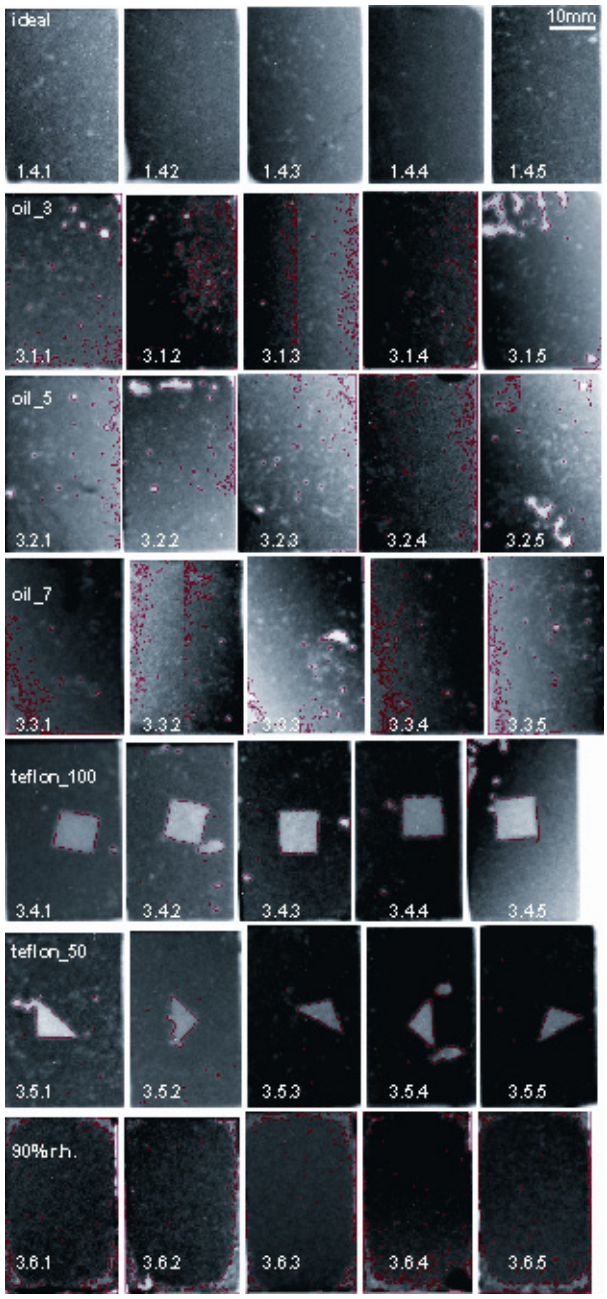

Fig. A4: Transmission images of steel-Terokal 5070 overlaps with 0,5mm bondline thickness.

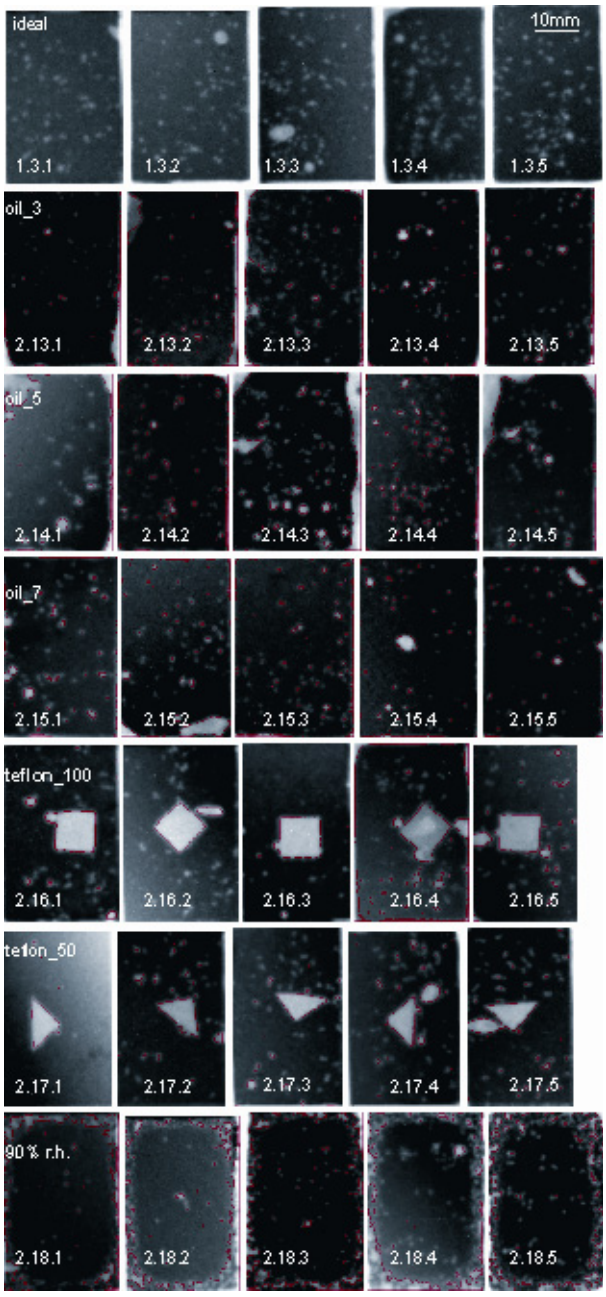

Fig. A5: Transmission images of steel-Betamate 1496 overlaps with 1,0mm bondline thickness.

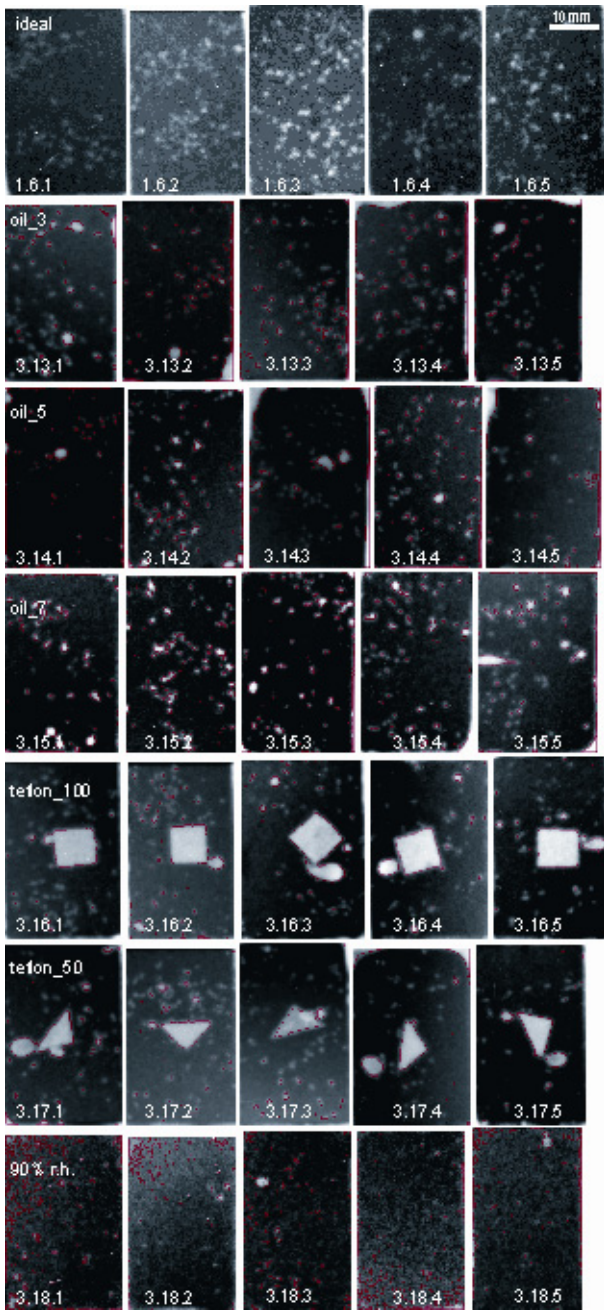

Fig. A6: Transmission images of steel-Terokal 5070 overlaps with 1,0mm bondline thickness.

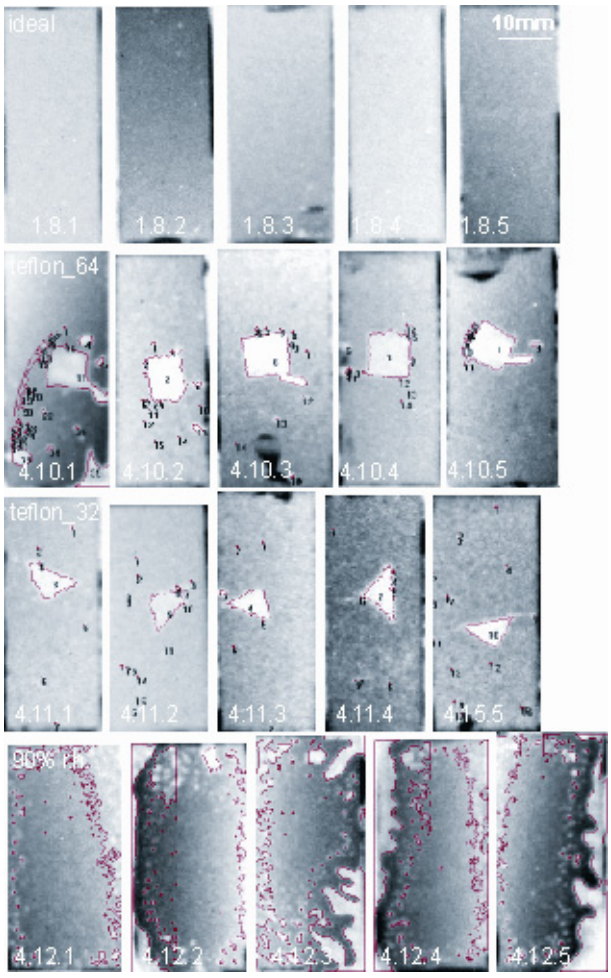

Fig. A7: Transmission images of aluminium-Betamate 1496 overlaps with 0,2mm bondline thickness.

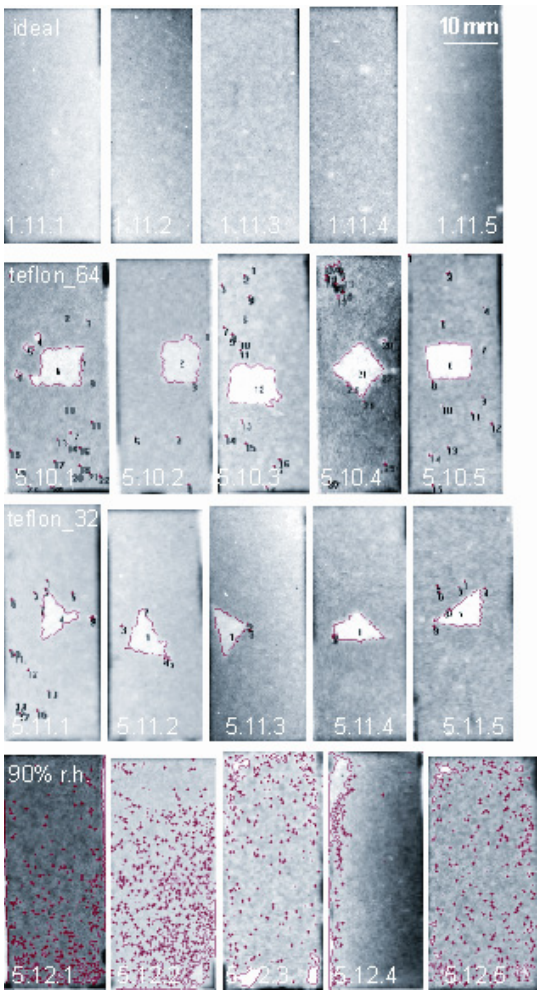

Fig. A8: Transmission images of aluminium-Terokal 5070 overlaps with 0,2mm bondline thickness.

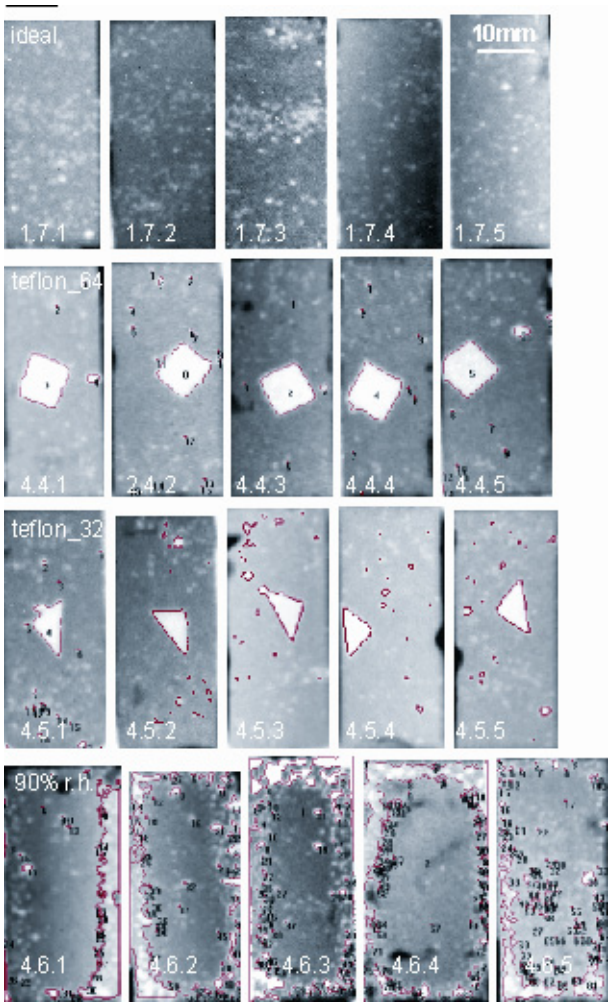

Fig. A9: Transmission images of aluminium-Betamate 1496 overlaps with 0,5mm bondline thickness.

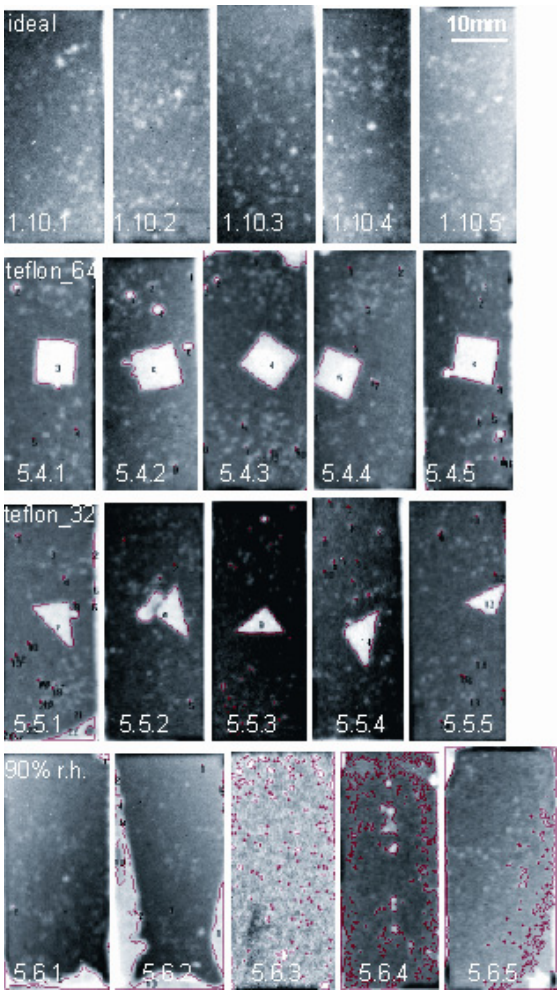

Fig. A10: Transmission images of aluminium-Terokal 5070 overlaps with 0,5mm bondline thickness.

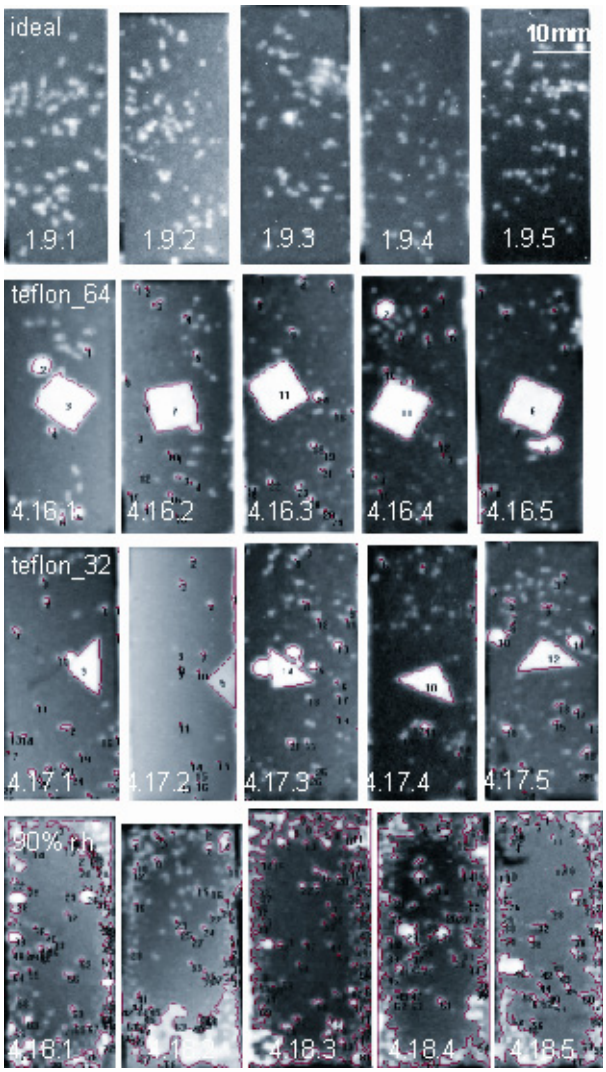

Fig. A11: Transmission images of aluminium-Betamate 1496 overlaps with 1,0mm bondline thickness.

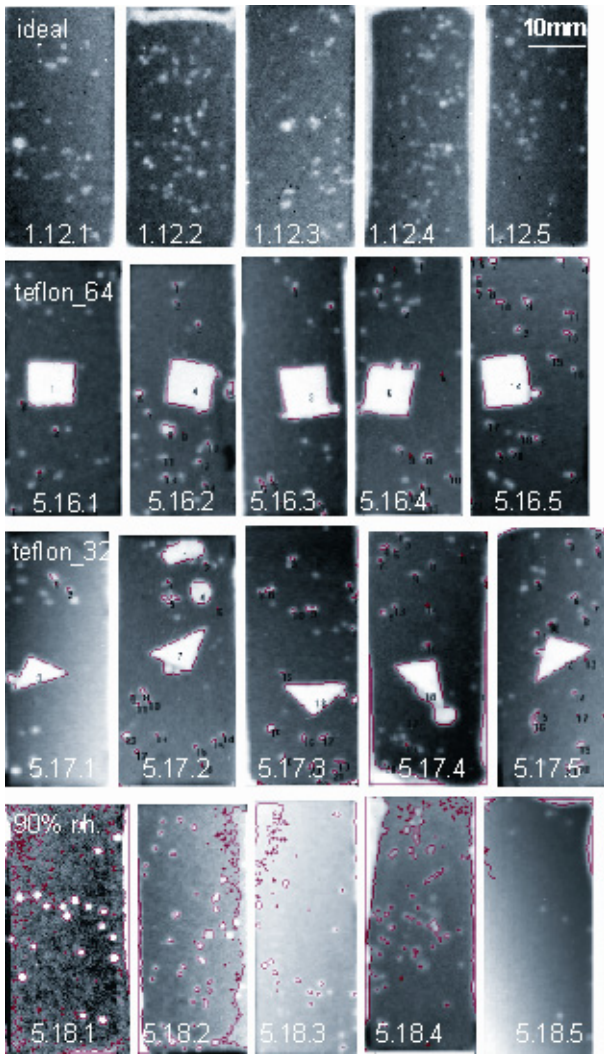

Fig. A12: Transmission images of aluminium-Terokal 5070 overlaps with 1,0mm bondline thickness.

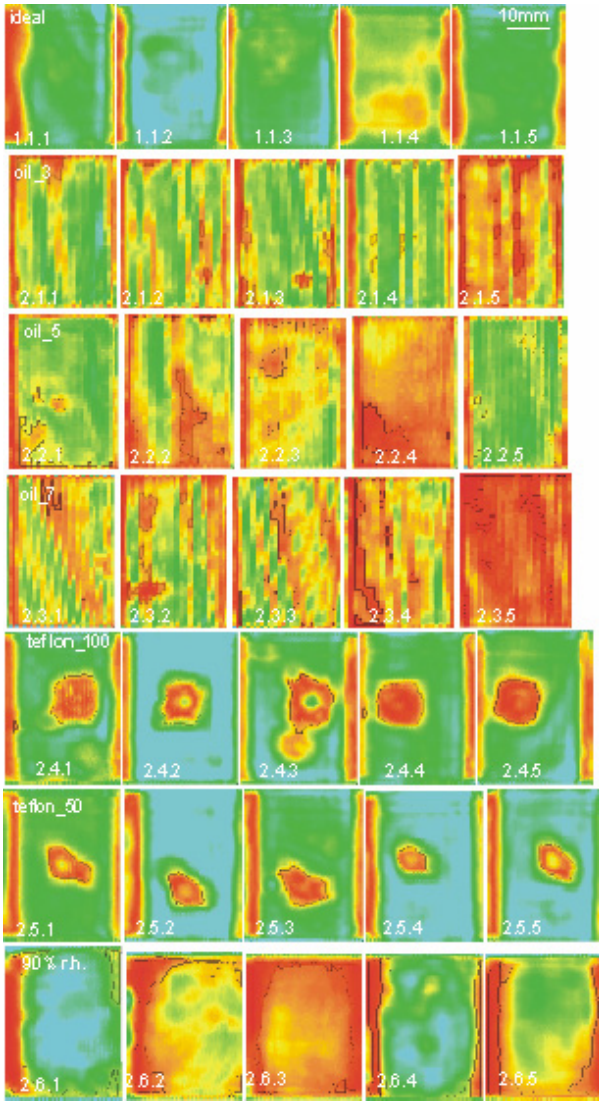

Fig. B3: C-scans of steel-Betamate 1496 overlaps with 0,5mm bondline thickness.

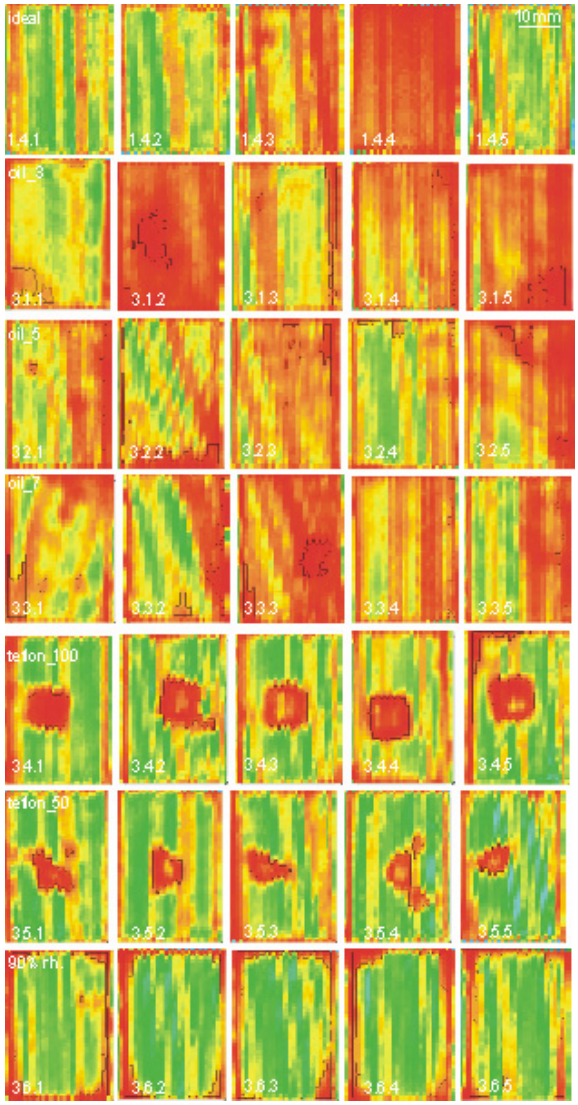

Fig. B4: C-scans of steel-Terokal 5070 overlaps with 0,5mm bondline thickness.

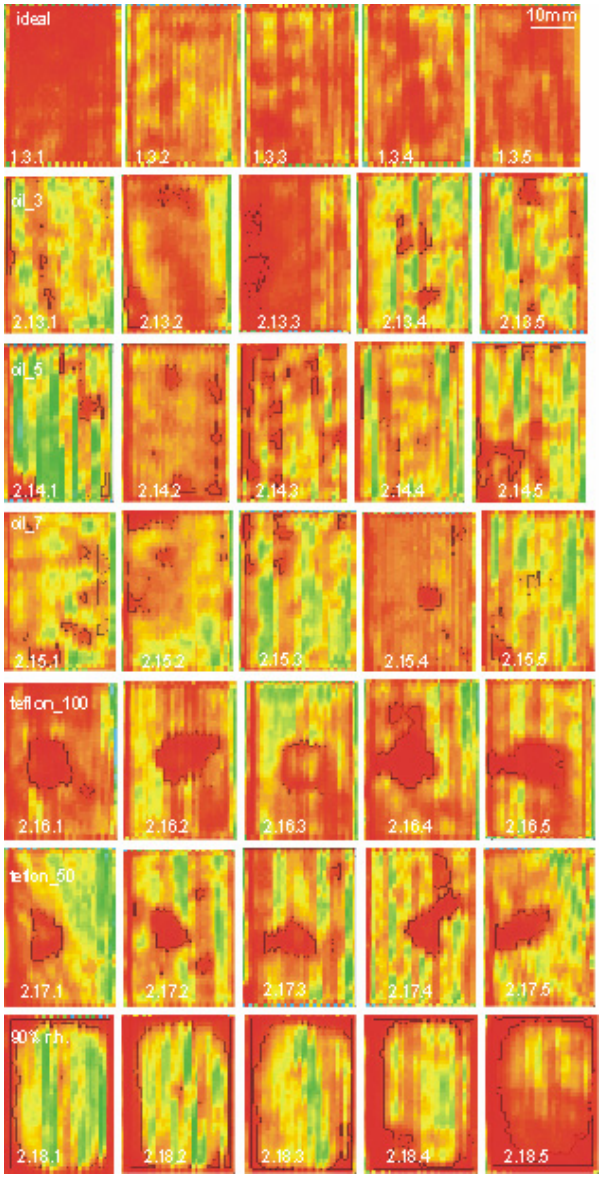

Fig. B5: C-scans of steel-Betamate 1496 overlaps with 1,0mm bondline thickness.

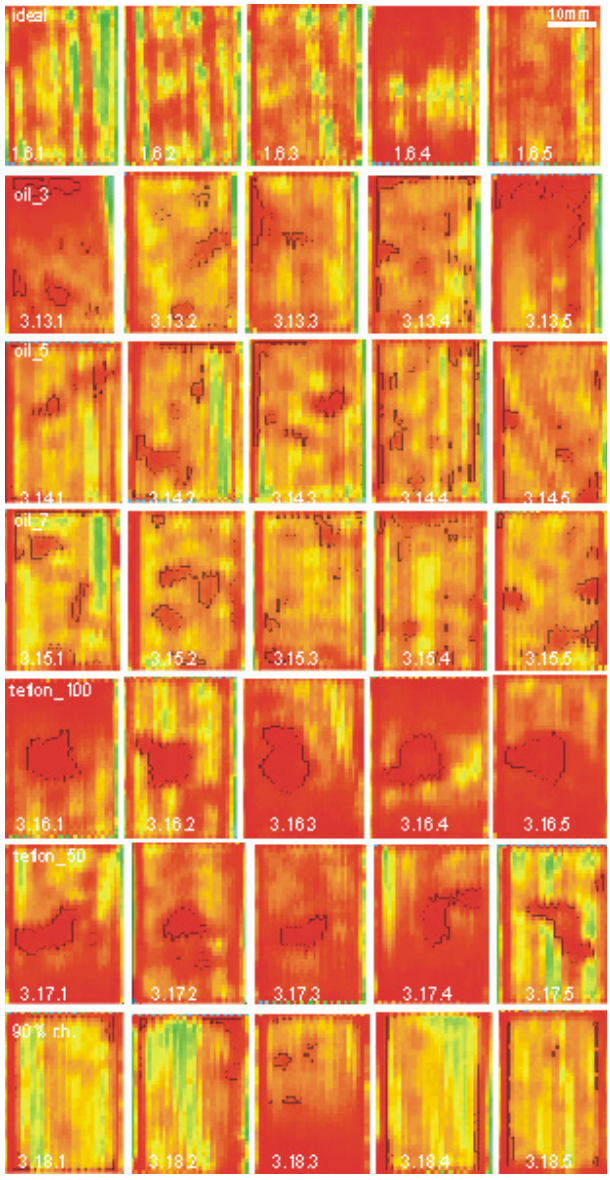

Fig. B6: C-scans of steel-Terokal 5070 overlaps with 1,0mm bondline thickness.

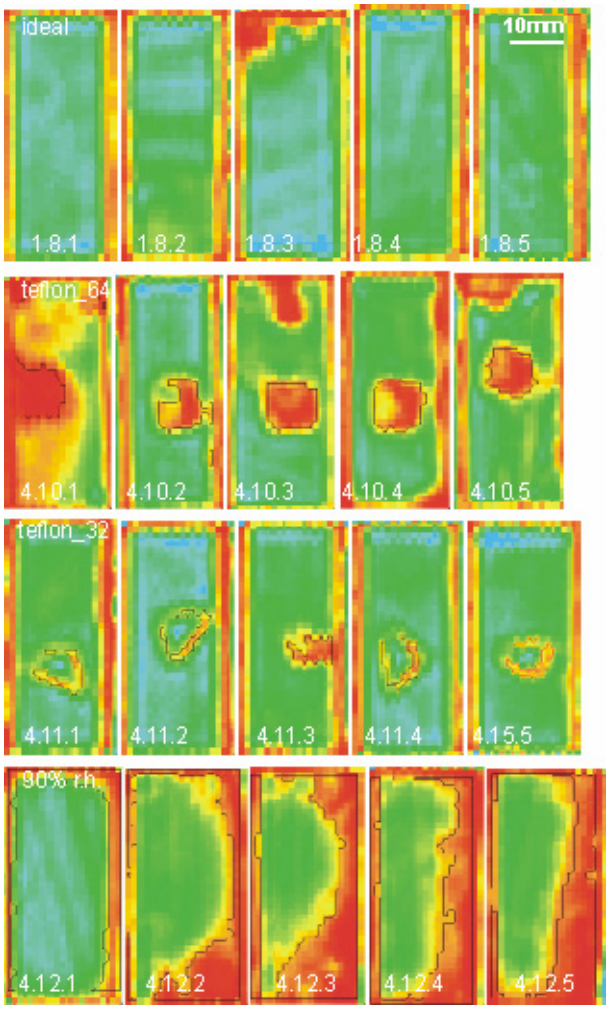

Fig. B7: C-scans of aluminium-Betamate 1496 overlaps with 0,2mm bondline thickness.

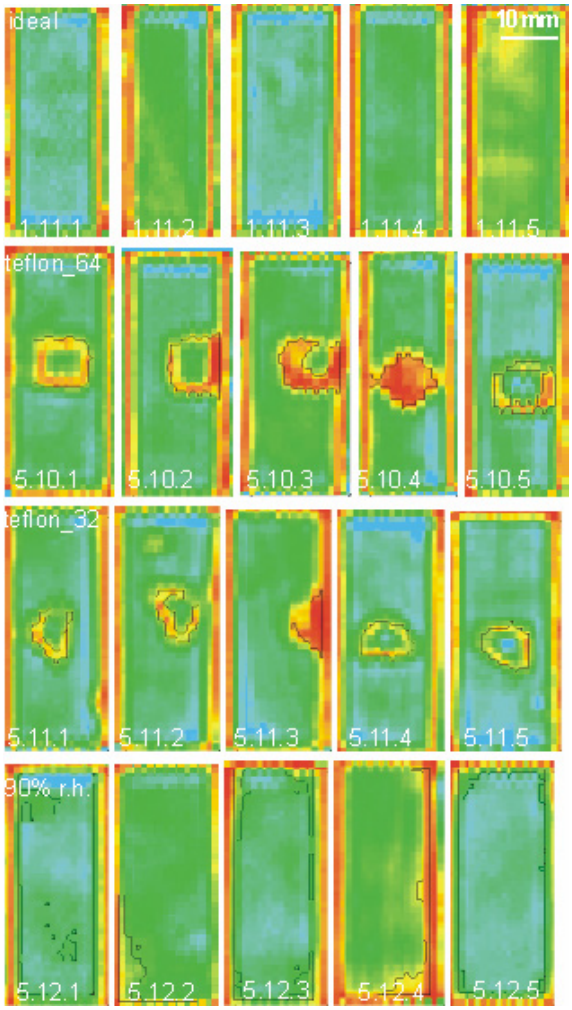

Fig. B8: C-scans of aluminium-Terokal 5070 overlaps with 0,2mm bondline thickness.

Annex B for Chapter 6

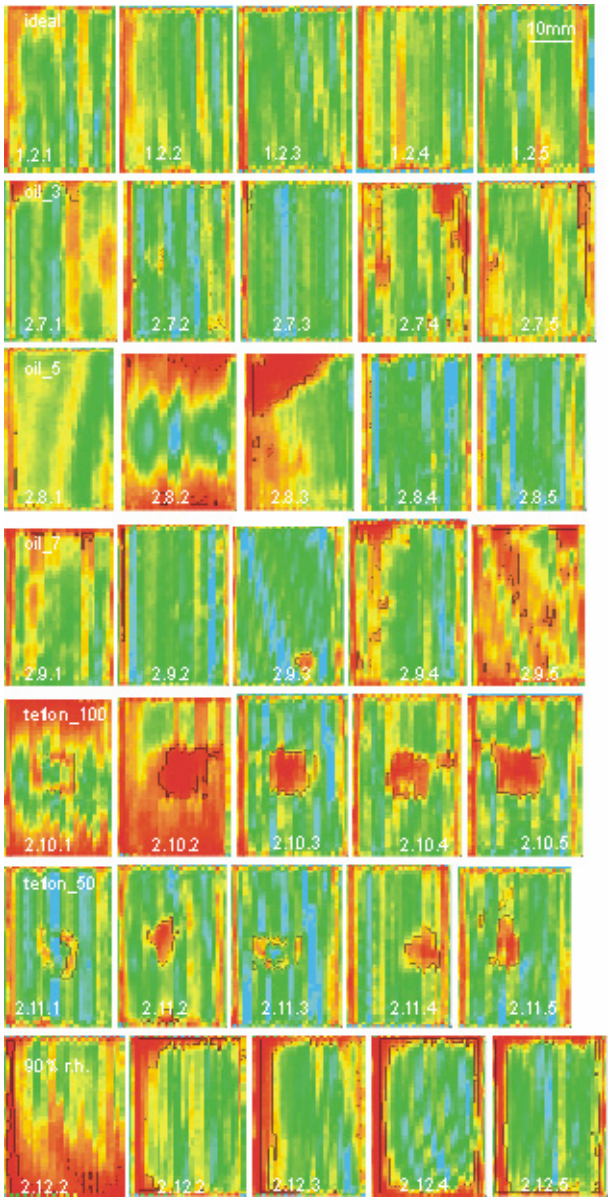

Fig. B1: C-scans of steel-Betamate 1496 overlaps with 0,2mm bondline thickness.

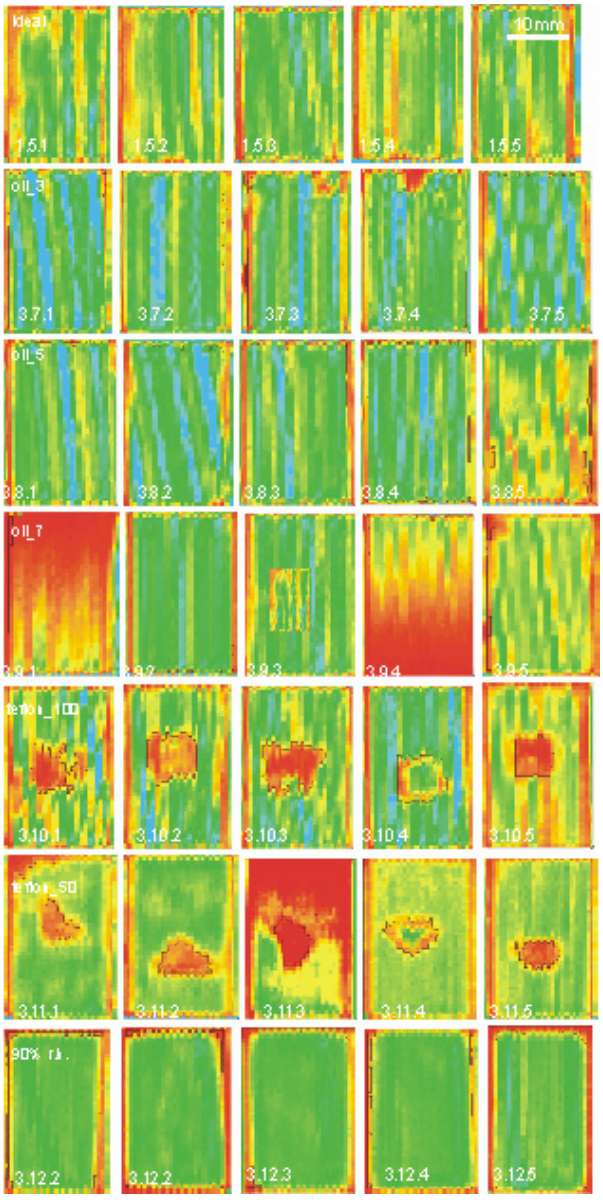

Fig. B2: C-scans of steel-Terokal 5070 overlaps with 0,2mm bondline thickness.

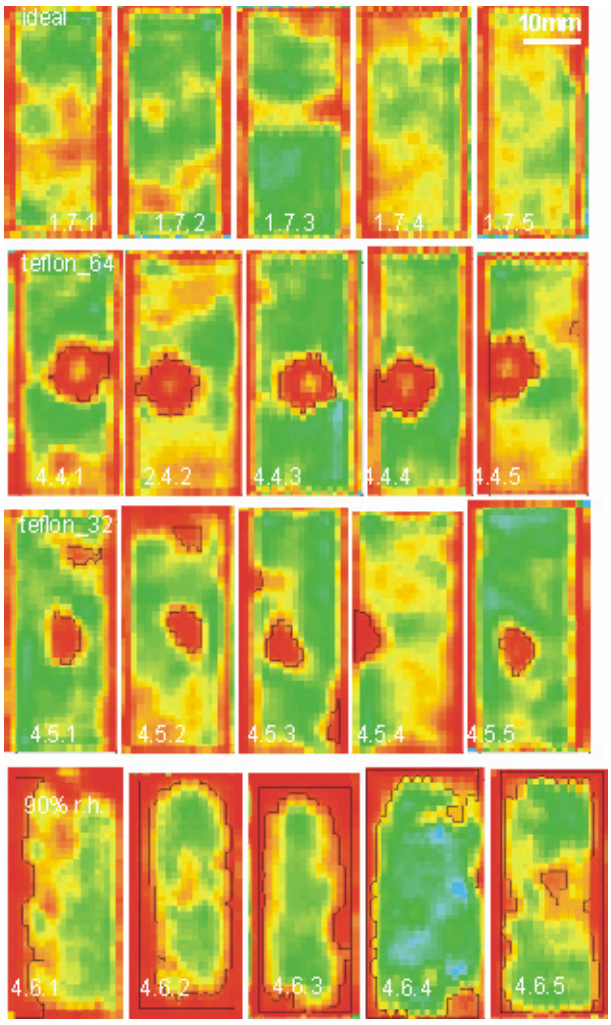

Fig. B9: C-scans of aluminium-Betamate 1496 overlaps with 0,5mm bondline thickness.

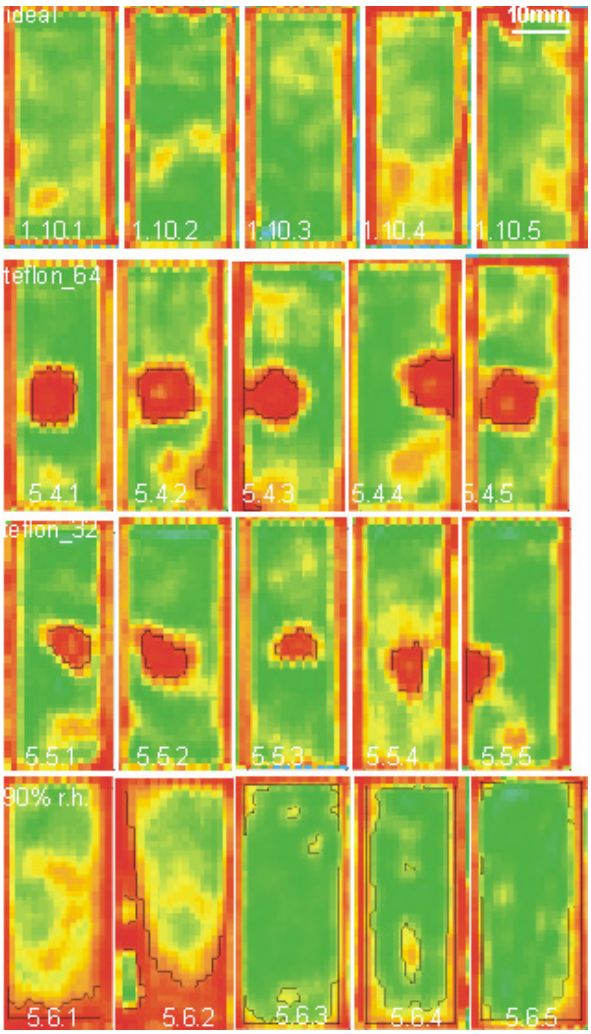

Fig. B10: C-scans of aluminium-Terokal 5070 overlaps with 0,5mm bondline thickness.

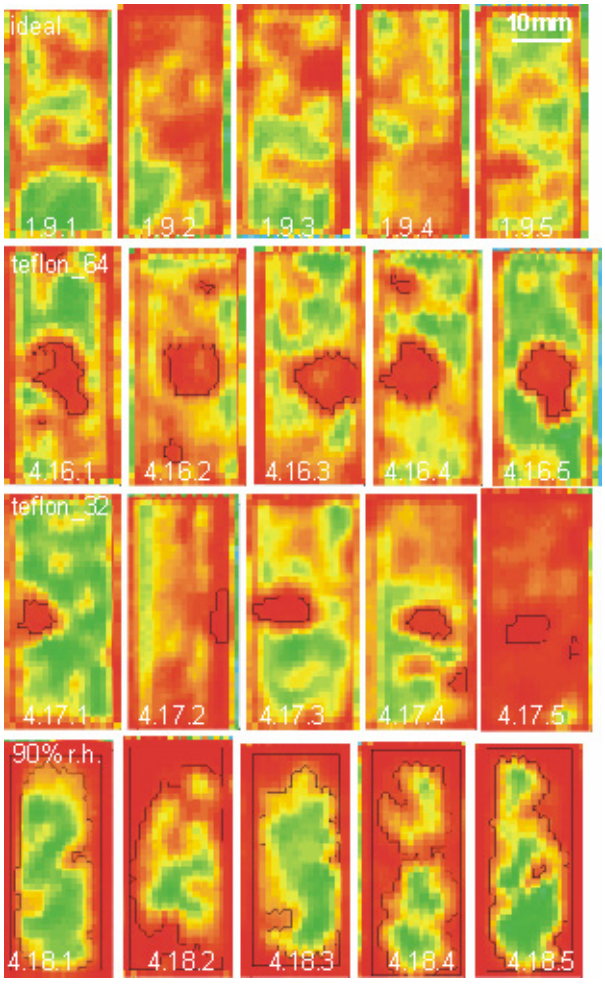

Fig. B11: C-scans of aluminium-Betamate 1496 overlaps with 1,0mm bondline thickness.

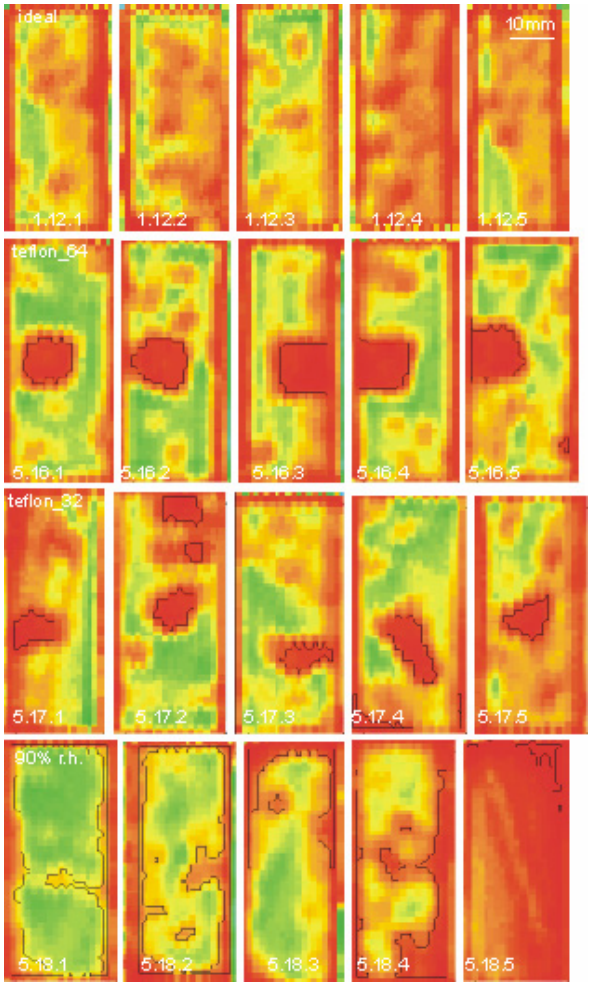

Fig. B12: C-scans of aluminium-Terokal 5070 overlaps with 1,0mm bondline thickness.

Annex C for Chapter 8

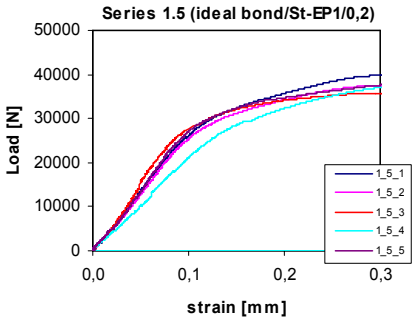

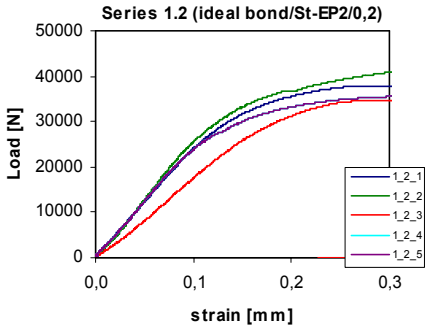

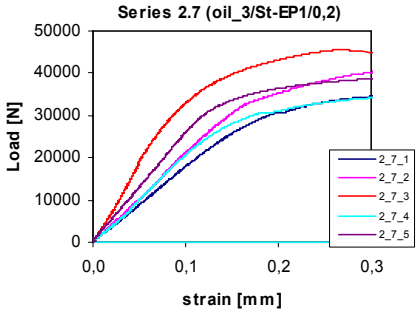

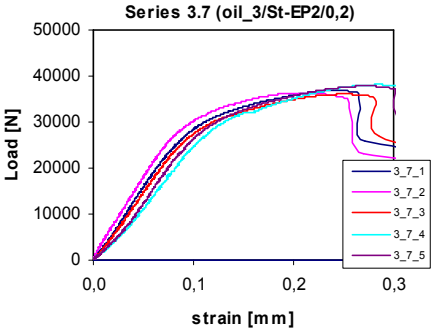

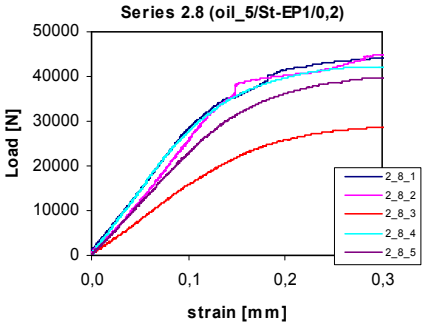

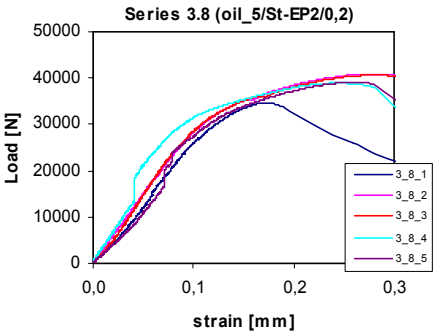

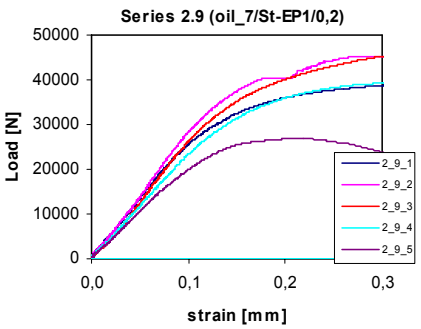

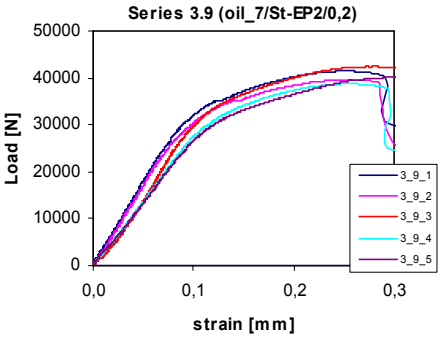

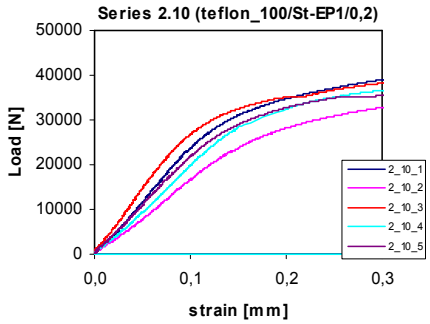

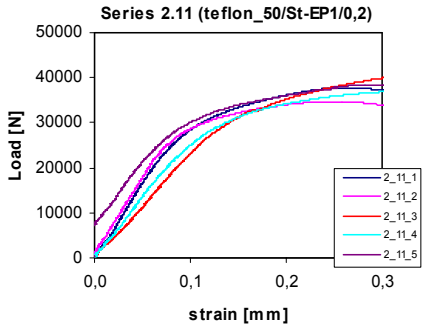

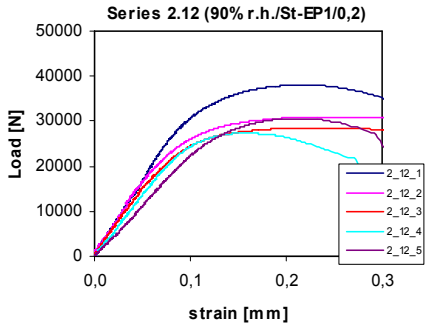

Fig. C1: Load-strain diagrams of ideal and defect bonds with steel-Betamate 1496 in 0,2 mm bondline thickness.

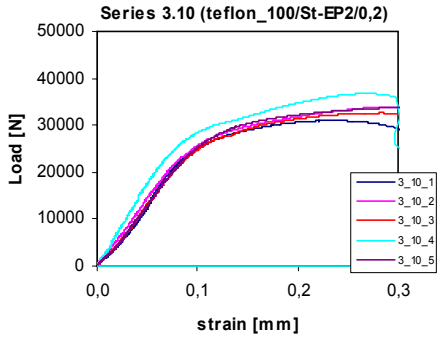

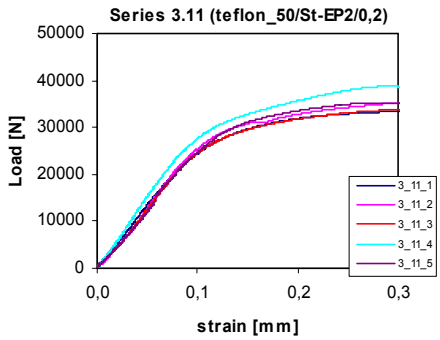

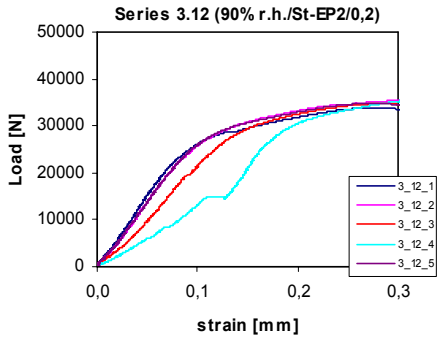

Fig. C2: Load-strain diagrams of ideal and defect bonds with steel-Terokal 5070 in 0,2 mm bondline thickness.

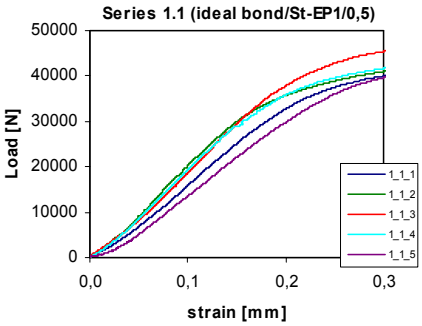
Series 1.1 (ideal bond/St-EP1/0,5)
Load [N]
strain [mm]
1_1_1
1_1_2
1_1_3
1_1_4
1_1_5

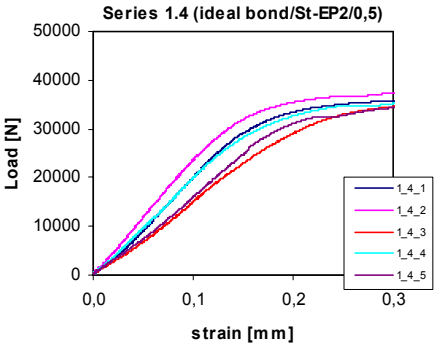
Series 1.4 (ideal bond/St-EP2/0,5)
Load [N]
strain [mm]
1_4_1
1_4_2
1_4_3
1_4_4
1_4_5

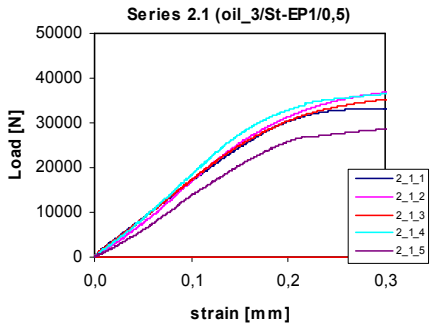
Series 2.1 (oil_3/St-EP1/0,5)
Load [N]
strain [mm]
2_1_1
2_1_2
2_1_3
2_1_4
2_1_5

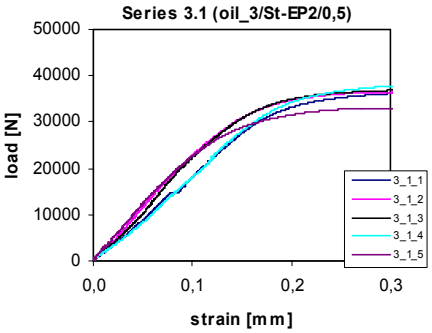
Series 3.1 (oil_3/St-EP2/0,5)
load [N]
strain [mm]
3_1_1
3_1_2
3_1_3
3_1_4
3_1_5

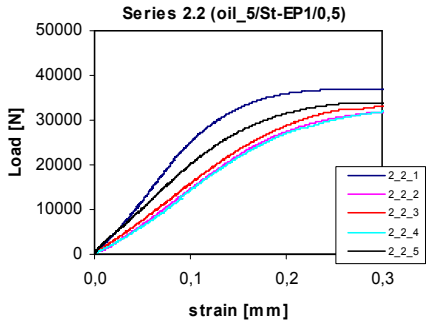
Series 2.2 (oil_5/St-EP1/0,5)
Load [N]
strain [mm]
2_2_1
2_2_2
2_2_3
2_2_4
2_2_5

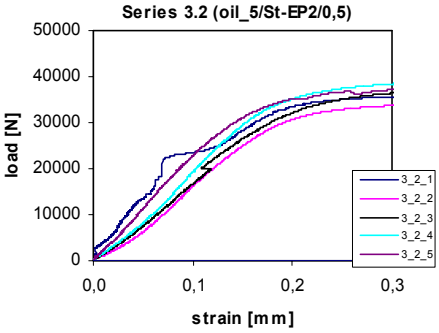
Series 3.2 (oil_5/St-EP2/0,5)
load [N]
strain [mm]
3_2_1
3_2_2
3_2_3
3_2_4
3_2_5

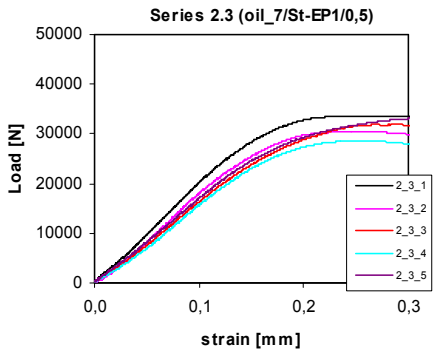
Series 2.3 (oil_7/St-EP1/0,5)
Load [N]
strain [mm]
2_3_1
2_3_2
2_3_3
2_3_4
2_3_5

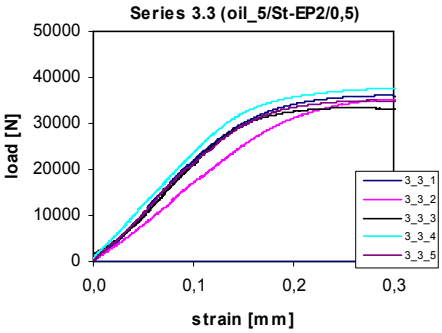
Series 3.3 (oil_5/St-EP2/0,5)
load [N]
strain [mm]
3_3_1
3_3_2
3_3_3
3_3_4
3_3_5

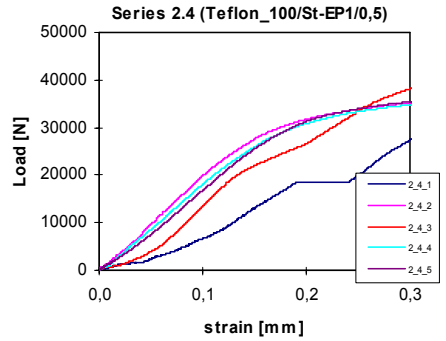

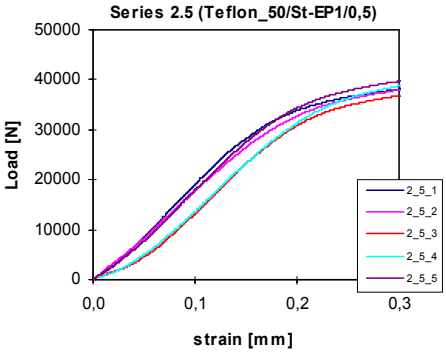

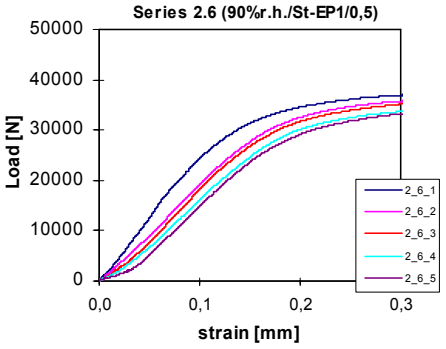

Fig. C3: Load-strain diagrams of ideal and defect bonds with steel-Betamate 1496 in 0,5 mm bondline thickness.

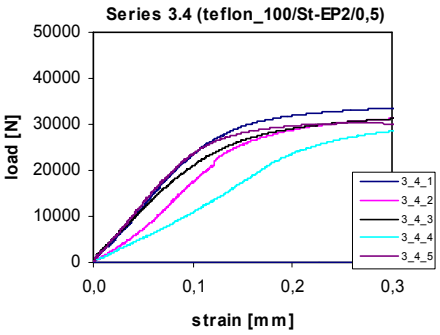

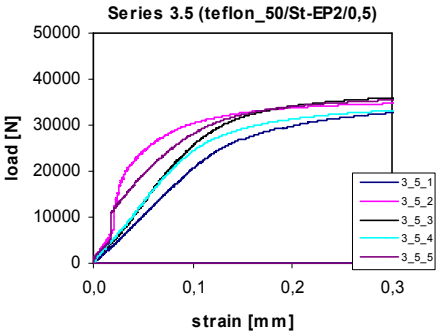

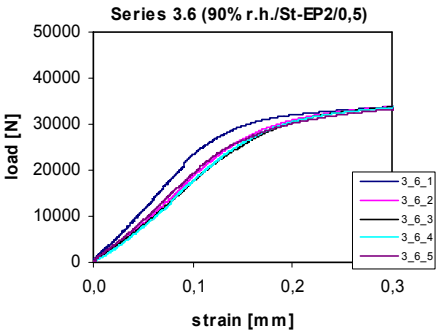

Fig. C4: Load-strain diagrams of ideal and defect bonds with steel-Terokal 5070 in 0,5 mm bondline thickness.

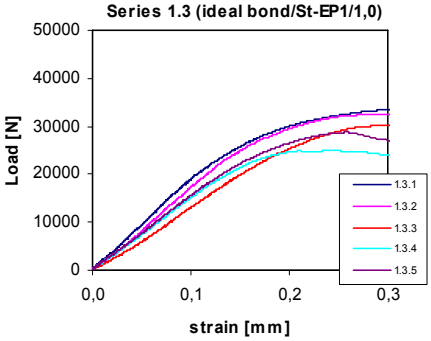
Series 1.3 (ideal bond/St-EP1/1,0)
Load [N]
strain [mm]
1.3.1
1.3.2
1.3.3
1.3.4
1.3.5

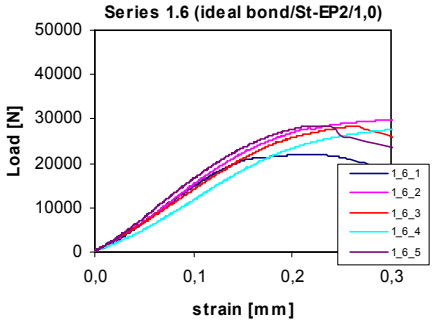
Series 1.6 (ideal bond/St-EP2/1,0)
Load [N]
strain [mm]
1_6_1
1_6_2
1_6_3
1_6_4
1_6_5

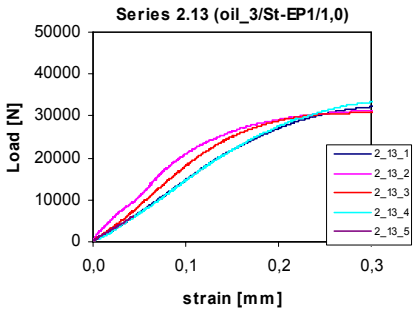
Series 2.13 (oil_3/St-EP1/1,0)
Load [N]
strain [mm]
2_13_1
2_13_2
2_13_3
2_13_4
2_13_5

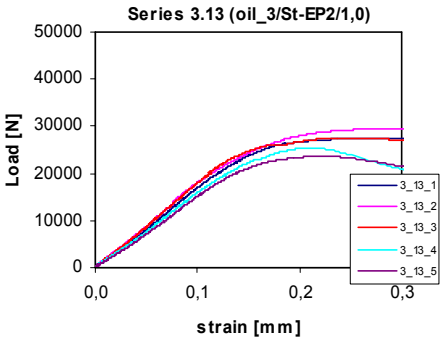
Series 3.13 (oil_3/St-EP2/1,0)
Load [N]
strain [mm]
3_13_1
3_13_2
3_13_3
3_13_4
3_13_5

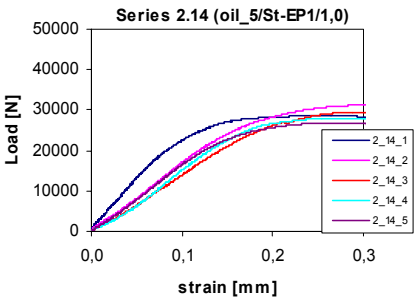
Series 2.14 (oil_5/St-EP1/1,0)
Load [N]
strain [mm]
2_14_1
2_14_2
2_14_3
2_14_4
2_14_5

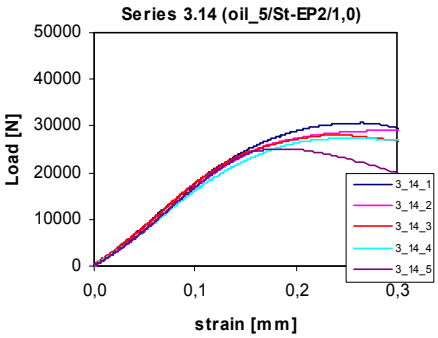
Series 3.14 (oil_5/St-EP2/1,0)
Load [N]
strain [mm]
3_14_1
3_14_2
3_14_3
3_14_4
3_14_5

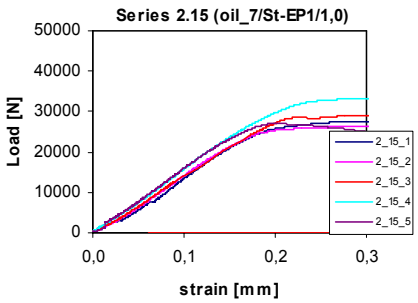
Series 2.15 (oil_7/St-EP1/1,0)
Load [N]
strain [mm]
2_15_1
2_15_2
2_15_3
2_15_4
2_15_5

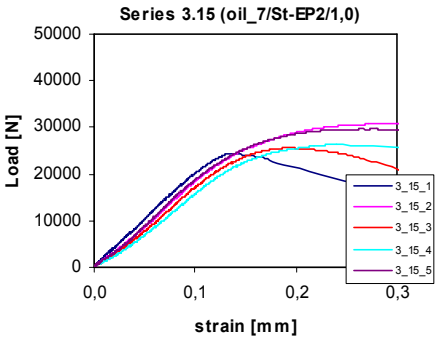
Series 3.15 (oil_7/St-EP2/1,0)
Load [N]
strain [mm]
3_15_1
3_15_2
3_15_3
3_15_4
3_15_5

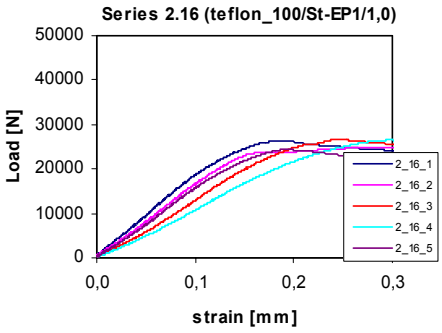

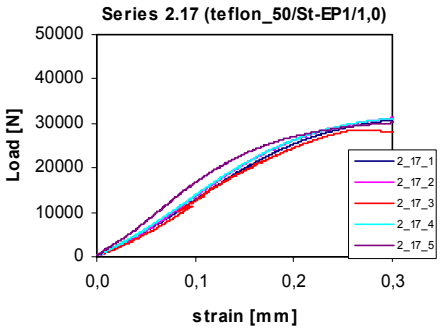

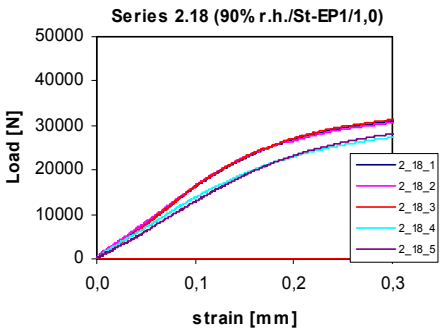

Fig. C5: Load-strain diagrams of ideal and defect bonds with steel-Betamate 1496 in 1,0 mm bondline thickness.

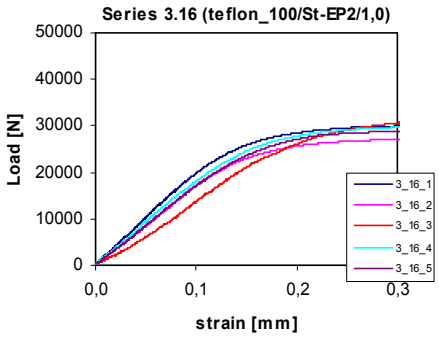

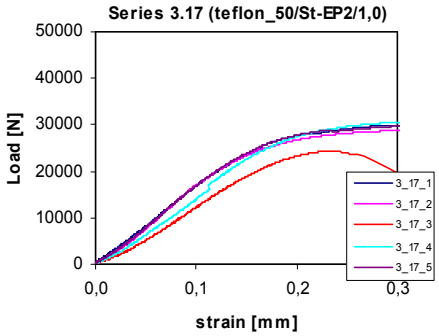

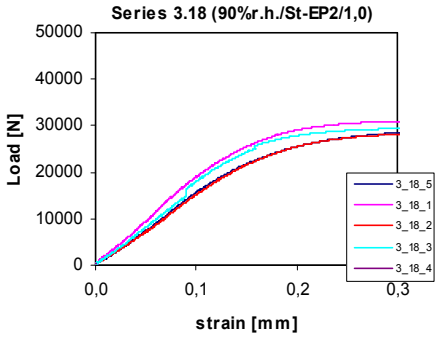

Fig. C6: Load-strain diagrams of ideal and defect bonds with steel-Terokal 5070 in 1,0 mm bondline thickness.

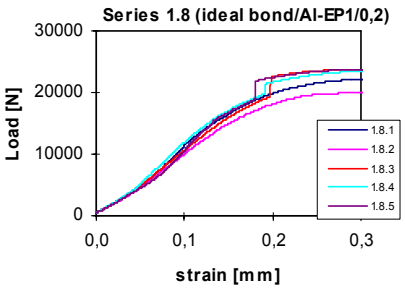

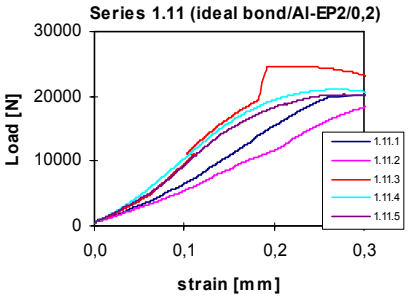

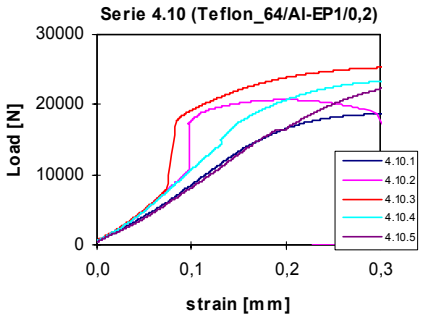

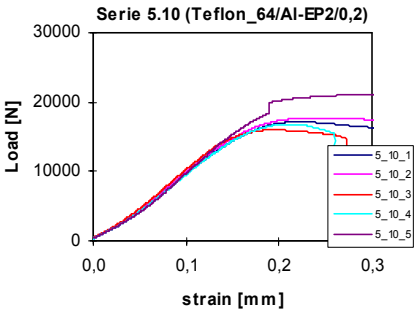

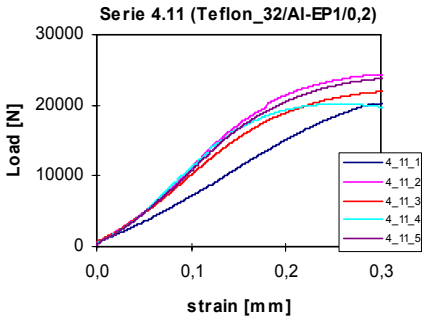

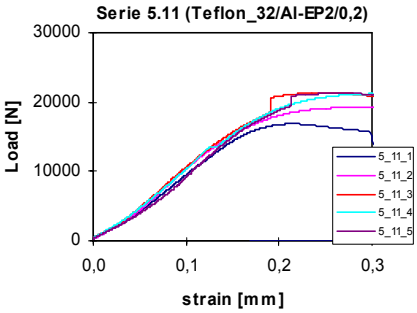

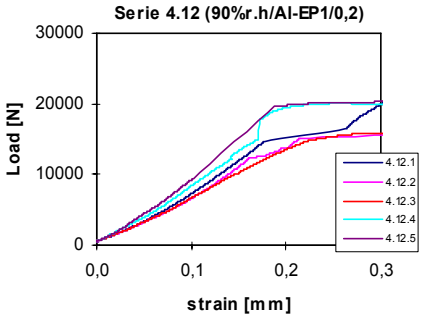

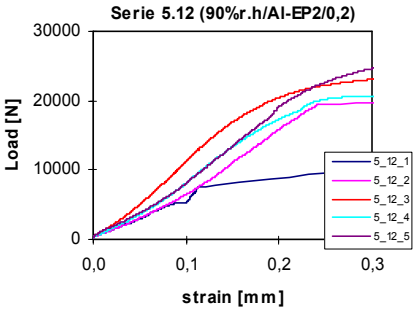

Fig. C7: Load-strain diagrams of ideal and defect bonds with aluminium-Betamate 1496 in 0,2 mm bondline thickness.

Fig. C8: Load-strain diagrams of ideal and defect bonds with aluminium-Terokal 5070 in 0,2 mm bondline thickness.

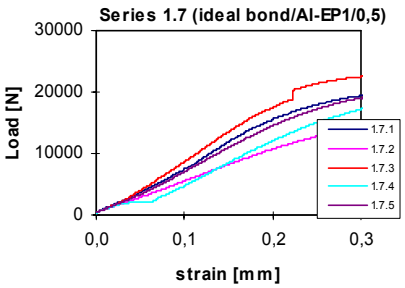

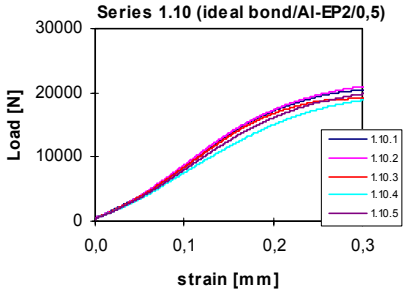

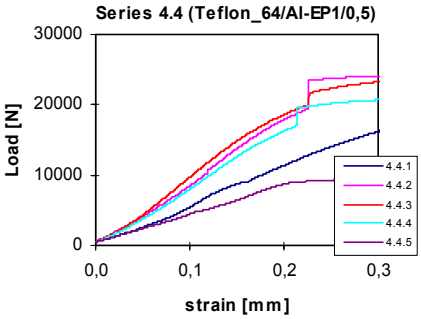

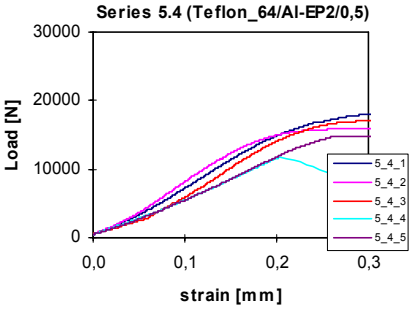

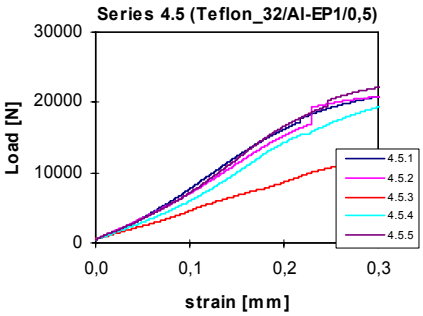

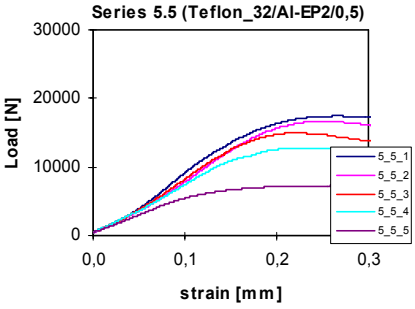

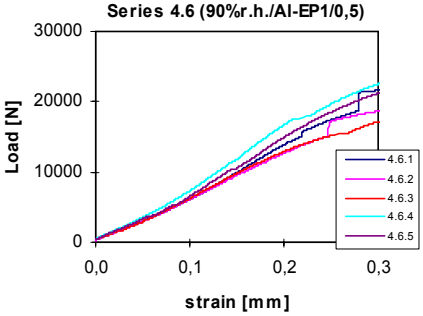

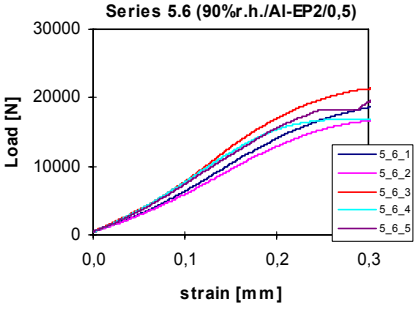

Fig. C9: Load-strain diagrams of ideal and defect bonds with aluminium-Betamate 1496 in 0,5 mm bondline thickness.

Fig. C10: Load-strain diagrams of ideal and defect bonds with aluminium-Terokal 5070 in 0,5 mm bondline thickness.

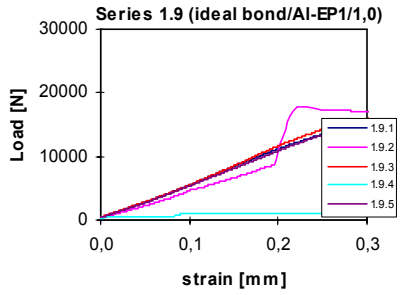

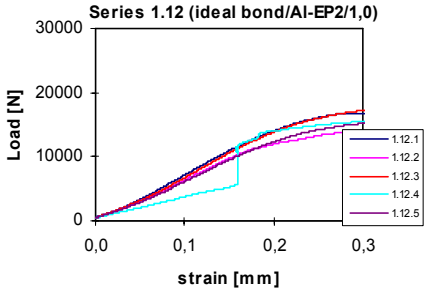

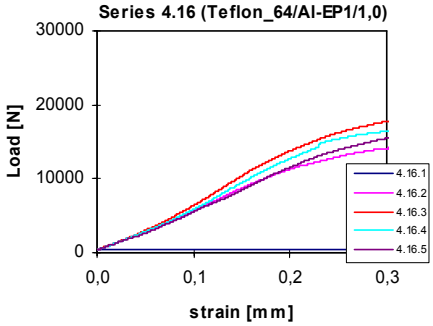

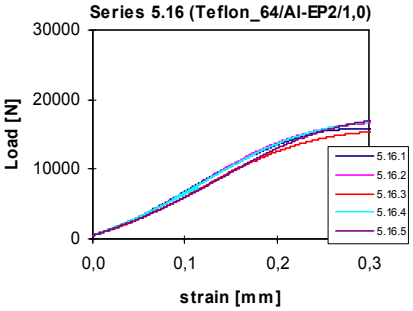

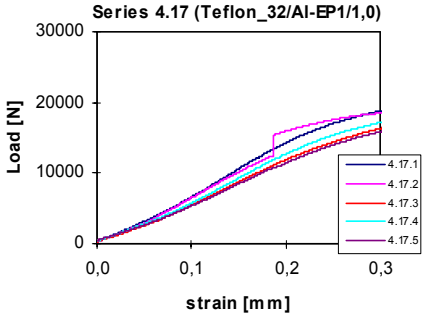

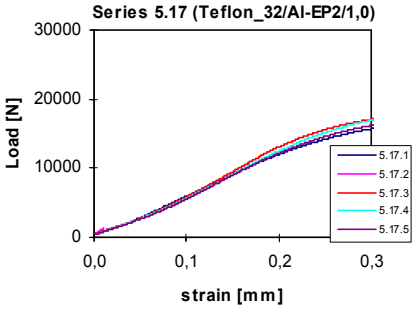

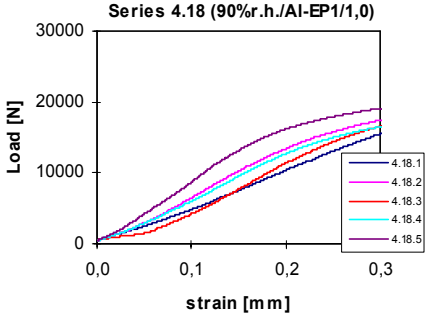

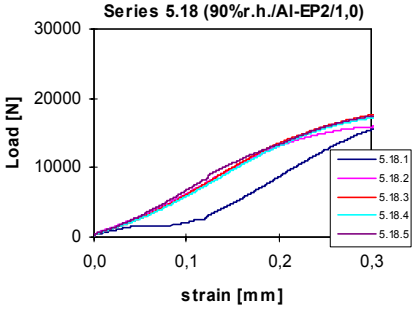

Fig. C11: Load-strain diagrams of ideal and defect bonds with aluminium-Betamate 1496 in 1,0 mm bondline thickness.

Fig. C12: Load-strain diagrams of ideal and defect bonds with aluminium-Terokal 5070 in 1,0 mm bondline thickness.

Annex D for Chapter 9

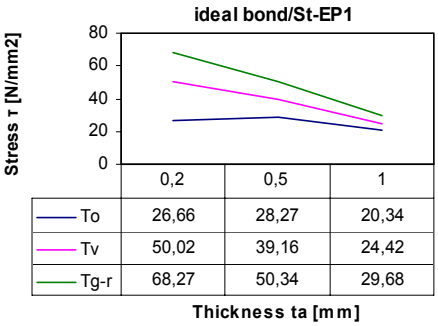

	0,2	0,5	1
To	26,66	28,27	20,34
Tv	50,02	39,16	24,42
Tg-r	68,27	50,34	29,68

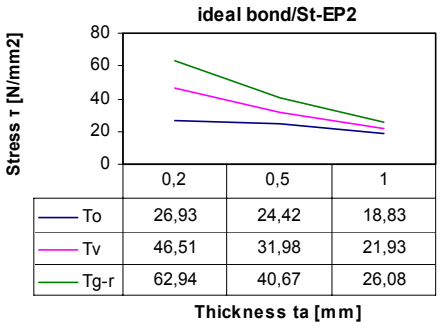

	0,2	0,5	1
To	26,93	24,42	18,83
Tv	46,51	31,98	21,93
Tg-r	62,94	40,67	26,08

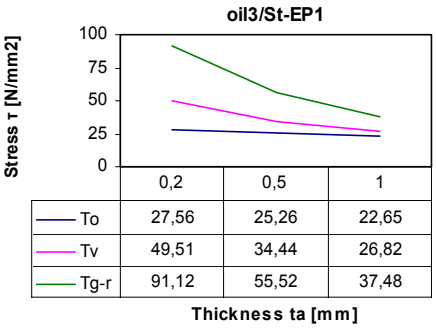

	0,2	0,5	1
To	27,56	25,26	22,65
Tv	49,51	34,44	26,82
Tg-r	91,12	55,52	37,48

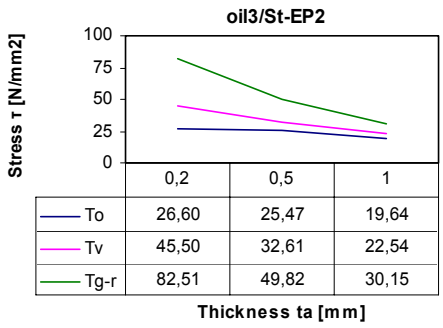

	0,2	0,5	1
To	26,60	25,47	19,64
Tv	45,50	32,61	22,54
Tg-r	82,51	49,82	30,15

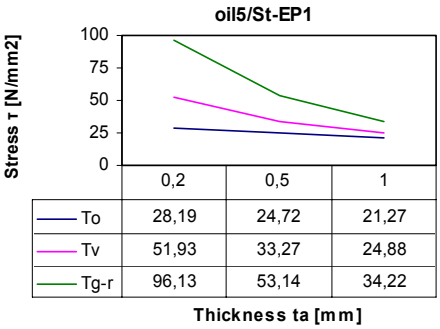

	0,2	0,5	1
To	28,19	24,72	21,27
Tv	51,93	33,27	24,88
Tg-r	96,13	53,14	34,22

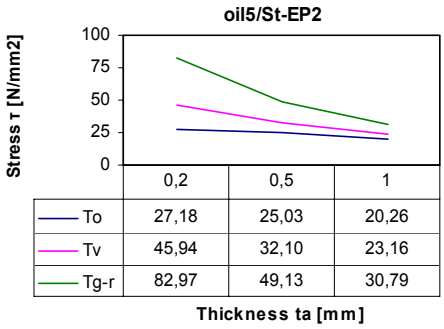

	0,2	0,5	1
To	27,18	25,03	20,26
Tv	45,94	32,10	23,16
Tg-r	82,97	49,13	30,79

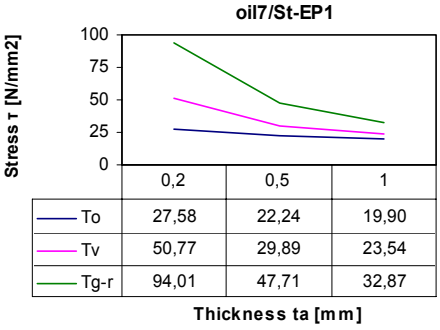

	0,2	0,5	1
To	27,58	22,24	19,90
Tv	50,77	29,89	23,54
Tg-r	94,01	47,71	32,87

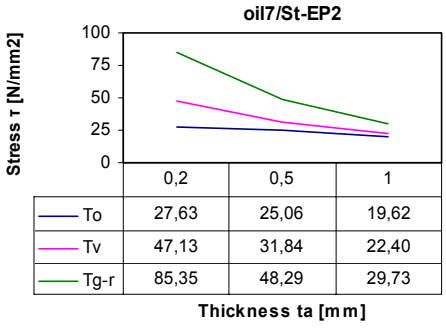

	0,2	0,5	1
To	27,63	25,06	19,62
Tv	47,13	31,84	22,40
Tg-r	85,35	48,29	29,73

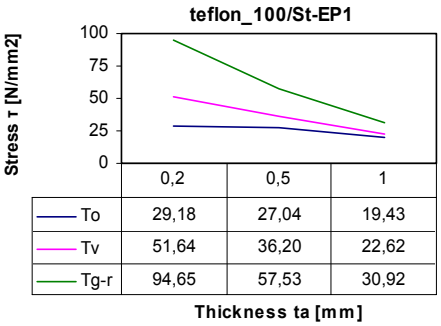

	0,2	0,5	1
To	29,18	27,04	19,43
Tv	51,64	36,20	22,62
Tg-r	94,65	57,53	30,92

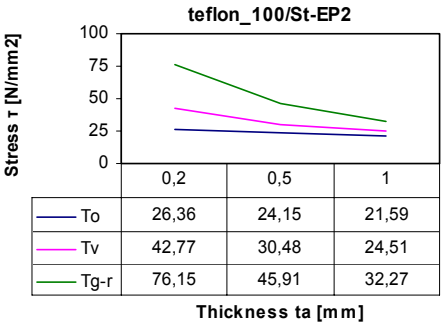

	0,2	0,5	1
To	26,36	24,15	21,59
Tv	42,77	30,48	24,51
Tg-r	76,15	45,91	32,27

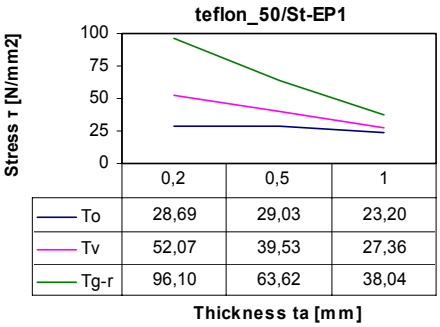

	0,2	0,5	1
To	28,69	29,03	23,20
Tv	52,07	39,53	27,36
Tg-r	96,10	63,62	38,04

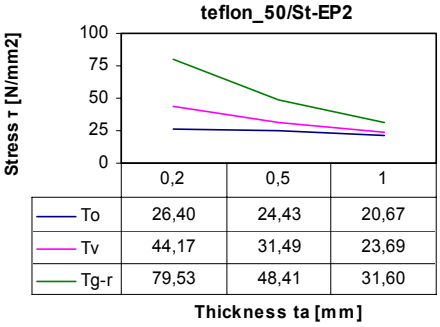

	0,2	0,5	1
To	26,40	24,43	20,67
Tv	44,17	31,49	23,69
Tg-r	79,53	48,41	31,60

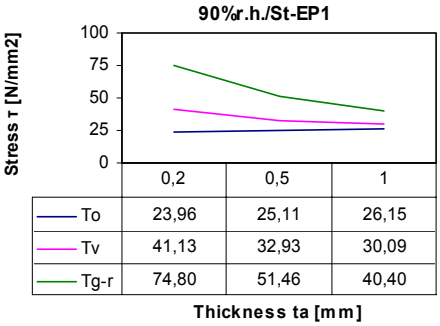

	0,2	0,5	1
To	23,96	25,11	26,15
Tv	41,13	32,93	30,09
Tg-r	74,80	51,46	40,40

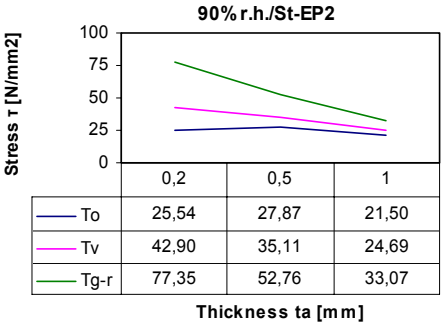

	0,2	0,5	1
To	25,54	27,87	21,50
Tv	42,90	35,11	24,69
Tg-r	77,35	52,76	33,07

Fig. D.1: Influence of bondline thickness upon experimental and theoretical failure stress of steel-EP1 single lap joints with defects

Fig. D.2: Influence of bondline thickness upon experimental and theoretical failure stress of steel-EP2 single lap joints with defects

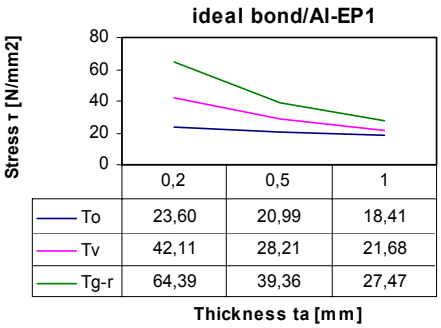

	0,2	0,5	1
To	23,60	20,99	18,41
Tv	42,11	28,21	21,68
Tg-r	64,39	39,36	27,47

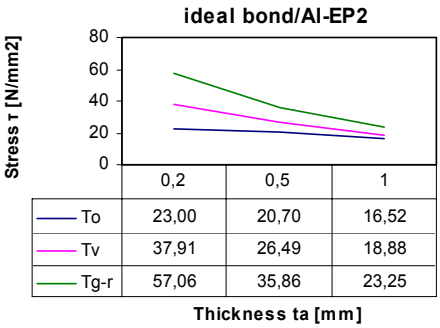

	0,2	0,5	1
To	23,00	20,70	16,52
Tv	37,91	26,49	18,88
Tg-r	57,06	35,86	23,25

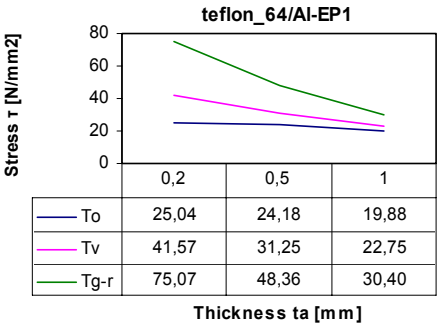

	0,2	0,5	1
To	25,04	24,18	19,88
Tv	41,57	31,25	22,75
Tg-r	75,07	48,36	30,40

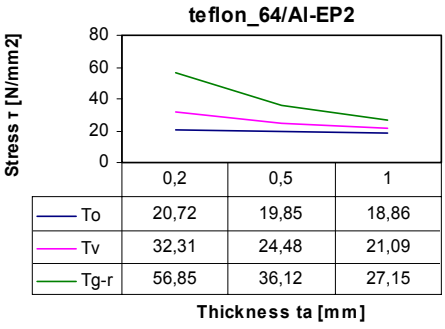

	0,2	0,5	1
To	20,72	19,85	18,86
Tv	32,31	24,48	21,09
Tg-r	56,85	36,12	27,15

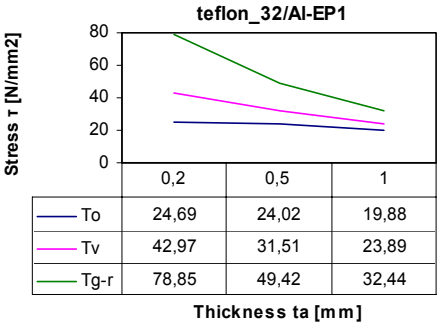

	0,2	0,5	1
To	24,69	24,02	19,88
Tv	42,97	31,51	23,89
Tg-r	78,85	49,42	32,44

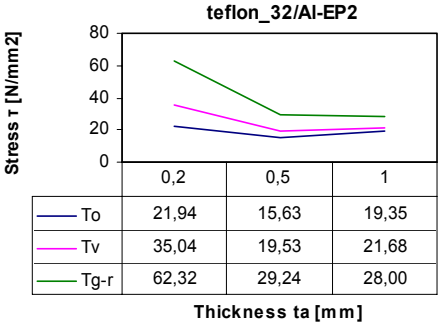

	0,2	0,5	1
To	21,94	15,63	19,35
Tv	35,04	19,53	21,68
Tg-r	62,32	29,24	28,00

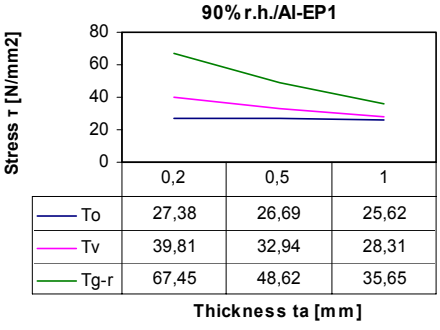

	0,2	0,5	1
To	27,38	26,69	25,62
Tv	39,81	32,94	28,31
Tg-r	67,45	48,62	35,65

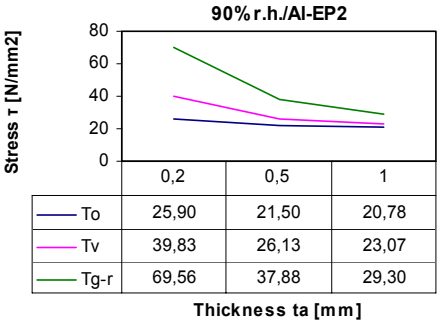

	0,2	0,5	1
To	25,90	21,50	20,78
Tv	39,83	26,13	23,07
Tg-r	69,56	37,88	29,30

Fig. D.3: Influence of bondline thickness upon experimental and theoretical failure stress of aluminium-EP1 single lap joints with defects

Fig. D.4: Influence of bondline thickness upon experimental and theoretical failure stress of aluminium-EP2 single lap joints with defects